Library Declaration and Deposit Agreement

1. STUDENT DETAILS

Please complete the following:

Full name: ………………………………………………………………………………………………

University ID number: ………………………………………………………………………………

2. THESIS DEPOSIT

2.1 I understand that under my registration at the University, I am required to deposit my thesis with the University in BOTH hard copy and in digital format. The digital version should normally be saved as a single pdf file.

2.2 The hard copy will be housed in the University Library. The digital version will be deposited in the University's Institutional Repository (WRAP). Unless otherwise indicated (see 2.3 below) this will be made openly accessible on the Internet and will be supplied to the British Library to be made available online via its Electronic Theses Online Service (EThOS) service.
[At present, theses submitted for a Master's degree by Research (MA, MSc, LLM, MS or MMedSci) are not being deposited in WRAP and not being made available via EthOS. This may change in future.]

2.3 In exceptional circumstances, the Chair of the Board of Graduate Studies may grant permission for an embargo to be placed on public access to the hard copy thesis for a limited period. It is also possible to apply separately for an embargo on the digital version. (Further information is available in the *Guide to Examinations for Higher Degrees by Research*.)

2.4 *If you are depositing a thesis for a Master's degree by Research, please complete section (a) below. For all other research degrees, please complete both sections (a) and (b) below:*

(a)   Hard Copy

I hereby deposit a hard copy of my thesis in the University Library to be made publicly available to readers (please delete as appropriate) EITHER immediately OR after an embargo period of ………..................... months/years as agreed by the Chair of the Board of Graduate Studies.

I agree that my thesis may be photocopied.   YES / NO (*Please delete as appropriate*)

(b)   Digital Copy

I hereby deposit a digital copy of my thesis to be held in WRAP and made available via EThOS.

Please choose one of the following options:

EITHER   My thesis can be made publicly available online.   YES / NO (*Please delete as appropriate*)

OR   My thesis can be made publicly available only after…..[date] (Please give date)
                                                    YES / NO (*Please delete as appropriate*)

OR   My full thesis cannot be made publicly available online but I am submitting a   separately identified   additional, abridged version that can be made available online.
                                                    YES / NO (*Please delete as appropriate*)

OR   My thesis cannot be made publicly available online.   YES / NO (*Please delete as appropriate*)

3. **GRANTING OF NON-EXCLUSIVE RIGHTS**

Whether I deposit my Work personally or through an assistant or other agent, I agree to the following:

Rights granted to the University of Warwick and the British Library and the user of the thesis through this agreement are non-exclusive. I retain all rights in the thesis in its present version or future versions. I agree that the institutional repository administrators and the British Library or their agents may, without changing content, digitise and migrate the thesis to any medium or format for the purpose of future preservation and accessibility.

4. **DECLARATIONS**

(a)   I DECLARE THAT:

- I am the author and owner of the copyright in the thesis and/or I have the authority of the authors and owners of the copyright in the thesis to make this agreement. Reproduction of any part of this thesis for teaching or in academic or other forms of publication is subject to the normal limitations on the use of copyrighted materials and to the proper and full acknowledgement of its source.

- The digital version of the thesis I am supplying is the same version as the final, hard-bound copy submitted in completion of my degree, once any minor corrections have been completed.

- I have exercised reasonable care to ensure that the thesis is original, and does not to the best of my knowledge break any UK law or other Intellectual Property Right, or contain any confidential material.

- I understand that, through the medium of the Internet, files will be available to automated agents, and may be searched and copied by, for example, text mining and plagiarism detection software.

(b)   IF I HAVE AGREED (in Section 2 above) TO MAKE MY THESIS PUBLICLY AVAILABLE DIGITALLY, I ALSO DECLARE THAT:

- I grant the University of Warwick and the British Library a licence to make available on the Internet the thesis in digitised format through the Institutional Repository and through the British Library via the EThOS service.

- If my thesis does include any substantial subsidiary material owned by third-party copyright holders, I have sought and obtained permission to include it in any version of my thesis available in digital format and that this permission encompasses the rights that I have granted to the University of Warwick and to the British Library.

5. **LEGAL INFRINGEMENTS**

I understand that neither the University of Warwick nor the British Library have any obligation to take legal action on behalf of myself, or other rights holders, in the event of infringement of intellectual property rights, breach of contract or of any other right, in the thesis.

Please sign this agreement and return it to the Graduate School Office when you submit your thesis.

Student's signature: ....……… Date: ....

DESIGN AND MECHANISM OF ACTION OF ORGANOMETALLIC ANTICANCER COMPLEXES
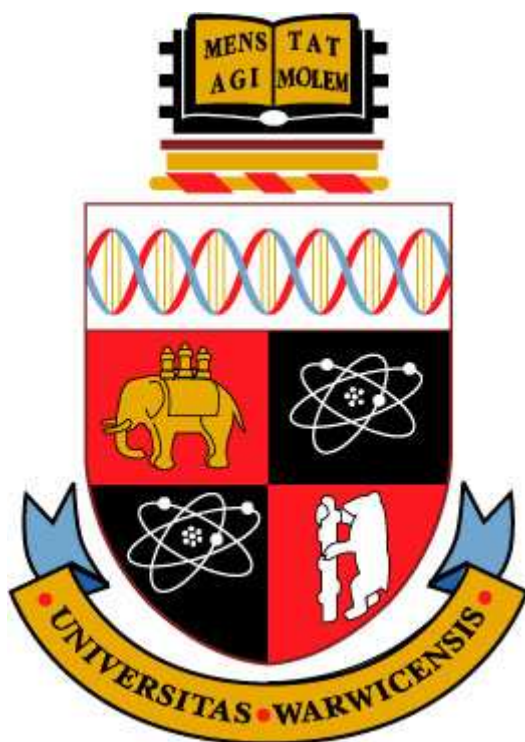
A Thesis Submitted for the Degree of
Doctor of Philosophy

Isolda Romero C., MSc

Supervisor: Prof. Peter J Sadler, FRS

University of Warwick, Department of Chemistry

August 2012.

Design and mechanism of action of organometallic anticancer compounds

Chapter 2. Experimental Methods   43

Acknowledgements

I would like to thank my supervisor Prof. Peter Sadler. I really appreciated all the support, encouragement and the challenges. Thanks for saying yes! Thanks for the opportunity. It has been quite an amazing ride!

Also, a big thanks to all past and present members of the PJS group, especially to all in C409, a very peculiar but enjoyable office! Abraha, thanks for all the advice, support and help in the lab. Ana, I cannot say thanks enough for teaching me so much. Every cultured cell will always remind me of you in the most fantastic way. Much more than that, thanks for all the smiles and all the "quality time" in biology. Luca, what can I say...my favourite Italian. Thanks for the support, for the chemistry, the laughter and the pasta. I have to say, the coffee club has never been the same. Sos grande Italiano! Sabine, thanks for your friendship and the reality checks. You were the first person to tell me.... It can be done within three years. You were right!. To my other two thirds of the fantastic organizational trio.... Ruth and LouNo thanks so much for everything: your help and support, the laughs and the tears. Especially for putting up with this very mean Latin. You made work much more enjoyable. Bushra and Jess, thanks for having kept biology going while I was writing. It is most appreciated. Ying thanks for all your encouraging "you will be fine".

Thanks to Dr. Ivan Prokes and Mr. Edward Tunnah for their help with the NMR, and Dr. Lijiang Song and Mr. Phillip Aston for their help with mass spectrometry.

Gracias....Totales

Isolda

Declaration

I hereby declare that except where specific reference is made to other sources, the work contained in this thesis is the original work of the author. It has been composed by myself and has not been submitted, in whole or in part, for any other degree, diploma or other qualification.

Isolda Romero Canelón

August 2012

Design and mechanism of
action of organometallic anticancer complexes

Abstract

Since the discovery of cisplatin, numerous attempts have been made to emulate its activity while reducing its collateral toxicity. Coordination complexes based on a wide number of transition metals have been developed in the search for improved bioavailability, selectivity and reduced adverse side-effects. Ruthenium(II) complexes have been widely developed in this field as a viable alternative to platinum chemotherapeutics.

This thesis is concerned with the synthesis, characterization and biological evaluation of three series of novel half-sandwich complexes of the general formula $[Ru^{II}(arene)(X)(YZ)]^{n+}$. These piano-stool Ru^{II} complexes have been designed as to allow the fine-tuning of their chemical and biological properties. In the first two series, the arene unit has been varied between *p*-cymene, biphenyl and terphenyl to investigate the correlation between hydrophobicity and antiproliferative activity, while the *N,N*-imino pyridine chelating ligand, YZ, has been modified to include either a higher number of aromatic units that could allow better DNA intercalation or substituent groups that could affect the overall charge distribution in the complex. Finally, the monodentate ligand, X, is either chloride or iodide. These compounds have been fully characterised by NMR, MS and elemental analysis. Their aqueous behaviour has been investigated together with the extent of 9-EtG binding, as an indication of the possible interaction with

nucleobases. The antiproliferative activity of these novel Ru^{II} complexes was determined, several of them show promising IC_{50} values, in the low µM range, against ovarian, colon, lung and breast cancer cell lines, in many cases the activities observed are better than cisplatin. The pathways for cellular accumulation were investigated. Complexes with an I as the monodentate ligand, X, exhibit partial energy-independent uptake. Overall results indicate that the novel Ru^{II} complexes synthesised in this thesis are most likely to be multi-targeted and that their mechanism of action depends to a great extent on the nature of the monodentate ligand, X. Two particularly active complexes in these series include the impy-NMe_2 ligand as YZ chelate. These have been compared to their isostructural azopyridine analogues and also to their Os^{II} equivalents. In this case, experiments were designed to study the activation of landmark events that lead to apoptosis, allowing contrasting the effects of different metal centres (Ru vs Os), isoelectronic ligands (impy-NMe_2 vs azpy-NMe_2) and monodentate ligands (Cl vs I). Results indicate that the molecular pathway followed by the iodido complexes is p53-independent. In comparison, the chlorido analogues activate the intrinsic apoptotic pathway and their activity relies on the existence of this tumour suppressor. DNA intercalation was also evaluated as a possible mechanism of action.

Finally, the third series includes inactive Ru^{II} complexes with tetrahydroquinoline derivatives, which were found to enhance the activity of platinum drugs in clinical use. These promising preliminary results in the use of Ru^{II} complexes in combination therapy open a world of possibilities for the dose-reduction of platinum-chemotherapeutics.

Abbreviations

9-EtA	9-Ethyl adenine
9-EtG	9-Ethyl guanine
APAF-1	Apoptosis activating factor 1
Azpy	Azopyridine
BCL2	B-cell lymphoma 2 protein
BCR	Breakpoint cluster region protein
BRCA1/2	Breast cancer type 1 susceptibility protein
CDDP	Cisplatin
CDK	Cyclin-dependent kinase
CIN	Chromosomal instability
CT-DNA	Calf thymus DNA
CTR1	Copper transport protein 1
DDW	Double deionised water
DISC	Death inducing signalling complex
DMEM	Dubelco's modified eagle medium
ECACC	European Collection of Cell Cultures
EGFR	Epidermal growth factor receptor
ERBB2 receptor	Human epidermal growth factor receptor 2 (HER2)
ESI	Electro spray ionisation
FDA	U.S. Food and Drug Administration
GSH	Glutathione
GSK3α	Glycogen synthase kinase 3

HIF-1	Hypoxia inducing factor 1
HIV	Human immunodeficiency virus
IC_{50}	50 % growth inhibition concentration
ICP	Inductively coupled plasma
Impy	Iminopyridine
L-BSO	L-Buthionine-sulfoximine
mDNA	Mitochondrial DNA
MDR	Multidrug resistance
MMR	Mismatch repair
MRP1/2/3	Multidrug resistance protein 1/2/3
MSI	Microsatellite instability
NER	Nucleotide excision repair
NSCLC	Non-Small Cell Lung Cancer
OXA	Oxaliplatin
P21/WAF	Cyclin-dependent kinase inhibitor 1
P53	Tumour suppresor protein 53
PAK1	Serine/threonine-protein kinase 1
PBS	Phosphate buffered saline
PDT	Photodynamic therapy
P-gp	P-glycoprotein 1
PI	Propidium iodide
PTEN	Phosphatase and tensin homolog protein
RB	Retinoblastoma tumour suppressor protein
RFA	Radiofrequency ablation
RNAse	Ribonuclease

ROS	Reactive oxygen species
RPMI-1640	Rosswell Park memorial institute medium 1640
SRB	Sulforhodamine B
TCA	Trichloroacetic acid
TFA	Trifluoracetic acid
TNF	Tumour necrosis factor
WHO	World Health Organization
WT1	Wilm's tumour gene

Chapter 1

Introduction

This thesis deals with the synthesis, characterization, chemical, and biological studies of the mechanism of action of novel Ru(II)half-sandwich arene complexes with antineoplastic activity. Understanding the molecular basis of cancer is crucial for the study of the metabolic pathways activated by metal-based anticancer agents. For this reason, this Chapter introduces core concepts in cancer biology. It also establishes the current approaches for treatment, including the new trend of single targeted therapy while recognising the benefits of multi-targeted agents. Platinum and ruthenium-based chemotherapeutics and their mechanism of action are summarised.

1.1. Cancer

Cancer, defined by the WHO as 'the uncontrolled growth and spread of cells', is responsible for at least 13% of world-wide deaths. Cancer, known since the early Greeks, was reported by Hippocrates (460-370 BC) as an ulcerous formation and by the roman physician Galen (130-200 AC), as a malignant swelling. However, current statistics indicate that 1 in every 3 people will develop some form of cancer during their life time. It is estimated that by 2030 there will be 21.4 million new cases diagnosed every year.[1]

Cancerogenesis is a process in which normal cells convert into neoplastic tissue, and disturbs cellular events such as proliferation, differentiation and development as a consequence of the lack of response to normal control mechanisms in cells.[2] Hanahan and Weinberg described tumour progression process as the result of six main events that are known as *the hallmarks of cancer*. They are: 1) self-

sufficiency in growth signals, 2) insensitivity to antigrowth signals, 3) evasion of apoptosis, 4) limitless replicative potential, 5) sustained angiogenesis and 6) tissue invasion and metastasis.[3]
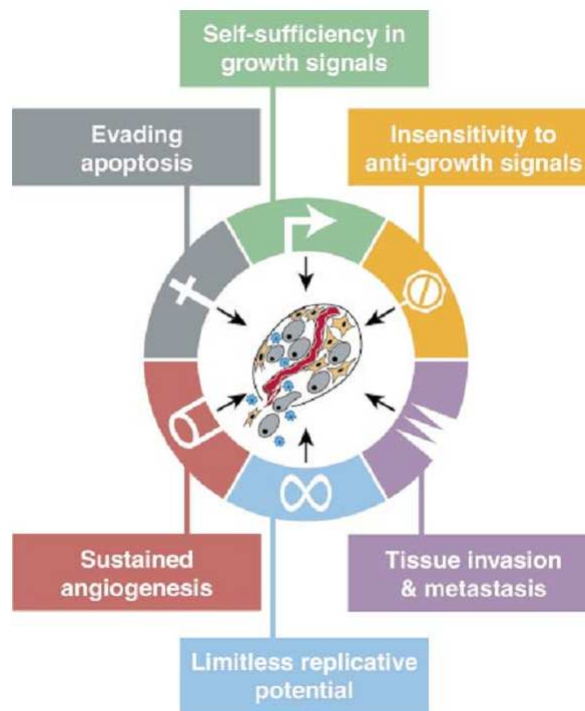
Figure 1.1. Hallmarks of cancer according to Hanahan and Weinberg.[3]

Cancers can be divided according to the tissue involved, for instance, carcinomas are cancers affecting the epithelium, while adenocarcinomas involve glandular tissue. Sarcoma is the generic name for malignant tumours of the mesenchyme (eg. fibrosarcoma, osteosarcoma, angiosarcoma, liposarcoma) and the hemato-lymphoid system gives origin to leukaemias and lymphomas, respectively. [2,4]

The generation of neoplastic tissue has often been associated to environmental, behavioural and genetic issues.[4,5] However, it is accepted that cancer is the result

of multi-factorial causes. As a leading cause of death, multiple approaches have been made to understand its molecular basis in the quest for a cure.

1.1.1 Molecular basis of cancer

1.1.1.1 Genetic instability

Genetic instability is a very common event in cancer development, it occurs as a result of the loss of DNA integrity and is present in all stages of the disease, from pre-cancerous lesions to advanced cancer.[6] This instability is critical in the process in which pre-cancerous lesions accumulate mutations characteristic of a cancerous state.[7] It is possible to classify genomic instability into three: firstly, the microsatellite instability MSI, which is characterised by expansion and contraction of oligonucleotide repeats in microsatellite sequences. Secondly, an instability defined by the increased frequency of base-pair mutations and thirdly, the most common of them all, chromosomal instability, CIN. This type of instability relates to the rate in which the number and structure of chromosomes varies over time in cancerous tissue[8] as a consequence of errors in chromosome segregation.[9] Chromosomal instability has been directly linked with colorectal cancers, which are ~ 80% aneuploid and with aggressive epithelial tumours in pancreatic, ovarian and lung tissue.[9]

1.1.1.2 Oncogene activation

An oncogene is defined as the altered manifestation of a normal gene that encodes a regulatory protein with dominant transforming proteins.[4] Molecular alterations leading to cancer include the de-regulation of oncogenes and/or the activation of proto-oncogenes.[10] This activation can occur by point-mutation or over-expression of the gene, the latter involving one of two distinctive genetic mechanisms: amplification (increase of the number of copies) or translocation.[2]

The most widely known oncogenes belong to the MYC and RAS families. De-regulated MYC gene is associated with several malignancies, including cancer.[11] c-myc, a member of this oncogene family, is generally over-expressed in rapidly proliferating tissue. Its de-regulation has been linked to Burkitt's lymphoma, invasive ductal breast carcinoma and colon adenocarcinoma amongst others. [10,11] This oncogene is thought to cause genomic instability, promote angiogenesis [5] and therefore represents an attractive target for anticancer agents, since its inhibition may be enough to stop tumour growth.[10]

RAS proteins are involved in multiple signalling pathways between cell surface receptors and intracellular pathways.[12] Its mutations are frequently observed in human cancers where it modulates the tumour micro-environment and promotes pro-angiogenic mechanisms.[13] Pancreatic, colon and lung adenocarcinoma have been associated with a high incidence of RAS oncogenic mutations which have lost the ability of becoming inactive after the external stimulus has ceased.[14] Table 1. 1. below shows the function associated to the principal human oncogenes and their mechanism of activation in cancer.

Table 1. 1. Principal human oncogenes (adapted from ref 15)

Oncogene	Function	Mechanism of activation in cancer
RAS	GTPase in mitogenic signaling	Mutation block GTPase
MYC	Regulatory factor in mitogenic signalling	Gene over expression
RAF	Protein kinase mitogenic signaling	Mutation inactivates kinase
BCL2	Protein kinase of multiple functions	Gene over expression or activation by mutation

1.1.1.3 Tumour suppressor gene inactivation

Tumour suppressor genes encode proteins whose absence, repression, inactivation or mutation promotes oncogenesis. These include DNA repair and cell cycle control proteins. Some examples of relevant tumour suppressor genes are shown in Table 1. 2 below, such as p53, WT1, PTEN, BRCA1 and BRCA2[2] amongst others, together with their familial cancer association. Mutations in the p53 protein are the most common event in human cancer. These occur in at least 50% of all cases. In normal tissue, activation of p53 allows the cell to respond to stress triggered by DNA-damaging agents amongst other external stimuli which in turn results in apoptosis.[5] More detailed explanation of the role of p53 can be found in Chapter 5 where the activity of Ru/Os organometallic anticancer complexes are evaluated against a colon carcinoma cell line with a p53 mutation. Tumour suppressor genes involved in the regulation of cell proliferation are usually inactivated during cancer. Their re-activation is the basis of the development of new anticancer therapies.

Table 1. 2. Principal human tumour suppressors (adapted from ref 16)

Tumour suppressor gene	Function	Familial cancer association
WT1	Transcription factor	Wilm's tumour
NF1	GTPase activating protein for RAS mitogenic signaling	Neurofibromatosis, sarcomas and gliomas
PTEN	Antagonist of PI3 kinase	Cowden syndrome
RB	Inhibitor of G1/S gene expression	Retinoblastoma
BRCA1, BRCA2	DNA repair, damage response	Familial breast cancer and ovarian cancer

1.1.1.4 Cell cycle-related events in neoplastic cells

Normal cells proliferate freely and only withdraw from the cell cycle after growth-factor deprivation or growth inhibitory signals. However, within the cell cycle, there are a number of checkpoints to ensure safe progression.[17] De-regulation of the cell cycle is a common event in human cancer. In this case persistent cell cycle progression occurs, losing the controls that limit the transition between phases. Check-point controls rely on cyclin-dependent kinases, CDKs. De-regulation of CDKs can cause excessive cell proliferation as well as genomic and chromosomal instability.[18]

1.1.1.5 Angiogenesis and metastasis

The microenvironment of solid tumours is usually associated with poor oxygenation[19] and low pH as consequences of accelerated metabolism.[20] Recent studies have demonstrated high correlation between this micro enviroment and

aggressive tumour progression. The presence of immune modulatory mediators together with the activation of inflammatory tissue surrounding the neoplasia are critical in tumour evolution towards metastasis.[21]

Tumour growth is closely related to the generation/improvement of vascularity. Drugs inhibiting angiogenesis have been used as antitumour agents. This type of therapeutic intervention suggests that targeting stromal events can affect tumour progression.[21] An example of this is *bevacizumab* for the treatment of metastatic colorectal cancer.[22] Neoplasms tend to disseminate, leaving the primary lesion and forming secondary tumours.[23] This process called metastasis has already occurred in two-thirds of cases by the time of diagnosis.[4] Critical events in the so called "metastatic cascade" include cell detachment from the primary tumour, invasion, penetration into the vascular system, extravastation and proliferation.[4,24]

1.1.1.6 Senescence and apoptosis as mechanisms of cell death

Cellular senescence refers to a cellular proliferation arrest triggered by stress stimuli, that can include telomere shortening, chemotherapeutic agent intervention or oncogene activation.[25] Different to quiescence, which is proliferative arrest caused by absence of growth factors, senescence can limit cancer progression in early neoplastic lesions.[26] and could be induced with therapeutic aims.[27]
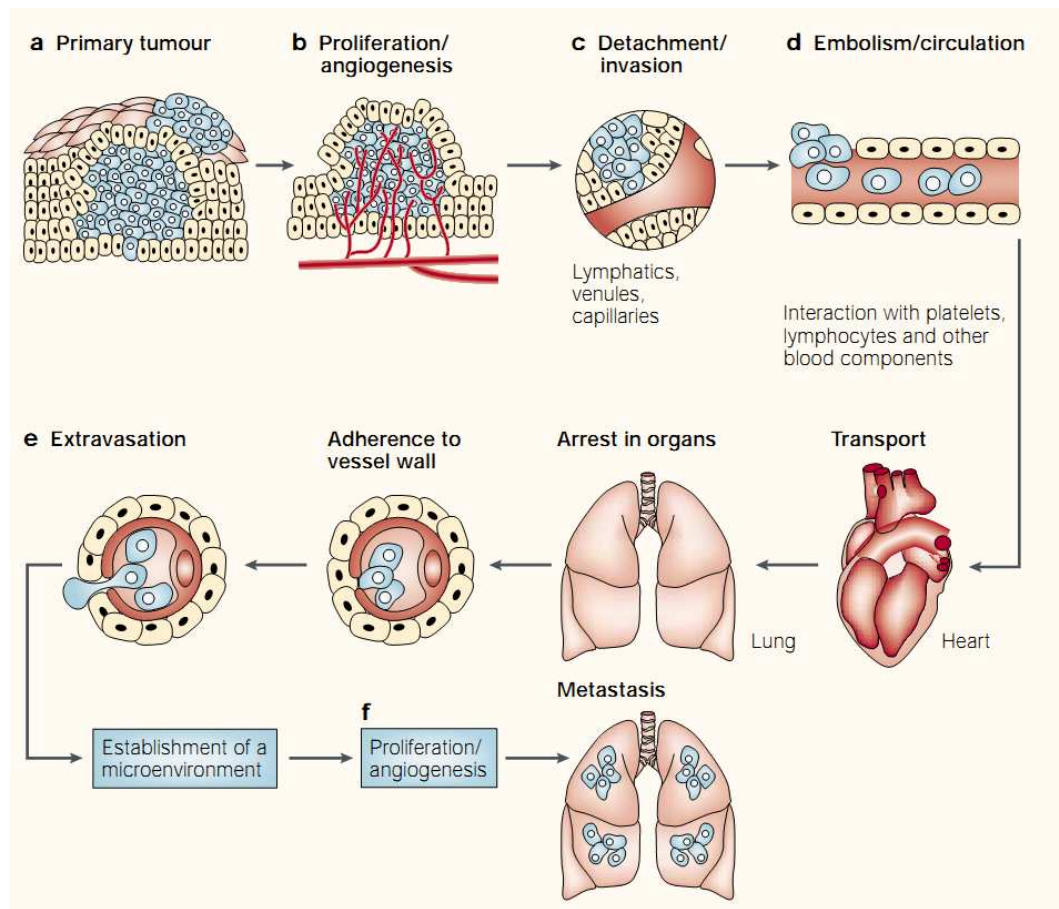
Figure 1.2. Angiogenesis and metastasis (adapted from ref 28). (a) generation of a primary neoplasia, (b) angiogenesis, (c) invasion of the stroma, (d) detachment of cancerous cells from the primary tumour, (e) extravasation, (f) proliferation into a new organ.

Normal cell proliferation is restrained by telomere degeneration as telomerase activity is usually absent in somatic cells. In early neoplastic lesions, dysfunctional telomere shortening can cause chromosomic instability and is associated oncogene activation.[29,30] At this point the lesions can activate cellular senescence. However, in advanced tumours, telomerase is activated, allowing

cells to exceed the regular limit of cell division cycles and progress towards malignancy and metastasis.[15,31]

Another cellular response to stress stimuli is apoptosis or programmed cell death. This energy-dependent process is based on morphological and biochemical changes that do not include inflammation.[32] Apoptosis can be activated by two main signalling pathways, however they both conclude in the formation of apoptotic bodies that surrounding fagocytic tissue can engulf.

1.2 Cancer Therapy

1.2.1 Surgery and other therapies

Surgery is the primary treatment for solid tumours; it involves the total removal of neoplastic tissue and the surrounding lymph nodes. This type of radical intervention depends to a great extent on the type of cancer, the affected organ and the stage of the diagnosed lesion. This treatment has strong limitations, especially for aggressive tumours with high rate of metastasis. Alternative therapies include the following.

- **Photodynamic therapy, PDT:** involves the administration of a non-toxic pro-drug and its subsequent selective activation at a specific wavelength. An example of a red-light activated antineoplastic agent is *photofrin*, while

levulan is activated by blue light. This therapy is widely used for skin cancers.

- **Radiotherapy**: based on the use of gamma radiation to treat neoplastic lesions; this radiation generates DNA damage in the affected tissue.

- **Hormone therapy**: the rate of growth and spread of neoplastic lesions that are hormone-dependent, such as breast, endometrial and prostate cancer, can be diminished by modulating hormonal levels in the patient. An example of this is the use of *tamoxifen* for the treatment of breast cancer.

- **Immunotherapy**: includes ligand-targeted therapeutics in which an immunotoxin or an immunoconjugate are used to improve drug-selectivity.[33]

- **Cryosurgery or cryotherapy:** an alternative to surgery for some types of cancer, for example liver, prostate and skin neoplastias.

- **Radiofrequency ablation, RFA:** Commonly used for liver and lung neoplastias, this intervention relies on high temperatures, generated by radiofrequencies, to destroy cancerous tissue.

1.2.2 Chemotherapy

Surgery and radiotherapy dominated cancer treatment during the first half of the 20th century. Chemotherapy, as a viable alternative, was first considered in the 1940s when nitrogen mustards were used against lymphomas. Since then, extensive research into the use of drugs against the proliferation of malignant

tissue has taken place. In time, important discoveries have been made that have allowed the cure and/or improvement of life expectancy for cancer patients.[34]

Selectivity has always been presented as the downside of chemotherapy, mostly because the severity of undesired side-effects which range from nausea and vomiting to acute renal failure. Theoretically, reduction of side-effects could be achieved by increasing the dose of drug that reaches the diseased tissue while reducing the dose that reaches and affects normal surrounding tissue/organs. However, in the practice, selectivity is a much more complicated issue, especially because of the lack of unique molecular targets in cancer cells.

Anticancer agents currently in clinical use rely on the high proliferation rate of neoplastic tissue as means for selectivity.[35] This results in side-toxicity in tissues that also exhibit frequent cellular replacement such as bone marrow and gastrointestinal tract.[33]

1.2.2.1 Single-targeted chemotherapeutic agents

Single-targeted chemotherapy aims to selectively deliver the drug to the neoplastic growth, avoiding the surrounding tissue. It also refers to some antineoplastic agents that are able to interrupt a particular metabolic pathway only present in cancerous cells or to directly interact with a unique molecular target. The benefits of such therapy are the increase in selectivity and the possibility of reducing adverse side-effects.

Molecularly-targeted therapies are in their early stages. However, several examples can be found, for instance *imatinib* targets the BCR-ABL oncogene that causes chronic myelogenous leukaemia and *trastuzumab* targets the ERBB2 receptor to stop proliferation of breast cancer. In both cases, these antineoplastic agents aim to target pathways that are specifically activated in cancers.[33] Frequent targets for cancer therapies are tyrosine kinase receptors. These receptors for growth factors are located in the cell surface and have a crucial role in oncogenesis.[36] One example of this is the use of *cetuximab* to target the family of epidermal growth factor receptors, EGFR, in metastatic colorectal and head and neck cancers or *gefitinib* in the analogous breast and lung cancers.[37]

Cellular metabolism in cancer is altered to allow cells to sustain a high rate of proliferation and to avoid cell death-signalling usually caused by increased cellular stress levels.[35,38] Such alterations in metabolism can be exploited by targeted agents,[39] such as *lonidamine,* which inhibits glycolysis and is currently in phase III clinical trials. Another example of this type is the use of arginine deiminase against metastatic melanoma and hepatocellular carcinomas, as it reduces arginine levels in plasma (clinical trials phases I/II).[35]

New possible targets are being investigated, such as those of the hypoxia-inducible factor 1, HIF-1, which is involved in cancer progression. HIF-1 is over expressed in solid tumours as result of microenvironment hypoxia and it activates the transcription of angiogenesis-promoting genes.[40,41]

Finding unique molecular targets in a disease not fully understood at molecular levels can prove to be a difficult endeavour[42]. Although there have been

advantages in single-targeted therapies, many workers insist they will not be the ultimate answer to increase chemotherapy's selectivity. Cancer is a very dynamic disease, resulting from sporadic mutations and genomic instability, which promotes rapid somatic evolution. Single-targeted therapy undoubtedly can be able to promote resistance as an evolutive answer.[43] This would only allow short-term use of the therapy with an increased risk of resistant recurrences.[32]

1.2.2.2 Multi-targeted chemotherapeutic agents

The efficiency achieved by the complete inhibition of one single molecular target can be over-estimated when compared to the partial inhibition of several targets, especially when the multi-targeting is the result of a single agent.[44] A recent view that a multi-targeted drug can prevent cells from developing resistance has quickly gained followers. Multiple target screenings are being developed[45] to tackle multi factorial diseases such as cancer or Alzheimer.[46] The aim is to find a single agent that would be able to stimulate/inhibit more than one molecular activity.[32] The best examples of successful multi-targeted antineoplastic agents are *cisplatin* (CDDP) and its derivative drugs *carboplatin* and *oxaliplatin*. These platinum chemotherapeutics have DNA as their principal target.[47] However, in the case of CDDP, only 1% of the administered metal reaches the cellular nucleus, allowing the rest of the drug to interact with other important biomolecules.[48–51]

1.2.2.3 Combination therapy in cancer treatment

Multi-targeted therapy can also be achieved by combination of several single-targeted agents or by co-administration of drugs with synergistic anti-tumour activity, which can block simultaneously multiple signalling pathways.[52,53] Several attempts have been made to understand the interaction of two or more drugs when they are co-administered. The most-accepted theory, developed by Chou and Talalay, indicates that two agents can interact in three different ways. 1) synergistically, 2) additively or 3) antagonistically. Synergistic interaction refers to the situation when the modulating effect of the combination of both drugs is greater than the addition of their single actions, in comparison, in an antagonist interaction the modulating result is lower.[54–56]

The best outcome of combination therapy in cancer would be a synergistic interaction that could allow the reduction of drug doses and subsequently the incidence of adverse side-effects. Another possible advantage of this type of therapy is the circumvention of drug resistance as is the case on the treatment of ovarian cystadenocarcinoma cells treated with tunicamycin and CDDP or vincristine.[57]

One particular cancer in which multi-targeted agents or the combination of single-targeted drugs are the best option is non-small cell lung cancer, NSCLC. Refractory advanced patients are best treated with EGFR *gefitinib* in combination with *erlotinib*. Other ongoing clinical trials include the co-administration of *ZD6474*, a kinase inhibitor with *gefitinib* or *docetaxel*.[52] Other approaches include *gemcitabine* combined with *etoposide* which also work on ovarian cancer.[58]

Activity of platinum agents such as CDDP can also be enhanced by the co-administration of secondary chemotherapeutics such as dichloroacetate[59] or aphidicolin glycinate.[60] Combination therapy of anti-angiogenic agents with regular chemotherapy increases the survival rate of patients with advanced cancers.[22]

1.2.2.4 Resistance to chemotherapeutics

One of the major challenges in the use of chemotherapy for cancer treatment is the high incidence of resistance.[61] Drug resistance is divided into two main categories, inherent and acquired resistance. Some of the most important molecular mechanisms of resistance include: increased drug efflux, mutations in drug targets, activation of downstream or parallel signalling pathways and altered drug metabolism.[62] The development of drug resistance is not limited to cancer treatment, and is a critical factor in the management of diseases such as malaria, tuberculosis and HIV.[63,64]

Inherent resistance usually has pleiotropic origins and determines the selectivity of a neoplastic lesion to chemotherapy. This resistance is the basis of the Goldie-Coldman hypothesis[65] that states that resistance can arise from spontaneous mutations that inevitably occur in cell proliferation as part of intrinsic genetic instability.[66]

In comparison, acquired resistance is developed after initial exposure to chemotherapeutics. Multidrug resistance, MDR, can emerge as a cellular response

to chemotherapeutic agents.[67] The family of proteins know as multidrug resistance-associated proteins, MRP are usually organic anion transporters, although MRP1, MRP2 and MRP3 can also transport neutral molecules, which function as efflux pumps in order to reduce intracellular drug concentrations. The most widely known protein of this family is the P-glycoprotein discovered in 1976.[68,69]

Mutations in drug targets as a mechanism of acquired resistance have been extensively investigated. Such is the case of chronic myeloid leukaemia. This type of cancer is often treated with *imatinib*, however up to 40% of the cases develop some kind of resistance due to a mutation in the kinase domain of BCR.[70–72]

Increased drug efflux and therefore impaired cellular accumulation is often related to CDDP and other platinum-drug resistance, particularly in the treatment of hormone dependent female cancers. For ovarian neoplastias the combination of platinum-*paclitaxel* improves rates of survival, although patients will eventually relapse with a median-survival of 18 months.[73] After platinum resistance has established, patients are often treated with *doxorubidicin*, *topotecan*, *etoposide* or other hormonal therapies, but still the relapse is frequent and associated with multiple drug resistance.[73]

1.3 Metal-based anticancer agents

1.3.1 Platinum-based anticancer agents

Since the serendipitous discovery that cisplatin, CDDP, could arrest cell division of *E. coli*, coordination complexes have been used as anticancer agents.[74] CDDP had been first reported in 1845 by M. Perone[75] and its structure proposed in 1893 by A. Werner, but it was not until 1965 when the observations of B. Rossenberg[76,77] started a new field for platinum chemistry and its medical applications.[78]

CDDP was the first platinum-based drug approved by the FDA with antineoplastic activity (1978). Currently, its use is accepted alone or in combination with other chemotherapeutic drugs against bladder and advanced cervical cancer that cannot be treated with surgery or radiotherapy, also in non-small cell lung or ovarian cancer that are locally advanced or have metastasised. Finally it can be used to treat malignant mesothelioma, squamous cell carcinoma of the head and neck and testicular cancer.[79]

Since its approval, several attempts have been made to improve the pharmacological properties of CDDP. Two important derivatives have gained FDA approval, *carboplatin* in 1989 and *oxaliplatin*, OXA, in 2002, the latter having European approval since 1996. In comparison to CDDP*, carboplatin* is approved to treat non-small cell lung cancer and ovarian cancer, in both cases the lesions should be locally advanced or derived from tumour recurrence. Advanced

or recurrent colorectal cancers or stage III colon cancers may be treated with OXA.[79]
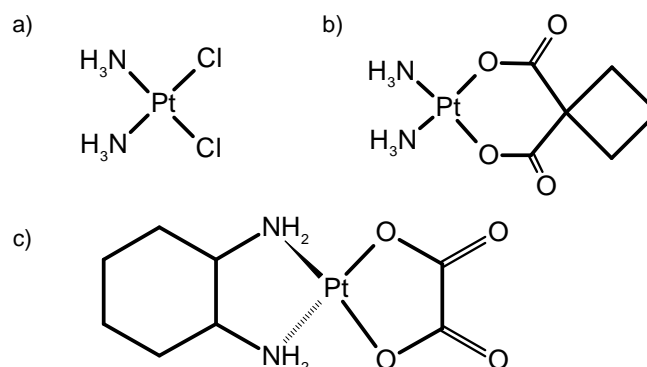
Figure 1.3. Cisplatin, CDDP (a), carboplatin (b) and oxaliplatin, OXA (c)

Despite the wide clinical application of CDDP and its derivatives, these platinum chemotherapeutics have strong disadvantages. Their administration causes severe side effects which include nephrotoxicity,[80,81] neurotoxicity,[82,83] ototoxicity,[84,85] nauseas and vomiting amongst others. These side-effects are mostly caused by the lack of drug selectivity. Numerous studies have been carried out to improve drug delivery including optimised solubility and selective activation of pro-drugs. In the latter case, platinum(IV) complexes have lead the research with complexes such as *tetraplatin*, *satraplatin*. The latter, although it has not yet received full FDA approval, is the first platinum antineoplastic agent that can be administered orally.[86]
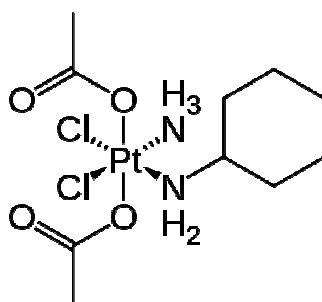
Figure 1.4. Structure of satraplatin

1.3.1.1 Mechanism of action of Pt-based anticancer agents

It is widely accepted that the antineoplastic properties of CDDP rely on the interaction with DNA which in turn activates apoptosis. However, this is a reductionist view of a process in which several important events are involved from drug administration to cellular death. A general scheme of these cellular events is shown in Figure 1.5 below.

CDDP is administered directly into the bloodstream. The chloride concentration in blood plasma is 100 mM,[87] and this allows the molecule to remain intact. It is thought that protein binding can deactivate the platinum drug at this stage, especially after S-binding to metallothioneins or thiol groups in eg. Albumin. Cellular accumulation of CDDP occurs by means of diffusion and active transport via the copper transporter CTR1. Once inside the cytoplasm of the cell, the concentration of chloride is reduced to 20 mM and partial aquation CDDP occurs. Aquated forms of CDDP are reactive and bind to DNA, forming monofunctional

adducts. The formation of inter-strand or intra-strand bifunctional adducts is possible.[87–90]
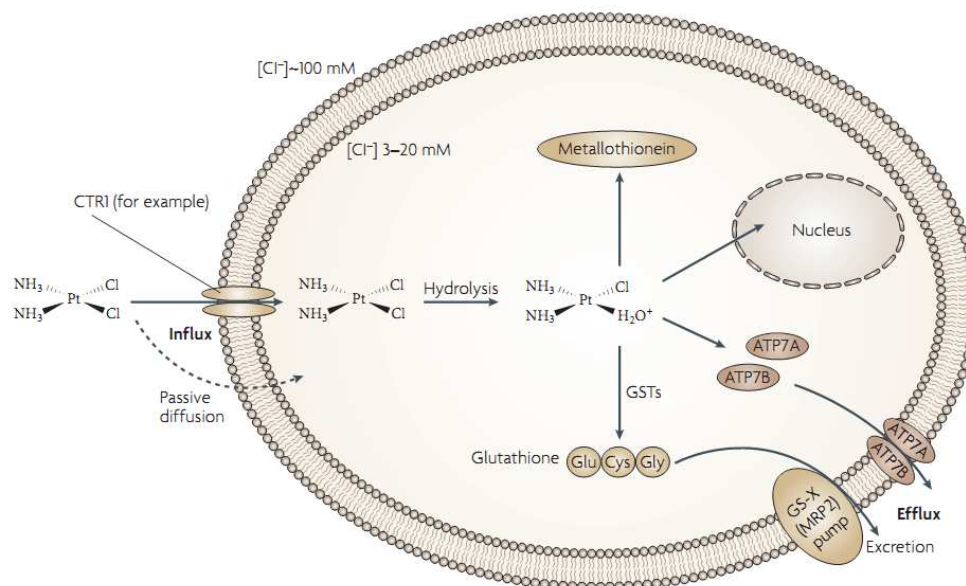
Figure 1.5. Cellular mechanism of action of CDDP (adapted from ref [87])
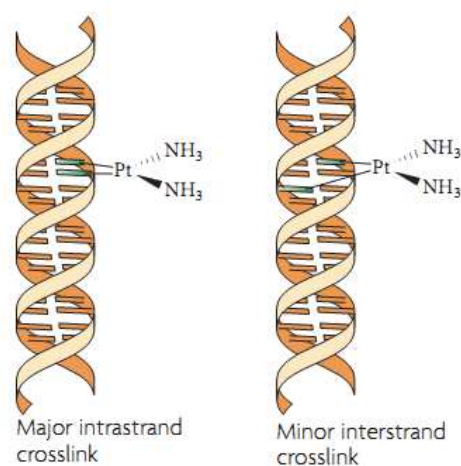
Figure 1.6. CDDP-DNA bifunctional adducts (adapted from ref [87])

Once the CDDP-DNA adducts have been formed, the lesions can be repaired by three distinct mechanisms: 1) nucleotide excision repair, NER, 2) mismatch

repair, MMR or 3) DNA-dependent protein kinase repair mechanisms, DNA-PK. NER mechanism is the most common of the three. It involves an ATP-dependent protein to recognise the DNA lesion, especially 1,2-intrastrand cross-links, and excise the damaged DNA strand-section for the subsequent filling of the gap by the DNA polymerase.[91] The general scheme for this repair process is shown in Figure 1.7. Although the DNA lesions caused by CDDP and their repair processes have been extensively investigated, the detailed mechanism by which they lead to apoptosis remains poorly understood.[87,92]

Carboplatin and OXA are thought to follow similar mechanisms of action to CDDP.[47] Although *carboplatin* shows reduced side-effects and OXA shows improved performance on colorectal cancers, CDDP is still the chemotherapeutic agent of choice and is more widely available.
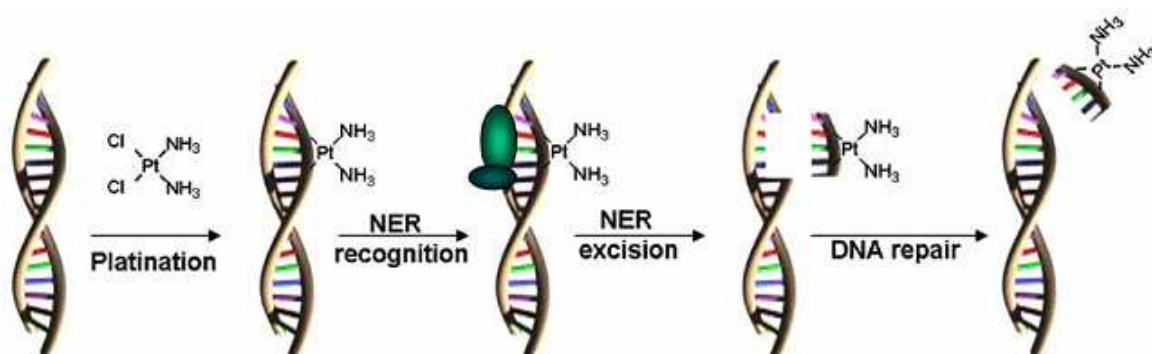
Figure 1.7. NER repair mechanism according to Cepeda *et al*. [91]

One major drawback of platinum chemotherapeutics is the high occurrence of inherent and acquired resistance. Such resistance against platinum drugs can be the result of one of the following mechanisms: a) impaired cellular accumulation

as a consequence of reduced cellular uptake or increased cellular efflux, b) deactivation by binding to sulfur containing proteins and c) increased repair of DNA lesions.[93–99]

1.3.2 Ruthenium-based anticancer agents

Since the discovery of CDDP, numerous attempts have been made to emulate its activity while reducing its side toxicity. Coordination complexes based on a wide number of metals have been developed in the search for improved bioavailability and increased selectivity.[100–102] Ruthenium (II/III) complexes have been widely developed in this field as a viable alternative to platinum chemotherapeutics.

Two Ru(III) antineoplastic complexes NAMI-A and KP1019, Figure 1.8, have reached human clinical trials.[103,104] NAMI-A has shown antimetastatic potential, while the latter induces apoptosis in primary tumours.
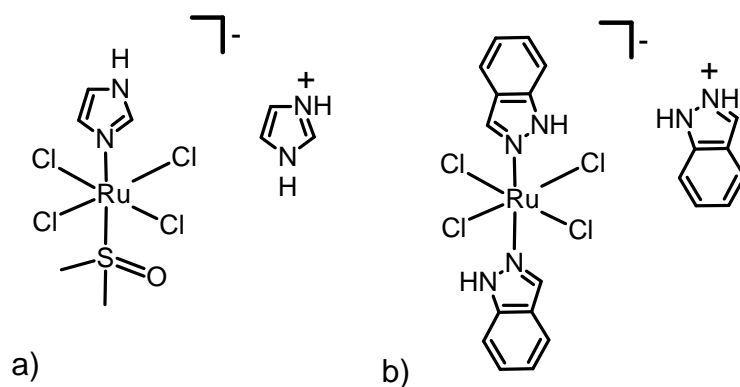
Figure 1.8. Structure of NAMI-A (a) and KP1019 (b).

Other promising series of Ru(II) complexes have been synthesised, Figure 1.9, including organometallic arene diamine complexes prepared in the Sadler Group like RM175,[105] phosphor-adamantane derivatives such as RAPTA-C[106] developed by the Dyson Group and polypyridyl complexes synthesised by the Sheldrick Group.[107]
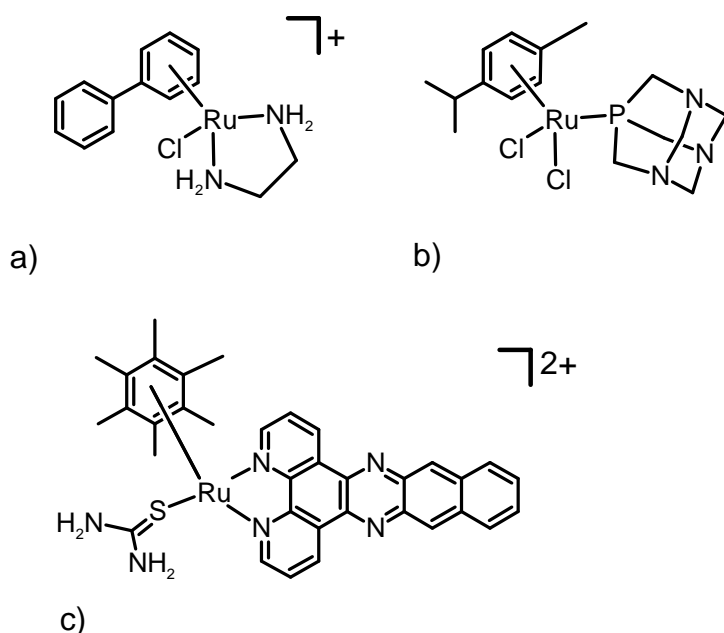
Figure 1.9. Structures of RM175 (a) and RAPTA-C (b) and Ru(II) complex synthesised by Sheldrick.

Organometallic Ru(II) 'piano-stool' complexes were designed to allow fine tuning of the physical and chemical properties which should result in optimised biological activity.[108–111] These complexes include three basic building units as shown in Figure 1.10: an arene ligand, used to stabilise the metal centre oxidation state and improve hydrophobicity, a monodentate ligand, X, initially included as an activation site, and a bidentate ligand, Y-Z. [100,112]
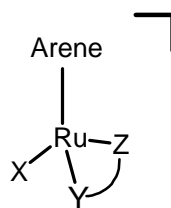
Figure 1.10. Basic structure of Ru(II) 'piano-stool' complexes.

1.3.2.1 Mechanism of action of Ru-based anticancer agents

Investigations into the mechanism of action of metal-based chemotherapeutics are still in the early stages. Ruthenium organometallic drugs are most likely to be multi-targeted. Although the DNA damage caused by most complexes is considerable, this mechanism may be only partly responsible for the antineoplastic activity observed. Investigations on non-DNA targets are extensive but the details of the mechanism of action of these drugs in still poorly understood.[113] However, significant progress has been made to link their biological activity to particular molecular targets that include protein kinases, carbonic anhydrases[114] and topoisomerases.[115–117]

Organometallic Ru(II) piano stool complexes can undergo activation by the loss/replacement of the monodentate ligand. This gives rise to a free coordinative position that can bind to DNA or other biologically-relevant molecules.[100] Some cell-free studies show that aquation of the complexes can occur with subsequent binding to nucleobases such as 9-EtG and 9-EtA, Figure 1.11. [118,119]
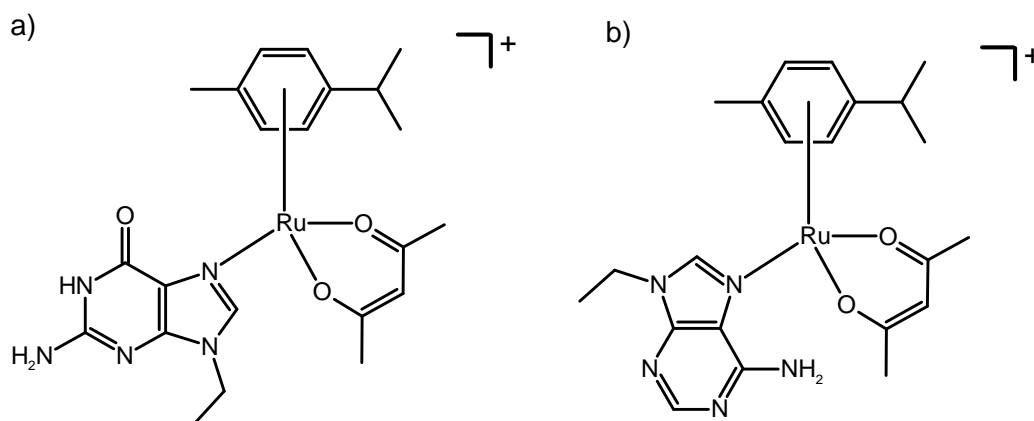
Figure 1.11. Structures of 9-EtG (a) and 9-EtA (b) ruthenium(II) adducts reported by Melchart *et al.*[118]

Under the same conditions several studies have shown how these complexes can interact with Calf Thymus-DNA.[120] Further, *in vitro* testing has shown the extent of the interaction between the Ru(II) complexes and cellular DNA[113,121] as well as the activation of nucleotide excision repair mechanisms after the formation of Ru-DNA adducts.[122] Metal complexes not only can be activated by aquation but also by reduction,[100] particularly in the case of Ru(III) complexes.[123, 124]

An important advantage of Ru(II) piano stool complexes is their ability to circumvent resistance to platinum chemotherapeutics. Such is the case of RM175 which is active in CDDP-resistant ovarian carcinoma cells A2780cis.[125] This Ru(II) complex causes G1/G2 arrest in HCT116 cells in a p53 and p21/WAF1-dependent manner after short drug-exposure periods.[126]

With P-donor ligands, pyridocarbazole half-sandwich Ru(II) complexes, such as that shown in Figure 1.12, are able to inhibit protein kinases GSK3α and

PAK1.[127] The same kinases can be inhibited by octahedral Ru(II) complexes as well.[128]
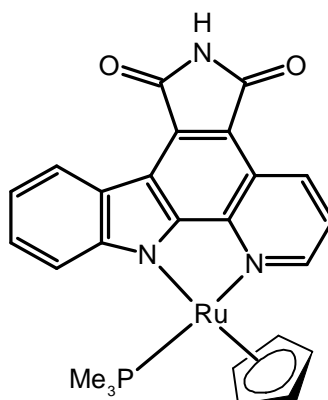
Figure 1.12. Half-sandwich ruthenium(II) complex inhibitor of GSK3α and PAK1.[127]

Ruthenium polypyridyl complexes can interact with DNA by intercalation,[115,129,130] but they can also induce mitochondria-mediated[131] and caspase-dependent[132] apoptosis. This mechanism of cell death activation is also observed in 'piano-stool' Ru(II) complexes.[133–135]

1.3.3. Anticancer agents based on other metals

Research into metal-based anticancer agents, other than Pt and Ru, has seen an abrupt increase in the last decades.[136] The use of osmium, iridium, gallium, or gold as metal centres for novel antineoplastics has achieved important steps towards the development of drugs with low side effects.[101]

Osmium, has been used to build piano-stool complexes similar to those of Ru(II), complexes such as $[Os(\eta^6\text{-bip})(en)Cl]^+$ or $[Os(\eta^6\text{-bip})(picolinate)Cl]$ which have shown to have good activity against A2780 ovarian cancer cells. More important, they are active in the CDDP resistant derived cell line, A2780cis.[120] Os complexes are more inert towards aquation and ligand exchange than their Ru analogues. They also exhibit lower rates for nucleobase binding than their Ru(II) complexes. In addition water molecules bound to the Os metal centre are significantly more acidic.[137] Attempts have been made to increase the selectivity of such complexes based on Os by using targeting peptides.[138]

Azopyridine Os(II) complexes such as $[Os(\eta^6\text{-bip})(azpy\text{-OH})I]PF_6$, $[Os(\eta^6\text{-}p\text{-cym})(azpy\text{-OH})I]PF_6$, $[Os(\eta^6\text{-bip})(azpy\text{-NMe}_2)I]PF_6$ and $[Os(\eta^6\text{-}p\text{-cym})(azpy\text{-NMe}_2)I]PF_6$ have shown to be an order of magnitude more active than CDDP in the ovarian cancer cell line A2780. In particular, $[Os(\eta^6\text{-}p\text{-cym})(azpy\text{-NMe}_2)I]PF_6$ exhibited sub-micro molar IC_{50} values in lung A549, colon HCT116, breast MCF7 and prostate cancer PC3. This complex has also shown good in vivo tumour reduction for HCT116 xenografs.[139]

Osmium(II) and rhodium(II) analogues of Ru(II) based anticancer agent such as RAPTA-C have also been used in order to improve antiproliferative activity. In this case, the Rh analogues showed to be twice as active than the original Ru complex in A549 lung cancer and T47D breast cancer cells.[140] Organometallic half-sandwich iridium complexes have also been explored as novel anticancer agents. In this case, negatively charged cyclopentadienes are needed in order to stabilise Ir(III) as a metal centre. Highly active complexes $[Ir(\eta^5\text{-}C_5Me_4C_6H_4C_6H_5)(phen)Cl]^+$ and $[Ir(\eta^5\text{-}C_5Me_4C_6H_4C_6H_5)(bpy)Cl]^+$ are reported to undergo hydrolysis and form nucleobase adducts after reaction with 9-EtG. However they do not react with 9-EtA. In both cases their IC_{50} values in A2780 ovarian cancer cells is in the sub-micro molar range (0.72 ± 0.01 and 0.57 ± 0.07 µM respectively).[141]

Gallium-based compounds have been explored in the clinic as antineoplastic agents. Oral administration of Ga salts results in low toxicity which allows for chronic treatment. Gallium nitrate has reached phase II clinical trials with promising results in the treatment of bladder carcinoma and lymphomas. Gallium chloride and maltolate have also been investigated,[142] as well as, tris(8-quinolinolato) gallium(III) (KP46) which is capable of inhibiting tumour growth and there is clinical evidence of its activity in renal cell carcinoma.[143,144] More recently, another gallium based compound, KP2235, which targets the functionality of the endoplasmic reticulum has completed pre-clinical trials.[145]

1.4 Aims

The general aim of this thesis was to synthesise and characterise novel ruthenium(II) complexes for subsequent investigation of their biological properties as antineoplastic agents, including their *in vitro* mechanism of action in cancer cells. More specific aims are as follows.

- Synthesise and characterise novel half-sandwich Ru(II) arene complexes.

- Investigate the aqueous chemistry of the novel Ru(II) complexes including the extent of their aquation and binding to 9-EtG, as a model for nucleobase interaction.

- Determine the antiproliferative activity *in vitro* and the total cellular accumulation of the Ru(II) complexes in cancer cells and investigate the molecular pathways involved in the cellular accumulation of the Ru(II) complexes.

- Investigate the mechanism of action of iminopyridine Ru(II) complexes and explore DNA as a possible target by means of intercalation.

- Investigate the differences in the molecular pathways activated by organometallic Ru/Os complexes when the monodentate ligand changes from chloride to iodide.

- Investigate the synergistic effect of inactive Ru(II) complexes in combination therapy by co-administration with Pt drugs currently in clinical use.

1.5 References

1. A. Jemal, F. Bray, M. Center, J. Ferlay, E. Ward, and D. Forman, *Ca. Cancer J. Clin.*, 2011, **61**, 69-90.

2. M. Knowles and P. Selby, Eds., *Introduction to the Cellular and Molecular Biology of Cancer*, Oxford University Press, Oxford, UK, Fourth Edi., 2006.

3. D. Hanahan and R. Weinberg, *Cell*, 2000, **100**, 57-70.

4. R. McKinnell, R. Parchment, A. Perantoni, and G. Pierce, *The Biological Basis of Cancer*, Cambridge University Press, Cambridge, UK, 1998.

5. H. Kiaris, *Understanding Carcinogenesis*, Wiley, Weinheim, First Edit., 2006.

6. C. Lengauer, K. W. Kinzler, and B. Vogelstein, *Nature*, 1998, **396**, 643-649.

7. J. Breivik, *Seminars in Cancer Biology*, 2005, **15**, 51-60.

8. S. Negrini, V. G. Gorgoulis, and T. D. Halazonetis, *Nat. Rev. Mol. Cell Biol.*, 2010, **11**, 220-228.

9. V. M. Draviam, S. Xie, and P. K. Sorger, *Curr. Opin. Genet. Dev.*, 2004, **14**, 120-125.

10. H. Hermeking, *Curr. Cancer Drug Targets*, 2003, **3**, 163-175.

11. C. E. Nesbit, J. M. Tersak, and E. V. Prochownik, *Oncogene*, 1999, **18**, 3004-3016.

12. M. Malumbres and M. Barbacid, *Nat. Rev. Cancer*, 2003, **3**, 459-465.

13. Y. Pylayeva-Gupta, E. Grabocka, and D. Bar-Sagi, *Nat. Rev. Cancer*, 2011, **11**, 761-74.

14. J. L. Bos, *Cancer Res.*, 1989, **49**, 4682-4689.

15. D. Morgan, *The Cell Cycle: Principles of Control*, Oxford University Press, London, 2007.

16. C. J. Sherr, *Cell*, 2004, **116**, 235-246.

17. M. B. Kastan and J. Bartek, *Nature*, 2004, **432**, 316-323.

18. M. Malumbres and M. Barbacid, *Nat. Rev. Cancer*, 2009, **9**, 153-166.

19. A. I. Minchinton and I. F. Tannock, *Nat. Rev. Cancer*, 2006, **6**, 583-592.

20. P. Subarsky and R. P. Hill, *Clin. Exp. Metastasis*, 2003, **20**, 237-250.

21. G. Lorusso and C. Rüegg, *Histochem. Cell Biol.*, 2008, **130**, 1091-103.

22. N. Ferrara and R. S. Kerbel, *Nature*, 2005, **438**, 967-974.

23. D. X. Nguyen and J. Massagué, *Nat. Rev. Genet.*, 2007, **8**, 341-352.

24. D. X. Nguyen, P. D. Bos, and J. Massagué, *Nat. Rev. Cancer*, 2009, **9**, 274-284.

25. L. Hoenicke and L. Zender, *Carcinogenesis*, 2012, **33**, 1123-1126.

26. A. Suram, J. Kaplunov, P. L. Patel, H. Ruan, A. Cerutti, V. Boccardi, M. Fumagalli, R. Di Micco, N. Mirani, R. L. Gurung, M. P. Hande, F. D'Adda, and U. Herbig, *EMBO J.*, 2012, **31**, 2839-2851.

27. R. R. Gordon and P. S. Nelson, *Drug Resist. Update*, 2012, **15**, 123-131.

28. I. J. Fidler, *Nat. Rev. Cancer*, 2003, **3**, 1-6.

29. D. M. Feldser, J. Hackett, and C. W. Greider, *Nat. Rev. Cancer*, 2003, **3**, 1-5.

30. S. Perera, R. S. Maser, H. Xia, K. McNamara, A. Protopopov, L. Chen, A. F. Hezel, C. F. Kim, R. T. Bronson, D. H. Castrillon, L. Chin, N. Bardeesy, R. Depinho, and K. K. Wong, *Carcinogenesis*, 2008, **29**, 747-753.

31. L. G. Larsson, *Seminars in Cancer Biology*, 2011, **21**, 367-376.

32. S. K. Mencher and L. G. Wang, *BMC Clin. Pharmacol.*, 2005, **5**, 3-10.

33. T. M. Allen, *Nat. Rev. Cancer*, 2002, **2**, 750-763.

34. V. T. DeVita and E. Chu, *Cancer Res.*, 2008, **68**, 8643-8653.

35. D. Tennant, R. V. Durán, and E. Gottlieb, *Nat. Rev. Cancer*, 2010, **10**, 267-277.

36. J. Zhang, P. L. Yang, and N. S. Gray, *Nat. Rev. Cancer*, 2009, **9**, 28-39.

37. A. Gschwind, O. M. Fischer, and A. Ullrich, *Nat. Rev. Cancer*, 2004, **4**, 361-370.

38. T. T. Tan and E. White, *Adv. Exp. Med. Biol.*, 2008, **615**, 81-104.

39. M. G. Vander Heiden, *Nat. Rev. Drug Discovery*, 2011, **10**, 671-684.

40. G. L. Semenza, *Nat. Rev. Cancer*, 2003, **3**, 721-732.

41. C. V. Dang, *J. Med. Sci.*, 2009, **2**, 46-51.

42. S. Surade and T. L. Blundell, *Chem. Biol.* , 2012, **19**, 42-50.

43. R. J. Gillies, D. Verduzco, and R. Gatenby, *Nat. Rev. Cancer*, 2012, **12**, 487-493.

44. P. Csermely, V. Agoston, and S. Pongor, *Trends Pharmacol. Sci.*, 2005, **26**, 178-182.

45. A. Borisy, P. J. Elliott, N. W. Hurst, M. S. Lee, J. Lehar, E. R. Price, G. Serbedzija, G. R. Zimmermann, M. Foley, B. R. Stockwell, and C. T. Keith, *Proc. Natl. Acad. Sci. USA.*, 2003, **100**, 7977-7782.

46. M. L. Bolognesi, M. Bartolini, A. Tarozzi, F. Morroni, F. Lizzi, A. Milelli, A. Minarini, M. Rosini, P. Hrelia, V. Andrisano, and C. Melchiorre, *Bioorg. Med. Chem. Lett.*, 2011, **21**, 2655-2658.

47. E. Raymond, S. Faivre, S. Chaney, J. Woynarowski, and E. Cvitkovic, *Mol. Cancer Ther.*, 2002, 227-235.

48. B. Benedetti, E. Peterson, P. Kabolizadeh, A. Martinez, R. Kipping, and N. P. Farrell, *Mol. Pharm.*, 2012, **8**, 940-948.

49. I. Khalaila, C. S. Allardyce, C. S. Verma, and P. J. Dyson, *ChemBioChem*, 2005, **6**, 1788-1795.

50. I. Ivanov, J. Christodoulou, J. Parkinson, K. J. Barnham, A. Tucker, J. Woodrow, and P. J. Sadler, *J. Biol. Chem.*, 1998, **273**, 14721-14730.

51. A. R. Timerbaev, S. S. Aleksenko, K. Polec-Pawlak, R. Ruzik, O. Semenova, C. G. Hartinger, S. Oszwaldowski, M. Galanski, M. Jarosz, and B. K. Keppler, *Electrophoresis*, 2004, **25**, 1988-1995.

52. P. Maione, C. Gridelli, T. Troiani, and F. Ciardiello, *The Oncologist. Lung Cancer*, 2006, **1**, 274-284.

53. J. B. Fitzgerald, B. Schoeberl, U. B. Nielsen, and P. K. Sorger, *Nat. Chem. Biol.*, 2006, **2**, 458-466.

54.   T. C. Chou, *Pharmacol. Rev.*, 2007, **58**, 621-681.

55.   T. C. Chou, *Cancer Res.*, 2010, **70**, 440-446.

56.   T. C. Chou and P. Talalay, *Adv. Enzyme Regul.*, 1984, **22**, 27-55.

57.   D. C. Hiss, G. Gabriels, and P. Folb, *Cancer Cell*, 2007, **7**, 5-15.

58.   C. J. van Moorsel, H. M. Pinedo, G. Veerman, A. Guechev, K. Smid, W. J. Loves, J. B. Vermorken, P. E. Postmus, and G. J. Peters, *Biochem. Pharmacol.*, 1999, **57**, 407-415.

59.   U. Olszewski and T. T. Poulsen, *Clin. Pharmacol.*, 2010, **2**, 177-183.

60.   P. J. O'Dwyer, J. D. Moyer, M. Suffness, S. D. Harrison, R. Cysyk, T. C. Hamilton, and J. Plowman, *Cancer Res.*, 1994, 724-729.

61.   J. M. Ford and W. N. Hait, *Cytotechnology*, 1993, **12**, 171-212.

62.   R. H. Wilting and J.-H. Dannenberg, *Drug Resist. Update*, 2012, **15**, 21-38.

63.   M. Hegreness, N. Shoresh, D. Damian, D. Hartl, and R. Kishony, *Proc. Natl. Acad. Sci. USA.*, 2008, **105**, 13977-13981.

64.   C. Bock and T. Lengauer, *Nat. Rev. Cancer*, 2012, **12**, 494-501.

65.   J. H. Goldie and A. J. Coldman, *Cancer Res.*, 1984, 3643-3653.

66.   G. K. Dy and A. Adjei, *Cancer*, 2008, **113**, 1857-1887.

67.   D. Fan, S. J. Kim, R. L. Langley, and I. J. Fidler, *Drug Resistance in Cancer Cells*, Springer US, New York, NY, 2009.

68.   P. Borst, R. Evers, M. Kool, and J. Wijnholds, *J. Natl. Cancer Inst.*, 2000, **92**, 1295-1302.

69. G. Szak, K. Kin, W. To, O. Polg, R. W. Robey, and S. E. Bates, in *Drug Resistance in Cancer Cells*, 2009, pp. 1-20.

70. A. Quintás-Cardama, H. M. Kantarjian, and J. E. Cortes, *Cancer Control*, 2009, **16**, 122-131.

71. J. F. Apperley, *The Lancet Oncology*, 2007, **8**, 1018-1029.

72. M. J. Mauro, *Hematology*, 2006, 219-225.

73. T. Yap, C. P. Carden, and S. Kaye, *Nat. Rev. Cancer*, 2009, **9**, 167-81.

74. B. Lippert, Ed., *Cisplatin*, Wiley, Zurich, 1999.

75. G. B. Kauffman, R. Pentimalli, S. Doldi, and M. D. Hall, *Platinum Metals Review*, 2010, **54**, 250-256.

76. B. Rosenberg, L. Van Camp, and T. Krigas, *Nature*, 1965, **200**, 698-699.

77. B. Rosenberg, L. Van Camp, E. B. Grimley, and J. Thomson, *J. Biol. Chem.*, 1967, **242**, 1347-1352.

78. S. P. Fricker, *Dalton Trans.*, 2007, 4903-4917.

79. N. C. Institute, *August 2012*, www.cancer.gov.

80. R. P. Miller, R. K. Tadagavadi, G. Ramesh, and W. B. Reeves, *Toxins*, 2010, **2**, 2490-2518.

81. X. Yao, K. Panichpisal, N. Kurtzman, and K. Nugent, *Am. J. Med. Sci.*, 2007, **334**, 115-124.

82. D. Screnci and M. J. McKeage, *J. Inorg. Biochem.*, 1999, **77**, 105-110.

83. S. R. McWhinney, R. M. Goldberg, and H. L. McLeod, *Mol. Cancer Ther.*, 2009, **8**, 10-16.

84.   R. L. Brown, R. C. Nuss, R. Patterson, and J. Irey, *Gynecol. Oncol.*, 1983, **16**, 254-262.

85.   S. S. More, O. Akil, A. G. Ianculescu, E. G. Geier, L. R. Lustig, and K. M. Giacomini, *J. Neurosci.*, 2010, **30**, 9500-9509.

86.   A. Bhargave and U. Vaishampayan, *Expert Opin. Invest. Drugs*, 2009, **18**, 1787-1797.

87.   L. Kelland, *Nat. Rev. Cancer*, 2007, **7**, 573-584.

88.   M. Fuertes, C. Alonso, and J. M. Pérez, *Chem. Rev.* , 2003, **103**, 645-662.

89.   J. Reedijk and P. Lohman, *Pharm. Weekbl*, 1985, **7**, 173-180.

90.   J. Reedijk, *Pure Appl. Chem.*, 1987, **59**, 181-192.

91.   V. Cepeda, M. Fuertes, J. Castilla, C. Alonso, C. Quevedo, and J. M. Pérez, *Anti. Canc. Agents Med. Chem.*, 2007, **7**, 3-18.

92.   V. M. Gonzalez, M. Fuertes, C. Alonso, and J. M. Perez, *Mol. Pharmacol.*, 2001, **59**, 657-663.

93.   P. J. Sadler and Z. Guo, *Pure Appl. Chem.*, 1998, **70**, 863-871.

94.   M. D. Hall, M. Okabe, D. W. Shen, X. Liang, and M. M. Gottesman, *Annu. Rev. Pharmacol. Toxicol.*, 2008, **48**, 495-535.

95.   D. P. Gately and S. B. Howell, *Br. J. Cancer*, 1993, **67**, 1171-1176.

96.   H. Timmer-Bosscha, N. H. Mulder, and E. G. de Vries, *Br. J. Cancer*, 1992, **66**, 227-238.

97.   M. Kartalou and J. M. Essigmann, *Mutat. Res.*, 2001, **478**, 23-43.

98. D. W. Shen, L. M. Pouliot, M. D. Hall, and M. M. Gottesman, *Pharmacol. Rev.*, 2012, **64**, 5637-.

99. M. M. Gottesman, *Annu. Rev. Med*, 2002, 615-627.

100. Y. K. Yan, M. Melchart, A. Habtemariam, and P. J. Sadler, *Chem. Commun.* , 2005, 4764-4776.

101. B. Desoize, *Anti-Cancer Res.*, 2004, **24**, 1529-1544.

102. I. Ott and R. Gust, *Archiv der Pharmazie*, 2007, **340**, 117-126.

103. E. S. Antonarakis and A. Emadi, *Cancer Chemoth. Pharm.*, 2010, **66**, 1-9.

104. I. Bratsos, S. Jedner, T. Gianferrara, and E. Alessio, *Chimia*, 2007, **61**, 692-697.

105. R. E. Morris, R. E. Aird, P. D. S. Murdoch, H. Chen, J. Cummings, N. D. Hughes, S. Parsons, A. Parkin, G. Boyd, D. I. Jodrell, and P. J. Sadler, *J. Med. Chem.*, 2001, **44**, 3616-3621.

106. C. Scolaro, A. Bergamo, L. Brescacin, R. Delfino, M. Cocchietto, G. Laurenczy, T. J. Geldbach, G. Sava, and P. J. Dyson, *J. Med. Chem.*, 2005, **48**, 4161-4171.

107. S. Schäfer, I. Ott, R. Gust, and W. S. Sheldrick, *Eur. J. Inorg. Chem.*, 2007, 3034-3046.

108. F. Wang, A. Habtemariam, E. van der Geer, R. Fernández, M. Melchart, R. J. Deeth, R. Aird, S. Guichard, F. P. Fabbiani, P. Lozano-Casal, I. D. H. Oswald, D. I. Jodrell, S. Parsons, and P. J. Sadler, *Proc. Natl. Acad. Sci. USA.*, 2005, **102**, 18269-18274.

109. A. Habtemariam, M. Melchart, R. Fernandez, S. Parsons, I. D. H. Oswald, A. Parkin, F. P. Fabbiani, J. E. Davidson, A. Dawson, R. E. Aird, D. I. Jodrell, and P. J. Sadler, *J. Med. Chem.*, 2006, **49**, 6858-6868.

110. A. F. A. Peacock, A. Habtemariam, R. Fernández, V. Walland, F. Fabbiani, S. Parsons, R. E. Aird, D. I. Jodrell, and P. J. Sadler, *J. Am. Chem. Soc.*, 2006, **128**, 1739-1748.

111. P. C. Bruijnincx and P. J. Sadler, *Adv. Inorg. Chem.*, 2011, **8838**, 1-59.

112. G. Süss-Fink, *Dalton Trans.*, 2010, **39**, 1673-1688.

113. A. Casini, C. G. Hartinger, A. A. Nazarov, and P. J. Dyson, *Top Organomet Chem*, 2010, **32**, 57-80.

114. B. T. Loughrey, M. L. Williams, P. C. Healy, A. Innocenti, D. Vullo, C. T. Supuran, P. G. Parsons, and S. A. Poulsen, *J. Biol.Inorg. Chem.*, 2009, **14**, 935-945.

115. F. Gao, H. Chao, J. Q. Wang, Y. X. Yuan, B. Sun, Y. F. Wei, B. Peng, and L. N. Ji, *J. Inorg. Chem.*, 2007, **12**, 1015-1027.

116. K. J. Du, J. Q. Wang, J. F. Kou, G. Y. Li, L. L. Wang, H. Chao, and L. N. Ji, *Eur. J. Med. Chem.*, 2011, **46**, 1056-1065.

117. Y. N. Vashisht Gopal and A. K. Kondapi, *J. Biosci.*, 2001, **26**, 271-276.

118. M. Melchart, A. Habtemariam, S. Parsons, and P. J. Sadler, *J. Inorg. Biochem.*, 2007, **101**, 1903-1912.

119. S. J. Dougan, M. Melchart, A. Habtemariam, S. Parsons, and P. J. Sadler, *Inorg. Chem.*, 2006, **45**, 10882-10894.

120. H. Kostrhunova, J. Florian, O. Novakova, A. Peacock, P. J. Sadler, and V. Brabec, *J. Med. Chem.*, 2008, **51**, 3635-3643.

121. T. Bugarcic, O. Nováková, A. Halámiková, L. Zerzánková, O. Vrána, J. Kaspárková, A. Habtemariam, S. Parsons, P. J. Sadler, and V. Brabec, *J. Med. Chem.*, 2008, **51**, 5310-5319.

122. O. Novakova, J. Kasparkova, V. Bursova, C. Hofr, M. Vojtiskova, H. Chen, P. J. Sadler, and V. Brabec, *Chem. Biol.* , 2005, **12**, 121-129.

123. M. J. Clarke, *Coord. Chem. Rev.*, 2002, **232**, 69-93.

124. A. M. Pizarro, A. Habtemariam, and P. J. Sadler, *Top Organomet Chem*, 2010, **32**, 21-56.

125. R. E. Aird, J. Cummings, A. A. Ritchie, M. Muir, R. E. Morris, H. Chen, P. J. Sadler, and D. I. Jodrell, *Br. J. Cancer*, 2002, **86**, 1652 - 1657.

126. R. L. Hayward, Q. C. Schornagel, R. Tente, J. S. Macpherson, R. E. Aird, S. Guichard, A. Habtemariam, P. J. Sadler, and D. I. Jodrell, *Cancer Chemoth. Pharm.*, 2005, **55**, 577-583.

127. C. Streu, L. Feng, P. J. Carroll, J. Maksimoska, R. Marmorstein, and E. Meggers, *Inorg. Chim. Acta*, 2011, **377**, 34-41.

128. J. Maksimoska, L. Feng, K. Harms, C. Yi, J. Kissil, R. Marmorstein, and E. Meggers, *J. Am. Chem. Soc.*, 2008, **130**, 15764-15765.

129. E. Corral, A. C. G. Hotze, H. den Dulk, A. Leczkowska, A. Rodger, M. J. Hannon, and J. Reedijk, *J. Biol.Inorg. Chem.*, 2009, **14**, 439-448.

130. X. Chen, F. Gao, W. Y. Yang, J. Sun, Z. X. Zhou, and L. N. Ji, *Inorg. Chim. Acta*, 2011, **378**, 140-147.

131. S. Ali Ezadyar, A. S. Kumbhar, A. Kumbhar, and A. Khan, *Polyhedron*, 2012, **36**, 45-55.

132. T. Chen, Y. Liu, W. J. Zheng, J. Liu, and Y. S. Wong, *Inorg. Chem.*, 2010, **49**, 6366-6368.

133. C. Gaiddon, P. Jeannequin, P. Bischoff, M. Pfeffer, C. Sirlin, and J. P. Loeffler, *Pharmacology*, 2005, **315**, 1403-1411.

134. X. Yang, L. Chen, Y. Liu, Y. Yang, T. Chen, W. Zheng, J. Liu, and Q. Y. He, *Biochimie*, 2011, **94**, 345-353.

135. C. Tan, S. Wu, S. Lai, M. Wang, Y. Chen, L. Zhou, Y. Zhu, W. Lian, W. Peng, L. Ji, and A. Xu, *Dalton Trans.*, 2011, **40**, 8611-8621.

136. S. H. van Rijt and P. J. Sadler, *Drug Discov. Today*, 2009, **14**, 1089-1097.

137. A. Peacock and P. J. Sadler, *Chem-Asian J.*, 2008, **3**, 1890-1899.

138. S. H. van Rijt, H. Kostrhunova, V. Brabec, and P. J. Sadler, *Bioconjugate Chem.*, 2011, **22**, 218-226.

139. Y. Fu, A. Habtemariam, A. M. Pizarro, S. H. van Rijt, D. J. Healey, P. Cooper, S. D. Shnyder, G. J. Clarkson, and P. J. Sadler, *J. Med. Chem.*, 2010, **53**, 8192-8196.

140. A. Dorcier, W. H. Ang, S. Bolaño, L. Gonsalvi, L. Juillerat-Jeannerat, G. Laurenczy, M. Peruzzini, A. D. Phillips, F. Zanobini, and P. J. Dyson, *Organometallics*, 2006, **25**, 4090-4096.

141. Z. Liu, A. Habtemariam, A. M. Pizarro, S. Fletcher, A. Kisova, O. Vrana, L. Salassa, P. C. Bruijnincx, G. J. Clarkson, V. Brabec, and P. J. Sadler, *J. Med. Chem.*, 2011, **54**, 3011-3026.

142. P. Collery, B. Keppler, C. Madoulet, and B. Desoize, *Crit. Rev. Oncol. Hemat.*, 2002, **42**, 283-296.

143. A. V. Rudnev, L. S. Foteeva, C. Kowol, R. Berger, M. Jakupec, V. B. Arion, A. R. Timerbaev, and B. K. Keppler, *J. Inorg. Biochem.*, 2006, **100**, 1819-1826.

144. A. R. Timerbaev, *Metallomics*, 2009, **1**, 193-198.

145. R. Baerga, J. Cobb, A. Ogden, and H. Sheshbaradaran, in *AACR 103rd Annual Meeting 2012 - Targeting Metabolism and Gene Expression*, American Association for Cancer Research, Chicago, IL, 2012.

Chapter 2

Experimental methods

This Chapter describes the general experimental techniques and instrumentation used in this Thesis. Particular methods for individual experiments are described in the appropriate chapters.

2.1 Materials

$RuCl_3.xH_2O$ was purchased from Precious Metals Online (PMO pty Ltd). All solvents (acetone, methanol and ether) were obtained from commercial sources such as Fisher Scientific and Sigma-Aldrich and were used without further purification; ethanol was obtained from the same suppliers but dried over Mg/I_2 before use. Alpha-phellandrene and cyclopentadiene were purchased also from Sigma Aldrich, the latter was obtained in its dimeric form and was freshly distilled before use. Octanol ($\geq$ 99%) for Log P determinations was purchased from the same provider. Deuterated solvents ($CDCl_3$, MeOD, D_2O, DMSO-d_6) were purchased from Cambridge Isotopes Limited. ICP-MS standards (Ru, Pt, Os) were obtained from Inorganic Ventures.

For the biological experiments, RPMI-1640, DMEM and McCoy 5A media, as well as foetal bovine serum, L-glutamine, penicillin/streptomycin mixture, trypsin, trypsin/EDTA, phosphate buffered saline (PBS) were purchased from PAA Laboratories GmbH. Cisplatin **CDDP** ($\geq$ 99.9%), oxaliplatin **OXA** ($\geq$ 98.9%), trichloroacetic acid ($\geq$ 99%), 9-EtG, sulforhodamine B (75%), sodium phosphate monobasic monohydrate ($\geq$ 99%), sodium phosphate dibasic

heptahydrate ($\geq$ 99%), acetic acid ($\geq$ 99%) formaldehyde (36.5–38% in H_2O) triton X-100 and Tris(hydroxymethyl) aminomethane (TRIS, $\geq$ 99%) were obtained from Sigma Aldrich.

2.1.1 Synthesis of the starting materials

Synthesis of the ruthenium *p*-cymene dimer, [(Ru(η^6-*p*-cymene)Cl$_2$)$_2$].[1,2]
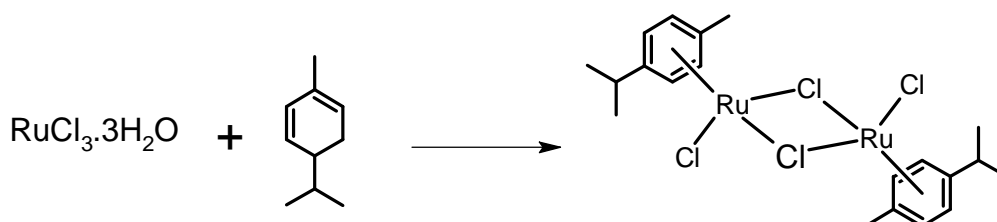
Scheme 2.1. Synthesis of the ruthenium *p*-cymene dimer [(Ru(η^6-*p*-cymene)Cl$_2$)$_2$].

$RuCl_3.3H_2O$ (150 mg, 0.66 mmol) was dissolved in freshly distilled ethanol (5 mL), the solution was placed in a round-bottom flask, then *alpha*-phellandrene (105 µL, 0.66 mmol) was added with constant stirring. The reaction mixture was heated under reflux for 18 h. The solvent was removed by rotary evaporation and the solid precipitate was washed with ethanol and ether, (98 mg, 48.0%). Elemental analysis calc. for $C_{20}H_{28}Cl_4Ru_2$, C: 39.23%, H: 4.58%. Found: C: 39.31%, H: 4.56%. NMR-δ_H (500 MHz; MeOD) 1.29 (6H, d, J =

7.10 Hz), 2.15 (3H, s), 2.98 (1H, m), 5.34 (2H, d, J = 5.80 Hz), 5.46 (2H, d, J = 5.80 Hz). m/z (ESI) found 576.9 (M^+ $C_{20}H_{28}Cl_3Ru_2$ = 576.93).

2.2 Instrumentation

2.2.1 Nuclear Magnetic Resonance Spectroscopy (NMR)[3,4]

In this thesis, NMR data (^1H, ^{13}C and 2D experiments) were acquired using 5 mm NMR tubes in the NMR Spectroscopy Facility of Warwick University on either a 500-MHz spectrometer Bruker DRX-500 or a 600-MHz Bruker AVA spectrometer, experiments were carried out at 298 K unless otherwise stated. ^1H-NMR chemical shifts were internally referenced to MeOD (3.49 ppm), DMSO-d_6 (2.50 ppm) 1,4-dioxane (3.71 ppm, for samples in D_2O) or $CHCl_3$ (7.26 ppm). Typically, 20 ppm were used as spectral width for ^1H-NMR and 200 ppm for ^{13}C-NMR experiments. Spectra were processed using Bruker Topspin 2.1.

2.2.2 Elemental Analysis

Elemental analysis (percentages of C, H and N) was carried out on a CE-440 Exeter Elemental Analyzer by the Warwick Analytical Service.

2.2.3 Absorption Spectroscopy (UV/Vis)

Electronic absorption spectroscopy spectra were recorded on a Varian Cary 300 or Cary 300Bio UV-Vis spectrometers using 1-cm path-length cuvettes (600 µL) and processed with Origin Lab 8.1 (Origin, USA). Experiments were carried out at 298 K unless otherwise stated; both spectrometers were fitted with PTP1 Peltier temperature controllers.

2.2.4 Electrospray Ionisation Mass Spectrometry (ESI-MS)[5]

Data were recorded in the Mass Spectrometry Facility of Warwick University using methanolic solutions (50% MeOH, 50% H_2O) on a Bruker Esquire 2000 instrument with electrospray as the ionization method. Usually experiments were based on scanning a range of up to 1000 m/z for positive ions, the cone voltage and source temperature varied depending on the sample.

2.2.5 Inductively Coupled Plasma Mass Spectrometry (ICP-MS)[6]

Inductively coupled plasma mass spectrometry was used to determine the metal content of cellular samples. Experiments were carried out using an ICP-MS

Agilent technologies 7500 series from the Mass Spectrometry Facility of Warwick University. The solvent used for all ICP-MS experiments was double deionised water (DDW) with 5% HNO_3. All metal standards (Ru, Os and Pt) were freshly prepared in double deionised water with 5% HNO_3 before each experiment. The concentrations used for the calibration curve were in all cases (0, 5, 10, 50, 200, 500, 1 x 10^3, 5 x 10^3, 10 x 10^3, 50 x 10^3, 200 x 10^3 ppt). The isotopes detected were ^{101}Ru, ^{195}Pt and ^{189}Os, and readings were made in duplicate (He gas and no gas mode).

2.2.6 Flow Cytometry [7–9]

All flow cytometry experiments were carried out using a Becton Dickinson FACScan Flow Cytometer in the School of Life Sciences at Warwick University. Typically, A2780 cells were seeded in Pietri dishes using 4 x 10^6 cells per plate. Experiments included 24 h of pre-incubation in drug-free media at 310 K in CO_2 humidified atmosphere (5%), followed by 24 h of drug exposure under the same conditions. After this, sample preparation and staining depended on the aim of the experiment being carried out; more detailed procedures can be found in the appropriate chapters.

2.3 Methods

2.3.1 Aquation studies

A 2 mM solution of each complex was prepared in D_2O water using 5% DMSO/MeOD, ^{1}H-NMR spectra were recorded at 298 K within the first 10 min after mixing and then again under the same conditions after 24 h. Results shown were obtained from a 500 MHz spectrometer. All experiments were carried out in triplicate and the standard deviations calculated. Aquation of the complexes was followed by the observation of a second set of signals after 24 h, in order to confirm that the process observed was indeed aquation, the reaction was inhibited by the addition of NaCl or KI, according to the details in the following section. The results presented reflect the extent of aquation after a given period of time (24 h); however no attempt was made to determine the kinetics of the reactions. In order to verify that after 24 h the reactions had reached equilibrium, a further spectrum of each sample was run after 48 h. No further changes were detected.

2.3.1.1 Suppression of aquation

A fresh 2 mM solution of each complex was prepared in a 200 mM solution of NaCl / KI in deuterated water (NaCl for chlorido complexes and KI for the iodido complexes) with 5% DMSO/MeOD. In order to prepare this solution,

the solid complex was dissolved first in DMSO/MeOD to be then diluted in deuterated water, already containing NaCl/KI. ^{1}H-NMR spectra were recorded at 298 K within the first 10 min of sample preparation and then again after 24 h. All experiments were carried out in triplicate and the standard deviations calculated. The suppression of aquation was monitored, signals generated by the complex remained unchanged after the 24 h period.

2.3.2 Determination of partition coefficient (Log P)

A 2 mM solution of each complex was prepared in octanol-saturated water (5 mL) and shaken overnight on a IKA Vibrax VXC basic shaker (500 g/min) with an equal volume of water-saturated octanol. Layers were separated and metal concentration in the aqueous layer was determined via ICP-MS after dilution with double distilled water to achieve concentrations within the ICP-MS standards range mentioned before (5–200 x 10^3 ppt). For these experiments the doubly-distilled water contained 200 mM of NaCl to avoid the aquation of the complexes. Partition coefficients were calculated using the formula log P = log ($[Ru]_{oct}/[Ru]_{aq}$).[10] Octanol-saturated water and water-saturated octanol were prepared before hand by stirring mixtures of octanol and water overnight. The value corresponding to the concentration of metal in the octanol layer was determined as the difference between the aqueous layer before mixing and the corresponding concentration after 24 h. Log P determinations were carried out

as duplicates of triplicates in independent experiments and the standard deviations were calculated.

2.3.3 Nucleobase binding

A fresh 2 mM solution of each complex was prepared in 50 mM sodium phosphate buffer (pH 7.5) with 5% DMSO. In order to prepare this solution, the solid complex was dissolved first in DMSO and then diluted with the corresponding buffer. The solution also contained 9-ethylguanine for a final mol. ratio 1:1.25 where the nucleobase was in excess. As in the case of aquation studies, ^{1}H-NMR spectra were recorded at 298 K within the first 10 min after sample preparation and again after 24 h at 500 MHz. All experiments were carried out in triplicate and the standard deviations calculated. Nucleobase binding was monitored by the formation of a second set of peaks that included bound-9-EtG.[11,12] The spectrum of free 9-EtG under the same conditions was recorded for comparison purposes.

2.3.4 pH* measurements

pH* measurements were carried out at ambient temperature in a Corning 240 pH meter equipped with a microcombination electrode (KNO_3, chloride free)

calibrated with Aldrich buffer solutions at pH 4, 7 and 10. pH meter readings without correction for effects of deuterium on the glass electrode.

2.3.5 Cancer cell studies

2.3.5.1 Cell maintenance [13,14]

Cell lines used in this work, A2780 human ovarian carcinoma, A549 human caucasian lung carcinoma, HCT116 human colon carcinoma, MCF7 human caucasian breast carcinoma and MRC5 human foetal lung fibroblasts were obtained from the European Collection of Cell Cultures (ECACC). Modified cell lines HCT116Ox and HCT116p53-/- were kindly provided by R. Sharma from Oxford University and J. Cherry from Johns Hopkins International Medical Center respectively. A2780 ovarian and MRC5 were grown in Roswell Park Memorial Institute medium (RPMI-1640), A549 and MCF7 were grown in Dulbecco's Modified Eagle medium (DMEM) and HCT116 and its derived cell lines in McCoy′s Modified 5A medium. All media were supplemented with 10% of foetal calf serum, 1% of 2 mM glutamine and 1% penicillin/streptomycin.

All cells were grown in 75 cm^2 culture flasks as adherent monolayers, and they were split two to three times a week when around 80-90% confluence was reached, using 0.25% trypsin for A2780 or 0.25% trypsin/EDTA for all other

cell lines. Between passages cells are kept in an incubator at 310 K with 5% CO_2 humidified atmosphere.

2.3.5.2 Antiproliferative activity

Antiproliferative activity was determined by the sulforhodamine B (SRB) colorimetric assay.[15,16] This assay was first developed by Skeham in 1990[17] and it is based on the ability of the sulforhodamine B (Figure 2.1) to bind electrostatically to basic amino acid residues of proteins from fixed cells. The process is pH-dependent, the binding occurs under mild acidic conditions, but under mild basic conditions it is possible to release quantitatively the dye. Absorbance measurements of solubilised dye are linear with the amount of cellular protein present, allowing for the determination of the amount of viable treated cells against an untreated control.
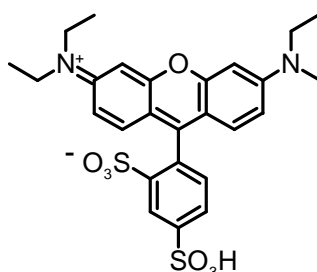
Figure 2.1. Structure of sulforhodamine B.

Typically, antiproliferative activity experiments involved the following:

- Cell preparation: human carcinoma cells and fibroblasts were grown as indicated above until approximately 80-90% confluence was achieved. The medium was removed and cells were washed twice with phosphate-buffered saline (PBS. This step allowed the removal of dead cells in the supernatant. Then the PBS was removed and 2 mM trypsin or trypsin/EDTA (2 mL) was added. The culture flask was left to stand for 3 min in the incubator. The trypsin or trypsin/EDTA was diluted using the corresponding medium and the solution was mixed to obtain a single cell suspension. A hemocytometer was used to determine the concentration of cells in the suspension.

- Plate seeding: the single cell suspension obtained in the previous step was diluted with medium in order to seed a 96-well plate with approximately 5000 cells per well using 180 μL per well. The plate was left in the incubator for two days.

- Sample preparation: a 2 mM solution of each compound to be tested was prepared using a 5% DMSO, 95% (saline: PBS) mixture. This stock was then used to prepare six different solutions by dilution with PBS. The concentration range of these solutions varied according to the screening results for each particular sample, and were adjusted to achieve three values above the expected IC_{50} and three values below.

- Positive control preparation: a 2 mM solution of cisplatin was prepared using a 5% DMSO, 95% saline. This stock was then used to prepare 2000, 1000, 500, 200, 50, and 1 μM solutions by dilution in PBS.

- Negative control preparation: this was obtained by 5 % of DMSO, 95% (saline: PBS) mixture.

- Drug addition: 20 μL of samples, cisplatin, positive and negative control solutions were added to the 96-well plate in triplicate. The plate was left in the incubator for 24 h.

- Drug removal: supernatant solutions were removed from each well by means of suction. Each well was then washed using 100 μL of PBS, finaly 200 μL of fresh medium were added to each well. The plate was left to stand for 72 h in the incubator, while the cells were allowed to recover.

- Sulforhodamine B (SRB) colorimetric assay: 50 μL of cold 10% trifluoroacetic acid (TCA), 277 K, were added to each well of the plate. This was left to incubate for 1 h at 277 K. The TCA was removed and the plate was washed with slow-running tap water 10 times. Excess moisture was removed and the plate was allowed to air-dry. This step fixed the cells to the surface of the wells.

  Aliquots of 50 μL of 0.4% SRB dye (prepared in 1% acetic acid) were added to each well. The plate was allowed to stand for 30 min at room temperature. This step stained the biomass present in each well. Excess

dye was removed by washing the plate 5 times with 1% acetic acid. Excess moisture was removed and the plate was allowed to air-dry. Aliquots of 10 mM Tris base solution (200 μL, pH 10.5) were added to each well and the plate was left to stand at ambient temperature for 1 h. This step solubilised the bound dye. The plate was measured in a multi reader at 570 nm. Those wells with absorbances over 3.00 units were diluted 1:6 and the absorbance was re-read. These dilutions were done by removing 150 μL of each of the wells and adding 250 μL of 10 mM Tris base solution.

- Cell viability determination: for each compound screened, survival percentages were obtained by dividing the absorbance data by the average of the negative-control readings and multiplying by one hundred. Then the data were plotted as the survival percentage versus the logarithm of the concentration used expressed in mili molar units. A sigmoidal curve was fitted using OriginPro 8.1 software, and the IC_{50} value was determined, as the half-maximal inhibitory concentration. By a way of validation for each plate, the IC_{50} of cisplatin was determined.

- Figure 2.2 below shows an example of the dose-response curve obtained for cisplatin.
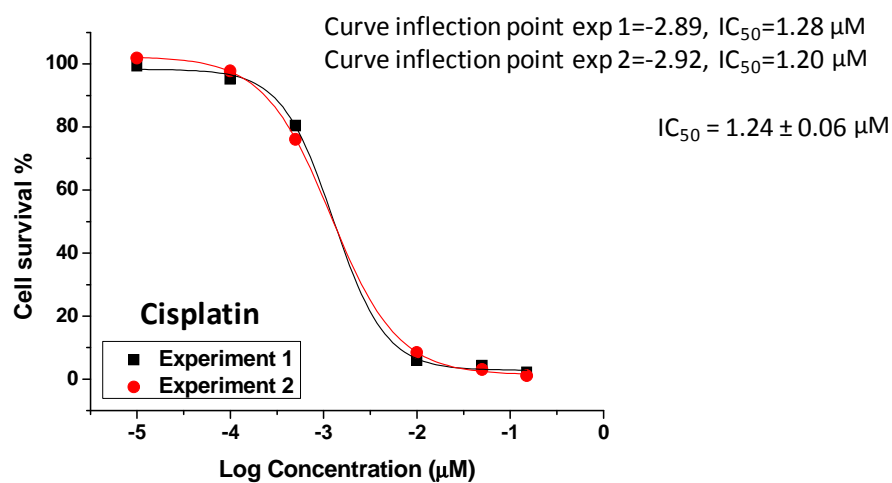
Figure 2.2. Dose-response curve for cisplatin.

2.3.5.3 Metal accumulation in cancer cells

- Cell preparation: A2780 human ovarian carcinoma cells were grown in a 75 cm^2 cell culture flask as indicated in above, until Ca. 80% confluence was achieved. The medium was removed and cells were washed twice with PBS: this step allowed the removal of supernatant dead cells, then the PBS was removed and 2 mL of 2 mM trypsin or trypsin/EDTA was added. The culture flask was left to stand for 3 min in the incubator. The trypsin was diluted using medium and the solution was mixed to obtain a single cell suspension. A hemocytometer was used to determine the concentration of cells in the suspension.

- Cell seeding: on day one of the experiment, 4×10^6 cells were seeded in a 68 mm Petri dish using 9 mL of medium. These cells were incubated at 319 K and 5% CO_2 levels for 24 h.

- Sample preparation: 2 mM solution of each compound to be tested for cellular uptake was prepared using a 5% DMSO, 95% (saline: PBS) mixture. This stock was then used to prepare diluted solutions in PBS.

- Negative control preparation: this was obtained by using 5% DMSO, 95% (saline: PBS) mixture.

- Drug addition: on day-two of the experiment, 1 mL of each compound to be tested was added to three pre-incubated Pietri dishes, this resulted in a final concentration of the ruthenium(II) complex which is a fifth of its IC_{50} value. On the same day three negative control plates were prepared accordingly. Cells were exposed to the drugs for 24 h.

- Drug removal: on day-three of the experiment, supernatants of the Pietri dishes were removed by suction. Cells were washed with PBS and treated with trypsin or trypsin/EDTA to obtain a single cell suspension as described before in the cell preparation section. Cell concentration was determined using a hemocytometer, before centrifuging the samples to obtain whole-cell pellets.

- Sample digestion: cell pellets were transferred into wheaton v-vials and digested using 225 µL of freshly distilled concentrated 72% v/v nitric acid. For full digestion, the vials were heated to 353 K overnight.

- Metal content determination: digested samples were diluted using double-distilled deionized water to obtain a final nitric acid concentration of Ca. 5% v/v and they were analysed for metal content using ICP-MS.

- The statistical significance of all cellular accumulation values was determined using a two-sided t-test with P<0.05.

2.4 References

1.   M. Bennett and A. K. Smith, *Dalton Trans.*, 1974, 233-241.

2.   E. S. Sk, R. A. Zelonka, and M. C. Baird, *J. Organomet. Chem.*, 1972, **35**, 43-46.

3.   P. Hore, *Nuclear magnetic resonance*, Oxford University Press, New York, 2001.

4.   T. Claridge, *High-resolution NMR techniques in organic chemistry series*, Pergamon, 1990.

5.   W. Henderson and J. McIndoe, *Mass spectrometry of inorganic, coordination, and organometallic compounds*, Wiley, Hoboken, NJ, 2005.

6.   R. Rhomas, *Practical guide to ICP-MS : a tutorial for beginners*, CRC Press, Boca Raton, Second Edi., 2008.

7.   M. G. Ormerod, Ed., *Flow cytometry : a practical approach*, Oxford University Press, Oxford, 1990.

8.   Z. Darzynkiewicz and H. Crissman, Eds., *Methods in cell biology. Vol.33, Flow cytometry*, London : Academic Press, 1990.

9.   H. Shapiro, *Practical flow cytometry*, Wiley, Hoboken, NJ, Fourth Edi., 2003.

10. A. Leo, C. Hansch, D. Elkins, A. H. Law, and B. N. Behavior, *Chem. Rev.* , 1971, **71**, 525-616.

11. M. Melchart, A. Habtemariam, S. Parsons, and P. J. Sadler, *J. Inorg. Biochem.*, 2007, **101**, 1903-1912.

12. A. Peacock, M. Melchart, R. J. Deeth, A. Habtemariam, S. Parsons, and P. J. Sadler, *Chemistry*, 2007, **13**, 2601-2613.

13. K. Maramorosch and H. Hirumi, Eds., *Practical tissue culture applications*, New York Academic Press, 1979.

14. J. Davis, Ed., *Basic cell culture : a practical approach*, Oxford University Press, Oxford, UK, 2002.

15. V. Vichai and K. Kirtikara, *Nat. Protoc.*, 2006, **1**, 1112-1116.

16. K. T. Papazisis, G. D. Geromichalos, K. Dimitriadis, and H. Kortsaris, *J. Immunol. Methods*, 1997, **208**, 151-158.

17. P. Skehan, R. Storeng, D. Scudiero, A. Monks, J. McMahon, D. Vistica, J. T. Warren, H. Bokesch, S. Kenney, and M. R. Boyd, *J. Natl. Cancer Inst.*, 1990, **82**, 1107-1112.

CHAPTER 3

Ruthenium iminopyridine arene complexes:

cellular uptake mechanisms.

3.1 Introduction

Ruthenium arene complexes have been widely studied in recent times as a viable alternative to platinum chemotherapeutics,[1–9] especially because acquired resistance to platinum-based drugs represents a major clinical drawback for compounds such as cisplatin (**CDDP**)[10,11] or oxaliplatin (**OXA**).[12,13] This type of resistance usually develops as a consequence of impaired cellular accumulation that can be caused by lower cellular uptake or increased cellular efflux. [10,14,15]

Several attempts have been made to understand platinum uptake and its accumulation.[16–18] However, there is a lack of knowledge on equivalent mechanisms involved in the accumulation of ruthenium anti-cancer drugs. Understanding of these pathways could allow rational design and further improvement of such complexes. In this Chapter cellular uptake and metal accumulation mechanisms for prospective ruthenium anticancer complexes have been investigated regarding their time-, concentration- and temperature-dependence as well as the extent of metal efflux. Further cellular accumulation pathways have been investigated, including the following.

- **Inhibition of P-gp mediated efflux by the use of verapamil:** this ATP-binding protein of the ABC super family[19] mediates the efflux of xenobiotics and endogenous compounds. Its substrates include antibiotics, steroid hormones and anticancer agents among others. P-gp is responsible for the development of multidrug resistance, [20] therefore, its interaction with diverse substrates has been widely studied.[21–23] P-gp-mediated efflux can be

inhibited by the use of verapamil,[23] which allows to investigate the role this efflux pathway has in the detoxification of chemotherapeutics.[24]

- **Role of Na^+/K^+ pump in cellular metal accumulation, as a facilitated diffusion endocytotic pathway by ouabain inhibition**: Na^+/K^+ pump is a P-type ATPase which pumps three Na^+ out of the cells while transporting two K^+ into it for each hydrolysed unit of ATP.[25] This allows the cell to keep low intracellular Na^+ concentrations,[26] a mechanism which has often been studied in relation to **CDDP** uptake. Ouabain is a cardiac glycoside with high bioavailability that inhibits the activity of the Na^+/K^+ -ATPase as it interacts with the extracellular surface of the pump, more specifically, it binds to the α subunit.[27] Co-incubation of chemotherapeutics with ouabain reflects on the role of the pump in drug cellular uptake.

- **Role of CTR1 in cellular accumulation:** CTR1 which is a high affinity copper uptake protein,[28] encoded in humans by the *SLC31A1* gene, is responsible to a great extent for **CDDP** uptake.[16,29–34] Also copper exporters ATP7A and ATP7B are involved in the efflux of **CDDP**.[35,36] Transporter protein, CTR1, can be down-regulated by high levels of intracellular copper.[37] Cells with a knocked out gene *h*CTR1 are resistant to **CDDP** in vitro.[38] CTR1 is normally expressed in **CDDP** resistant cell lines, but the transporter is not functional because of a lack of activation by glycosylation.[39] The details of this mechanism are not yet very clear, however it is known that the process is energy independent and highly influenced by pH.[40] In this study we investigate whether CTR1 is also involved in the uptake of ruthenium drugs.

- **Membrane disruption by amphotericin B as a model for protein mediated transport:** amphotericin B is an antifungal agent that has been used to potentiate the antiproliferative activity of chemotherapeutic drugs *in vivo* and *in vitro*, at non-toxic concentrations of up to 15 μM.[41] The mechanism of action of amphotericin B involves depletion of intracellular potassium and therefore modification of membrane permeability. It is assumed that amphotericin B binds to sterol molecules and forms pores in the membrane of up to 8 Å in diameter which improve cellular uptake of exogenous molecules. This antifungal agent has been used in the present Chapter to find out wether the uptake of ruthenium(II) from half-sandwich arene complexes can be improved by increased facilitated transport.

- **The role of caveolae endocytotic pathway in metal accumulation:** caveolaes are cholesterol-rich microdomains in the cell membrane[42] and β-methyl cyclodextrin is known to inhibit caveolae-related uptake by binding to cholesterol.[31,42,43] Therefore co-incubation with β-methyl cyclodextrin could be used to investigate whether this pathway is involved in the cellular uptake of a particular drug, in this case, the uptake of ruthenium half-sandwich complexes.

In this Chapter the synthesis and characterisation of novel ruthenium arene complexes containing imine ligands are described. It also reports on their aquation and extent of binding to 9-EtG as a model for nucleobase interaction. The antiproliferative activity of all ligands and complexes has been investigated using A2780 ovarian, A549 lung, HCT116 colon and MCF7 breast cancer cell lines,

these activities were related to their cellular accumulation and hydrophobicity. Finally, complex **15** [Ru(η^6-*p*-cym)(*p*-Impy-NMe$_2$)Cl]PF$_6$ and its iodido analogue **16** [Ru(η^6-*p*-cym)(*p*-Impy-NMe$_2$)I]PF$_6$ were used to investigate some of the pathways involved in cellular uptake and accumulation of ruthenium in comparison to platinum uptake and accumulation from **CDDP**. These two compounds were selected because of their structural similarities (only differ in their monodentate ligand Cl vs I) and with the aim to study the effect of the monodentate ligand on the cellular uptake behaviour.

Figure 3.1 summarises the Overview of the cellular accumulation pathways investigated in Chapter 3.
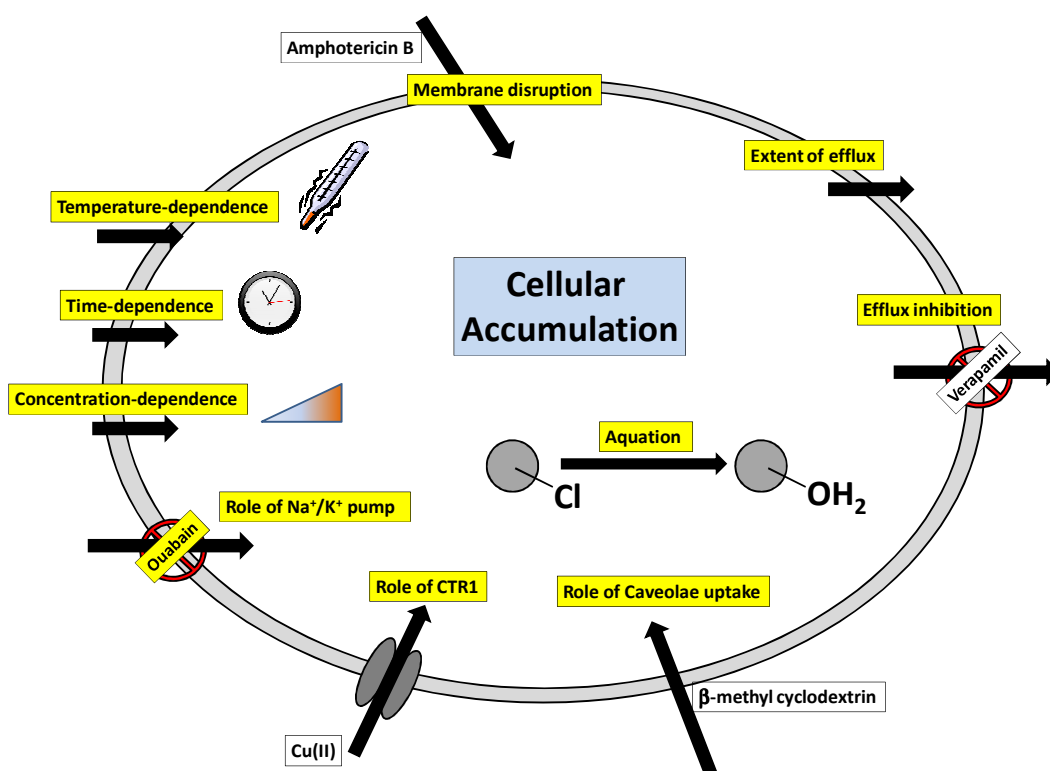
Figure 3.1. Overview of the cellular accumulation pathways investigated in Chapter 3.

3.2 Experimental section

3.2.1 Materials

Ruthenium half-sandwich arene dimers used in this Chapter include [(η^6-*p*-cymene)RuCl$_2$]$_2$, reported in Chapter 2, [(η^6-*p*-cymene)RuI$_2$]$_2$, [(η^6-*m*-terp)RuCl$_2$]$_2$, and [(η^6-bip)RuCl$_2$]$_2$, kindly provided by Dr. Abraha Habtemariam. 2-Pyridine carboxaldehyde (99%), 2-aminophenol (99%), 4-aminophenol (98%) were purchased from Sigma-Aldrich. 4-Aminobenzoic acid (≥99.0%) and ammonium hexafluorophosphate (≥98.0%) were obtained from Fluka. *N,N*-Dimethyl-4-[(*E*)-(pyridin-2-ylmethylidene) amino]aniline, (*p*-Impy-NMe$_2$, **6**) was kindly provided by Dr. Ying Fu. All deuterated solvents (D$_2$O, MeOD, DMSO-*d$_6$*, acetone-*d$_6$*, CDCl$_3$) were obtained from Cambridge Isotope Laboratories. For the biological assays, verapamil hydrochloride (≥99.0%), ouabain octahydrate (≥95%), antimycin A from *Streptomyces* sp., amphotericin B also from *Streptomyces* sp., methyl β-cyclodextrin and copper(II) chloride dihydrate (≥99.0%) were all purchased form Sigma Aldrich.

3.2.2 Preparation of ligands and complexes

The synthetic procedure 1, described below was used to generate all the imines used as ligands in this Chapter and listed in Figure 3. 2.

Impy, **1**   *o*-Impy-OH, **2**   *p*-Impy-OH, **3**

p-Impy-COOH, **4**   *p*-Impy-(CH$_2$)$_3$COOH, **5**
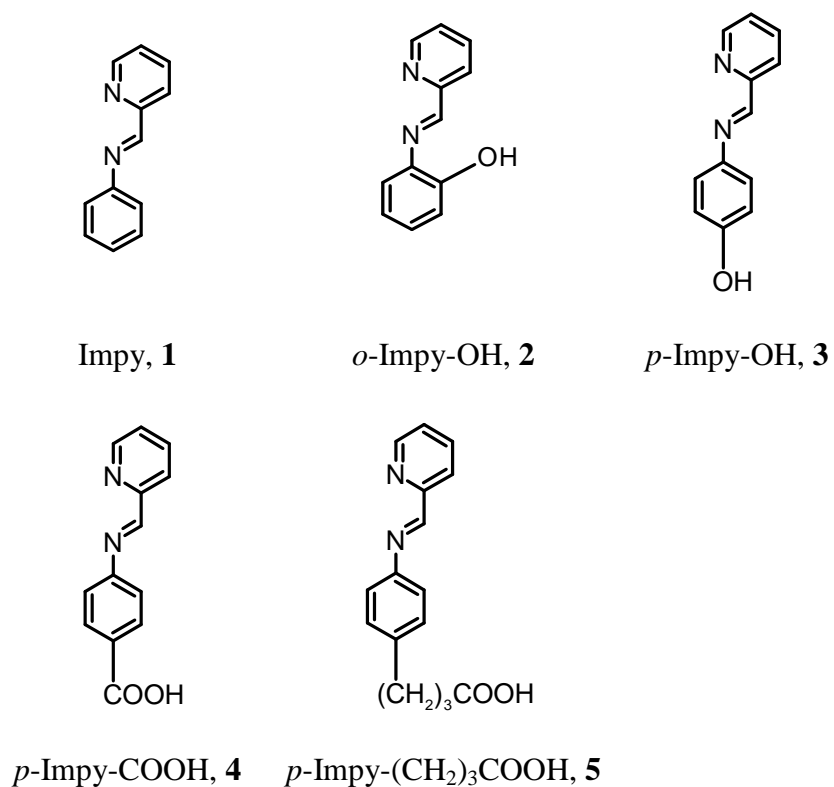
Figure 3. 2. Imines synthesised in Chapter 3.

Synthetic Procedure 1.
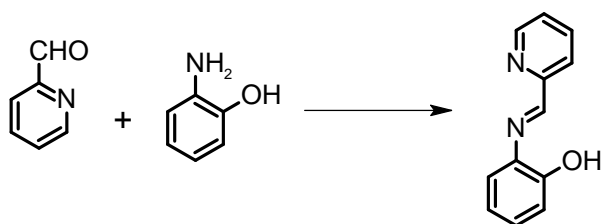
Scheme 3.1. Synthesis of 2-{[(*E*)-pyridin-2-ylmethylidene]amino}phenol **[*o*-Impy-OH, 2]**.

2-{[(E)-pyridin-2-ylmethylidene]amino}phenol [*o*-Impy-OH, 2]. Solid *o*-hydroxy aniline (200 mg, 1.832 mmol) was dissolved in acetonitrile (5 mL) at ambient temperature with stirring, 1 mol equiv. of the pyridine carboxaldehyde was then added (196 mg, 175 μL, 1.83 mmol). The reaction was left to stand with stirring for 4 h. The solvent was removed by rotary evaporation. A yellow solid was obtained, which was washed with ether (74 mg, 81.5%). Elemental analysis calc. for $C_{12}H_{10}N_2O$, C: 72.71%; H: 5.08%; N: 14.13%. Found: C: 72.40%; H: 5.05%; N: 14.15%. NMR-δ_H (500 MHz; CDCl$_3$) 7.15 (1H, td, J = 13.9, 7.8, 1.3 Hz) 7.22 (1H, dd, J = 8.1, 1.3 Hz) 7.46 (1H, td, J = 13.9, 8.1, 1.51 Hz) 7.60 (1H, dd, J = 7.8, 1.5 Hz) 7.65 (1H, dd, J = 4.8, 1.6 Hz) 8.07 (1H, td, J = 15.4, 7.9, 1.6 Hz) 8.38 (1H, d, J = 7.9 Hz) 8.92 (1H, d, J = 4.8 Hz) 9.03 (1H, s). m/z (ESI) found 199.0 (calc. M + H$^+$. $C_{12}H_{11}N_2O$ = 199.22), found 221.0 (calc. M + Na$^+$ $C_{12}H_{10}N_2NaO$ = 221.21).

***N*-[(1*E*)-pyridin-2-ylmethylene]aniline [Impy, 1].** As synthetic procedure 1, using aniline (100 mg, 98 μL, 1.07 mmol) and pyridine carboxaldehyde (115 mg, 102 μL, 0.46 mmol). Yield 95.3%. Elemental analysis calc. for $C_{12}H_{10}N_2$, C: 79.10%; H: 5.53%; N: 15.37%. Found: C: 78.85%; H: 5.49%; N: 15.69%. NMR-δ_H (500 MHz; CDCl$_3$) 7.31 (3H, m) 7.39 (1H, qd, J = 4.7, 7.6, 12.8 Hz) 7.44 (2H, t, J = 7.8, 15.4 Hz) 7.83 (1H, td, J = 7.8, 15.3 Hz) 8.32 (1H, d, J = 7.9 Hz) 8.64 (1H, s) 8.74 (1H, dq, J = 1.4, 4.6 Hz). m/z (ESI) found 184.0 (calc. M + H$^+$ $C_{12}H_{11}N_2$ = 184.22).

4-[(*E*)-(pyridin-2-ylmethylidene)amino]phenol [*p*-Impy-OH, 3]. As synthetic procedure 1, using *p*-hydroxy aniline (100 mg, 0.92 mmol) and pyridine

carboxaldehyde (98 mg, 87 μL, 0.92 mmol). Yield 92%. Elemental analysis calc. for $C_{12}H_{10}N_2O$ C: 72.71%; H: 5.08%; N: 14.43%. Found: C: 72.50%; H: 5.02%; N: 14.01%. NMR-δ_H (500 MHz; DMSO-d_6) 6.87 (2H, d, J = 8.6 Hz) 7.30 (2H, d, J = 8.6 Hz) 7.50 (1H, cd, J = 1.5, 4.8, 7.6, 15.7 Hz) 7.96 (1H, td, J = 0.5, 7.8, 15.7 Hz) 8.19 (1H, dt, J = 1.2, 2.2, 8.0 Hz) 8.63 (1H, s) 8.66 (1H, dc, J = 0.9, 1.6, 2.6, 4.9 Hz). m/z (ESI) found 199.0 (calc. M + H$^+$ $C_{12}H_{10}N_2O$ = 199.22).

4-[(E)-(pyridin-2-ylmethylidene)amino]benzoic acid [p-Impy-COOH, 4]. As synthetic procedure 1, using *p*-amino benzoic acid (100 mg, 0.73 mmol) and pyridine carboxaldehyde (78 mg, 69 μL, 0.73 mmol). Yield 70%. Elemental analysis calc. for $C_{13}H_{10}N_2O_2$ C: 69.02%; H: 4.46%; N: 12.38%. Found: C: 69.15%; H: 4.52%; N: 12.08%. NMR-δ_H (500 MHz; DMSO-d_6) 5.80 (1H, s) 6.88 (2H, d, J = 8.8 Hz) 7.44 (1H, cd, J = 1.1, 4.8, 7.6, 12.6 Hz) 7.69 (1H, d, J = 7.8 Hz) 7.86 (2H, d, J = 8.9 Hz) 7.93 (1H, td, J = 1.9, 7.2, 15.6 Hz). m/z (ESI) found 227.1 (calc. M + H$^+$ $C_{13}H_{11}N_2O_2$ = 227.23).

4-{4-[(E)-(pyridin-2-ylmethylidene)amino]phenyl}butanoic acid [p-Impy-(CH$_2$)$_3$COOH, 5]. As synthetic procedure 1, using 4-(4-aminophenyl)butanoic acid (100 mg, 0.56 mmol) and pyridine carboxaldehyde (60 mg, 53 μL, 0.56 mmol). Yield 64%. Elemental analysis calc. for $C_{16}H_{16}N_2O_2$, C: 71.62%; H: 6.01%; N: 10.44%. Found: C: 71.50%; H: 6.08%; N: 10.52%. NMR-δ_H (500 MHz; DMSO-d_6) 1.95 (2H, q, J = 7.4, 15.0, 22.7, 30.7 Hz) 2.29 (4H, d, J = 1.4 Hz) 2.35 (2H, t, J = 6.2, 14.5 Hz) 2.71 (2H, t, J = 7.6, 15.9 Hz) 7.53 (1H, cd, J = 1.1, 4.9, 7.4, 15.2 Hz) 7.99 (1H, td, J = 2.1, 7.7, 15.2 Hz) 8.22 (1H, td, J = 1.1, 2.0,

7.9 Hz) 8.63 (1H, s) 8.69 (1H, dc, J = 0.8, 1.8, 2.8, 4.9 Hz). m/z (ESI) found 291.1

(calc. M + H$^+$ C$_{16}$H$_{17}$N$_2$O$_2$ = 291.33).

Synthetic procedure 2, was used to synthesise all the ruthenium complexes described in this Chapter and listed in Table 3.2, on page 84.

Synthetic procedure 2.
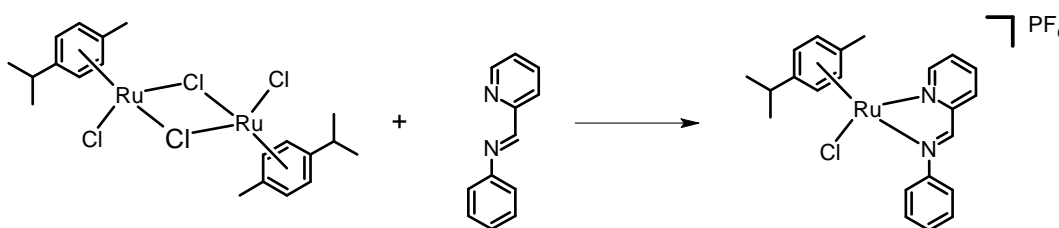
Scheme 3.2. Synthesis of [Ru(η^6-p-cym)(Impy)Cl]PF$_6$ [**7**].

[Ru(η^6-p-cym)(Impy)Cl]PF$_6$, [7]. Ruthenium p-cymene dimer [(η^6-p-cymene) RuCl$_2$]$_2$ (100 mg, 0.16 mmol) was dissolved in methanol (5 mL). and two mol equiv. of the appropriate ligand was added, in this case, N-[(1E)-pyridin-2-ylmethylene]aniline, (242 mg, 0.33 mmol). The reaction mixture was left at ambient temperature with constant stirring for 5 h. After this time, 5 mol. equiv. of NH$_4$PF$_6$ were added to the mixture, followed by stirring for a further hour. The solid precipitate was filtered off under vacuum and recrystallised. (87 mg, 44%). Elemental analysis calc. for C$_{22}$H$_{24}$N$_2$ClF$_6$PRu, C: 44.19%, H: 4.05%, N: 4.69%. Found: C: 44.25%, H: 4.06%; N: 4.72%. NMR-δ_H (500 MHz; DMSO-d$_6$) 1.10

(6H, d, J = 9.4 Hz) 2.26 (3H, s) 2.62 (1H, m) 5.49 (1H, dd, J = 6.3, 0.9 Hz) 5.60 (1H, dd, J = 6.3, 0.9 Hz) 5.67 (1H, q, J = 6.4, 1.1 Hz) 5.97 (1H, dd, J = 6.4, 1.1 Hz), 7.64 (3H, m) 7.82 (2H, m) 7.85 (1H, m) 8.27 (2H, m) 8.77 (1H, s) 9.51 (1H, d, J = 5.6 Hz). m/z (ESI) found 453.1 (calc. M$^+$ C$_{22}$H$_{24}$N$_2$ClRu = 452.96).

[Ru(η^6-*p*-cym)(Impy)I]PF$_6$ [8]. As synthetic procedure 2, using [Ru(η^6-*p*-cym)$_2$I$_2$]I$_2$ (50 mg, 0.06 mmol) and Impy (65 mg, 0.13 mmol). Yield 74%. Elemental analysis calc. for C$_{22}$H$_{24}$N$_2$F$_6$IPRu, C: 38.33%, H: 3.51%, N: 4.06%. Found: C: 38.10%, H: 3.68%; N: 4.10%. NRM-δ_H (500 MHz; DMSO-d$_6$) 0.99 (6H, dd, J = 8.1, 10.5 Hz) 2.37 (3H, s,) 2.61 (1H, m) 5.63 (1H, d, J = 6.7 Hz) 5.67 (1H, d, J = 5.5 Hz) 5.82 (1H, d, J = 5.5 Hz) 6.03 (1H, d, J = 6.7 Hz) 7.86 (1H, dd, J = 6.0, 13.2 Hz) 8.35 (1H, d, J = 7.0 Hz) 8.93 (1H, s) 9.59 (1H, d, J = 6.7 Hz). m/z (ESI) found 544.9 (calc. M$^+$ C$_{22}$H$_{24}$N$_2$IRu = 544.41).

[Ru(η^6-*p*-cym)(*o*-Impy-OH)Cl]PF$_6$ [9]. As synthetic procedure 2, using [Ru(η^6-*p*-cym)$_2$Cl$_2$]Cl$_2$ (100 mg, 0.16 mmol) and *o*-Impy-OH (65 mg, 0.33 mmol). Yield 87%. Elemental analysis calc. for C$_{22}$H$_{24}$N$_2$ClF$_6$OPRu, C: 43.04%, H: 3.94%, N: 4.56%. Found: C: 43.28%, H: 3.98%; N: 4.62%. NRM-δ_H (500 MHz; DMSO-d$_6$) 1.07 (3H, d, J = 4.2 Hz) 1.09 (3H, d, J = 4.2 Hz) 2.24 (3H, s) 2.64 (1H, q, J = 7.0, 13.9, 20.9, 27.7 Hz) 5.34 (1H, dd, J = 0.9, 6.2 Hz) 5.56 (1H, dd, J = 1.0, 6.2 Hz) 5.64 (1H, dd, J = 0.9, 6.2 Hz) 5.96 (1H, dd, J = 0.9, 6.2 Hz) 7.07 (1H, td, J = 1.2, 7.6, 15.3 Hz) 7.15 (1H, dd, J = 1.2, 8.2 Hz) 7.37 (1H, td, J = 1.5, 8.9, 15.3 Hz) 7.75 (1H, dd, J = 1.5, 8.1 Hz) 7.85 (1H, td, J = 1.9, 5.6, 12.9 Hz) 8.25 (2H, m) 8.77 (1H, s) 9.51 (1H, d, J = 5.4 Hz). m/z (ESI) found 469.0 (calc. M$^+$ C$_{22}$H$_{24}$N$_2$ClORu = 468.96).

[Ru(η⁶-*p*-cym)(*p*-Impy-OH)Cl]PF₆ [10]. As synthetic procedure 2, using [Ru(η⁶-
p-cym)₂Cl₂]Cl₂ (100 mg, 0.16 mmol) and *p*-Impy-OH (65 mg, 0.33 mmol). Yield
81%. Elemental analysis calc. for $C_{22}H_{24}N_2ClF_6OPRu$, C: 43.04%, H: 3.94%, N:
4.56%. Found: C: 43.01%, H: 3.90%; N: 4.75%. NMR-δ_H (500 MHz; DMSO-d₆)
1.10 (6H, d, J = 7.2 Hz) 2.25 (3H, s) 2.60 (1H, q, J = 6.7, 14.0, 20.5, 28.0 Hz) 5.52
(1H, d, J = 6.0), 5.59 (1H, d, J = 6.5 Hz) 5.65 (1H, d, J = 6.0 Hz) 5.96 (1H, d, J =
6.5 Hz) 7.00 (2H, d, J = 8.2 Hz) 7.71 (2H, d, J = 8.2 Hz) 7.80 (1H, m) 8.19 (1H,
dd, J = 1.2, 7.7 Hz) 8.24 (1H, td, J = 1.8, 7.3, 15.7 Hz) 9.45 (1H, d J = 6.0 Hz).
m/z (ESI) found 469.0 (calc. M⁺ $C_{22}H_{24}N_2ClORu$ = 468.96).

[Ru(η⁶-*p*-cym)(*p*-Impy-OH)I]PF₆ [11]. As synthetic procedure 2, using [Ru(η⁶-
p-cym)₂I₂]I₂ (150 mg, 0.19 mmol) and *p*-Impy-OH (76 mg, 0.38 mmol). Yield
64%. Elemental analysis calc. for $C_{22}H_{24}N_2F_6IPORu$, C: 37.46%, H: 3.43%, N:
3.97%. Found: C: 37.30%, H: 3.38%; N: 4.01%. NRM-δ_H (500 MHz; DMSO-d₆)
0.98 (6H, dd, J = 6.0, 13.4 Hz) 2.40 (3H, s,) 2.60 (1H, m) 5.61 (1H, d, J = 6.8 Hz)
5.66 (1H, d, J = 6.4 Hz) 5.77 (1H, d, J = 6.4 Hz) 6.07 (1H, d, J = 6.8 Hz) 6.97
(2H, d, J = 8.8 Hz) 7.74 (2H, d, J = 9.6 Hz) 8.25 (2H, d, J = 4.8 Hz) 8.52 (1H, d, J
= 5.6 Hz) 10.24 (1H, s). m/z (ESI) found 560.0 (calc. M⁺ $C_{22}H_{24}N_2IORu$ =
560.41).

[Ru(η⁶-*p*-cym)(*p*-Impy-COOH)Cl]PF₆ [12]. As synthetic procedure 2, using
[Ru(η⁶-*p*-cym)₂Cl₂]Cl₂ (100 mg, 0.16 mmol) and *p*-Impy-COOH (37 mg, 0.33
mmol). Yield 65%. Elemental analysis calc. for $C_{23}H_{24}N_2ClF_6O_2PRu$, C: 43.03%,
H: 3.77%, N: 4.36%. Found: C: 42.98%, H: 3.61%; N: 4.54%. NMR-δ_H (500
MHz; DMSO-d₆) 0.98 (3H, d, J = 2.4 Hz) 0.99 (3H, d, J = 2.4 Hz) 2.16 (3H, s)

2.84 (1H, m) 5.61 (1H, d, J = 6.8 Hz) 5.69 (1H, d, J = 6.1 Hz) 5.79 (1H, d, J = 6.1 Hz) 6.10 (1H, d, J = 6.8 Hz) 7.90 (3H, m) 8.18 (2H, d, J = 8.4 Hz) 8.32 (2H, m) 8.99 (1H, s) 9.60 (1H, d, J = 5.4 Hz). m/z (ESI) found 498.0 (calc. M$^+$ C$_{23}$H$_{24}$N$_2$ClO$_2$Ru = 497.93).

[Ru(η^6-*p*-cym)(*p*-Impy-COOH)I]PF$_6$ [13]. As synthetic procedure 2, using [Ru(η^6-*p*-cym)$_2$I$_2$]I$_2$ (50 mg, 0.05 mmol) and *p*-Impy-COOH (24 mg, 0.10 mmol). Yield 52%. Elemental analysis calc. for C$_{23}$H$_{24}$N$_2$F$_6$IO$_2$PRu, C: 37.67%, H: 3.30%, N: 3.82%. Found: C: 37.54%, H: 3.18%; N: 3.69%. NRM-δ$_H$ (500 MHz; DMSO-d$_6$) 1.00 (6H, d, J = 7.9 Hz) 2.18 (3H, s,) 2.62 (1H, m) 5.62 (1H, d, J = 6.0 Hz) 5.71 (1H, d, J = 6.0 Hz) 5.81 (1H, d, J = 5.7 Hz) 6.13 (1H, d, J = 5.7 Hz) 7.91 (2H, d, J = 8.7 Hz) 7.98 (1H, d, J = 8.4 Hz) 8.16 (1H, t, J = 7.84 15.4 Hz) 8.19 (2H, d, J = 8.7 Hz) 8.34 (2H, m) 9.03 (1H, s) 9.62 (1H, d, J = 5.1 Hz). m/z (ESI) found 588.4 (calc. M$^+$ C$_{23}$H$_{24}$N$_2$IO$_2$Ru = 588.42).

[Ru(η^6-*p*-cym)(*p*-Impy-(CH$_2$)$_3$COOH)Cl]PF$_6$ [14]. As synthetic procedure 2, using [Ru(η^6-*p*-cym)$_2$Cl$_2$]Cl$_2$ (100 mg, 0.16 mmol) and *p*-Impy-(CH$_2$)$_3$COOH (44 mg, 0.33 mmol). Yield 72%. Elemental analysis calc. for C$_{26}$H$_{30}$N$_2$ClF$_6$PO$_2$Ru, C: 57.93%, H: 5.61%, N: 5.20%. Found: C: 57.50%, H: 5.75%; N: 5.18%. NMR-δ$_H$ (500 MHz; DMSO-d$_6$) 1.09 (3H, d, J = 4.4 Hz) 1.33 (3H, d, J = 4.4 Hz) 2.02 (2H, q, J = 7.0, 14.5, 21.5, 29.1 Hz) 2.24 (3H, s) 2.40 (2H, t, J = 6.6, 14.1 Hz) 2.61 (1H, q, J = 6.1, 12.3, 16.5, 20.3 Hz) 2.84 (2H, t, J = 7.0, 15.02 Hz) 5.48 (1H, d, J = 6.3 Hz) 5.57 (1H, d, J = 6.3 Hz) 5.64 (1H, d, J = 7.0 Hz) 5.96 (1H, d, J = 6.8 Hz) 7.49 (2H, d, J = 8.4 Hz) 7.76 (2H, d, J = 8.5 Hz) 7.83 (1H, td, J = 2.7, 6.7,

12.2 Hz) 8.24 (2H, m) 8.71 (1H, s) 9.48 (1H, d, J = 5.1 Hz). m/z (ESI) found 539.2 (calc. M^+ $C_{26}H_{30}N_2ClO_2Ru$ = 539.05).

[Ru(η^6-p-cym)(p-Impy-NMe$_2$)Cl]PF$_6$ [15]. As synthetic procedure 2, using [Ru(η^6-p-cym)$_2$Cl$_2$]Cl$_2$ (100 mg, 0.16 mmol) and p-Impy-NMe$_2$ (74 mg, 0.33 mmol). Yield 84%. Elemental analysis calc. for $C_{22}H_{29}N_3ClF_6PRu$, C: 42.83%, H: 4.74%, N: 6.81%. Found: C: 42.68%, H: 4.81%; N: 6.74%. NMR-δ_H (500 MHz; DMSO-d$_6$) 0.99 (6H, dd, J = 1.1, 2.3, 6.9, 9.3 Hz) 2.20 (3H, s) 2.46 (1H, m) 3.12 (6H, s) 5.62 (2H) 5.78 (1H, d, J = 7.3 Hz) 6.11 (1H, d, J = 6.7 Hz) 6.89 (2H, d, J = 8.4 Hz) 7.70 (2H, d, J = 9.0 Hz) 7.81 (1H, t, J = 7.9, 14.1 Hz) 8.18 (1H, d, J = 6.7 Hz) 8.26 (1H, t, J = 7.3, 14.7 Hz) 8.78 (1H, s) 9.51(1H, d, J = 4.0 Hz). m/z (ESI) found 472.0 (calc. M^+ $C_{22}H_{29}N_3ClRu$ = 472.01).

[Ru(η^6-p-cym)(p-Impy-NMe$_2$)I]PF$_6$ [16]. As synthetic procedure 2, using [Ru(η^6-p-cym)$_2$I$_2$]I$_2$ (150 mg, 0.19 mmol) and p-Impy-NMe$_2$ (89 mg, 0.38 mmol). Yield 64%. Elemental analysis calc. for $C_{24}H_{29}N_3F_6IPRu$, C: 39.36%, H: 3.99%, N: 5.74%. Found: C: 39.24%, H: 3.98%; N: 5.81%. NMR-δ_H (500 MHz; DMSO-d$_6$) 1.00 (6H, dd, J = 7.3, 12.2, 18.1 Hz) 2.45 (3H, s) 2.56 (1H, m) 3.07 (6H, s) 5.59 (1H, d, J = 8.8 Hz) 5.65 (1H, d, J = 8.1 Hz) 5.77 (1H, d, J = 8.8 Hz) 6.08 (1H, d, J = 8.1 Hz) 7.73 (1H, d, J = 3.8, 6.6 Hz) 7.77 (1H, d, J = 10.8 Hz) 8.19 (1H, t, J = 7.9, 14.1 Hz) 8.21 (1H, d, J = 7.5 Hz) 8.72 (1H, s) 9.48(1H, d, J = 4.8 Hz). m/z (ESI) found 587.4 (calc. M^+ $C_{24}H_{29}N_3IRu$ = 587.48).

[Ru(η^6-bip)(p-Impy-NMe$_2$)Cl]PF$_6$ [17]. As synthetic procedure 2, using [Ru(η^6-bip)$_2$Cl$_2$]Cl$_2$ (50 mg, 0.07 mmol) and p-Impy-NMe$_2$ (35 mg, 0.15 mmol). Yield 76%. Elemental analysis calc. for $C_{26}H_{25}N_3ClF_6PRu$, C: 47.24%, H: 3.81%, N:

6.36%. Found: C: 47.12%, H: 3.74%; N: 6.30%. NMR-δ_H (500 MHz; DMSO-d_6) 3.05 (6H, s) 6.16 (3H, m) 6.34 (1H, d, J = 6.1 Hz) 6.45 (1H, d, J = 7.2 Hz) 6.71 (2H, d, J = 7.2 Hz) 7.43 (2H, m) 7.51 (3H, m) 7.59 (2H, t, J = 6.2 Hz) 7.69 (1H, t, J = 7.1, 13.1 Hz) 8.15 (1H, d, J = 6.8 Hz) 8.21 (1H, t, J = 6.8, 14.3 Hz) 8.72 (1H, s) 9.37 (1H, d, J = 5.9 Hz). m/z (ESI) found 515.9 (calc. M^+ $C_{26}H_{25}N_3ClRu$ = 516.02).

[Ru(η^6-*m*-terp)(*p*-Impy-NMe$_2$)Cl]PF$_6$ [18]. As synthetic procedure 2, using [Ru(η^6-*m*-terp)$_2$Cl$_2$]Cl$_2$ (80 mg, 0.01 mmol) and *p*-Impy-NMe$_2$ (45 mg, 0.20 mmol). Yield 83%. Elemental analysis calc. for $C_{32}H_{29}N_3ClF_6PRu$, C: 52.14%, H: 3.97%, N: 5.70%. Found: C: 52.28%, H: 3.85%; N: 5.78%. NMR-δ_H (500 MHz; DMSO-d_6) 3.02 (6H, s) 6.26 (3H, t, J = 6.5, 12.4 Hz) 6.55 (3H, t, J = 9.5, 16.86 Hz) 7.29 (2H, d, J = 9.5 Hz) 7.51 (7H, m) 7.78 (2H, d, J = 7.6 Hz) 7.83 (2H, d, J = 7.6 Hz) 8.15 (2H, m) 8.68 (1H, s) 9.10 (1H, d, J = 5.4 Hz). m/z (ESI) found 592.0 (calc. M^+ $C_{32}H_{29}N_3ClRu$ = 592.12).

3.2.3 Methods

3.2.3.1 Aquation studies

Aquation of complexes **7** - **18** was studied using ^{1}H-NMR (500 and 600 MHz) as described in Chapter 2, using 2 mM solutions of each complex in D$_2$O with 5% DMSO/MeOD at 298 K. To suppress the aquation observed in all the chlorido

complexes, 200 mM NaCl was added to the deuterated solvent, and, 200 mM KI was used to suppress the aquation of iodido complexes.

3.2.3.2 Nucleobase binding

The extent of binding over 24 h at 298 K for complexes **7** - **18** to 9-ethylguanine, as a nucleobase model, was followed by ^{1}H-NMR (500 MHz). The details of these experiments can be found in Chapter 2. Briefly, a fresh 2 mM solution of each complex was prepared in 50 mM sodium phosphate buffer (pH 7.5) with 5% DMSO. The solution also contained 9-EtG for a final mol. ratio 1:1.25 where the nucleobase was in excess. As in the case of aquation studies, ^{1}H-NMR spectra were recorded at 298 K within the first 10 min after sample preparation and again after 24 h at 500 MHz. All experiments were carried out in triplicate and the standard deviations calculated. Nucleobase binding was monitored by the formation of a second set of peaks that included bound-9-EtG.

3.2.3.3 Antiproliferative activity

The antiproliferative activity of ligands **1**-**6** and complexes **7**-**18** was determined in A2780 ovarian, A549 lung, HCT116 colon and MCF7 breast carcinoma cell lines. The experiments to determine IC_{50} values were carried out as described in Chapter 2. Briefly, 96 well plates were used to seed 5000 cells per well, they were left to pre-incubate in drug-free media at 310 K for 48 h before adding various

concentrations of the compounds to be tested. A drug exposure period of 24 h was allowed. After this, supernatants were removed by suction and each well was washed with PBS (100 μL). A further 48 h was allowed for the cells to recover in drug-free medium (200 μL per well) at 310 K. The SRB assay was used to determine cell viability, as described in Chapter 2. IC_{50} values, as the concentration which caused 50% of inhibition of cell growth, were determined as duplicates of triplicates in two independent sets of experiments, and their standard deviations were calculated.

3.2.3.4 Metal accumulation in cancer cells

Metal accumulation studies for complexes **7**-**18** were conducted on the A2780 ovarian carcinoma cell line. Briefly, 4 x 10^6 cells were seeded on a Petri dish, after 24 h of pre-incubation time in drug-free medium, the test complexes were added to give final concentrations equal to $IC_{50}/3$ and then allowed a further 24 h of drug exposure. After this time, cells were counted, treated with trypsin and cell pellets were collected. Each pellet was digested overnight in concentrated nitric acid (73%) at 353 K; the resulting solutions were diluted (HNO_3 5%) and the amount of ruthenium taken up by the cells was determined by ICP-MS. These experiments did not included any cell recovery time in drug-free media. They were all carried out in triplicate and the standard deviations were calculated. Results are compared to the corresponding data for **CDDP**. More experimental details can be found in Chapter 2.

For following cellular uptake studies, only complexes **15** [Ru(η^6-*p*-cym)(*p*-Impy-NMe$_2$)Cl]PF$_6$ and its iodido analogue **16** [Ru(η^6-*p*-cym)(*p*-Impy-NMe$_2$)I]PF$_6$ were used and compared to the corresponding data for **CDDP.** These two compounds were selected because their structural similarities (same arene unit, *p*-cym, and *N,N*-ligand *p*-Impy-NMe$_2$) and with the aim of studying the effect of the monodentate ligand on cellular accumulation behaviour. The procedure was carried out as described above including the following experimental variations. In all cases, 4 per 10^6 A2780 cells were seeded in Petri dishes, the pre-incubation time in drug-free medium was 24 h, and the drug concentrations used were equipotent and equal to IC$_{50}$/3 (**CDDP**= 0.4 µM, **15** = 5 µM and **16** = 1 µM), unless otherwise stated.

- **Time dependence:** these experiments involved variable drug exposure time but no recovery time in drug-free medium. The chosen time points for drug exposure were: 1 h, 4 h, 8 h, 24 h, 48 h, 72 h and 96 h.

- **Temperature dependence:** experiments were carried out using 8 h of drug exposure and no recovery time in drug-free medium. The chosen temperature points for incubation with the drugs were: 277 K, 293 K, 310 K and 323 K.

- **Concentration dependence:** these experiments used 24 h of drug exposure and no recovery time in drug-free medium. The chosen drug concentrations were: 0.16, 0.33, 1.6, 3.2, 6.4 and 9.6 x IC$_{50}$

- **Extent of efflux:** In these experiments drugs were removed after 24 h and fresh drug-free medium was added to the Petri dishes. Cells were

incubated again in drug-free medium for 24 h, 48 h and 72 h to allow them to recover before being treated with trypsin to collect the cell pellets.

- **Inhibition of efflux:** Experiments were done using 24 h of drug exposure and 24 h of recovery time using drug-free fresh medium with 5 µM, 10 µM or 20 µM of verapamil.

- **Role of Na$^+$/K$^+$ pump in cellular metal accumulation, as a facilitated diffusion endocytotic pathway:** these experiments involved 24 h of drug exposure, co-administration of the drug with 5 µM, 10 µM, 20 µM, 0.1 mM or 0.2 mM of ouabain. No recovery time in drug-free medium was allowed.

- **Role of of CTR1 in cellular metal accumulation:** experiments were carried out using 24 h of drug exposure time and co-administration of the drug with 10 µM, 20 µM, 40 µM, 0.1 mM or 0.2 mM of copper(II) chloride. No recovery time in drug-free medium was allowed.

- **Effect of ATP depletion in cellular metal accumulation:** experiments were performed using 24 h of drug exposure time and co-administration of the drug with 5 µM and 20 µM of antimycin A. No recovery time in drug-free medium was allowed.

- **Membrane disruption by amphotericin B as a model for protein-mediated uptake:** these experiments were done using 24 h of drug exposure and co-administration of the drug with 1 µM, 5 µM, 10 µM or 20 µM of amphotericin B. No recovery time in drug-free medium was allowed.

- **The role of caveolae endocytotic pathway in metal accumulation:** these experiments involved 24 h of drug exposure and co-administration of the drug with 10 μM, 20 μM, 0.5 mM or 1 mM of methyl β-cyclodextrin. No recovery time in drug-free medium was allowed.

3.2.3.5 Determination of partition coefficient (Log P)

The partition coefficients of the chlorido complexes **15** $[Ru(\eta^6\text{-}p\text{-cym})(p\text{-Impy-}NMe_2)Cl]PF_6$, **17** $[Ru(\eta^6\text{-bip})(p\text{-Impy-}NMe_2)Cl]PF_6$ and **18** $[Ru(\eta^6\text{-}m\text{-terp})(p\text{-}Impy\text{-}NMe_2)Cl]PF_6$ were determined using the shaking flask method. These three complexes were selected with the aim of studying the effect of the changes in the arene on the lipophilicity of the complexes. They all have the same *N,N*-chelating ligand (*p*-Impy-NMe$_2$, **6**), and the same monodentate ligand (Cl).

This method used 3 mL of 2 mM octanol-saturated aqueous solutions of the complexes which were shaken with equal volumes of water-saturated octanol for 24 h. The amount of ruthenium in the aqueous layer was determined by ICP-MS and the Log P values calculated. Aqueous solutions included 150 mM of NaCl to avoid aquation of the complexes. More details of this procedure can be found in Chapter 2.

3.2.3.6 HPLC analysis for I to Cl conversion

6 mM stock solutions of complexes **15** and **16** were prepared in 5% MeOH and water; separately 30 mM solutions of NaCl and KI were prepared in the same solvent. Aquation of each complex was studied using 40 µL of the stock solution and diluting it to 1 mL, chromatograms were recorded after 10 min of sample preparation and again after 24 h. Inhibition of aquation was studied by mixing 40 µL of the stock solutions of **1** or **2** and 40 µL of NaCl/KI (NaCl for complex **1** and KI for complex **2**) and diluting to 1 mL. Chromatograms were recorded after 10 min of sample preparation and again after 24 h. Finally for the I to Cl conversion, a fresh 1 mL solution was prepared containing together 40 µL of the stock of each complex and 40 and µL of NaCl. Chromatograms were recorded after 10 min of sample preparation and again after 24 h.

All chromatograms were obtained using an Agilent 1100 system with a DAD and a 100 µL loop with a mobile phase H_2O 0.1%TFA/ACN 0.1% TFA and a Agilent ZORBAX Eclipse Plus C18, 250 x 4.6 mm column with 5 µm pore size. Detection wavelength: 254 nm.

3.3 Results

3.3.1 Synthesis and characterization

In all cases the synthesis of the imines involved a nucleophilic attack by the lone pair of electrons from the aniline nitrogen on the carbonyl group of the aldehyde,

followed by dehydration. Imines **1**-**6** shown in Table 3.1 below were synthesised and characterised using ^{1}H and ^{13}C-NMR (1D, 2D experiments), ESI-MS, and elemental analysis.

Table 3.1. Imine ligands studied in Chapter 3.
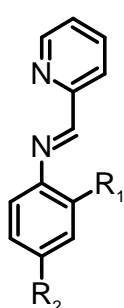
	Ligands	R$_1$	R$_2$
1	Impy	H	H
2	*o*-Impy-OH	OH	H
3	*p*-Impy-OH	H	OH
4	*p*-Impy-COOH	H	COOH
5	*p*-Impy-(CH$_2$)$_3$COOH	H	(CH$_2$)$_3$COOH
6	*p*-Impy-NMe$_2$	H	N(CH$_3$)$_2$

Once the proposed ligands were fully characterised, complexes **7**-**18** in Table 3.2 were synthesised. They were characterised using the same techniques as for the ligands, ^{1}H and ^{13}C-NMR (1D, 2D experiments), ESI-MS, and elemental analysis, as well as, ICP-MS for metal quantification. All the experiments were consistent with the proposed formulation for all the complexes. In all cases the chirality of the metal centre is inferred by the ^{1}H-NMR spectra which show four sets of peaks for the aromatic *p*-cymene protons. In the case of ligands/complexes containing –COOH residues the deprotonation of the carboxylic acid is shown as dependent on the particular experiments set up (working pH value). No pKa determinations were carried out.

Table 3.2. Ruthenium(II) arene complexes studied in Chapter 3.
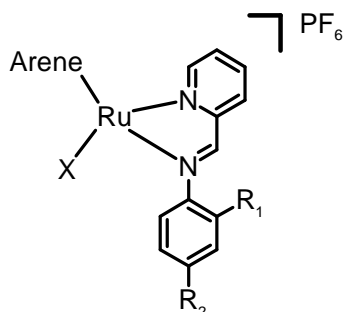
Complexes	Arene	Ligand	R_1	R_2	X
7	η^6-p-cym	Impy	H	H	Cl
8					I
9		o-Impy-OH	OH	H	Cl
10		p-Impy-OH	H	OH	Cl
11					I
12		p-Impy-COOH	H	COOH	Cl
13					I
14		p-Impy-(CH$_2$)$_3$COOH	H	(CH$_2$)$_3$COOH	Cl
15		p-Impy-NMe$_2$	H	N(CH$_3$)$_2$	Cl
16					I
17	η^6-bip		H	N(CH$_3$)$_2$	Cl
18	η^6-m-terp		H	N(CH$_3$)$_2$	Cl

3.3.2 Aqueous solution chemistry

Aquation of complexes **7**-**16** was followed using ^{1}H -NMR of 2 mM solutions of each complex in deuterated water. Each value for the percentage of aquation reported represents the mean ± SD for three independent NMR experiments at 298 K. In the case of chlorido complex **7** [Ru(η^6-p-cym)(Impy)Cl]PF$_6$, Figure 3.3 shows the ^{1}H -NMR spectrum **(A)** taken within 10 min of sample preparation. This spectrum has only one set of four p-cymene signals between 5.4 and 6.2 ppm

which is evidence of only one chiral species being present. The asymmetric ligand generates chirality on the metal centre, which causes these four protons to be magnetically inequivalent. Also there is only one signal that corresponds to the iminic proton. Spectrum **(B)** was recorded after 24 h of sample preparation, in which two set of peaks are observed. Particularly, a new set of signals for the *p*-cymene and the presence of two different imine protons indicate the formation of a second product. In order to confirm that this second set of peaks corresponded to the aqua adduct, another sample was run in the presence of 200 mM NaCl (as described in Chapter 2). This time, spectrum **(C)** only shows one set of *p*-cymene signals with the same chemical shifts as the original spectrum, confirming that the process observed was indeed aquation and that it can be suppressed by addition of an excess chloride in the media. The addition of $AgNO_3$ to a solution of the chloride complex also resulted in the generation of the aqua adduct observed in spectrum **(B)**. A similar set of results was obtained when the experiments were carried out using 100 mM phosphate buffer pH 7.4 as solvent, instead of deuterated water. This indicated that there is no formation of phosphate adducts.
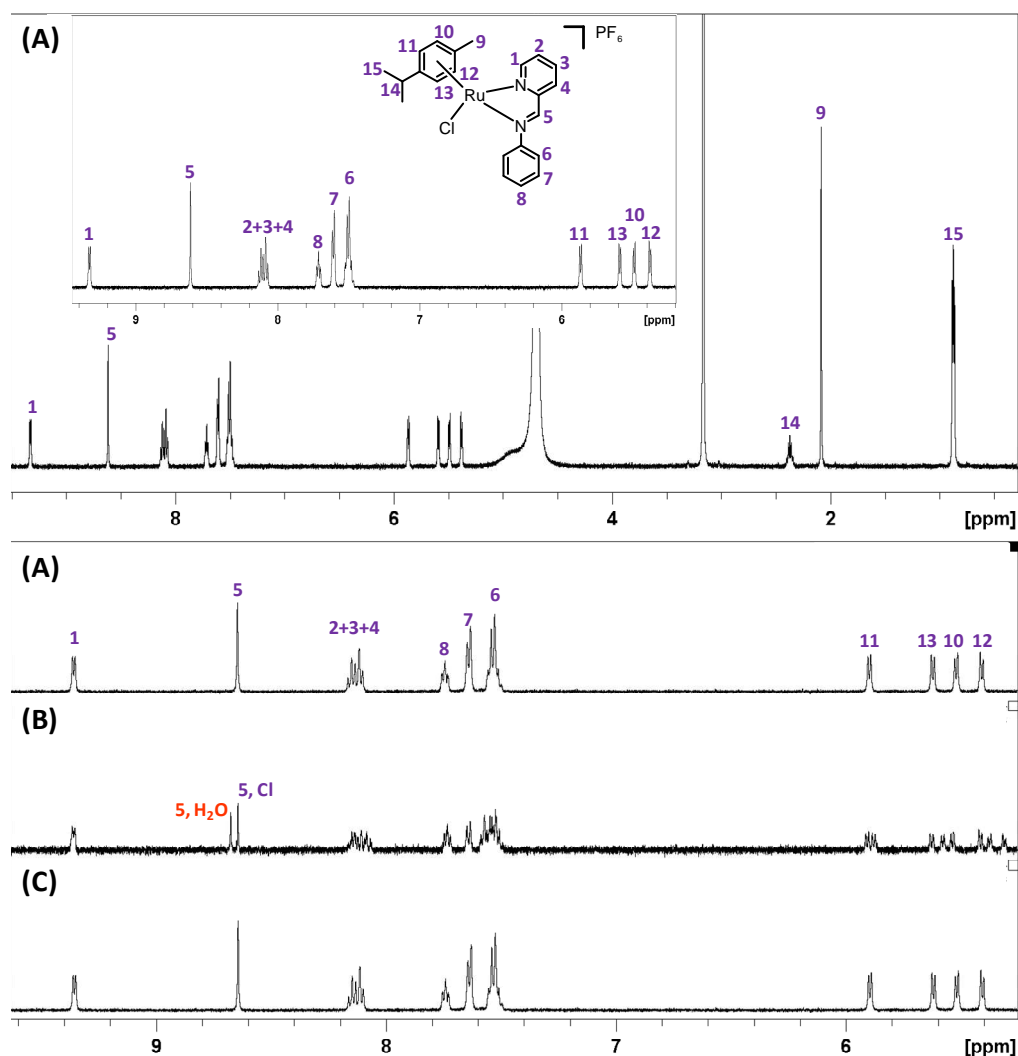
Figure 3.3. ^{1}H-NMR studies of the aquation of a 2 mM solution of complex **15** in 95% D_2O, 5% MeOD at 298 K. **(A)** After 8 min of sample preparation **(B)** After 24 h (highlighted: proton 5 in complex **15** and its analogous in the aqua complex). **(C)** A fresh solution with 200 mM of NaCl to suppress aquation taken after 24 h of sample preparation.

Table 3.3 shows the extent of the aquation after 24 h for all complexes. No aquation was observed for complexes **8** and **10**, while complexes **9**, **11**, **12** and **14** only hydrolysed partially ($< 20\%$). The highest extent of aquation is exhibited by

complexes **15** and **16**, (66% and 63% respectively) which have in common the same ligand, **6** *p*-Impy-NMe$_2$.

Table 3.3. Extent of aquation and extent 9-ethylguanine binding for complexes **7** - **16** after 24 h, using 2 mM solutions of each complex in phosphate buffer (pH 7.4) and a final ratio 1 : 1.25 for 9-EtG binding where the nucleobase was in excess.

	Compound a	% Aquation [b]	% 9-EtG binding [b]
7	[Ru(η^6-*p*-cym)(Impy)Cl]PF$_6$	37 ± 4	30 ± 3
8	[Ru(η^6-*p*-cym)(Impy)I]PF$_6$	0 ± 2	49 ± 4
9	[Ru(η^6-*p*-cym)(*o*-Impy-OH)Cl]PF$_6$	15 ± 5	22 ± 4
10	[Ru(η^6-*p*-cym)(*p*-Impy-OH)Cl]PF$_6$	0 ± 3	0 ± 4
11	[Ru(η^6-*p*-cym)(*p*-Impy-OH)I]PF$_6$	5 ± 2	4 ± 2
12	[Ru(η^6-*p*-cym)(*p*-Impy-COOH)Cl]PF$_6$	9 ± 3	9 ± 5
13	[Ru(η^6-*p*-cym)(*p*-Impy-COOH)I]PF$_6$	32 ± 4	47 ± 3
14	[Ru(η^6-*p*-cym)(*p*-Impy-(CH$_2$)$_3$COOH)Cl]PF$_6$	8 ± 3	16 ± 4
15	[Ru(η^6-*p*-cym)(*p*-Impy-NMe$_2$)Cl]PF$_6$	66 ± 6	68 ± 5
16	[Ru(η^6-*p*-cym)(*p*-Impy-NMe$_2$)I]PF$_6$	63 ± 3	75 ± 2

[a] Complexes 12, 13 and 14 contain carboxyl groups that are likely to be deprotonated at pH 7.4.
[b] Each value represents the mean ± SD for three independent NMR experiments at 310 K.

Independent NMR experiments were also used to follow the complexes binding to 9-ethylguanine (9-EtG) as a model for nucleobase interaction. In the case of complex **15** Figure 3.4 shows spectrum **(C)** which corresponds to the proton NMR taken within 10 min of sample preparation, followed by spectrum **(B)** that shows the formation of a 9-EtG adduct after 24 h of sample preparation (ratio 1: 1.25 where the nucleobase is in excess). As in the case of aquation, there are two sets of *p*-cymene signals, as well as two signals for the imine proton. A new peak for

bound 9-EtG is observed. Finally spectrum **(A)** corresponds to free 9-EtG for comparison purposes.
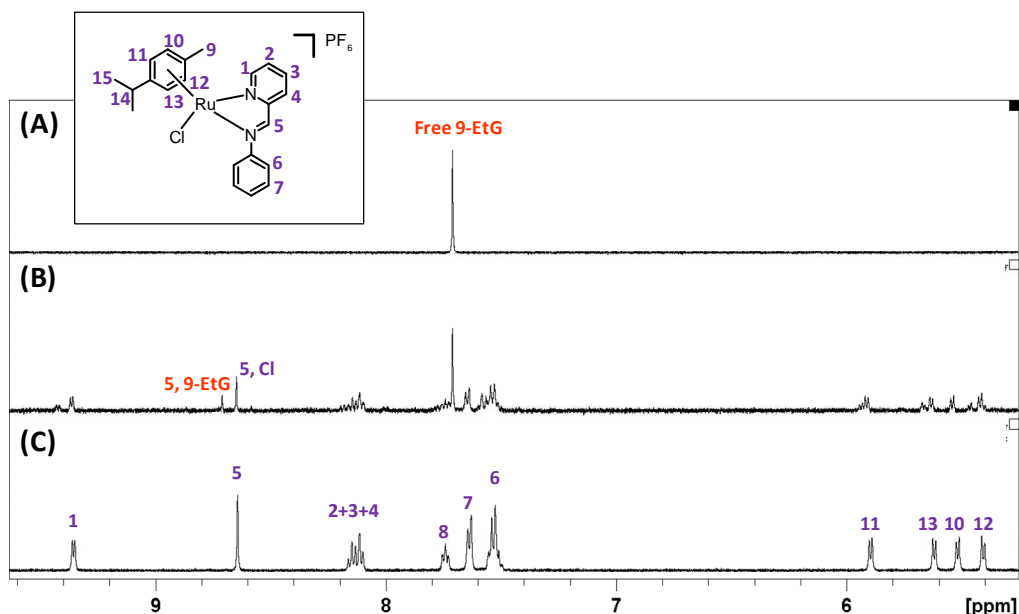
Figure 3.4. ^{1}H-NMR studies to determine the extent of binding of 9-EtG (1.25 mol. equiv.) to 2 mM complex **15** using in 100 mM phosphate buffer pH 7.4 at 298 K. **(A)** Free 9-EtG. **(B)** A fresh solution of complex **15** with adding excess of 9-EtG after 24 h of sample preparation (highlighted: proton 5 in complex **15** and its analogous in the 9-EtG complex). **(C)** Complex **15**.

Table 3.3, on page 87, also includes the extent of nucleobase adduct formation after 24 h for all complexes. Binding of complexes **10** [Ru(η^6-*p*-cym)(*p*-Impy-OH)Cl]PF$_6$, **11** [Ru(η^6-*p*-cym)(*p*-Impy-OH)I]PF$_6$ and **12** [Ru(η^6-*p*-cym)(*p*-Impy-COO)Cl]PF$_6$ to 9-EtG was found to be negligible ($< 10\%$).

Complexes **15** and **16,** the ones with the greater extent of aquation, are also the ones that bind to a greater extent to the nucleobase model. These results do not reflect the kinetics involved in the process.

3.3.3 Antiproliferative activity

3.3.3.1 IC$_{50}$ determination in A2780, A549, HCT116, MCF7 cells

Antiproliferative activity for ligands **1**-**6** and complexes **7**-**18** was determined using the SRB assay (Table 3.4), for which the protocol is described in detail in Chapter 2. For these assays, IC$_{50}$ values above 100 μM are considered inactive, while compounds with IC$_{50}$ values between 50 and 100 μM as moderately active. Values within the 15 - 50 μM range define a compound as active while below this range, compounds are considered to be highly active. All ligands tested were inactive against the chosen cell lines under the conditions described, as their IC$_{50}$ values were above 200 μM. Complexes **7**, **10**, **12**, **13** and **14** are also inactive as their IC$_{50}$ value are > 100 μM, while **8**, **9** and **11** are moderately active. Complexes **15** - **18** exhibited promising antiproliferative activity in all cell lines. A sample dose-response curve for IC$_{50}$ determinations can be found in Chapter 2.

Table 3.4. Part A. Antiproliferative activity of ligands **1**-**6** in A780, A549, HCT116 and MCF7 cell lines. IC$_{50}$ is expressed as the concentration in which each ligand/complex causes 50% cancer cell growth inhibition.

	Compound	IC$_{50}$ (μM)			
		A2780	A549	HCT116	MCF7
	1	>200	>200	>200	>200
	2	>200	>200	>200	>200
Ligands	3	>200	>200	>200	>200
	4	>200	>200	>200	>200
	5	>200	>200	>200	>200
	6	>200	>200	>200	>200

Table 3.4 Part B. Antiproliferative activity of complexes **7**-**18** in A780, A549, HCT116 and MCF7 cell lines.

	Compound	A2780	A549	HCT116	MCF7
		IC_{50} (µM)			
Ru^{II} complexes	7	160 ± 3	145 ± 1	158 ± 2	154 ± 3
	8	73 ± 3	54 ± 1	48 ± 4	46 ± 3
	9	84 ± 2	17 ± 3	85 ± 3	88 ± 2
	10	>200	>200	>200	>200
	11	48 ± 2	36 ± 2	51 ± 3	12.9 ± 0.6
	12	>200	>200	>200	>200
	13	135 ± 6	110 ± 3	122 ± 2	118 ± 3
	14	>200	>200	>200	>200
	15	16.2 ± 0.9	10.5 ± 0.8	3.4 ± 0.4	12.1 ± 0.3
	16	3.0 ± 0.2	15.3 ± 0.9	8.6 ± 0.8	4.4 ± 0.4
	17	38 ± 2	18.4 ± 0.3	5.1 ± 0.2	8.8 ± 0.2
	18	2.1 ± 0.2	8.8 ± 0.1	6.9 ± 0.5	5.9 ± 0.3

3.3.3.2 IC_{50} Time Dependence

The variation of IC_{50} values of complexes **15** [Ru(η^6-p-cym)(p-Impy-NMe$_2$)Cl]PF$_6$ and **16** [Ru(η^6-p-cym)(p-Impy-NMe$_2$)I]PF$_6$ in the A2780 cell line, after different exposure times (8-72 h) was evaluated using the protocol described in Chapter 2. These data were compared to that of **CDDP**. Results in Figure 3.5 indicate that there is no significant difference in the antiproliferative activity of the ruthenium(II) complexes after 24 h of drug exposure when the maximum potency was recorded.

| | | IC$_{50}$ (µM) | | |
| | | Exposure time (h) | | |
	8	**24**	**48**	**72**
CDDP	1.42 ± 0.09	1.22 ± 0.08	1.16 ± 0.07	1.1 ± 0.09
15	37.6 ± 0.9	16.2 ± 0.9	14 ± 1	12.7 ± 0.6
16	8.1 ± 0.8	3 ± 0.2	2.1 ± 0.8	1.65 ± 0.09
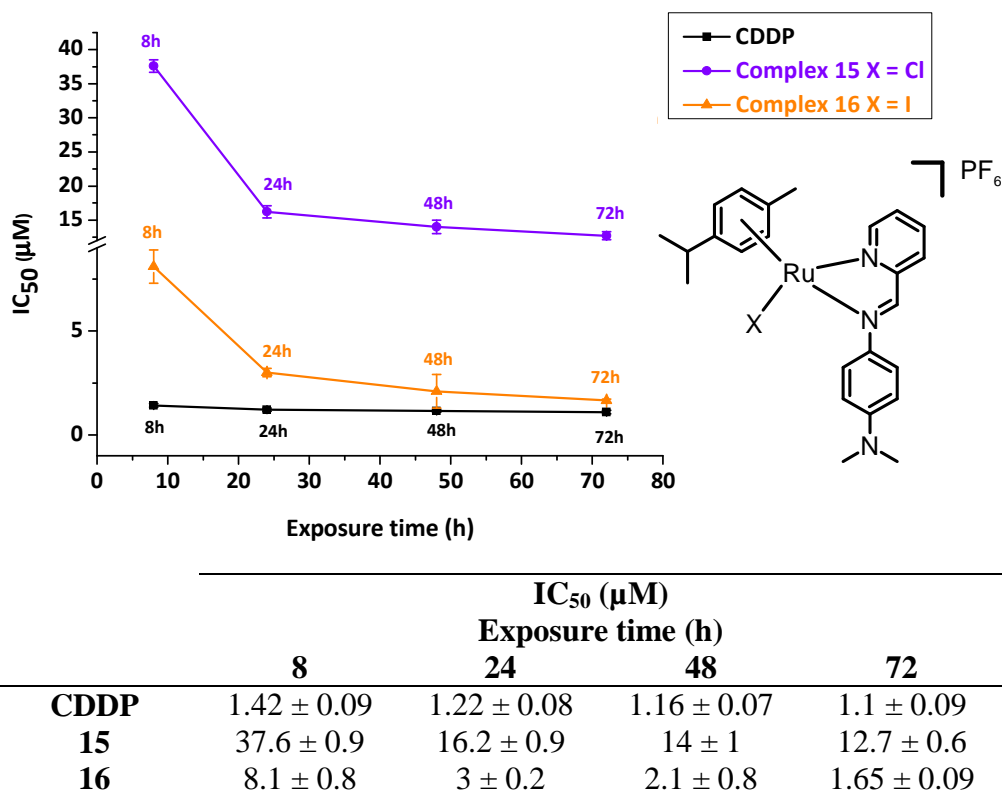
Figure 3.5. Dependence of IC$_{50}$ value in A2780 cell line on time of exposure for complexes **15** (−◆−)**, 16** (−▲−) and **CDDP** (−■−)**.** In all cases the pre-incubation time was 48 h before adding the drugs, and the cell recovery time was 72 h in drug-free medium.

3.3.3.3 Metal accumulation in cancer cells.

One time point, one concentration. Total cellular accumulation of ruthenium for complexes **7**-**18** was determined in A2780 ovarian cells line in order to relate the amount of Ru accumulated to cytotoxicity and to relate it to their hydrophobicity (Log P) in the case of complexes **15** [Ru(η^6-p-cym)(p-Impy-NMe$_2$)Cl]PF$_6$, **17** [Ru(η^6-bip)(p-Impy-NMe$_2$)Cl]PF$_6$ and **18** [Ru(η^6-m-terp)(p-

Impy-NMe$_2$)Cl]PF$_6$. For these experiments drug exposure time was 24 h and cells were not allowed to recover. Values are expressed as ng of Ru per million cells and were determined as independent duplicates of triplicates. The statistical significance of all cellular accumulation values was determined using a two-sided t-test with P<0.05. Results are shown in Table 3.5.

Table 3.5. Total accumulation of Ru in A2780 cells for complexes **7 - 18** after 24 h of drug exposure at 310 K with no recovery time, compared to their IC$_{50}$ values.

	Compound	ng Ru x10^6 cells[a]	IC$_{50}$ (µM)
7	[Ru(η^6-p-cym)(Impy)Cl]PF$_6$	5.3 ± 0.2	160 ± 3
8	[Ru(η^6-p-cym)(Impy)I]PF$_6$	0.88 ± 0.06	73 ± 3
9	[Ru(η^6-p-cym)(o-Impy-OH)Cl]PF$_6$	0.97 ± 0.09	84 ± 2
10	[Ru(η^6-p-cym)(p-Impy-OH)Cl]PF$_6$	6.9 ± 0.3	> 200
11	[Ru(η^6-p-cym)(p-Impy-OH)I]PF$_6$	28 ± 2	48 ± 2
12	[Ru(η^6-p-cym)(p-Impy-COOH)Cl]PF$_6$	7.2 ± 0.3	> 200
13	[Ru(η^6-p-cym)(p-Impy-COOH)I]PF$_6$	0.88 ± 0.06	135 ± 6
14	[Ru(η^6-p-cym)(p-Impy-(CH$_2$)$_3$COOH)Cl]PF$_6$	3.8 ± 0.3	> 200
15	[Ru(η^6-p-cym)(p-Impy-NMe$_2$)Cl]PF$_6$	7.5 ± 0.5	15.8 ± 0.6
16	[Ru(η^6-p-cym)(p-Impy-NMe$_2$)I]PF$_6$	11.9 ± 0.8	3.1 ± 0.3
17	[Ru(η^6-bip)(p-Impy-NMe$_2$)Cl]PF$_6$	10.2 ± 0.3	38 ± 2
18	[Ru(η^6-m-terp)(p-Impy-NMe$_2$)Cl]PF$_6$	4.6 ± 0.2	2.1 ± 0.2

[a] In all cases concentrations used were IC$_{50}$/3.

No clear trend was observed that correlates the total cellular accumulation of ruthenium with the antiproliferative activity. The highest cellular accumulation is for complex **11** [Ru(η^6-p-cym)(p-Impy-OH)I]PF$_6$ (28 ± 2 ng of Ru per 10^6 cells) which is only moderately active in the A2780 cell line (IC$_{50}$ value 48 ± 2 µM). The most active complexes **15** - **18** (IC$_{50}$ values 2-16 µM) have cellular accumulation in the range of 4.5 - 12 ng of metal per 10^6 cells, in this same range

as the cellular uptake of complex **10** [Ru(η^6-*p*-cym)(*p*-Impy-OH)Cl]PF$_6$ (6.9 $\pm$ 0.3 ng of Ru per 10^6 cells) which is completely inactive.

For following cellular accumulation studies, only complexes **15** and its iodido analogue **16** [Ru(η^6-*p*-cym)(*p*-Impy-NMe$_2$)I]PF$_6$ were used and compared to **CDDP.**

Time dependence. Cellular accumulation of ruthenium from complexes **15** and **16** was determined at different time points to find out the time of maximum uptake. It was also investigated whether the uptake is linear or if there is a saturation point, which would indicate the period in which the influx/efflux equilibrium is reached. These data, in Figure 3.6, were compared to **CDDP**. The general trend shows that the maximum cellular accumulation is reached at 48 h, after which an infflux/efflux equilibrium is reached.

Temperature dependence. Cellular accumulation studies of ruthenium from complexes **15**, **16** and platinum from **CDDP** shown in Figure 3.7, was determined at four different temperatures (277, 293, 310 and 323 K), At 277 K there is no observable cellular accumulation of platinum from **CDDP** which indicates the active nature of its uptake. Both ruthenium complexes were taken up even at this temperature, which suggests that their uptake is partially passive and not energy-dependent, especially for iodido complex **16**.

	ng Ru/Pt x10^6 cells						
	Drug exposure time (h)						
	1	**4**	**8**	**24**	**48**	**72**	**96**
CDDP	0.0011 ± 0.0001	0.014 ± 0.004	0.11 ± 0.08	0.25 ± 0.03	0.29 ± 0.02	0.26 ± 0.01	0.25 ± 0.02
15	1.32 ± 0.09	3.5 ± 0.4	4.2 ± 0.1	7.6 ± 0.8	8.9 ± 0.6	5.8 ± 0.4	4.0 ± 0.2
16	6.5 ± 0.4	8.2 ± 0.4	9 ± 2	11 ± 1	13.0 ± 0.7	10.7 ± 0.3	7.4 ± 0.1
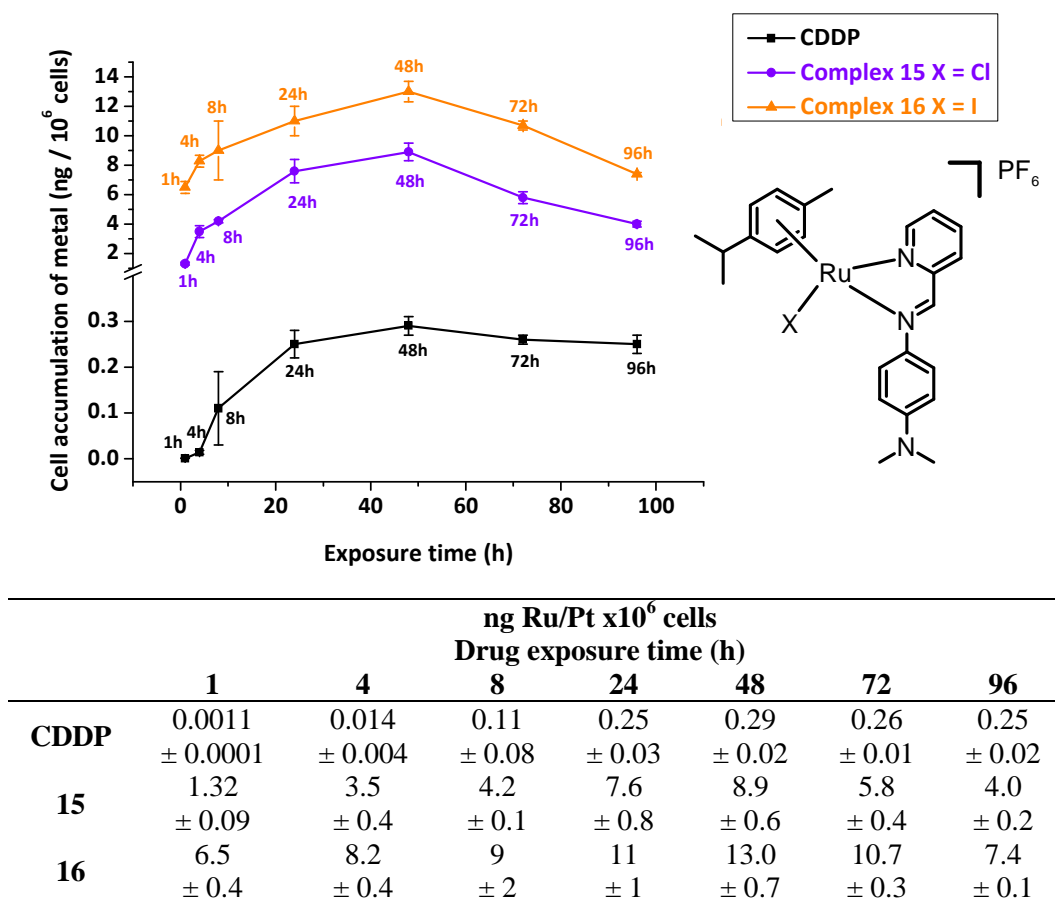
Figure 3.6. Time dependence of Ru/Pt accumulation in A2780 cells for complexes **15** (–◆–)**, 16** (–▲–) and **CDDP** (–■–) at 310 K**.** In all cases pre-incubation time before adding the drug was 48 h and cell recovery time was 72 h in drug-free medium. Concentrations used were **CDDP** = 0.4 μM, **15** = 5 μM and **16** = 1 μM.

	ng Ru/Pt x10^6 cells Temperature (K)		
	277	**293**	**310**
CDDP	N/D	0.005 ± 0.002	0.12 ± 0.03
15	0.14 ± 0.04	0.61 ± 0.06	4.6 ± 0.6
16	0.8 ± 0.1	4.1 ± 0.9	10.7 ± 0.6
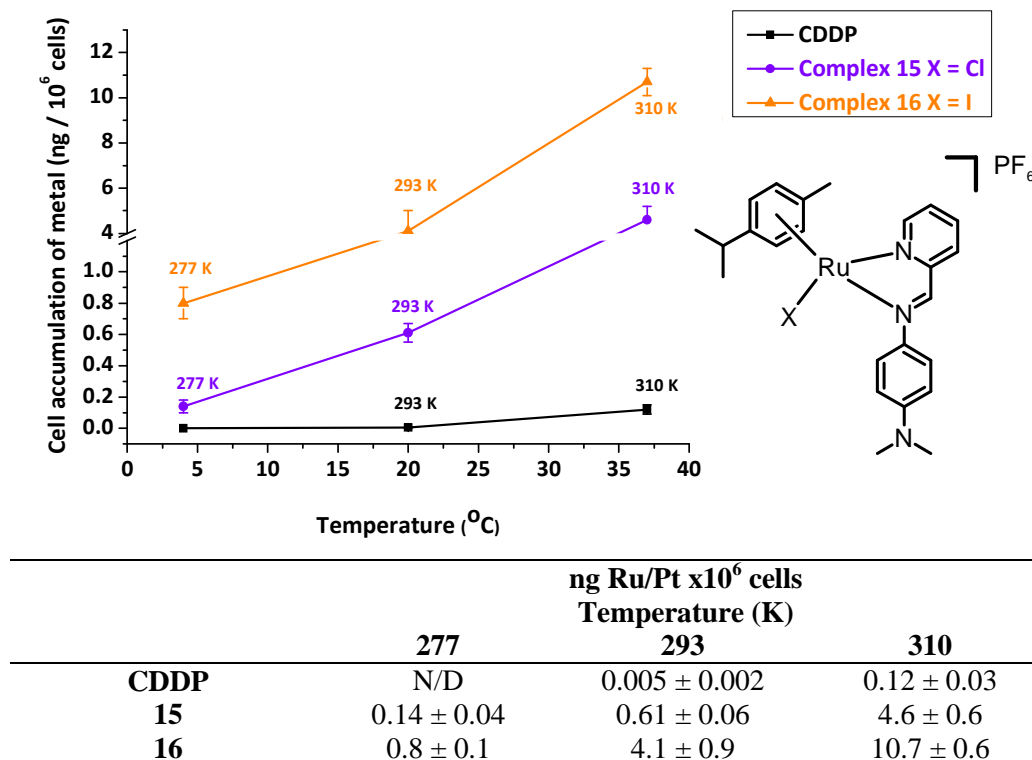
Figure 3.7. Temperature dependence of Ru/Pt accumulation in A2780 cells for complexes **15** ($-\blacklozenge-$), **16** ($-\blacktriangle-$) and **CDDP** ($-\blacksquare-$) expressed as ng of metal per 10^6 cells. Experiments were carried out using 8 h drug exposure time at 277 K, 293 K and 310 K. The experiments were also carried out at 323 K, but at this temperature no cell viability was observed. Concentrations used were **CDDP** = 0.4 µM, **15** = 5 µM and **16** = 1 µM. N/D = not detected.

Concentration dependence. The dose dependence of cellular accumulation of ruthenium for complexes **15** and **16** was determined in order to investigate whether saturation of the system was reached. These experiments were carried out using equipotent concentrations of each complex so the data are comparable. As

shown in Figure 3.8, chlorido complex **15** [Ru(η^6-*p*-cym)(*p*-Impy-NMe$_2$)Cl]PF$_6$ does not seem to saturate the uptake pathway up to more than three times its IC$_{50}$ (50 µM). At higher concentrations both ruthenium(II) complexes cause total cell death. **CDDP** does not saturate the system up to almost 10 times its IC$_{50}$ value (11.5 µM).
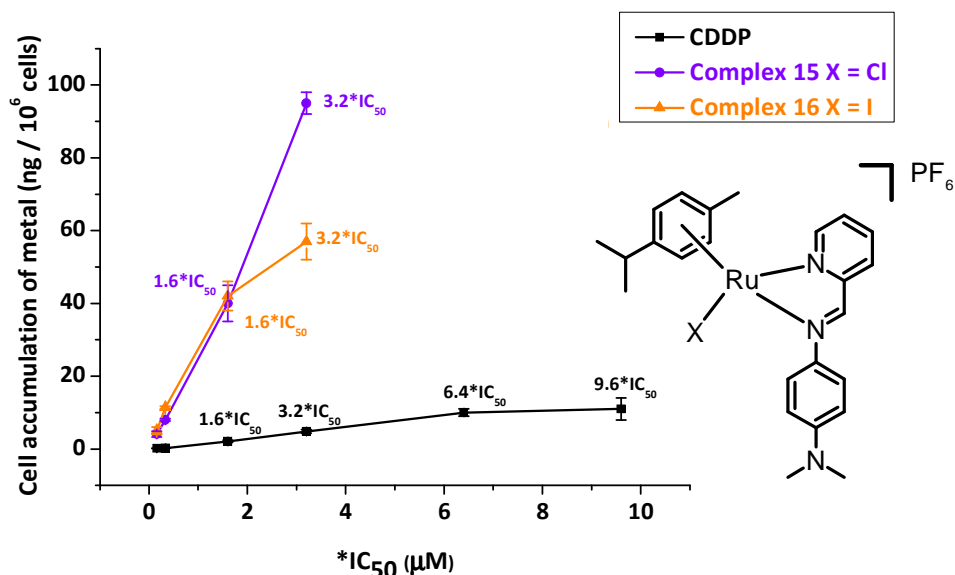
	ng Ru/Pt x10^6 cells Concentration (µM)					
	0.16 x IC$_{50}$	**0.33 x IC$_{50}$**	**1.6 x IC$_{50}$**	**3.2 x IC$_{50}$**	**6.4 x IC$_{50}$**	**9.6 x IC$_{50}$**
CDDP	0.16 ± 0.02	0.28 ± 0.05	2.1 ± 0.3	4.8 ± 0.5	10 ± 1	11 ± 3
15	4.1 ± 0.8	8.0 ± 0.3	40 ± 7	95 ± 3	N/V	N/V
16	5 ± 1	11.4 ± 0.4	42 ± 5	57 ± 6	N/V	N/V

Figure 3.8. Concentration dependence of Ru/Pt accumulation in A2780 cells for complexes **15** (−◆−), **16** (−▲−) and **CDDP** (−■−) at 310 K expressed as ng of metal per 10^6 cells. Experiments were carried out using 24 h drug exposure time, no recovery time and equipotent concentrations. N/V = no cell viability.

Extent of efflux. Total cellular accumulation of metal depends on cellular uptake and on the extent of efflux. Complexes **15** [Ru(η^6-*p*-cym)(*p*-Impy-NMe$_2$)Cl]PF$_6$ and **16** [Ru(η^6-*p*-cym)(*p*-Impy-NMe$_2$)I]PF$_6$ were used to investigate the extent of drug efflux during variable recovery times. These data are compared to the maximum cellular accumulation after 24 h exposure time studied earlier (see one-time-point one-concentration section). Results shown in Figure 3.9 indicate that even after 72 h in drug-free media, none of the ruthenium(II) complexes was completely excreted from the cell, being retained in both cases to more than 25% of the original uptake. Moreover, the extent of the efflux seems to reach a plateau after 48 h.

Inhibition of efflux. In this study complexes **15** and **16** were co-incubated with verapamil and their cellular accumulation as the amount of Ru was determined. In both cases ruthenium accumulation increased with verapamil concentration, as seen in Figure 3.10. Under normal conditions iodido complex **16** undergoes a high extent of efflux during the first 24 h of recovery, and ruthenium accumulation decreases by two thirds (from 11.5 ± 0.8 to 3.7 ± 0.2 ng of Ru per 10^6 cells). At the highest concentration of verapamil used (20 μM), Ru accumulation is reduced to only 7.2 ± 0.2 ng of Ru per 10^6 cells.
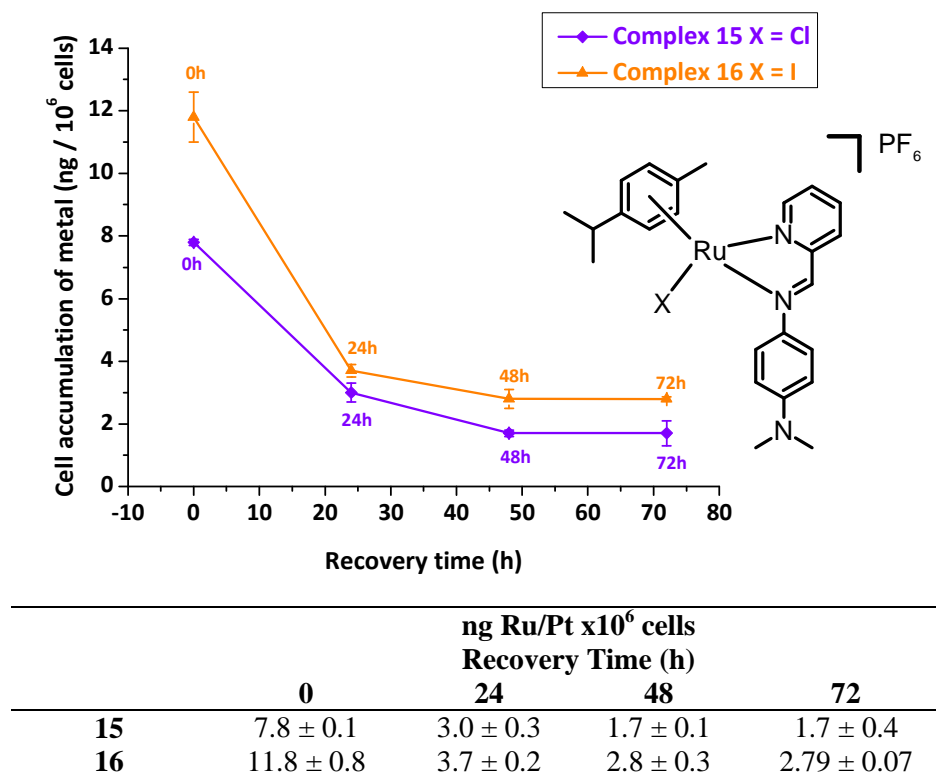
Figure 3.9. Accumulation of Ru/Pt in A2780 cells after variable recovery time for complexes **15** (–◆–) and **16** (–▲–). Extent of efflux was determined at 310 K after 0 h, 24 h, 48 h and 72 h recovery time in drug-free medium and results are expressed as ng of metal per 10^6 cells. Concentrations used were **CDDP** = 0.4 µM, **15** = 5 µM and **16** = 1 µM.

	ng Ru/Pt x10^6 cells Recovery Time (h)			
	0	**24**	**48**	**72**
15	7.8 ± 0.1	3.0 ± 0.3	1.7 ± 0.1	1.7 ± 0.4
16	11.8 ± 0.8	3.7 ± 0.2	2.8 ± 0.3	2.79 ± 0.07

		ng Ru/Pt x10^6 cells			
	Cellular Accumulation[A]	Verapamil (μM)			
		0[B]	5[C]	10[D]	20[E]
15	7.5 ± 0.5	3.0 ± 0.3	4.1 ± 0.5	4.9 ± 0.2	5.3 ± 0.4
16	11.9 ± 0.8	3.7 ± 0.2	4.8 ± 0.3	6.1 ± 0.4	7.2 ± 0.2
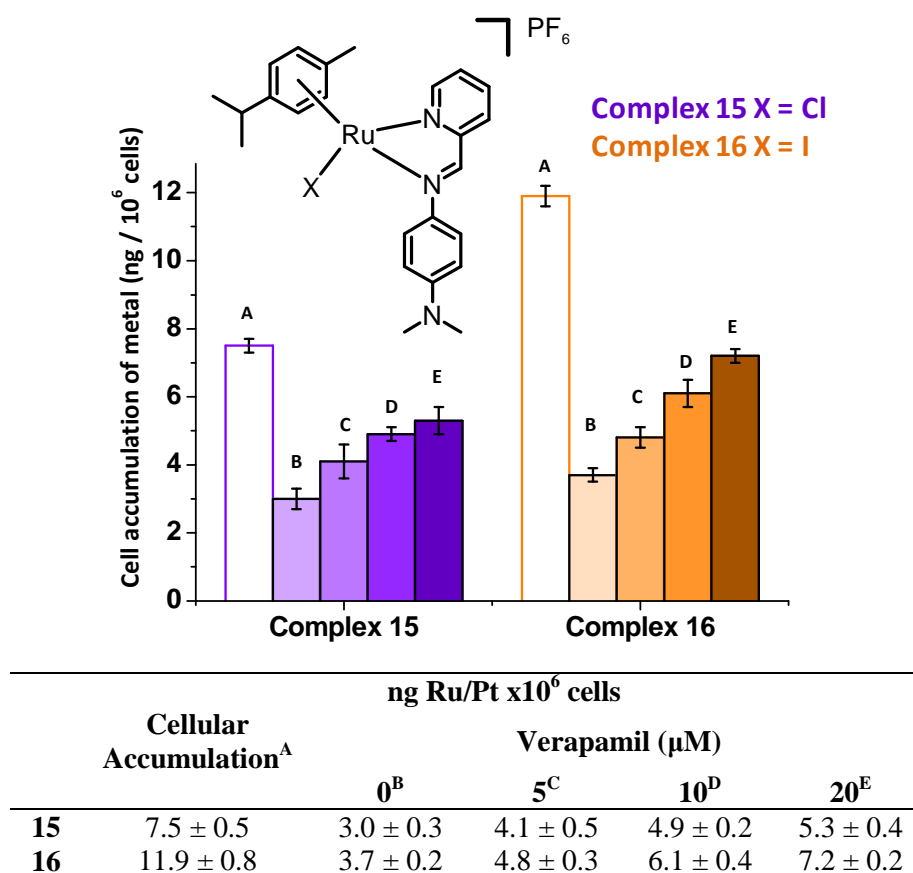
Figure 3.10. Accumulation of Ru/Pt in A2780 cells for complexes **15** (■) and **16** (■) at 310 K after co-incubation with variable concentration of verapamil. Results are expressed as ng of metal per 10^6 cells. Concentrations used were **CDDP** = 0.4 µM, **15** = 5 µM and **16** = 1 µM. In both complexes **(A)** metal accumulation with no recovery time, **(B)** metal accumulation with 24h recovery time and 0 μM verapamil, **(C)** 5 μM, **(D)** 10 μM and **(E)** 20 μM of verapamil.

Role of Na$^+$/K$^+$ pump in cellular metal accumulation, as a facilitated diffusion endocytotic pathway. In order to investigate if membrane potential plays a role in the cellular accumulation of ruthenium, cells were incubated with complexes **15**, **16** or **CDDP** and variable concentrations of ouabain. Results in Figure 3.11, show that in all cases cellular metal accumulation decreases as the ouabain

concentration increases. In the case of **CDDP**, Pt accumulation decreases to one half of its original value (to 0.12 ± 0.03 from 0.24 ± 0.05 ng of Pt per 10^6 cells). The same is true for the accumulation of ruthenium from chlorido complex **15**, which decreases from 7.5 ± 0.2 to 3.8 ± 0.3 ng of Ru per 10^6 cells, and complex 16 that decreases from 11.9 ± 0.8 to 7.5 ± 0.2 ng of Ru per 10^6 cells.

Role of CTR1 in cellular metal accumulation. Complexes **15** and **16** were co-incubated with variable amounts of copper(II) chloride to study the role on ruthenium accumulation, and therefore the involvement of the copper transporter CTR1 in the cellular uptake. Results shown in Figure 3.12 indicate that with 200 μM of Cu(II), Pt accumulation from **CDDP** is reduced by approximately 40%. At a concentration of 200 μM of Cu(II), ruthenium from chlorido complex **15** is 26% less taken up by A2780 cells, while for iodido complex **16**, uptake is reduced to a third of its original value.

Role of ATP depletion in cellular metal accumulation. Antimycin A_1, which can deplete ATP levels,[44] was used as co-incubating agent with complexes **15**, **16** and **CDDP** in order to investigate whether cellular accumulation is influenced by changes in the levels of ATP in the cell. Results shown in Figure 3.13 suggest that accumulation of platinum from **CDDP** and Ru from iodido complex **16** are unaffected after changes in ATP levels. However cellular accumulation of ruthenium from chlorido complex **15** increases markedly from 7.5 ± 0.2 to 32 ± 2 ng of Ru per 10^6 cells when co-incubated with 5μM of Antimycin.

	ng Ru/Pt x10^6 cells					
	Ouabain (µM)					
	0	**5**	**10**	**20**	**100**	**200**
CDDP	0.24 ± 0.05	0.22 ± 0.02	0.21 ± 0.04	0.27 ± 0.06	0.18 ± 0.0.5	0.12 ± 0.03
15	7.5 ± 0.2	5.7 ± 0.4	5.5 ± 0.2	5.1 ± 0.6	4.9 ± 0.6	3.8 ± 0.3
16	11.9 ± 0.3	9.7 ± 0.4	9.2 ± 0.3	8.9 ± 0.5	8.5 ± 0.4	7.5 ± 0.2
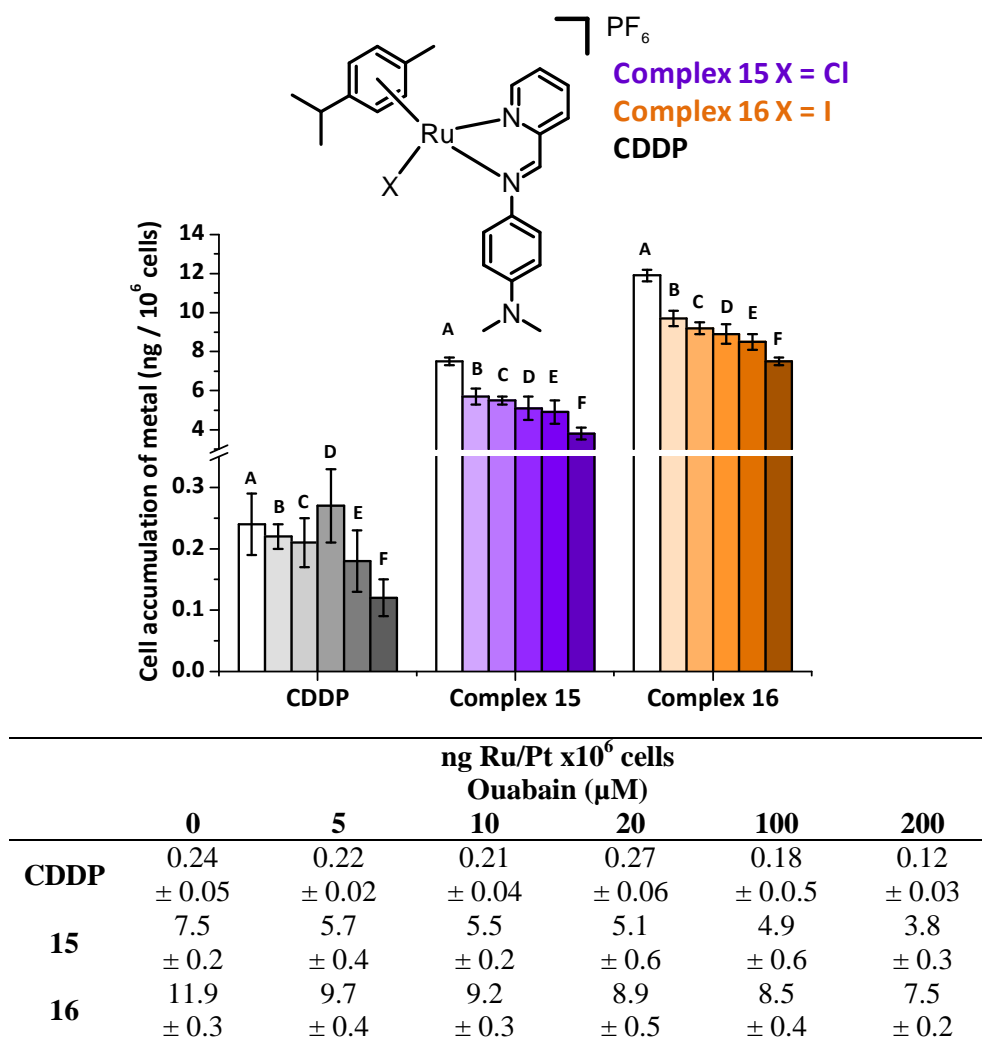
Figure 3.11. Accumulation of Ru/Pt in A2780 cells for **CDDP** (➡) complex **15** (➡) and **16** (➡) at 310 K after co-incubation with variable concentrations of ouabain. Results are expressed in ng of metal per 10^6 cells. Concentrations used were **CDDP** = 0.4 µM, **15** = 5 µM and **16** = 1 µM. For all complexes the concentrations of ouabain used were **(A)** 20 µM, **(B)** 5 µM, **(C)** 10 µM, **(D)** 20 µM, **(E)** 0.1 mM and **(F)** 0.2 mM.
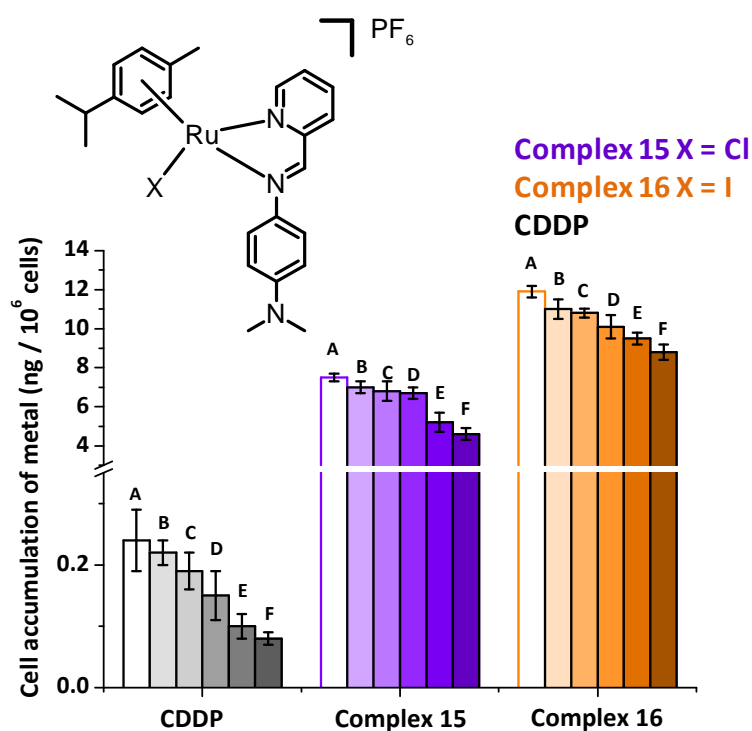
ng Ru/Pt x10^6 cells						
	Copper(II) chloride (µM)					
	0	**10**	**20**	**40**	**100**	**200**
CDDP	0.24 ± 0.05	0.22 ± 0.02	0.19 ± 0.03	0.15 ± 0.04	0.10 ± 0.2	0.08 ± 0.01
15	7.5 ± 0.2	7.0 ± 0.3	6.8 ± 0.5	6.7 ± 0.3	5.2 ± 0.5	4.6 ± 0.3
16	11.9 ± 0.3	11.0 ± 0.5	10.8 ± 0.2	10.1 ± 0.6	9.5 ± 0.3	8.8 ± 0.4

Figure 3.12. Accumulation of Ru / Pt in A2780 cell line for **CDDP** (➡), complex **15** (➡) and **16** (➡) at 310 K after co-incubation with various concentrations of Cu(II) . Results are expressed as ng of metal per 10^6 cells. Concentrations used were **CDDP** = 0.4 µM, **15** = 5 µM and **16** = 1 µM. For all complexes Cu(II) concentrations were **(A)** 0 µM, **(B)** 5 µM, **(C)** 10 µM, **(D)** 20 µM, **(E)** 0.1 mM and **(F)** 0.2 mM.

ng Ru/Pt x10^6 cells		
Antimycin A$_1$ (μM)		
	0	**5**
CDDP	0.24 ± 0.05	0.22 ± 0.02
15	7.5 ± 0.2	32 ± 2
16	11.9 ± 0.3	13.6 ± 0.4

Figure 3.13. Accumulation of Ru / Pt in A2780 cells for **CDDP** (➡), complex **15** (➡) and **16** (➡) at 310 K after co-incubation with antimycin. Results are expressed as ng of metal per 10^6 cells. Concentrations used were **CDDP** = 0.4 μM, **15** = 5 μM and **16** = 1 μM. For all complexes the antimycin concentrations were **(A)** 0 μM, **(B)** 5 μM.

Membrane disruption by amphotericin B as a model for protein-mediated uptake. Complexes **15** [Ru(η^6-p-cym)(p-Impy-NMe$_2$)Cl]PF$_6$, **16** [Ru(η^6-p-cym)(p-Impy-NMe$_2$)I]PF$_6$ and **CDDP** were co-incubated with variable amounts of amphotericin B to observe the changes in their cellular accumulation caused by the formation of pores caused by this antifungal drug. Figure 3.14 shows that platinum accumulation from **CDDP** is doubled with 10 μM amphotericin, A

similar behaviour was observed for ruthenium accumulation from the iodido complex **16**.

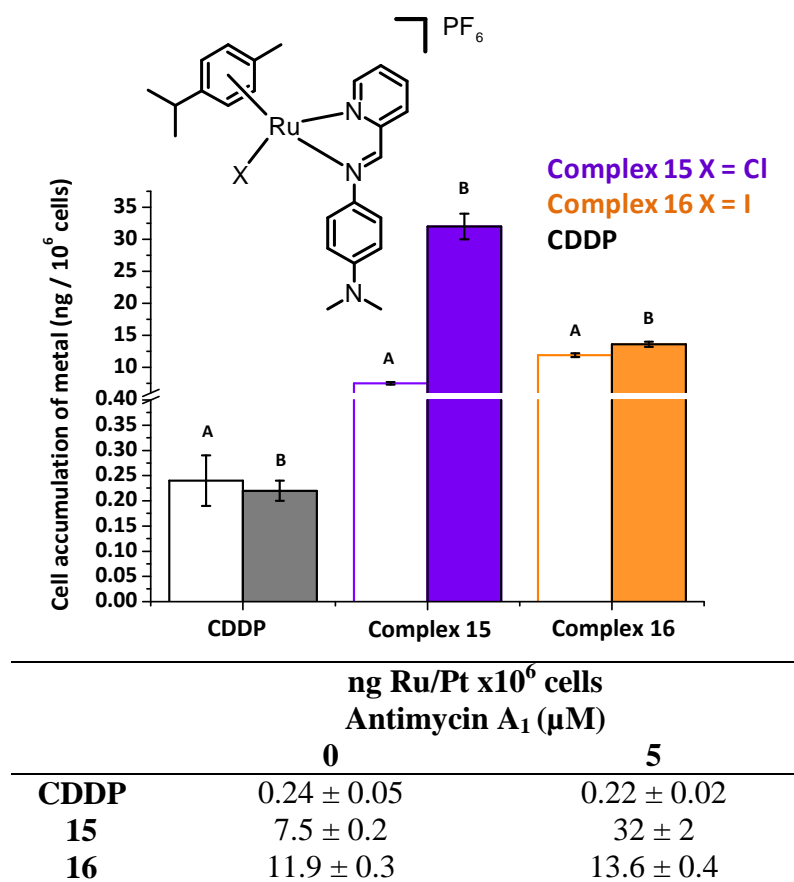| ng Ru/Pt x10^6 cells				
Amphotericin B (µM)				
	0	**1**	**5**	**10**
CDDP	0.24 ± 0.05	0.28 ± 0.03	0.35 ± 0.05	0.49 ± 0.05
15	7.5 ± 0.2	7.7 ± 0.2	9.8 ± 0.3	10.2 ± 0.5
16	11.9 ± 0.3	13.0 ± 0.4	18.5 ± 0.7	25.4 ± 0.6

Figure 3.14. Accumulation of Ru/Pt in A2780 cells for **CDDP** (➡), complex **15** (➡) and **16** (➡) at 310 K after co-incubation with various concentration of amphotericin B. Results are expressed as ng of metal per 10^6 cells. Concentrations used were **CDDP** = 0.4 µM, **15** = 5 µM and **16** = 1 µM. For all complexes amphotericin concentrations were **(A)** 0 µM, **(B)** 1 µM, **(C)** 5 µM and **(D)** 10 µM.

The role of caveolae endocytotic pathway in metal accumulation. Complexes **15**, **16** and **CDDP** were co-incubated with variable amounts of β-methyl

cyclodextrin and the changes in metal accumulation determined. These experiments were carried out in order to investigate the role of the caveolae pathway in Ru / Pt cellular accumulation. The results are shown in Figure 3.15 In all cases there is no significant change in platinum or ruthenium accumulation in cells.

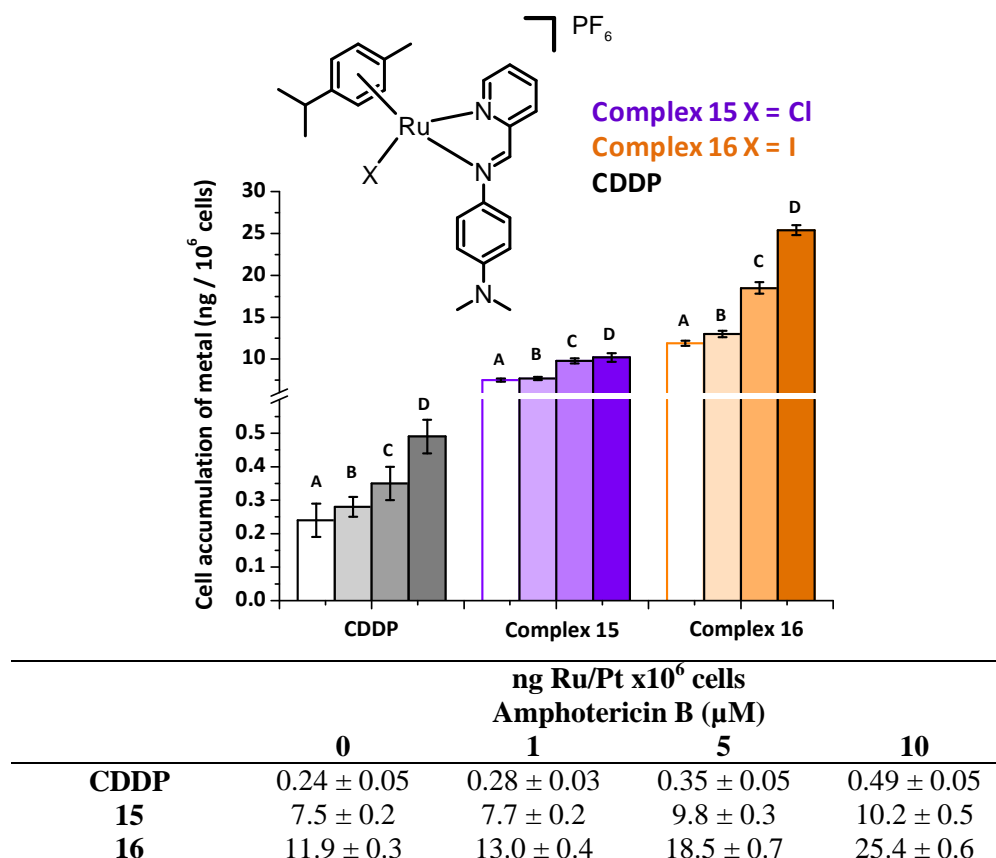| ng Ru/Pt x10^6 cells					
β-methyl cyclodextrin (μM)					
	0	**10**	**20**	**500**	**1000**
CDDP	0.24 ± 0.05	0.20 ± 0.06	0.26 ± 0.03	0.23 ± 0.05	0.27 ± 0.02
15	7.5 ± 0.2	7.8 ± 0.4	7.5 ± 0.2	7.6 ± 0.4	7.3 ± 0.3
16	11.9 ± 0.3	11.2 ± 0.5	11.9 ± 0.5	12.2 ± 0.4	12.1 ± 0.6
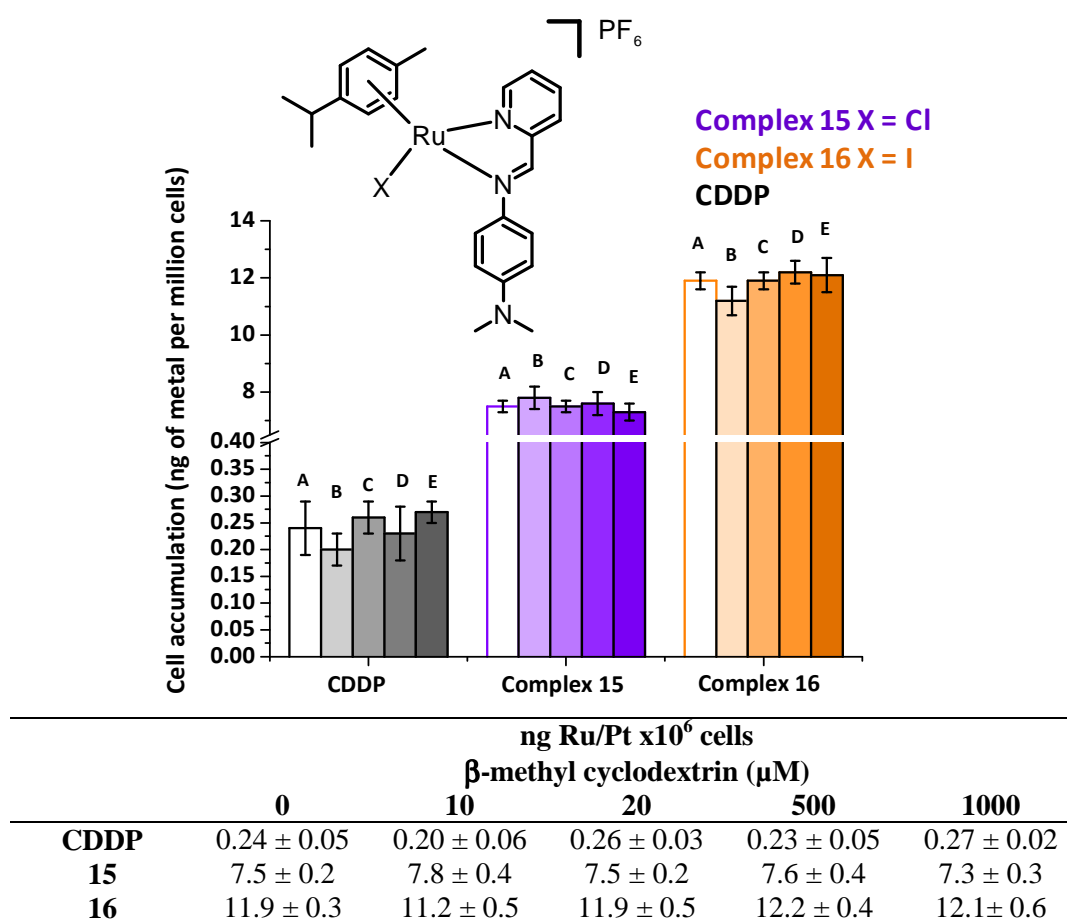
Figure 3.15. Accumulation of Ru/Pt in A2780 cells for **CDDP** (➡), complex **15** (➡) and **16** (➡) at 310 K after co-incubation with various concentratiosn of β-methyl cyclodextrin. Results are expressed as ng of metal per 10^6 cells. Concentrations used were **CDDP** = 0.4 μM, **15** = 5 μM and **16** = 1 μM. For all complexes β-methyl cyclodextrin concentrations were **(A)** 0 μM, **(B)** 10 μM **(C)** 20 μM, **(D)** 0.5 mM and **(E)** 1 mM.

3.3.4 Determination of partition coefficient (Log P)

The partition coefficients of chlorido complexes **15**, **17** and **18** were determined using the shaking-flask method. These three complexes were selected with the aim of studying the effect of changes in the arene group on the lipophilicity of the complexes. They all include the same *N,N*-chelating ligand (*p*-Impy-NMe$_2$) and the same monodentate ligand (Cl).To ensure that the complexes would not exist in the aquated form during the experiments 150 mM NaCl was added to the octanol-saturated water. Results are presented in Table 3.6. It is notable that all values obtained are negative.

Table 3.6. Log P values for ruthenium complexes **15**, **17** and **18** determined using the shaking-flask method.

	Compound	Log P
15	[Ru(η^6-*p*-cym)(*p*-Impy-NMe$_2$)Cl]PF$_6$	-0.98 ± 0.03
17	[Ru(η^6-bip)(*p*-Impy-NMe$_2$)Cl]PF$_6$	-0.34 ± 0.02
18	[Ru(η^6-*m*-terp)(*p*-Impy-NMe$_2$)Cl]PF$_6$	-0.08 ± 0.01

3.4 Discussion

3.4.1 Aqueous solution chemistry

The aquation of complexes **7** - **16** was investigated, as this step is believed to be crucial in the activation of metal pro-drugs that contain a halido ligand.[45] The aqua adducts formed after the release of the monodentate ligand, chloride and iodide in this case, are believed to be responsible for the antiproliferative activity

of piano-stool metal arene complexes, as they bind covalently to DNA causing irreparable lesions. [46]

Figure 3.16 shows that in the case of the chlorido complexes, aquation follows a clear trend that is also found for nucleobase adduct formation. The chlorido complexes exhibit extent of aquation following the order: **15 > 7 > 9 > 14 > 12 > 10.** The same order is also found in the extent of their binding to the nucleobase 9-EtG. This trend was not observed for the iodido analogues. When comparing the extent of 9-EtG binding between the chlorido and their corresponding iodido complexes (see Table 3.3), it is evident that the iodido analogues bind to a greater extent to 9-EtG regardless of the complexes' aquation. This observation can be explained as a consequence of direct substitution of the iodide by the nucleobase.

Complex	15	7	9	12	14	10
N,N- Ligand	*p*-Impy -NMe$_2$	Impy	*o*-Impy -OH	*p*-Impy -COOH	*p*-Impy- (CH$_2$)$_3$COOH	*p*-Impy -OH
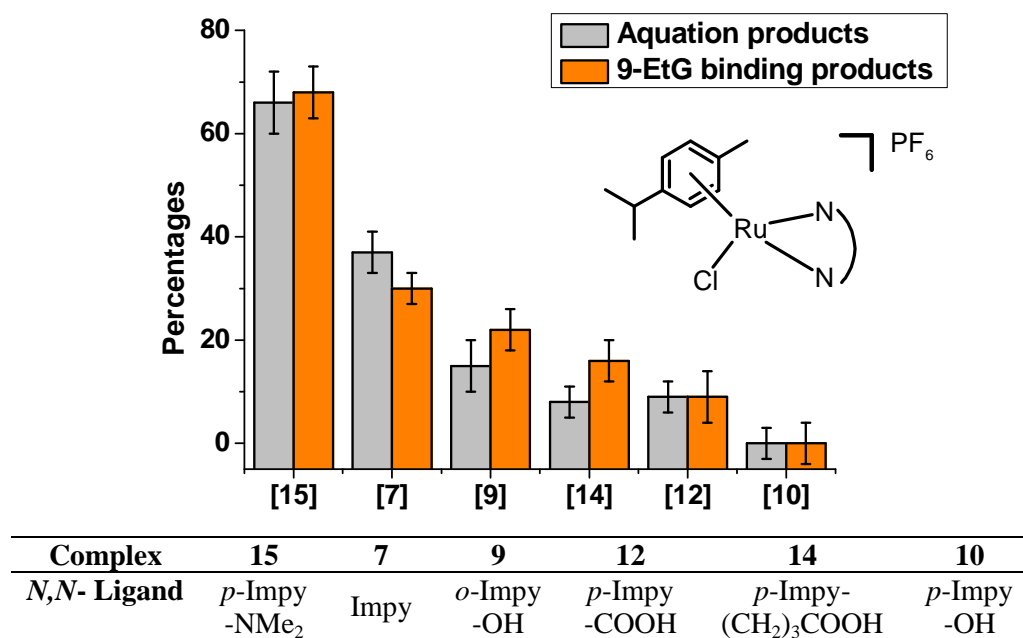
Figure 3.16. Comparison of the extent of aquation and 9-EtG binding of chlorido complexes followed by ^{1}H-NMR at 310 K.

Chlorido complexes **9** [Ru(η^6-*p*-cym)(*o*-Impy-OH)Cl]PF$_6$ and **10** [Ru(η^6-*p*-cym)(*p*-Impy-OH)Cl]PF$_6$ contain the same electron donating hydroxyl group on the Impy chelating ligand, although it is placed in different positions (*o*-substitution for complex **9,** R$_1$ and *p*-subtitution for complex **10,** R$_2$). Interestingly, there are major differences in the extent of aquation and 9-EtG binding for these complexes, which suggests that the position of the electron-donating group is highly relevant. Previous reports indicate that similar ruthenium arene complexes with chelating ligands can decompose in aqueous solution, in those cases, loss of the arene unit has been observed after the aquation has occurred.[47,48] To investigate this possibility, aqueous solutions of complexes **7-16** were kept after aquation studies and they were re-analysed after 96 h. No arene loss was detected by NMR in any of the cases.

Aquation of iodido complexes in the presence of high chloride concentration could result in the conversion to their chlorido analogues, this conversion could also be the result of direct substitution of the iodide by the chloride. However, HPLC studies show that after 24 h of incubation at 310 K, a 1:1 mixture of complexes **15** and **16** in the presence of NaCl (ca. 10X) remained unchanged as the iodido to chlorido conversion is less than 5%. This is consistent with our NMR results that indicate that complex **16** is stable after 48 h in cell culture media. A similar complex [Ru(η^6-bip)(*p*-Azpy-NMe2)I]PF$_6$ has been previously reported not to undergo conversion to its chlorido analogue after 24h. [49]
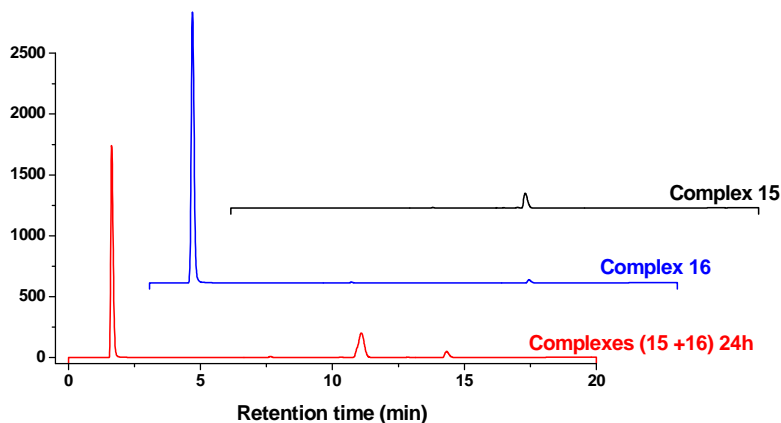
Figure 3.17. HPLC studies of complexes **15** and **16**.

3.4.2 Antiproliferative activity

Ligands **1** - **6** were tested in four cancer cell lines, A2780, A549, HCT116 and MCF7 of ovarian, lung, colon and breast tissue origin, respectively. In all cases the chelating imine ligands were found to be inactive (IC_{50} values > 200 μM). Chlorido complexes **12** [Ru(η^6-p-cym)(p-Impy-COO)Cl]PF$_6$ and **14** [Ru(η^6-p-cym)(p-Impy-(CH$_2$)$_3$COO)Cl]PF$_6$ were also inactive in all cell lines. These compounds include in their structure ligands **4** p-Impy-COOH and **5** p-Impy-(CH$_2$)$_3$COOH which have electron withdrawing groups (-COOH) in position R$_2$. The activity of complex **12** seems to be enhanced when the monodentate ligand in the complex is changed from chloride to iodide. This observation is also true when comparing the analogous complexes **7** [Ru(η^6-p-cym)(Impy)Cl]PF$_6$ and **8**

$[Ru(\eta^6\text{-}p\text{-cym})(Impy)I]PF_6$ which have Impy as their chelating ligand. The antiproliferative activity increases from 160 μM in A2780 ovarian cancer cells for the chlorido complex **7** to 73 μM for the corresponding iodido analogue **8**, the same effect is observed in all cell lines (see Table 3.4).

The active complexes in these series, contain electron-donating groups such as -OH and -NMe$_2$, as substituents on the phenyl ring of the imine ligand (in position R$_2$). The effect of the moderately activating hydroxyl group differs according to the position in the phenyl ring of the imine ligand. Comparing chlorido complexes **9** $[Ru(\eta^6\text{-}p\text{-cym})(o\text{-Impy-OH})Cl]PF_6$ and **10** $[Ru(\eta^6\text{-}p\text{-cym})(p\text{-Impy-OH})Cl]PF_6$, the *ortho-* substituent, R$_1$, generates a more active complex than the *para-* substituent, R$_2$. The most active complexes include ligand **6** which has the strongest electron donating group -NMe$_2$ in position R$_2$. These compounds have antiproliferative activities comparable to **CDDP** in A2780 ovarian, HCT116 colon and MCF7 breast cancer cells.

The above trend relating the nature of the substituents to the biological activity of the complexes is consistent as well with the extent of nucleobase binding as shown in Figure 3.18. Results in A2780 ovarian and MCF7 breast cell lines show that iodido complexes **8**, **10**, **13** and **16** exhibit a higher extent of binding to 9-EtG and are always more active than their respective chlorido analogues **7**, **11**, **12** and **15**, respectively. Complexes **10**, **12** and **14** particularly, are inactive in all cell lines and bind only weakly to 9-EtG (extent 0 - 16%). Complex **13** $[Ru(\eta^6\text{-}p\text{-cym})(p\text{-Impy-COO})I]PF_6$, which include an electron-withdrawing substituent and iodide as monodentate ligand is more active than its chlorido analogue **12**

$[Ru(\eta^6\text{-}p\text{-cym})(p\text{-Impy-COO})Cl]PF_6$ and it binds to a greater extent to 9-EtG. Once again, *ortho-* substitution, R_1 with an electron-donating group improves interaction with the nucleobase, thereby increasing its activity. Finally the most active complexes **15** and **16**, that include the group NMe_2 in position R_2 bind to 9-EtG to a greater extent in this series.

Protocols published in the literature to determine the antiproliferative activity vary considerably regarding the length of the drug exposure time, ranging between 24 to 96 h.[50–52] However, the protocol used to determine the IC_{50} values reported here (see Chapter 2), includes a drug exposure period of 24 h. Complexes **15** $[Ru(\eta^6\text{-}p\text{-cym})(p\text{-Impy-NMe}_2)Cl]PF_6$, **16** $[Ru(\eta^6\text{-}p\text{-cym})(p\text{-Impy-NMe}_2)I]PF_6$ and **CDDP** were used to investigate the dependence of biological activity on the length of drug exposure time and to confirm that 24 h was the optimum period. For this, A2780 ovarian cells were exposed to the ruthenium complexes for a variable number of hours. Figure 3.5 in page 91, showed that there is a difference in the antiproliferative activity between 8 and 24 h of drug exposure, however longer exposure times have no significant effect after 24 h. A stability plateau is reached at 72 h of exposure. This confirms that the protocol used to determine IC_{50} values is optimised.
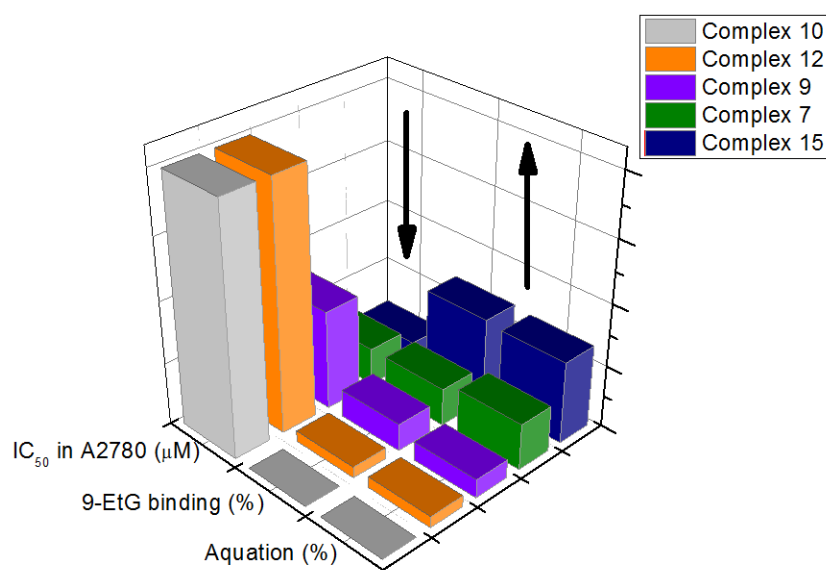
Complex	15	7	9	12	10
N,N- Ligand	*p*-Impy-NMe$_2$	Impy	*o*-Impy-OH	*p*-Impy-COOH	*p*-Impy-OH

Figure 3.18. Relation between aquation, 9-EtG binding and antiproliferative activity in A2780 cells for chlorido complexes

3.4.2.1 Metal accumulation in cancer cells

The extent of the ruthenium accumulation in A2780 ovarian cancer cells was determined using equipotent concentrations (IC$_{50}$/3) of complexes **7**-**16**. Results in Table 3.5 on page 88 indicate that there is no correlation between the amount of ruthenium that is found in the cells after a 24 h drug exposure period and the potency of the complexes as anticancer agents (Figure 3.19). For example iodido complex **11** [Ru(η^6-*p*-cym)(*p*-Impy-OH)I]PF$_6$ exhibited high accumulation, reaching intracellular concentrations of 28 ± 2 ng Ru per 10^6 cells, however it is only moderately active, with an IC$_{50}$ value of 48 ± 2 μM. Meanwhile chlorido complex **15** [Ru(η^6-*p*-cym)(*p*-Impy-NMe$_2$)Cl]PF$_6$ only reaches concentrations of

7.8 ± 0.5 ng Ru per 10^6 cells, but is considerably more active towards A2780 cells (IC_{50} 16.2 ± 0.9 µM). This indicates that the cytotoxic effects caused by complex **15** inside A2780 cells are more efficient than those caused by complex **11**. Such observations have been previously reported for other related ruthenium arene complexes.[53]
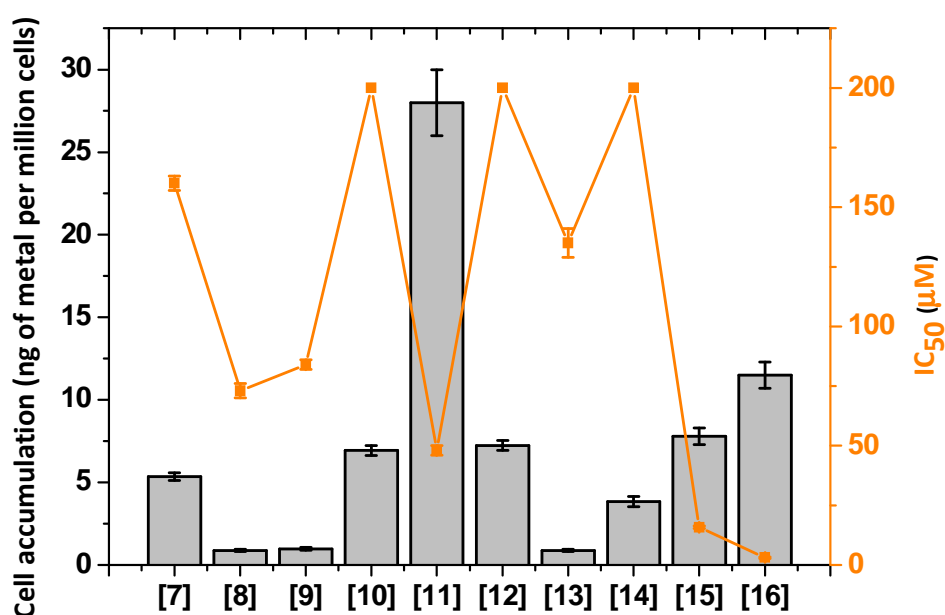
Figure 3.19. Comparison between cellular accumulation (left axis) and antiproliferative activity (right axis) of ruthenium complexes **7**-**16.**

Ruthenium accumulation from chlorido complexes cannot be related to the complexes ability to form aqua adducts as it is known that extracellular concentrations of chloride (100 mM in blood plasma) would not allow this process to occur. In fact, it is accepted that **CDDP** only hydrolyses after it has been taken up into the cell,[54,55] as intracellular chloride concentration only reaches

22.7 mM.[56] Also, in the previous section it has been shown that complex **7** does not undergo aquation in cell culture medium after 24h.

Hydrophobicity is often associated with cellular uptake and therefore with metal accumulation. In the case of complexes **7**-**16** there are no differences in the number of aromatic rings present, nor in the arene unit, nor in the *N,N*-chelating ligand. As a consequence, it is expected that their log P values should not vary significantly as to determine different patterns in metal accumulation. Calculation of the partition coefficient of ligands **1**-**6** using XLOGP3[57] software confirms that there is no significant variations amongst the ligands (value range 3.84 to 4.81) as shown in Table 3. 7. This is consistent with the idea of no significant changes in the log P values of complexes **7**-**16.**

Table 3. 7. Calculated Log P values for ligands **1**-**6**.

	Ligand	Calculated Log P
1	Impy	4.81
2	*o*-Impy-OH	3.84
3	*p*-Impy-OH	4.09
4	*p*-Impy-COOH	4.39
5	*p*-Impy-$(CH_2)_3$COOH	4.69
6	*p*-Impy-NMe_2	4.57

3.4.2.2 Pathways involved in cellular uptake and accumulation

For following cellular uptake studies, only complexes **15** [Ru(η^6-*p*-cym)(*p*-Impy-NMe_2)Cl]PF_6 and its iodido analogue **16** [Ru(η^6-*p*-cym)(*p*-Impy-NMe_2)I]PF_6 were used and compared to the corresponding data for **CDDP.** These two compounds

were selected because of their structural similarities and with the aim to study the effect of the monodentate ligand on the cellular uptake behavior.

Mechanisms of cellular Pt uptake from cisplatin and cellular accumulation of Pt have been widely investigated,[11,14] however little is known about analogous pathways involved in the uptake of half-sandwich ruthenium anticancer complexes.[58] One of the aims of the research presented in this Chapter was to gain a more in-depth understanding of this crucial step. It has been reported that **CDDP** uptake is linear with respect to time in the first 60 min of drug exposure,[37] however the present investigation involves a longer time frame. A2780 ovarian cells were exposed to complex **15**, its iodido analogue complex **16** and **CDDP** at seven different time points ranging from 1 h to 96 h. In all cases, maximum metal cellular accumulation occurs between 24 - 48 h of drug exposure, after this time, the amount of Pt / Ru decreases slightly, indicating that influx/efflux equilibrium may have been reached. The **CDDP** accumulation seems to reach a concentration plateau at 96 h as shown in Figure 3.6 on page 95.

The temperature dependence of the cellular uptake and accumulation of Ru was also investigated. Experiments were carried out at three different temperatures, 277 K, 295 K and 310 K. As shown in Figure **3.7**, on page 95, **CDDP** influx is nonexistent at the lowest temperature (277 K), this is consistent with previous reports which indicate that **CDDP** uptake is energy dependent.[59] As expected for an energy dependent process, **CDDP** influx begins at 295 K and increases as the temperature is raised to 310 K (from 0.005 ± 0.002 ng of Pt to 0.12 ± 0.03 ng of Pt per 10^6 cells). Ru accumulation curves for complexes **15** and **16** are very different.

Although an increased uptake is accompanied by an increase in temperature, ruthenium complex **16** exhibits significant energy independent uptake at 277 K (0.8 ± 0.1 ng of Ru per 10^6 cells).

Another important factor investigated was the saturation of the cellular uptake with increasing drug concentration. Experiments were carried out at equipotent concentrations of complex **15**, **16** and **CDDP**. Figure 3.8, on page 96 shows that **CDDP** uptake is slowed down after reaching 6.4 x IC_{50} concentration values (7.6 mM) as the gradient of the graph decreases, but does not reach a plateau. This is consistent with previous reports that indicate that **CDDP** accumulation does not saturate up to 100 μM.[17] Meanwhile, ruthenium complexes exhibit a much sharper gradient, indicating that concentrations of up to 3.2 x IC_{50} values do no cause saturation of the uptake pathways. It is also relevant that at concentrations equal to 6.4 x IC_{50} and 9.6 x IC_{50} total cell death was observed. Therefore the exact saturation of Ru concentration could not be established.

Cellular accumulation of metal (Ru/Pt) arises as the result of the equilibrium of two important processes: cellular uptake and cellular efflux. The latter is especially important in antiproliferative activity measurements that involve a cell recovery period in drug-free media. The extent of the efflux of Ru for complexes **15** [Ru(η^6-*p*-cym)(*p*-Impy-NMe$_2$)Cl]PF$_6$ and its iodido analogue **16** was investigated over time. For this, A2780 ovarian cells were exposed to the ruthenium complexes for 24 h and then left to recover at various periods of time. Figure 3.9 on page 98, shows that although there is a significant efflux during the first 24 h of recovery, the concentration of metal retained in the cells reaches a

plateau after 48 h with no marked difference between 24 and 48 h. Most important of all, at the lowest metal concentration point, at least 25% of the original ruthenium is retained.

One of the most important mechanisms of resistance of anticancer pharmaceuticals involves impaired cellular accumulation as a result of an increased extent of efflux.[60] Therefore investigating the mechanism of efflux of a drug can provide insights into the mechanism of resistance. Verapamil, an L-type calcium channel blocker shown in Figure 3.20 effectively abrogates P-gp mediated active efflux of anticancer drugs in ovarian cancer cells by competitive inhibition of drug transport and is capable of reversing multi-drug resistance.[61,62] Although it is not fully understood how verapamil interacts with P-gp to decrease cellular efflux, it has been reported that 50 μM of verapamil is capable of restoring doxorubicin sensitivity in MDR cell lines[61] by blocking active efflux.[63] Accordingly, complexes **15** and **16** were used to investigate the extent of Ru efflux when cells are allowed to recover in drug-free media that contains verapamil.
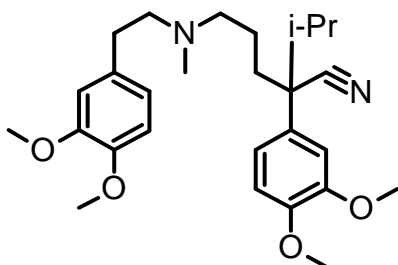
Figure 3.20. Structure of verapamil.

Results shown in Figure 3.10 on page 99, indicate that by increasing the concentration of verapamil it is possible to impair the efflux process of ruthenium complexes **15** and **16**. This result is especially important for chlorido complex **15** which is retained by more than 70% in the presence of 20 μM of this calcium channel blocker. This result is consistent with P-gp taking part in the efflux of complex **15**. However, it is remarkable that preliminary molecular docking calculations[21] carried out for ligands **1-6** seem to indicate that they are not P-gp substrates.

The involvement of P-gp in ruthenium complexes resistance has been demonstrated previously, as it is possible to achieve restoration of the sensitivity to this type of metal complexes by use of verapamil.[6] Particularly, sensitivity to RM175, (Figure 3.21) is restored by verapamil in adriamycin resistant A2780AD cells.[61] Verapamil does not restore **CDDP** sensitivity, as it is not recognized by P-gp.[64]
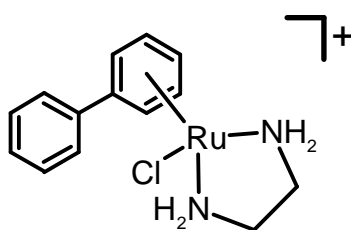
Figure 3.21. Structure of RM175.

Polar molecules cannot diffuse freely through the cell membrane; instead, they need to rely on membrane proteins or membrane channels to reach the interior of

cell compartments. One of these proteins in the plasma membrane is the sodium-potassium adenosine triphosphatase enzyme or Na^+/K^+ pump which is responsible for maintaining cellular volume and most important of all for maintaining the resting potential of the cell.[14,17,65,66] The function of this pump can be altered by the use of ouabain (Figure 3.22) which reduces the sodium gradient across the cell membrane causing the membrane potential to change.[67] There are no previous reports that investigate the effect of co-administering ouabain and ruthenium drugs. To analyse cellular accumulation of Ru under these conditions, complexes **15** [Ru(η^6-*p*-cym)(*p*-Impy-NMe$_2$)Cl]PF$_6$ and **16** [Ru(η^6-*p*-cym)(*p*-Impy-NMe$_2$)I]PF$_6$ were co-incubated with 5 µM, 10 µM, 20 µM, 0.1 mM or 0.2 mM of ouabain. Corresponding data for **CDDP** was also obtained.
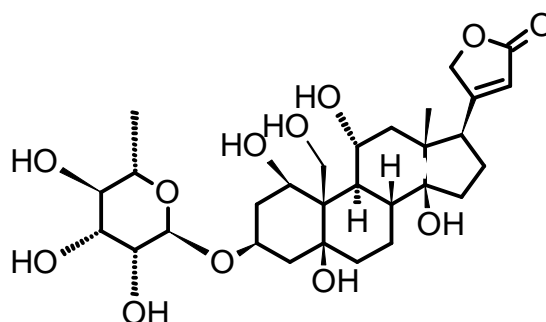
Figure 3.22. Structure of ouabain

Results in Figure 3.11 on page 101, show that in the case of complexes **15** and **16** co-incubation with the cardiac glycoside, ouabain, impaired metal cellular accumulation. Ru accumulation from complex **15** decreases from 7.5 ± 0.2 ng of Ru to 3.8 ± 0.3 ng of Ru per 10^6 cells when co-incubated with 200 µM of

ouabain. In the case of complex **16,** its metal accumulation decreases from 11.9 ± 0.3 ng of Ru to 7.2 ± 0.2 ng of Ru per 10^6 cells when co-incubated with the same concentration of ouabain. These results suggest that there may be a percentage of the cellular uptake pathway of these ruthenium complexes that relies on facilitated diffusion and in particular that is dependent on the membrane potential.

Figure 3.11 on page 101, also shows the corresponding results for **CDDP** co-incubation with ouabain. As expected from previous reports,[17,37] cisplatin uptake is also reduced with increasing concentrations of ouabain, changing from 0.24 ± 0.05 ng of Pt to 0.12 ± 0.05 ng of Pt per 10^6 cells when co-incubated with 200 μM of the glycoside. Although this mechanism is still not very clear, previous reports propose that the sodium gradient in the membrane determines the facilitated transport of **CDDP** into the cells.[14,68] This suggests that **CDDP** transport is dependent on the membrane potential, therefore any agent that affects the electrochemical gradient in the cell could potentially modify the **CDDP** uptake.[59] The use of ouabain to modify the action of the Na^+/K^+-ATPase pump impairs **CDDP** cellular accumulation.[11] This effect is indeed caused by changes in the electrochemical gradient and not because the pump itself transports the drug into the cell.[59]

Cellular accumulation of **CDDP** has been linked to copper transport pathways in mammalian cells.[36,69] Hence, complexes **15** and **16** were co-incubated with various concentration of a copper(II) salt with the aim of investigating whether CTR1 is also involved in the transport of these complexes across the cellular

membrane. Corresponding data for **CDDP** was also obtained for comparison purposes.

Results suggest that the CTR1 pathway may also be involved in the uptake of ruthenium complexes **15** and **16**. Figure 3.12 on page 101 shows that chlorido complex **15** exhibits a 26% decrease in its accumulation in the presence of the highest concentration of copper used (0.2 mM). The results for complex **16** are still more striking as Ru accumulation is lowered by 33% of its original value (from 11.9 ± 0.3 ng of Ru per 10^6 cells to 8.8 ± 0.4 ng of Ru per 10^6 cells when coincubated with 200 µM of $Cu^{(II)}$).

A2780 ovarian cancer cells were also co-incubated with **CDDP** together with various concentrations of a copper(II) salt that ranged between 10 µM, and 0.2 mM. Under these conditions Pt accumulation from **CDDP** was reduced from 0.24 ± 0.05 ng of Pt to 0.08 ± 0.01 ng of Pt per 10^6 cells, a reduction in accumulation of 40%. Previous reports indicate that CTR1 regulates **CDDP** toxicity by regulating **CDDP** uptake[70] and that the expression of CTR1 alters sensitivity to **CDDP** and other platinum- containing anticancer drugs.

Although the full extent of this transport remains poorly understood, recent developments in NMR analysis show that **CDDP** binds to the methionine sulfur atoms on extracellular CTR1, which might involve the formation of monosulfur adducts (*cis*-$[PtCl(Met)(NH_3)_2]^+$) that facilitate the transport and activation of the drug.[71] This could also be an activation step involved in the antiproliferative

mechanism of other metal based- chemotherapeutic drugs such as ruthenium arene complexes.

Some energy dependent pathways can be inhibited by lowering the levels of ATP. Such reduction of ATP concentrations can be achieved by co-administering antimycin A, shown in Figure 3.23, which is a mitochondrial ATP synthesis inhibitor that interferes with oxidative phosphorylation.[44] In order to investigate the role of ATP depletion on cellular accumulation of Ru, complexes **15** and **16** were co-incubated with 5 μM of antimycin A. These experiments were also carried out using **CDDP**.
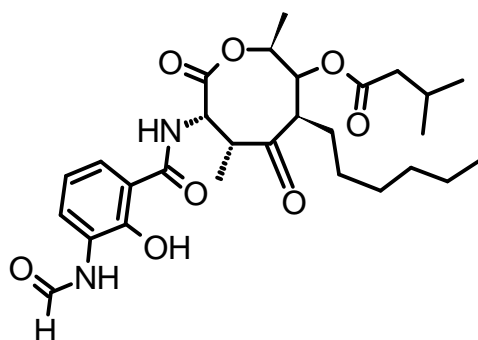
Figure 3.23. Structure of antimycin A.

It is expected that if the cellular uptake process of complexes **15** and **16** was ATP dependent, its depletion should cause a decrease in Ru cellular accumulation. However, only a small, non significant variation is observed in the cellular accumulation of Ru from complex **16** [Ru(η^6-*p*-cym)(*p*-Impy-NMe$_2$)I]PF$_6$ (Figure 3.13, on page 103). These results suggest a significant extent of ATP- independent

uptake. This is consistent with cellular accumulation results when the uptake process takes place at low temperatures (277 K) (see temperature- dependence above). The figure also shows a major increase in cellular accumulation of ruthenium for complex **15** [Ru(η^6-*p*-cym)(*p*-Impy-NMe$_2$)Cl]PF$_6$, this behaviour suggests that an ATP-dependent efflux pump is involved in the detoxification of this complex. This is consistent with the possibility of an ABC transporter, such as the MRP2 pump being involved in complex **15** efflux. MRP2 pump is inhibited by antimicyn caused- ATP depletion, therefore its inhibition could allow intracellular Ru concentrations to increase. The ATP-dependent pump has been reported to be involved in the efflux of **CDDP** conjugated to glutathione and to several multidrug resistance mechanisms.[73]

Figure 3.13, on page 103 also shows that co-incubation of A2780 cells with **CDDP** and 5 μM of antimycin A does not reduce Pt uptake significantly (from 0.24 ± 0.05 ng of Pt per 10^6 cells to 0.22 ± 0.02 ng of Pt per 10^6 cells). Such observation could be interpreted as inconsistent with the results shown above, regarding the temperature-dependence of **CDDP** uptake. Although it is reported that antimycin (1.5 µM) can achieve 90% of ATP depletion in LLC-PK cells (Pig kidney cells) when exposed for 5h,[72] the present work did not include the determination of ATP levels in A2780 ovarian cells. It is possible that the depletion in this case was not effective enough to cause an observable decrease in the **CDDP** uptake. The use of antimycin causes striking results when used with carboplatin, as it is possible to inhibit 90% of its uptake in the BEL-7404 cell line

by using 50 μg/mL of antimycin A.[44] However it is important to recognise that the concentrations needed for efficient ATP depletion are cell-dependent.

Enhanced protein-mediated transport across cell membranes has been reported as a means of increasing cellular accumulation.[74] Consequently, the role of protein-mediated transport in the cellular accumulation of Pt and Ru drugs was investigated. Complexes **15**, **16** and **CDDP** were co-incubated with variable concentrations of amphotericin B (Figure 3.24) which forms pores in the cellular membrane.[41,75–77]
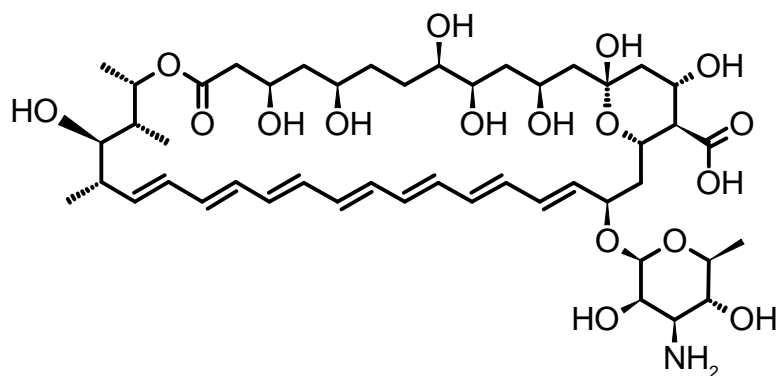
Figure 3.24. Structure of amphotericin B.

These pores, permeable to water and non-electrolytes, may allow increased influx and therefore higher cellular accumulation of the chemotherapeutic drugs. Experimental results of co-incubation with amphotericin B (Figure 3.14 on page 104) show that there is no significant variation in the cellular accumulation of Ru from complex **15** [Ru(η^6-p-cym)(p-Impy-NMe$_2$)Cl]PF$_6$, suggesting that facilitated diffusion may not be involved in the uptake pathway of this complex. In contrast,

cellular accumulation of Ru from complex **16** [Ru(η^6-*p*-cym)(*p*-Impy-NMe$_2$)I]PF$_6$ is enhanced from 11.9 ± 0.3 ng of Ru per 10^6 cells to 25.4 ± 0.6 ng of Ru per 10^6 cells by the use of 10 μM of amphotericin B, supporting results that involve passive diffusion of this complex through the cell membrane (See temperature-dependence of cellular uptake above).

Results in Figure 3.14 on page 104 also show that **CDDP** accumulation increases from 0.24 ± 0.05 ng to 0.49 ± 0.05 ng of Pt per 10^6 cells. This is consistent with previous reports that indicate that amphotericin B increases **CDDP** cellular accumulation [41,14] This effect of amphotericin B on **CDDP** accumulation has been used to reverse resistance in non-small cell lung cancer.[17] Although when **CDDP** resistance develops, cells may also develop resistance to amphotericin B, 5-fluorouracil and aphidicolin.[78]

Finally, the role of caveolae endocytotic pathway in cellular metal accumulation was explored. Complexes **15**, **16** and **CDDP** were co-incubated with increasing concentrations of β-methyl cyclodextrin. Results shown in Figure 3.15 on page 105, indicate that this endocytotic pathway is not involved either in the uptake of Pt from **CDDP** nor in the uptake of Ru for complexes **15**, **16** as there are no significant changes in metal cellular concentration when increasing concentrations of β-methyl cyclodextrin are used.

3.4.2.3 Effects of changing the arene.

Relationship between log P values and cellular

accumulation

Hydrophobicity is also thought to play an important role in the antiproliferative activity of a given drug.[79] Increments in this factor have been related to enhanced cellular uptake and therefore enhanced cellular accumulation.[80] Negative Log P values indicate higher solubility of a given compound in water than in octanol. This can affect its transport through cellular membranes. Complex **15** [Ru(η^6-*p*-cym)(*p*-Impy-NMe$_2$)Cl]PF$_6$, has been studied in comparison to complexes **17** [Ru(η^6-bip)(*p*-Impy-NMe$_2$)Cl]PF$_6$ and **18** [Ru(η^6-*m*-terp)(*p*-Impy-NMe$_2$)Cl]PF$_6$. All three compounds bear the same imine **6,** *p*-Impy-NMe$_2$ as ligand and they all have chloride as their monodentate ligand. However, in this series, the number of phenyl rings in the arene unit varies. As expected, the increase in aromatic rings in the structure results in higher hydrophobicity, although they all have negative Log P values.

Figure 3.25, compares Log P values and the corresponding cellular accumulation data. Although hydrophobicity decreases in the series **18** > **17** > **15** it is observed that there is a significant drop in Ru concentration for complex **18**, which indicates that the shape of the arene unit might play a significant role in cellular uptake. However, it is interesting that complex **18** with the lowest cellular accumulation of the series (4.6 ± 0.2 ng of Ru per 10^6 cells) has the greater potency against A2780 ovarian cells (IC$_{50}$ = 2.1 ± 0.2 μM) while complex **17** which is highly taken up (10.2 ± 0.3 ng of Ru per 10^6 cells) is only moderately

active in the same cell line ($IC_{50} = 38 \pm 2$ µM). This shows that the antiproliferative mechanism of complex **18** is more efficient than that of **17**.
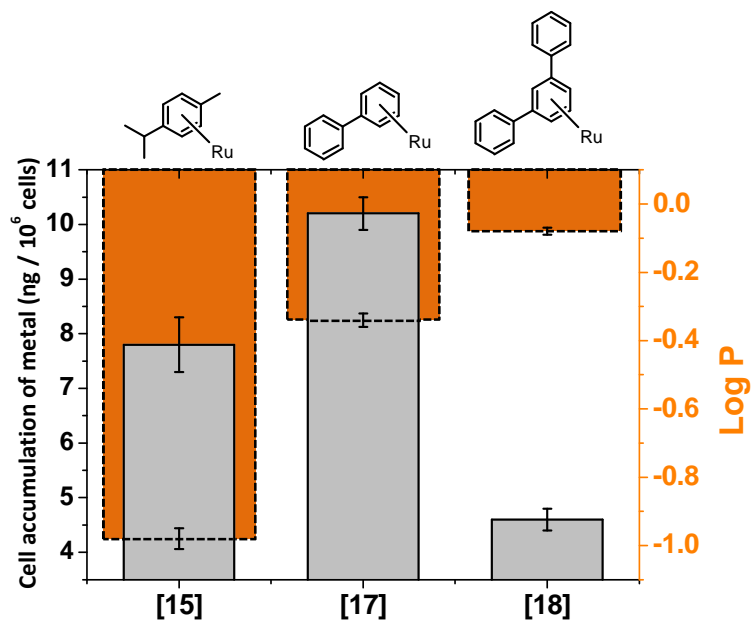
Figure 3.25. Comparison of total cellular accumulation for complexes **15, 17** and **18** in A2780 ovarian cell line expressed in ng of metal per million cells against the corresponding Log P values.

3.5 Conclusions

This study shows that ruthenium(II) Impy complexes that include in their structure (as R_2 substituents) electron-donating groups such as NMe_2 are more active towards cancer cell lines (A2780, A549, HCT116 and MCF7) than those which include electron withdrawing groups (COOH, C_3H_6COOH). Also, is has been demonstrated that there is a correlation between the presence of these groups and the extent of aquation exhibited by the complexes after 24 h. The same correlation can be drawn to include the ability of the complexes to bind to 9-EtG as a nucleobase model. Further analysis on the interaction of Ru(II) half-sandwich complexes with DNA is included in Chapter 4. Potency of the complexes towards A2780 cell lines does not correlate with their cellular accumulation, showing that, the different ruthenium arene complexes may use different antiproliferative pathways (See Chapter 5).

Complexes **15** [Ru(η^6-p-cym)(p-Impy-NMe$_2$)Cl]PF$_6$ and **16** [Ru(η^6-p-cym)(p-Impy-NMe$_2$)I]PF$_6$ were used to investigate the possible pathways for cellular accumulation in comparison with **CDDP** in A2780 ovarian cancer cells. These two complexes were chosen as they have in common the arene unit (p-cym) an the *N,N*-chelating ligand (p-Impy-NMe$_2$) with the aim to investigate the role of the halide ligand in determining the cellular uptake mechanism involved. It was demonstrated that maximum Ru accumulation from both complexes occurs between 24 h and 48 h of exposure. Also, they exhibit partial energy-independent uptake in comparison to **CDDP** which is not taken up at low temperatures (277K). This is especially true for iodido complex **16**, for which uptake is greatly

enhanced by amphotericin B, a facilitative diffusion agent. Cellular accumulation of ruthenium in A2780 cells was enhanced by inhibition of efflux pathways by verapamil, indicating that a MDR protein, such as P-gp, could be involved in ruthenium efflux and detoxification. This is also supported by results of co-incubation with antimycin A, these show that the enhanced accumulation of chlorido complex **15** is consistent with the inhibition of MRP2 pump which is ATP-dependent. Changes in the resting membrane potential induced by ouabain have been shown to reduce Ru accumulation in A2780 ovarian cancer cells, which suggests that electrochemical gradient can modulate uptake. CTR1 copper transporter, which is involved in the cellular uptake of **CDDP**, is likely to be involved as well in the uptake of complex **16**. Finally it was shown that that the caveolae endocytotic pathway is not involved in the uptake of either of the ruthenium complexes **15** or **16**.

3.6 References

1. A. Casini, C. G. Hartinger, A. A. Nazarov, and P. J. Dyson, *Top Organomet Chem*, 2010, **32**, 57-80.

2. P. J. Dyson and G. Sava, *Dalton Trans.*, 2006, 1929-1933.

3. A. Peacock and P. J. Sadler, *Chem-Asian J.*, 2008, **3**, 1890-1899.

4. G. Gasser, I. Ott, and N. Metzler-Nolte, *J. Med. Chem.*, 2011, **54**, 3-25.

5. L. Ronconi and P. J. Sadler, *Coord. Chem. Rev.*, 2007, **251**, 1633-1648.

6. Y. K. Yan, M. Melchart, A. Habtemariam, and P. J. Sadler, *Chem. Commun.* , 2005, 4764-4776.

7. J. Reedijk, *Macromol. Symp.*, 2008, **270**, 193-201.

8. P. C. Bruijnincx and P. J. Sadler, *Curr. Opin. Chem. Biol.*, 2008, **12**, 197-206.

9. C. G. Hartinger, A. D. Phillips, and A. Nazarov, *Curr. Top. Med. Chem.* , 2011, **11**, 2688-2702.

10. H. Timmer-Bosscha, N. H. Mulder, and E. G. de Vries, *Br. J. Cancer*, 1992, **66**, 227-238.

11. M. Kartalou and J. M. Essigmann, *Mutat. Res.*, 2001, **478**, 23-43.

12. M. Jones, J. Siracky, L. R. Kelland, and K. R. Harrap, *Br. J. Cancer*, 1993, **67**, 24-29.

13. D. Trachootham, W. Zhang, and P. Huang, *Oxidative stress and drug resistance in cancer*, Springer US, New York, NY, 2009.

14. M. D. Hall, M. Okabe, D. W. Shen, X. Liang, and M. M. Gottesman, *Annu. Rev. Pharmacol. Toxicol.*, 2008, **48**, 495-535.

15. A. M. Florea and D. Büsselberg, *Cancers*, 2011, **3**, 1351-1371.

16. S. Ishida, J. Lee, D. J. Thiele, and I. Herskowitz, *Proc. Natl. Acad. Sci. USA.*, 2002, **99**, 14298-14302.

17. D. P. Gately and S. B. Howell, *Br. J. Cancer*, 1993, **67**, 1171-1176.

18. D. Sinani, D. J. Adle, H. Kim, and J. Lee, *J. Biol. Chem.*, 2007, **282**, 26775-26785.

19. D. Fu and I. M. Arias, *Int. J. Biochem. Cell Biol.*, 2012, **44**, 461-464.

20. M. M. Cornwell, I. Pastan, and M. M. Gottesman, *J. Biol. Chem.*, 1987, **262**, 2166-2170.

21. Z. Bikadi, I. Hazai, D. Malik, K. Jemnitz, Z. Veres, P. Hari, Z. Ni, T. W. Loo, D. M. Clarke, E. Hazai, and Q. Mao, *PloS one*, 2011, **6**, e25815.

22. R. B. Wang, C. L. Kuo, L. L. Lien, and E. J. Lien, *J. Clin. Pharm. Ther.*, 2003, **28**, 203-228.

23. J. Karwatsky, M. C. Lincoln, and E. Georges, *Biochemistry*, 2003, **42**, 12163-12173.

24. R. M. Laberge, R. Ambadipudi, and E. Georges, *Arch. Biochem. Biophys.*, 2009, **491**, 53-60.

25. A. Takeuchi, N. Reyes, P. Artigas, and D. C. Gadsby, *Nature*, 2008, **456**, 413-416.

26.   H. Yu, I. M. Ratheal, P. Artigas, and B. Roux, *Nat. Struct. Mol. Biol.*, 2011, **18**, 1159-1163.

27.   C. M. Canessa, J. D. Horisberger, D. Louvard, and B. C. Rossier, *EMBO J.*, 1992, **11**, 1681-1687.

28.   B. E. Kim, T. Nevitt, and D. J. Thiele, *Nat. Chem. Biol.*, 2008, **4**, 176-185.

29.   C. J. De Feo, S. G. Aller, G. S. Siluvai, N. J. Blackburn, and V. M. Unger, *Proc. Natl. Acad. Sci. USA.*, 2009, **106**, 4237-4242.

30.   Y. Nose, E. M. Rees, and D. J. Thiele, *Trends Biochem. Sci.*, 2006, **31**, 604-607.

31.   A. K. Holzer and S. B. Howell, *Cancer Res.*, 2006, **66**, 10944-10952.

32.   K. Katano, A. Kondo, R. Safaei, P. Copper, A. Holzer, G. Samimi, M. Mishima, and Y. ming Kuo, *Cancer Res.*, 2002, **62**, 6559-6565.

33.   X. Lin, T. Okuda, A. Holzer, and S. B. Howell, *Mol. Pharmacol.*, 2002, **62**, 1154-1159.

34.   Z. D. Liang, D. Stockton, N. Savaraj, and M. T. Kuo, *Mol. Pharmacol.*, 2009, **76**, 843-853.

35.   G. Samimi and S. B. Howell, *Cancer Chemoth. Pharm.*, 2006, **57**, 781-788.

36.   J. Lee, M. J. Petris, and D. J. Thiele, *J. Biol. Chem.*, 2002, **277**, 40253-40259.

37.   V. Cepeda, M. Fuertes, J. Castilla, C. Alonso, C. Quevedo, and J. M. Pérez, *Anti. Canc. Agents Med. Chem.*, 2007, **7**, 3-18.

38.   P. Abada and S. B. Howell, *Met Based Drugs*, 2010, **2010**, 317581.

39. S. B. Howell, R. Safaei, C. A. Larson, and M. J. Sailor, *Mol. Pharmacol.*, 2010, **77**, 887-894.

40. J. Lee, M. M. O. Peña, Y. Nose, and D. J. Thiele, *J. Biol. Chem.*, 2002, **277**, 4380-4387.

41. S. Y. Sharp, P. Mistry, M. R. Valenti, P. Bryant, and L. R. Kelland, *Cancer Chemoth. Pharm.*, 1994, **35**, 137-143.

42. D. Garmann, A. Warnecke, G. V. Kalayda, F. Kratz, and U. Jaehde, *J. Controlled Release*, 2008, **131**, 100-106.

43. B. Razani, S. E. Woodman, and M. P. Lisanti, *Pharmacol. Rev.*, 2002, **54**, 431-467.

44. D. W. Shen, S. Goldenberg, and I. R. A. Pastan, *J. Cell. Physiol.*, 2000, **116**, 108 -116.

45. A. M. Pizarro, A. Habtemariam, and P. J. Sadler, *Top Organomet Chem*, 2010, **32**, 21-56.

46. A. M. Pizarro and P. J. Sadler, *Biochimie*, 2009, **91**, 1198-1211.

47. T. Bugarcic, A. Habtemariam, R. J. Deeth, F. P. Fabbiani, S. Parsons, and P. J. Sadler, *Inorg. Chem.*, 2009, **48**, 9444-9453.

48. S. J. Dougan, M. Melchart, A. Habtemariam, S. Parsons, and P. J. Sadler, *Inorg. Chem.*, 2006, **45**, 10882-10894.

49. S. J. Dougan, University of Edinburgh, 2007.

50. E. Lindhagen, P. Nygren, and R. Larsson, *Nat. Protoc.*, 2008, **3**, 1364-1369.

51. P. Skehan, R. Storeng, D. Scudiero, A. Monks, J. McMahon, D. Vistica, J. T. Warren, H. Bokesch, S. Kenney, and M. R. Boyd, *J. Natl. Cancer Inst.*, 1990, **82**, 1107-1112.

52. K. T. Papazisis, G. D. Geromichalos, K. Dimitriadis, and H. Kortsaris, *J. Immunol. Methods*, 1997, **208**, 151-158.

53. T. Bugarcic, O. Nováková, A. Halámiková, L. Zerzánková, O. Vrána, J. Kaspárková, A. Habtemariam, S. Parsons, P. J. Sadler, and V. Brabec, *J. Med. Chem.*, 2008, **51**, 5310-5319.

54. G. Chu, *J. Biol. Chem.*, 1994, **269**, 787-790.

55. J. K. C. Lau and B. Ensing, *Phys. Chem. Chem. Phys.*, 2010, **12**, 10348-10355.

56. J. Reedijk, *Eur. J. Inorg. Chem.*, 2009, 1303-1312.

57. T. Cheng, Y. Zhao, X. Li, F. Lin, Y. Xu, X. Zhang, Y. Li, R. Wang, and L. Lai, *J. Chem. Inf. Model.*, 2007, **47**, 2140-2148.

58. M. Groessl, O. Zava, and P. J. Dyson, *Metallomics*, 2011, **3**, 591-599.

59. P. A. Andrews, S. Velury, S. C. Mann, and B. I. Stephen, *Cancer Res.*, 1988, **48**, 68-73.

60. M. M. Gottesman, S. V. Ambudkar, and D. Xia, *Nat. Biotechnol.*, 2009, **27**, 546-547.

61. R. E. Aird, J. Cummings, A. A. Ritchie, M. Muir, R. E. Morris, H. Chen, P. J. Sadler, and D. I. Jodrell, *Br. J. Cancer*, 2002, **86**, 1652 - 1657.

62. S. G. Aller, J. Yu, A. Ward, Y. Weng, S. Chittaboina, P. M. Harrell, Y. T. Trinh, Q. Zhang, I. L. Urbatsch, and G. Chang, *Science*, 2009, **323**, 1718-1722.

63. J. Cummings, J. S. Macpherson, I. Meikle, and J. F. Smyth, *Biochem. Pharmacol.*, 1996, **52**, 979-990.

64. J. D. Allen, R. F. Brinkhuis, L. V. Deemter, J. Wijnholds, and A. H. Schinkel, *Cancer Res.*, 2000, **60**, 5761-5766.

65. J. Q. Chen, R. G. Contreras, R. Wang, S. V. Fernandez, L. Shoshani, I. H. Russo, M. Cereijido, and J. Russo, *Breast Cancer Res. Treat.*, 2006, **96**, 1-15.

66. W. Zhang, H. Takeuchi, M. Kurono, and M. Emaduddin, *Gen Pharmac*, 1997, **29**, 625-632.

67. N. Ramu and R. Gorodetsky, *Biochem. Pharmacol.*, 1991, **42**, 1699-1704.

68. J. Uozumi and C. L. Litterst, *Cancer Chemoth. Pharm.*, 1995, **15**, 93-96.

69. A. K. Holzer, K. Katano, L. W. J. Klomp, and S. B. Howell, *Clin. Cancer Res.*, 2004, **10**, 6744-6749.

70. A. K. Holzer, G. H. Manorek, and S. B. Howell, *Mol. Pharmacol.*, 2006, **70**, 1390-1394.

71. X. Wang, X. Du, H. Li, D. S. B. Chan, and H. Sun, *Angew. Chem., Int. Ed.*, 2011, **50**, 2706-2711.

72. M. Venkatachalam, Y. Patel, J. Kreisberg, and J. Weingberg, *J. Clin. Invest*, 1988, **81**, 745-758.

73. K. Taniguchi, M. Wada, K. Kohno, and M. Kawakami, *Cancer Res.*, 1996, **56**, 4124-4129.

74. H. Resat and M. Baginski, *Eur. Biophys. J.*, 2002, **31**, 294-305.

75. B. Venegas, J. González-Damián, H. Celis, and I. Ortega-Blake, *Biophys. J.*, 2003, **85**, 2323-2332.

76. G. Fujii, J. E. Chang, T. Coley, and B. Steere, *Biochemistry*, 1997, **36**, 4959-4968.

77. E. Romero, E. Valdivieso, and B. E. Cohen, *J. Membr. Biol.*, 2009, **230**, 69-81.

78. T. Tanaka, H. Kurokawa, K. Matsuno, S. Matsumoto, and Y. Hayashida, *Anti-Cancer Res.*, 2008, **28**, 2663-2668.

79. D. Aguirre, A. Angeles-Bosa, A. Chouai, C. Turro, J. Pellois, and K. Dunbar, *Dalton Trans.*, 2009, 10651-10659.

80. A. Leo, C. Hansch, D. Elkins, A. H. Law, and B. N. Behavior, *Chem. Rev.*, 1971, **71**, 525-616.

Chapter 4

N,N-Chelated ruthenium arene complexes: exploring DNA intercalation.

4.1 Introduction

DNA is generally accepted to be the main target of cisplatin, which has been demonstrated to bind most frequently to guanine residues through their N7 position, thereby generating a kink in the DNA structure.[1] The most abundant adducts formed by cisplatin in linear DNA are 1,2-d(GpG) ($\sim$65%) or 1,2-d(ApG) (25%) intrastrand and 1,2-d(GG) ($\sim$6%) interstrand cross-links[2]

Piano-stool metal complexes were originally designed to have a similar behaviour. These complexes could be activated by the loss of the monodentate ligand, usually a halogen that undergoes aquation. The result of this reaction is the generation of a coordinative vacancy that can be used to target biomolecules such as DNA. Some ruthenium compounds have shown a direct correlation between their antiproliferative activity and DNA binding.[2] It is also known that Ru(II) complexes such as $[(\eta^6\text{-arene})\text{Ru(en)Cl}]^+$ bind strongly to nucleobase models like 9-EtG and 9-EtA, showing preference for the guanine base.[3] However, it remains unclear if nuclear DNA is the principal target of such compounds.[4,5]

Interactions with DNA can also include non-covalent binding, in the form of DNA-intercalation, in such interaction a planar aromatic unit of the metal complex gets inserted between the base pairs of the DNA double helix.[6] Stabilization of the double helix caused by intercalation allows the DNA to be unwinded, leading to functional changes that may include inhibition of repair processes.[7] This in turn can lead to cell death. Ruthenium complexes with polypyridyl ligands have been widely used to study DNA intercalation.[8–15]

The present Chapter explores DNA-intercalation as a possible mechanism of action for Ru(II) piano-stool complexes that include in their structures *N,N*-ligands with an increasing number of aromatic units.

4.2 Experimental section

4.2.1 Materials

Ruthenium arene dimers used in this Chapter include $[(\eta^6\text{-}p\text{-cymene})RuCl_2]_2$, reported in Chapter 2. $[(\eta^6\text{-bip})RuCl_2]_2$, and $[(\eta^6\text{-terp})RuCl_2]_2$, were kindly provided by Dr. Abraha Habtemariam. Quinoline-2-carbaldehyde, aniline (ACS Reagent $\geq$99.5%), 2-aminoanthracene (96%), pyridine-2-carbaldehyde 2-aminoquinoline (97%), 1H-indol-5-amine (96%) were purchased from Sigma Aldrich. All deuterated solvents (D$_2$O, MeOD, DMSO-d_6, acetone-d_6, CDCl$_3$) were obtained from Cambridge Isotope Laboratories. For the biological assays: CT-DNA was also obtained from Sigma Aldrich.

4.2.2 Preparation of ligands and complexes

The synthetic procedure 1, described below was used to obtain all the imines used as ligands in this Chapter and listed in Figure 4.1.

Phimqn, **19**   Anthimqn, **20**

Anthimpy, **21**   Qnimpy, **22**   Indoimpy, **23**
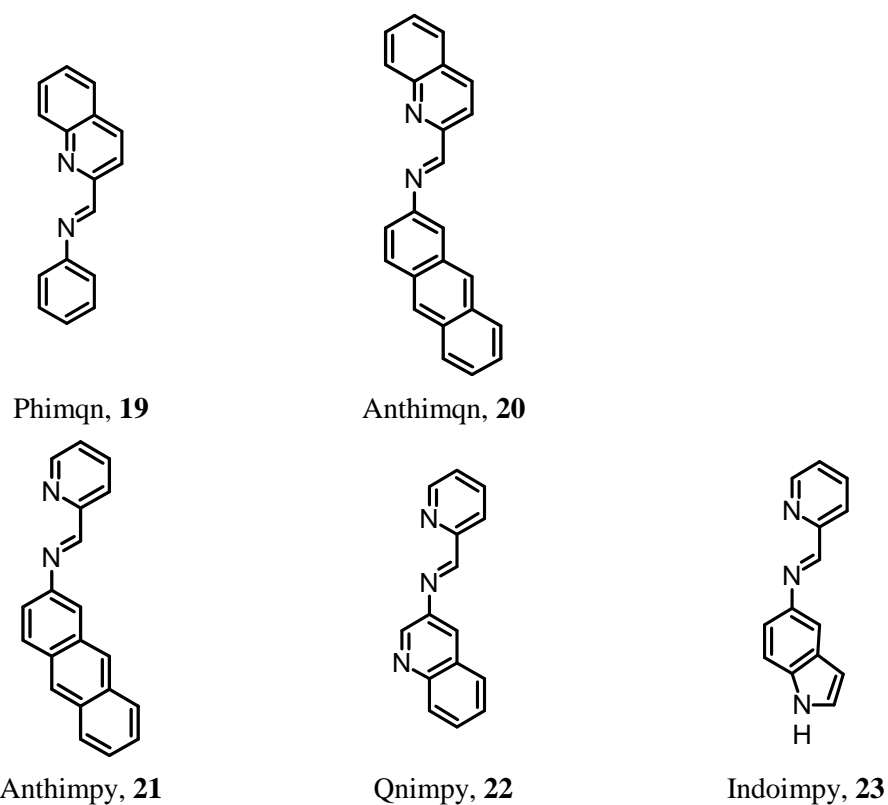
Figure 4.1 Ligands investigated in this Chapter**.**

Synthetic Procedure 1.
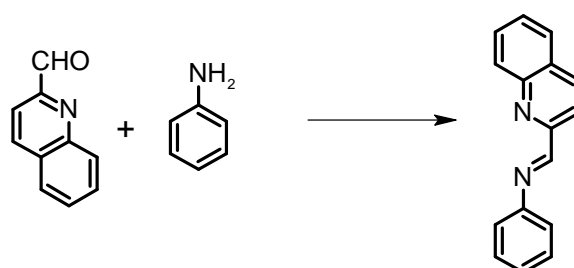
Scheme 4.1. Synthesis of (*E*)-*N*-phenyl-1-(quinolin-2-yl)methanimine **[Phimqn, 19].**

(*E*)-*N*-phenyl-1-(quinolin-2-yl)methanimine [19]. Quinoline-2-carbaldehyde

(50 mg, 0.32 mmol) was dissolved in acetonitrile (5 mL) at ambient temperature

with stirring. Then 1 mol. equiv. of aniline was added (30 mg, 29 μL, 0.32 mmol). The reaction was left to stand with stirring for 4 h. The solvent was removed by rotary evaporation. A pale solid was obtained, which was washed with ether (Yield 70%). Elemental analysis calc. for $C_{16}H_{12}N_2$, C: 82.73%; H: 5.21%; N: 12.06%. Found: C: 82.85%; H: 5.18%; N: 12.32%. NMR-δ_H (500 MHz; CDCl$_3$) 7.33 (1H, t, J = 7.4, 14.2 Hz) 7.43 (2H, dd, J = 1.3, 7.5 Hz) 7.48 (2H, m) 7.70 (1H, t, J = 8.4, 15.5 Hz) 7.85 (1H, t, J = 7.4, 15.3 Hz) 8.07 (1H, d, J = 9.0 Hz) 8.14 (1H, d, J = 9.0 Hz) 8.30 (1H, d, J = 9.5 Hz) 8.50 (1H, d, J = 9.5 Hz) 8.78 (1H, s). m/z (ESI) found 234.0 (calc. M + H$^+$. $C_{16}H_{13}N_2$ = 234.27).

(*E*)-*N*-(anthracen-2-yl)-1-(quinolin-2-yl)methanimine [Anthimqn, 20] As synthetic procedure 1, using quinoline-2-carbaldehyde (50 mg, 0.32 mmol) and 2-aminoanthracene (62 mg, 0.32 mmol). Yield 86%. Elemental analysis calc. for $C_{24}H_{16}N_2$ C: 86.72%; H: 4.85%; N: 8.42%. Found: C: 86.64%; H: 4.81%; N: 8.36%. NMR-δ_H (500 MHz; CDCl$_3$) 7.51 (2H, m) 7.66 (2H, m) 7.82 (1H, m) 7.93 (1H, d, J = 8.0 Hz) 7.98 (1H, d, J = 1.8 Hz) 8.05 (2H, m) 8.11 (1H, d, J = 8.1 Hz) 8.23 (1H, d, J = 8.2 Hz) 8.33 (1H, d, J = 8.6 Hz) 8.48 (1H, d, J = 2.2 Hz) 8.50 (2H, m) 9.04 (1H, s). m/z (ESI) found 332.4 (calc. M + H$^+$ $C_{24}H_{17}N_2$ = 332.39).

(*E*)-*N*-(anthracen-2-yl)-1-(pyridin-2-yl)methanimine [Anthimpy, 21] As synthetic procedure 1, using pyridine-2-carbaldehyde (28 mg, 25 μL, 0.26 mmol) and 2-aminoanthracene (50 mg, 0.26 mmol). Yield 65%. Elemental analysis calc. for $C_{20}H_{14}N_2$ C: 85.08%; H: 5.00%; N: 9.92%. Found: C: 85.95%; H: 4.92%; N: 9.78%. NMR-δ_H (500 MHz; CDCl$_3$) 7.54 (2H, m) 7.58 (1H, qd, J = 1.0, 4.5, 6.0, 7.5 Hz) 7.67 (1H, dd, J = 2.0, 9.1 Hz) 8.01 (2H, m) 8.10 (2H, c, J = 5.4, 9.0, 15.3

Hz) 8.19 (1H, d, J = 9.1 Hz) 8.26 (1H, d, J = 8.3 Hz) 8.63 (2H, d, J = 3.5 Hz) 8.77 (1H, dc, J = 0.8, 1.7, 2.6, 4.7 Hz) 8.84 (1H, s). m/z (ESI) found 282.0 (calc. M + H$^+$ $C_{20}H_{15}N_2$ = 283.33).

(*E*)-1-(pyridin-2-yl)-*N*-(quinolin-3-yl)methanimine [Qnimpy, 22] As synthetic procedure 1, using pyridine-2-carbaldehyde (37 mg, 34 µL, 0.35 mmol) and 2-aminoquinoline (50 mg, 0.35 mmol). Yield 86%. Elemental analysis calc. for $C_{15}H_{11}N_3$ C: 77.23%; H: 4.75%; N: 18.01%. Found: C: 77.50%; H: 4.89%; N: 18.22%. NMR-δ_H (500 MHz; CDCl$_3$) 7.58 (1H, qd, J = 5.0, 6.2, 7.6, 12.1 Hz) 7.64 (1H, t, J = 7.7, 14.9 Hz) 7.75 (1H, td, J = 1.4, 6.1, 15.4 Hz) 8.03 (3H, m) 8.25 (1H, d, J = 7.9 Hz) 8.30 (1H, d, J = 2.6 Hz) 8.77 (1H, d, J = 4.6 Hz) 8.85 (1H, s) 8.97 (1H, d, J = 2.5 Hz). m/z (ESI) found 234.3 (calc. M + H$^+$ $C_{15}H_{12}N_3$ = 234.26).

(*E*)-*N*-(1*H*-indol-5-yl)-1-(pyridin-2-yl)methanimine [Indoimpy, 23] As synthetic procedure 1, using pyridine-2-carbaldehyde (40 mg, 38 µL, 0.38 mmol) and 1H-indol-5-amine (50 mg, 0.38 mmol). Yield 86%. Elemental analysis calc. for $C_{14}H_{11}N_3$ C: 76.00%; H: 5.01%; N: 18.99%. Found: C: 76.15%; H: 5.19%; N: 19.09%. NMR-δ_H (500 MHz; CDCl$_3$) 7.33 (1H, m) 7.36 (1H, s) 7.48 (1H, d, J = 9.5 Hz) 7.58 (1H, t, J = 1.6 Hz) 7.79 (1H, td, J = 1.9, 7.8, 15.2 Hz) 7.84 (1H, s) 7.94 (1H, s) 8.10 (1H, d, J = 8.0 Hz) 8.61 (1H, s) 8.68 (1H, d, J = 3.5 Hz). m/z (ESI) found 222.3 (calc. M + H$^+$ $C_{14}H_{12}N_3$ = 222.25).

Synthetic procedure 2, was used to synthesise all the ruthenium complexes described in this Chapter and listed in Figure 4.2.

Complex **24**, X = Cl

Complex **25**, X = Cl
Complex **26**, X = I

Complex **27**, X = Cl
Complex **28**, X = I

Complex **29**, X = Cl
Complex **30**, X = I

Complex **31**, X = Cl

Complex **32**, arene = η^6-bip
Complex **33**, arene = η^6-*m*-terp
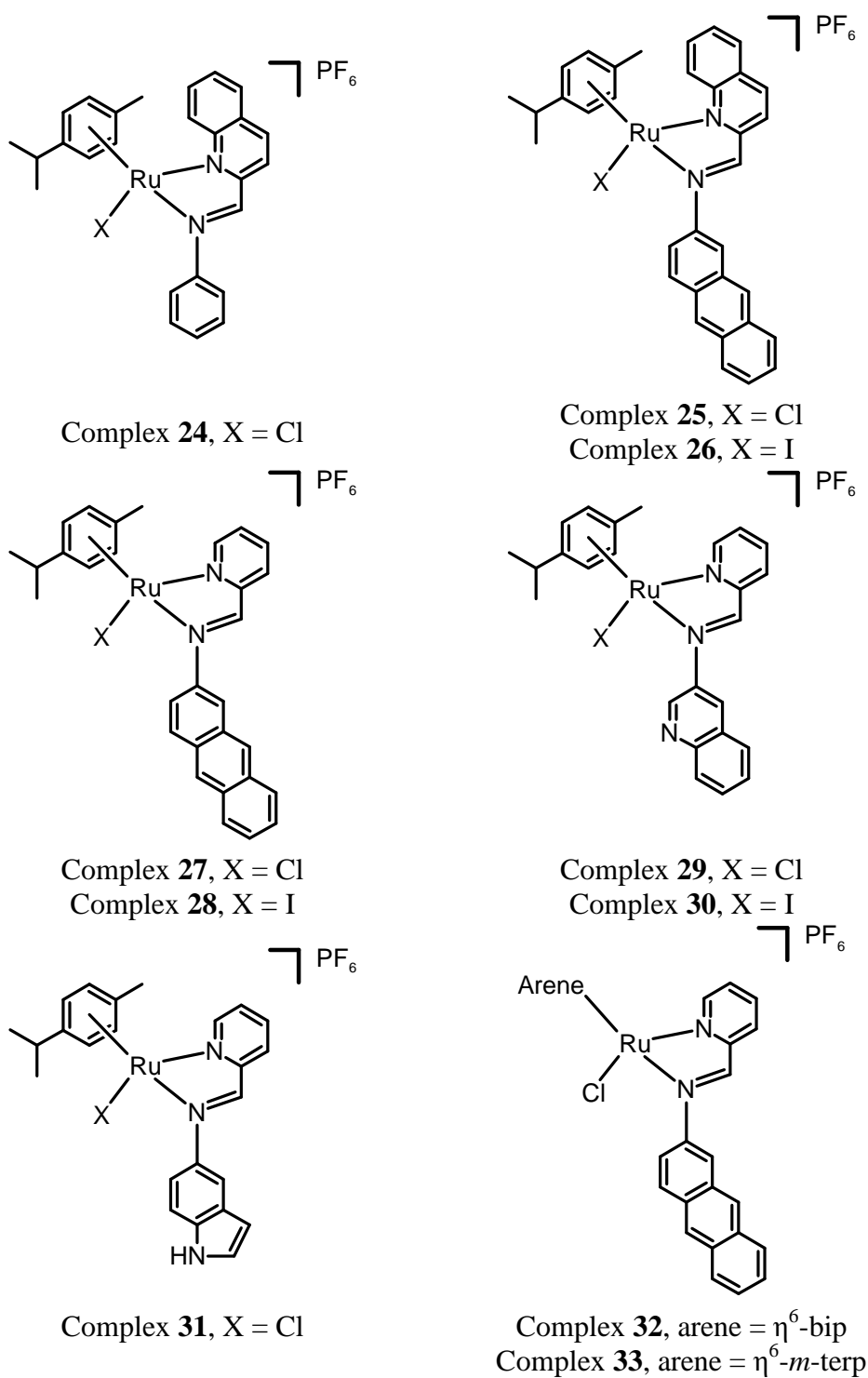
Figure 4.2 Complexes investigated in this Chapter**.**
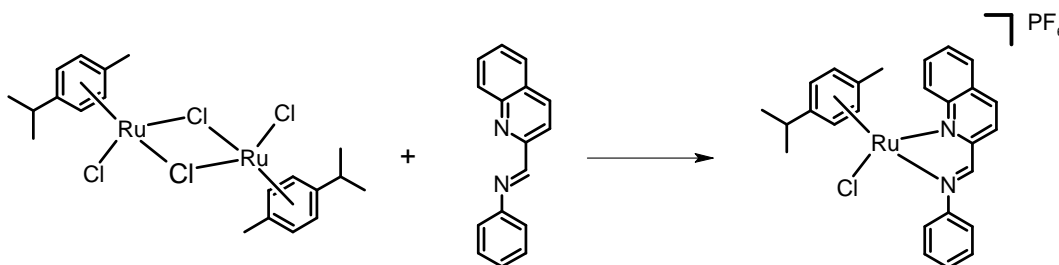
Synthetic procedure 2.

Scheme 4.2. Synthesis of the ruthenium complex [Ru(η^6-*p*-cym)(Phimqn)Cl]PF$_6$, **[24].**

[Ru(η^6-*p*-cym)(Phimqn)Cl]PF$_6$, [24]. Ruthenium *p*-cymene dimer [(η^6-*p*-cym)RuCl$_2$]$_2$ (100 mg, 0.16 mmol) was dissolved in methanol (5 mL). This mixture was placed in a round bottom flask, then two mol equiv of the appropriate ligand was added, in this case, Phimqn (76 mg, 0.32 mmol). The reaction was left at ambient temperature with constant stirring for 5 h. After this time 5 equiv of NH$_4$PF$_6$ were added to the mixture, and left stirring for a further hour. The solid residue was filtered off under vacuum and recrystallised. (Yield 52%). Elemental analysis calc. for C$_{26}$H$_{26}$N$_2$ClF$_6$PRu, C: 48.19%, H: 4.04%, N: 4.32%. Found: C: 48.28%, H: 4.07%; N: 4.29%. NMR -δ_H (500 MHz; DMSO-d$_6$) 0.76 (3H, d, J = 6.7 Hz) 0.92 (3H, d, J = 6.7 Hz) 2.22 (3H, s) 2.36 (1H, m) 5.36 (1H, d, J = 6.7 Hz) 5.78 (1H, d, J = 6.1 Hz) 5.88 (1H, d, J = 6.1 Hz) 6.12 (1H, d, J = 6.7 Hz), 7.65 (1H, m) 7.70 (2H, t, J = 7.1, 14.7 Hz) 7.98 (2H, d, J = 7.4 Hz) 8.04 (1H, t, J = 6.7, 14.5 Hz) 8.19 (1H, t, J = 8.3, 15.6 Hz) 8.34 (2H, t, J = 8.9, 18.4) 8.79 (1H, d, J = 10.4 Hz) 8.94 (1H, d, J = 8.3 Hz) 9.20 (1H, s). m/z (ESI) found 503.0 (calc. M$^+$ C$_{26}$H$_{26}$N$_2$ClRu = 503.02).

[Ru(η⁶-*p*-cym)(Anthimqn)Cl]PF₆ [25]. As synthetic procedure 2, using [Ru(η⁶-*p*-cym)₂Cl₂]Cl₂ (54 mg, 0.09 mmol) and Anthimqn (50 mg, 0.18 mmol). Yield 68%. Elemental analysis calc. for $C_{30}H_{28}N_2ClF_6PRu$ C: 51.62%, H: 4.04%, N: 4.01%. Found: C: 51.72%, H: 4.12 %; N: 4.09%. NMR -δ_H (500 MHz; DMSO-d₆) 0.95 (6H, d, J = 4.8 Hz) 2.10 (3H, s) 2.35 (1H, m) 5.54 (1H, d, J = 7.0 Hz) 5.80 (1H, d, J = 6.4 Hz) 6.02 (1H, d, J = 7.0 Hz) 6.35 (1H, d, J = 6.5 Hz) 7.45 (2H, m) 7.58 (2H, m) 7.90 (1H, m) 8.02 (1H, d, J = 7.6 Hz) 8.10 (1H, d, J = 2.3 Hz) 8.15 (2H, m) 8.32 (1H, d, J = 9.0 Hz) 8.45 (1H, d, J = 7.4 Hz) 8.54 (1H, d, J = 9.1 Hz) 8.72 (1H, d, J = 3.0 Hz) 8.85 (2H, m) 9.24 (1H, s). m/z (ESI) found 553.0 (calc. M⁺ $C_{30}H_{28}N_2ClRu$ = 553.08).

[Ru(η⁶-*p*-cym)(Anthimqn)I]PF₆ [26]. As synthetic procedure 2, using [Ru(η⁶-*p*-cym)₂I₂]I₂ (50 mg, 0.08 mmol) and anthimqn (54 mg, 0.16 mmol). Yield 71%. Elemental analysis calc. for $C_{34}H_{30}N_2IF_6PRu$ C: 48.64%, H: 3.60%, N: 3.34%. Found: C: 48.60%, H: 3.58%; N: 3.30%. NMR-δ_H (500 MHz; DMSO-d₆) 0.79 (3H, d, J = 6.8 Hz) 0.94 (3H, d, J = 6.8 Hz) 2.10 (3H, s,) 2.42 (1H, m) 5.45 (1H, d, J = 6.0 Hz) 5.87 (1H, d, J = 6.3 Hz) 5.95 (1H, d, J = 6.3 Hz) 6.18 (1H, d, J = 6.0 Hz) 7.62 (2H, m) 8.06 (1H, t, J = 8.4, 13.0 Hz) 8.13 (1H, d, J = 8.1 Hz) 8.23 (3H, m) 8.36 (1H, d, J = 8.3 Hz) 8.41 (2H, dd, J = 5.0, 8.4 Hz) 8.67 (1H, s) 8.81 (2H, d, J = 9.0 Hz) 8.86 (1H, s) 8.98 (1H, d, J = 9.6 Hz) 9.40 (1H, s). m/z (ESI) found 694.6 (calc. M⁺ $C_{34}H_{30}N_2IRu$ = 694.59).

[Ru(η⁶-*p*-cym)(Anthimpy)Cl]PF₆ [27]. As synthetic procedure 2, using [Ru(η⁶-*p*-cym)₂Cl₂]Cl₂ (50 mg, 0.08 mmol) and Anthimpy (38 mg, 0.16 mmol). Yield 54%. Elemental analysis calc. for $C_{30}H_{28}N_2ClF_6PRu$, C: 51.62%, H: 4.04%, N:

4.01%. Found: C: 51.80%, H: 4.11%; N: 4.09%. NMR -δ_H (500 MHz; DMSO-d$_6$) 1.01 (6H, t, J = 7.3, 15.2 Hz) 2.23 (3H, s) 2.56 (1H, m) 5.63 (1H, d, J = 5.6 Hz) 5.72 (1H, d, J = 5.6 Hz) 5.83 (1H, d, J = 6.3 Hz) 6.16 (1H, d, J = 6.3 Hz) 7.63 (2H, m) 7.93 (1H, c, J = 5.7, 9.0, 14.2 Hz) 7.98 (1H, d, J = 9.7 Hz) 8.20 (1H, q, J = 5.7, 9.5, 15.1 Hz) 8.35 (3H, m) 8.47 (1H, s) 8.77 (1H, s) 8.83 (1H, s) 9.14 (1H, s) 9.64 (1H, d, J = 5.5Hz). m/z (ESI) found 553.1 (calc. M$^+$ C$_{30}$H$_{28}$N$_2$ClRu = 553.08).

[Ru(η^6-*p*-cym)(Anthimpy)I]PF$_6$ [28]. As synthetic procedure 2, using [Ru(η^6-*p*-cym)$_2$I$_2$]I$_2$ (50 mg, 0.08 mmol) and Anthimpy (30 mg, 0.16 mmol). Yield 70%. Elemental analysis calc. for C$_{30}$H$_{28}$N$_2$F$_6$IPRu C: 45.64%, H: 3.57%, N: 3.55%. Found: C: 45.58%, H: 3.60 %; N: 3.47%. NMR -δ_H (500 MHz; DMSO-d$_6$) 0.99 (3H, d, J = 7.2 Hz) 1.05 (3H, d, J = 7. 2 Hz) 2.46 (3H, s) 2.67 (1H, m) 5.70 (1H, d, J = 6.2 Hz) 5.75 (1H, d, J = 6.4 Hz) 5.90 (1H, d, J = 6.2 Hz) 6.11 (1H, d, J = 6.4 Hz) 7.65 (2H, m) 7.88 (1H, t, J = 6.6, 13.2 Hz) 8.09 (1H, d, J = 9.2 Hz) 8.23 (2H, m) 8.34 (1H, t, J = 8.4, 16.1 Hz) 8.40 (1H, d, J = 8.7 Hz) 8.55 (1H, s) 8.80 (1H, s) 8.85 (1H, s) 9.11 (1H, s) 9.63 (1H, d, J = 4.8 Hz).). m/z (ESI) found 644.6 (calc. M$^+$ C$_{30}$H$_{28}$N$_2$IRu = 644.53).

[Ru(η^6-*p*-cym)(Qnimpy)Cl]PF$_6$ [29]. As synthetic procedure 2, using [Ru(η^6-*p*-cym)$_2$Cl$_2$]Cl$_2$ (100 mg, 0.16 mmol) and Qnimpy (76 mg, 0.32 mmol). Yield 75%. Elemental analysis calc. for C$_{25}$H$_{25}$N$_3$ClF$_6$PRu C: 46.27%, H: 3.88%, N: 6.47%. Found: C: 46.40%, H: 3.95%; N: 6.61%. NMR-δ_H (500 MHz; DMSO-d$_6$) 0.98 (3H, d, J = 4.4 Hz) 1.03 (3H, d, J = 4.4 Hz) 2.18 (3H, s) 2.56 (1H, m) 5.68 (1H, d, J = 6.1 Hz) 5.80 (1H, d, J = 6.4 Hz) 5.85 (1H, d, J = 6.1 Hz) 6.13 (1H, d, J = 6.4

Hz) 7.80 (1H, t, J = 7.7, 15.3 Hz) 7.93 (2H, m) 8.20 (2H, t, J = 8.01, 16.5 Hz) 8.34 (2H, d, J = 4.0 Hz) 8.34 (2H, d, J = 4.0 Hz) 8.75 (1H, d, J = 2.6 Hz) 9.14 (1H, s) 9.35 (1H, d, J = 2.3 Hz) 9.64 (1H, d, J = 5.8Hz). m/z (ESI) found 504.0 (calc. M^+ $C_{22}H_{24}N_2IRu$ = 504.01).

[Ru(η^6-*p*-cym)(Qnimpy)I]PF$_6$ [30]. As synthetic procedure 2, using [Ru(η^6-*p*-cym)$_2$I$_2$]I$_2$ (50 mg, 0.08 mmol) and Qnimpy (24 mg, 0.16 mmol). Yield 70%. Elemental analysis calc. for $C_{25}H_{25}N_3F_6IPRu$, C: 40.55%, H: 3.40%, N: 5.68%. Found: C: 40.75%, H: 3.54%; N: 5.74%. NMR-δ_H (500 MHz; DMSO-d$_6$) 0.97 (3H, d, J = 6.8 Hz) 1.02 (3H, d, J = 6.8 Hz) 2.41 (3H, s,) 2.68 (1H, m) 5.72 (1H, d, J = 6.3 Hz) 5.85 (1H, d, J = 6.9 Hz) 5.92 (1H, d, J = 6.3 Hz) 6.08 (1H, d, J = 6.9 Hz) 7.82 (1H, t, J = 7.7, 14.8 Hz) 7.89 (1H, td, J = 1.7, 5.9, 13.0 Hz) 7.95 (1H, t, J = 7.4, 15.0 Hz) 8.21 (2H, t) 8.33 (1H, t, J = 8.2, 15.1 Hz) 8.37 (1H, d, J = 7.3 Hz) 8.81 (1H, d, J = 2.3 Hz) 9.09 (1H, s) 9.45 (1H, d, J = 2.3 Hz) 9.63 (1H, d, J = 5.7 Hz). m/z (ESI) found 595.5 (calc. M^+ $C_{25}H_{25}N_3IRu$ = 595.46).

[Ru(η^6-*p*-cym)(Indoimpy)Cl]PF$_6$ [31]. As synthetic procedure 2, using [Ru(η^6-*p*-cym)$_2$Cl$_2$]Cl$_2$ (69 mg, 0.11 mmol) and Indoimpy (50 mg, 0.23 mmol). Yield 66%. Elemental analysis calc. for $C_{24}H_{25}N_3ClF_6RuP$ C: 45.26%, H: 3.96%, N: 6.60%. Found: C: 45.50%, H: 3.82%; N: 6.54%. NRM-δ_H (500 MHz; DMSO-d$_6$) 0.95 (6H, d, J = 7.1 Hz) 2.14 (3h, s) 2.35 (1H, m) 5.85 (1H, d, J = 6.2 Hz) 5.96 (1H, d, J = 7.1 Hz) 6.12 (1H, d, J = 6.1 Hz) 6.54 (1H, d, H = 7.1 Hz) 7.42 (1H, m) 7.54 (1H, s) 7.62 (1H, d, J = 8.0 Hz) 7.74 (1H, t, J = 2.1 Hz) 7.86 (1H, td, J = 2.1, 8.0, 14.6 Hz) 7.93 (1H, s) 8.08 (1H, s) 8.17 (1H, d, J = 8.6 Hz) 8.47 (1H, s) 8.82 (1H, d, J = 4.3 Hz). m/z (ESI) found 492.0 (calc. M^+ $C_{24}H_{25}N_3ClRu$ = 492.06).

[Ru(η[6]-bip)(Anthimpy)Cl]PF$_6$ [32]. As synthetic procedure 2, using [Ru(η[6]-bip)$_2$Cl$_2$]Cl$_2$ (50 mg, 0.08 mmol) and Anthimpy (44 mg, 0.16 mmol). Yield 73%. Elemental analysis calc. for C$_{32}$H$_{24}$N$_2$ClF$_6$PRu C: 53.52%, H: 3.36%, N: 3.90%. Found: C: 53.48%, H: 3.28%; N: 3.99%. NRM-δ_H (500 MHz; DMSO-d$_6$) 6.08 (1H, d, J = 5.5 Hz) 6.23 (2H, m) 6.26 (1H, m) 6.44 (2H, m) 7.37 (2H, t, J = 7.5, 15.0 Hz) 7.49 (2H, m) 7.62 (3H, m) 7.83 (2H, m) 8.18 (3H, m) 8.32 (1H, d, J = 4.9 Hz) 8.50 (1H, s) 8.71 (1H, s) 9.09 (1H, s) 9.54 (1H, d, J = 5.5 Hz). m/z (ESI) found 572.9 (calc. M[+] C$_{32}$H$_{24}$N$_2$ClRu = 573.0).

[Ru(η[6]-*m*-terp)(Anthimpy)Cl]PF$_6$ [33]. As synthetic procedure 2, using [Ru(η[6]-*p*-terp)$_2$Cl$_2$]Cl$_2$ (80 mg, 0.09 mmol) and Anthimpy (56 mg, 0.18 mmol). Yield 54%. Elemental analysis calc. for C$_{38}$H$_{28}$N$_2$ClF$_6$PRu C: 57.47%, H: 3.55%, N: 3.52%. Found: C: 57.60%, H: 3.48%; N: 4.11%. NRM-δ_H (500 MHz; DMSO-d$_6$) 6.41 (1H, t, J = 6.1, 12.2 Hz) 6.60 (1H, s,) 6.68 (1H, d, J = 7.0 Hz) 6.72 (1H, d, J = 6. 3 Hz) 7.41 (2H, t, J = 7.6, 15.1 Hz) 7.51 (3H, m) 7.63 (2H, m) 7.72 (1H, d, J = 7.4 Hz) 7.87 (1H, m) 7.92 (2H, d, J = 8.0 Hz) 8.04 (1H, d, J = 9.0Hz) 8.16 (1H, m) 8.29 (3H, m) 8.67 (1H, s) 9.03 (1H, s) 9.29 (1H, d, J = 5.4 Hz). m/z (ESI) found 649.0 (calc. M[+] C$_{38}$H$_{28}$N$_2$ClRu = 649.16).

4.2.3 Methods

4.2.3.1 Aquation studies

Aquation of complexes **24–33** was studied by proton NMR (500 and 600 MHz) as described in Chapter 2, using fresh solutions of each complex in D$_2$O at 310 K. In

order to suppress the aquation observed in all chlorido complexes, 150 mM NaCl was added to the deuterated solvent, and, 150 mM KI was used to suppress the aquation of iodido complexes.

4.2.3.2 Nucleobase binding

Complexes **24–33** were reacted with 9-ethylguanine, as a nucleobase model, the extent of binding was followed by ^{1}H-NMR (500 and 600 MHz). The details of these experiments can be found in Chapter 2. Briefly, a fresh 2 mM solution of each complex was prepared in 50 mM sodium phosphate buffer (pH 7.5) with 5% DMSO. The solution also contained 9-ethylguanine for a final mol. ratio 1:1.25 where the nucleobase was in excess. As in the case of aquation studies, ^{1}H-NMR spectra were recorded at 298 K within the first 10 min after sample preparation and again after 24 h at 500 MHz. All experiments were carried out in triplicate and the standard deviations calculated. Nucleobase binding was monitored by the formation of a second set of peaks that included bound-9-EtG.

4.2.3.3 Antiproliferative activity

The antiproliferative activity of ligands **19–23** and complexes **24–33** were determined in A2780 ovarian, A549 lung, HCT116 colon and MCF7 breast carcinoma cell lines. The experiments to determine IC_{50} values were carried out as described previously in Chapter 2. Briefly, 96 well plates were used to seed

5000 cells per well, they were left to pre-incubate in drug-free media at 310 K for 48 h before adding various concentrations of the compounds to be tested. A drug exposure period of 24 h was allowed, after this, supernatants were removed by suction and each well was washed with PBS (100 µL). Further 72 h were allowed for the cells to recover in drug-free media (200 µL per well) at 310 K. SRB assay was used to determine cell viability. IC_{50} values, as the concentration which caused 50% of cell growth inhibition, were determined as duplicate of triplicates in two independent set of experiments, their standard deviations were calculated.

4.2.3.4 Metal accumulation in cancer cells

Metal accumulation studies for complexes **24–33** were conducted on A2780 ovarian carcinoma cell line. Briefly, 4 x 10^6 cells were seeded on a Petri dish, after 24 h of pre-incubation time in drug-free medium at 310 K, the test complexes were added to give final concentrations equal to $IC_{50}/3$ and allowed further 24 h of drug exposure at the same temperature. After this time, cells were treated with trypsin, counted and cell pellets were collected. Each pellet was digested overnight in concentrated nitric acid (73%) at 353 K; the resulting solutions were diluted in double distilled water (to HNO_3 5%) and the amount of ruthenium taken up by the cells was determined by ICP-MS. These experiments did not allow any cell recovery time in drug-free media. They were all carried out in triplicate and the standard deviations were calculated. Results are compared to

the corresponding data for **CDDP**. More experimental details can be found in Chapter 2.

4.2.3.5 Determination of partition coefficient (Log P)

Partition coefficient of chlorido complexes **25** [Ru(η^6-p-cym)(Anthimpy)Cl]PF$_6$, **32** [Ru(η^6-bip)(Anthimpy)Cl]PF$_6$ and **33** [Ru(η^6-m-terp)(Anthimpy)Cl]PF$_6$ were determined using the shaking flask method. These three complexes were selected with the aim of studying the effect of the changes of the arene group on the lipophilicity of the complexes and how this relates to their antiproliferative activity. They all include the same ligand (Anthimpy, **23**) and the same leaving group (Cl). In the method used, 2 mM octanol-saturated aqueous solutions of the complexes were shaken with equal volumes of water-saturated octanol for 24 h. The amount of metal in the aqueous layer was determined by ICP-MS and the Log P values were calculated. Aqueous solutions were prepared including 150 mM of NaCl to avoid hydrolysis of the complexes. More details on this procedure can be found in Chapter 2.

4.2.3.6 DNA interactions

CT-DNA experiments were carried out in 10 mM phosphate buffer with 100 mM NaCl (for chlorido complexes) or 100 mM KI (for iodido complexes), at pH 7.5. In order to confirm that the CT-DNA was free from protein, a UV-VIS spectrum

was carried out in the phosphate buffer, giving an absorbance ratio of 1.92:1 at 260 nm/280 nm. Its concentration was determined using the UV absorbance at 260 nm and the known extinction coefficient at this wavelength (6600 $dm^3mol^{-1}cm^{-1}$).[16]

CT-DNA Melting. Thermal denaturation of CT-DNA was recorded by measuring the absorbance at 260 nm while increasing the temperature between 323 and 368 K. The melting curves of unruthenated and ruthenated CT-DNA were recorded using a fixed ratio of 1 : 5 Ru(II):CT-DNA (40 µM of the complex and 200 µM of CT-DNA). The value of the melting temperature (T_m) as the temperature when 50% of the present double-stranded CT-DNA converts into single-stranded CT-DNA was determined as the corresponding maximum on the first-derivative profile of the melting curves.

CT-DNA Binding Kinetics. Solutions of CT-DNA at a concentration of 200 µM were incubated with Ru(II) arene complexes **24, 25, 27, 28, 32** and **33** using a fixed complex concentration of 40 µM. The solutions were stabilised for 5 min at ambient temperature before being incubated at 310 K. At various time intervals (ranging from 1h to 72 h), a sample aliquot was withdrawn from the incubator, quickly cooled on an ice bath, and precipitated by ethanol (in a final alcohol concentration of 70%). The content of ruthenium in the supernatant of these samples was determined by ICP-MS. The amount of bound metal was calculated subtracting the free metal determined by ICP-MS from the original metal concentration.

CT-DNA UV-Vis Titrations. UV-Vis spectra titrations were performed to determine the DNA-binding affinity of complexes **24, 25, 27, 28, 32** and **33**. Experiments were carried out keeping fixed the concentration of the ruthenium(II) complexes (40 µM) while varying the concentration of CT-DNA (0, 20, 40, 60, 80, 100, 120, 160 and 200 µM) . The absorbance spectra were recorded after 10 min of each addition. This data allowed the calculation of CT-DNA binding constants for complexes **24–33** using the equation 4.1:[17,18]

$$\frac{A_0}{A-A_0} = \frac{\varepsilon_G}{\varepsilon - \varepsilon_G} + \frac{\varepsilon_G}{\varepsilon - \varepsilon_G} \, K \, [CT - DNA] \qquad \textbf{Eq. 4.1}$$
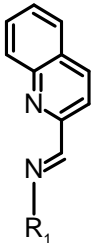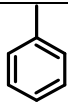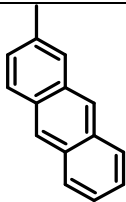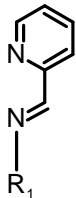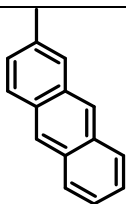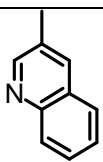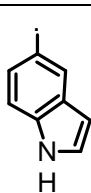
Where A_0 is the absorbance of the ruthenium complex on its own and A is the absorbance values in the presence of different concentrations of CT-DNA. The linear fitting of the plot $A_0/(A-A_0)$ vs 1/[CT-DNA] allowed the determination of the binding constant K.

4.3 Results

4.3.1 Synthesis and characterization
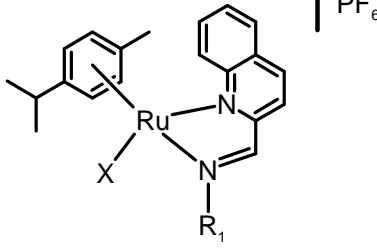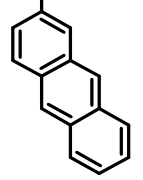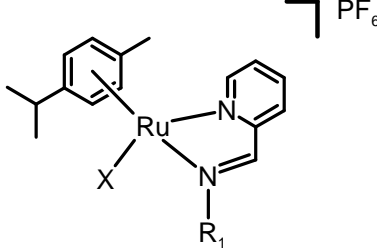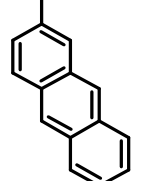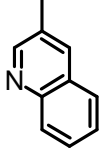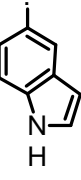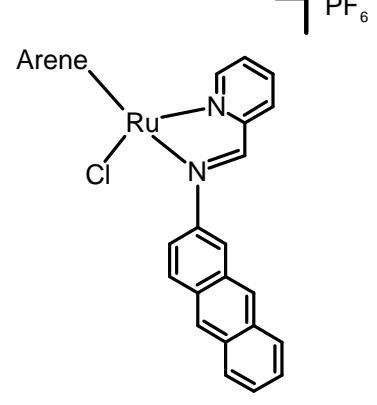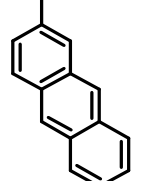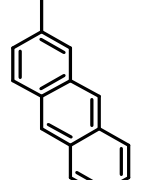
Iminopyridine ligands **19–23** shown in Table 4.1 below, were synthesised and characterised using ^{1}H and ^{13}C-NMR (1D, 2D experiments), ESI-MS, and elemental analysis.

Table 4.1. Imine ligands studied in Chapter 4.

	Ligands		R$_1$
	19	Phimqn	
	20	Anthimqn	
	21	Anthimpy	
	22	Qnimpy	
	23	Indoimpy	

Once the proposed ligands were fully characterised, complexes **24–33** in Table 4.2 were synthesised. They were characterised using the same techniques as for the ligands, ^{1}H and ^{13}C-NMR (1D, 2D experiments), ESI-MS, and elemental analysis, as well as, ICP-MS for metal quantification. The structures proposed in the table below are consistent with all experimental data.

Table 4.2. Ruthenium(II) arene complexes studied in Chapter 4.

	Complex	Arene	Ligand	R$_1$	X
	24		Phimqn		Cl
	25	p-η^6-cym	Anthimqn		Cl
	26				I
	27		Anthimpy		Cl
	28				I
	29	p-η^6- cym	Qnimpy		Cl
	30				I
	31		Indoimpy		Cl
	32	η^6-bip	Anthimpy		Cl
	33	η^6-m-terp	Anthimpy		Cl

155

4.3.2 Aqueous solution chemistry

Aquation of complexes **24–33** was followed using ^{1}H-NMR of freshly prepared solutions of each complex in Tris buffer (pH 7.5). Each value represents the mean ± SD for three independent NMR experiments at 310 K. Results are shown in Table 4.3. Extent of aquation of the complexes follow the order **29 > 25 > 31 > 30 > 28 > 27** with values that vary between 43 and 5% of the complex forming the aqua product. Remarkably, complexes **24** and **26** do not appear to undergo aquation.

Table 4.3. Extent of hydrolysis and extent 9-ethylguanine binding for complexes **24–33** after 24 h, using freshly prepared solutions of each complex in tris buffer (pH 7.5) and a final ratio 1 : 1.25 for 9-EtG binding where the nucleobase was in excess.

	Compound	% Aquation[a]	% 9-EtG binding[a]
24	$[Ru(\eta^6$-p-cym)(Phimqn)Cl]PF$_6$	0 ± 3	0 ± 2
25	$[Ru(\eta^6$-p-cym)(Anthimqn)Cl]PF$_6$	32 ± 3	0 ± 3
26	$[Ru(\eta^6$-p-cym)(Anthimqn)I]PF$_6$	0 ± 2	8 ± 3
27	$[Ru(\eta^6$-p-cym)(Anthimpy)Cl]PF$_6$	5 ± 2	13 ± 2
28	$[Ru(\eta^6$-p-cym)(Anthimpy)I]PF$_6$	12 ± 3	0 ± 2
29	$[Ru(\eta^6$-p-cym)(Qnimpy)Cl]PF$_6$	43 ± 2	38 ± 1
30	$[Ru(\eta^6$-p-cym)(Qnimpy)I]PF$_6$	24 ± 4	16 ± 3
31	$[Ru(\eta^6$-p-cym)(Indoimpy)Cl]PF$_6$	26 ± 3	5 ± 1

[a] Each value represents the mean ± SD for three independent NMR experiments at 310 K.

^{1}H -NMR was also used to follow the complexes binding to 9-ethylguanine (9-EtG) as a model for nucleobase binding. Table 4.3 also includes the extent of nucleobase adduct formation after 24 h. There is no clear trend that relate the

extent of aquation observed in the complexes with the extent of 9-EtG binding. Complexes **27, 29, 30** and **31** undergo aquation and subsequently they bind to the nucleobase model. However complexes **25** and **28** do not react with 9-EtG even though they can generate the aqua product. Particularly complex **24** does not undergo aquation nor binds to the nucleobase and complex **26** appears to undergo direct substitution, as it does not hydrolyse but forms approximately 8% of nucleobase adduct.

4.3.3 Antiproliferative activity

4.3.3.1 IC$_{50}$ determination in A2780, A549, HCT116, MCF7 cells

Antiproliferative activity for ligands **19–23** and complexes **24–33** was determined using the SRB assay, this protocol is detailed in Chapter 2. For these experiments compounds with IC$_{50}$ values (concentration at which 50% of cell growth is inhibited) above 100 μM are termed as inactive, while compounds with IC$_{50}$ values between 50 and 100 μM are moderately active. Values within the 15 - 50 μM range define a compound as active while below this range, compounds are considered highly active. All ligands tested were inactive against the chosen cell lines under the conditions described. Their IC$_{50}$ values are above 200 μM. All values reported in Table 4.4 were obtained as duplicates of triplicates in two independent experiments.

Table 4.4. Antiproliferative activity of ligands **19–23** and complexes **24–33** in A780, A549, HCT116 and MCF7 cell lines. IC_{50} is expressed as the concentration in which each ligand/complex causes 50% cancer cell growth inhibition. n/d = value not determined due to poor water solubility.

| | Compound | IC_{50} (µM) | | | |
		A2780	A549	HCT116	MCF7
Ligands	**19**	>200	>200	>200	>200
	20	n/d	n/d	n/d	n/d
	21	n/d	n/d	n/d	n/d
	22	>200	>200	>200	>200
	23	>200	>200	>200	>200
Ru^{II} complexes	**24**	15 ± 1	19 ± 1	17 ± 2	20.4 ± 0.9
	25	28 ± 3	56 ± 4	34 ± 2	28 ± 2
	26	1.56 ± 0.08	3.4 ± 0.8	2.7 ± 0.1	7.8 ± 0.4
	27	4.4 ± 0.7	24 ± 2	16 ± 2	6.9 ± 0.5
	28	1.7 ± 0.3	4.40 ± 0.09	2.6 ± 0.2	3.7 ± 0.5
	29	>200	>200	>200	>200
	30	156 ± 4	>200	180 ± 2	>200
	31	>200	>200	>200	>200
	32	9.2 ± 0.4	16 ± 1	23 ± 1	15.8 ± 0.4
	33	1.7 ± 0.3	8.3 ± 0.6	2.4 ± 0.2	2.7 ± 0.5

Complexes **29**, **30** and **31** are inactive in all cell lines tested, especially complexes **29** and **31**, as all their IC_{50} values are above 200 µM. Complexes **24** and **25** are considered active, showing their highest potency in ovarian cancer cells A2780. Finally, complexes **26**, **27**, **28**, **32** and **33** are highly active in the four cell lines tested. Complexes **26**, **28** and **33** show potency values equivalent to **CDDP**.

4.3.3.2 IC$_{50}$ Time dependence in A2780 cells

The variation of IC$_{50}$ values of complexes **24**, **25**, **26**, and **27** in the A2780 cell line, after different exposure times was evaluated using the protocol described in Chapter 2. These data were compared to that of **CDDP**.
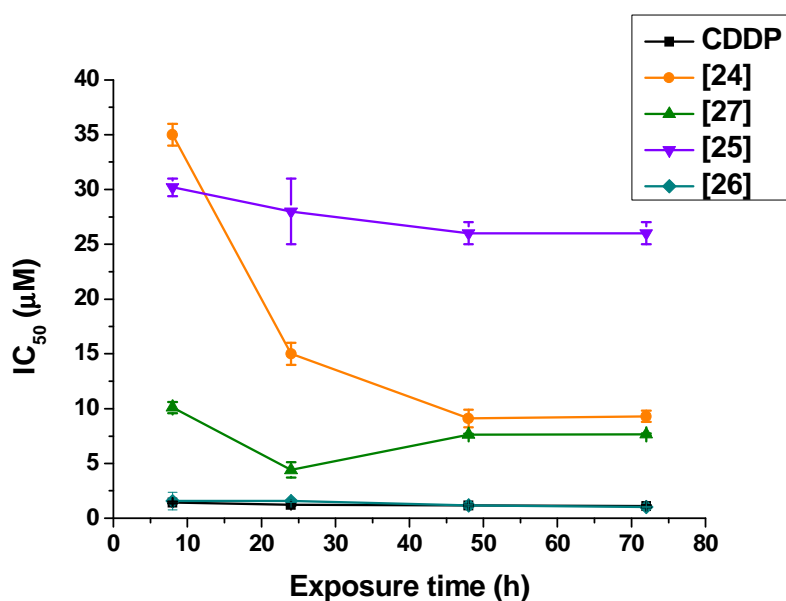
Exposure time (h)	IC$_{50}$ (μM)			
	8 h	**24 h**	**48 h**	**72 h**
24	35 ± 1	15 ± 1	9.1 ± 0.8	9.3 ± 05
25	30.2 ± 0.8	28 ± 1	26 ± 1	26 ± 1
26	1.57 ± 0.09	1.56 ± 0.08	1.17 ± 0.07	1.02 ± 0.06
27	10.1 ± 0.5	4.4 ± 0.7	7.62 ± 0.09	7.65 ± 0.09
CDDP	1.42 ± 0.09	1.22 ± 0.08	1.16 ± 0.07	1.10 ± 0.09

Figure 4.3. Dependence of IC$_{50}$ value in A2780 cell line on time of exposure for complexes **24, 25, 26,** and **27**. In all cases the pre-incubation time was 48 h before adding the drugs, and the cell recovery time was 72 h in drug-free médium at 310 K.

Results in Figure 4.3 indicate that there is no significant difference in the antiproliferative activity of the ruthenium(II) complexes after 24 h of drug exposure. Behaviour of complex **26** is very similar to that of CDDP, the IC_{50} values do not change significantly over time. The same is true for complex **25**. In the case of complex **24** there is a there is a big increase in potency between 8 h and 24 h, however the value stabilises after 48 h. A different behaviour is observed in complex **27**, its IC_{50} value reaches a minimum value at 24 h but it loses potency in the two following time points (48 and 72 h).

4.3.3.3 Metal accumulation in cancer cells

One time point, one concentration. Total cellular accumulation of ruthenium for complexes **24–33** was determined in the A2780 ovarian cancer cell line in order to relate the amount of Ru accumulated to cytotoxicity and to compare with their hydrophobicity (Log P). For these experiments drug exposure time was 24 h and cells were not allowed to recover. Values are expressed in ng of Ru per million cells and were determined as independent duplicates of triplicates. Results are shown in Table 4.5. Values determined for total cell accumulation follow the order **31** > **28** > **26** > **27** = **32** > **25** > **33** > **29** > **24** > **30**, with values ranging from 4.2 ng of ruthenium per 10^6 cells to 22 ng of the metal. This trend does not correlate to the IC_{50} values determined in the same cell line. Highly active complexes such as **24**, with an IC_{50} value of 15 ± 1 µM only exhibits a low accumulation of ruthenium (6.19 ± 0.09 ng Ru x10^6 cells) while inactive complex **31** (IC_{50} > 200 µM) shows the highest accumulation in the series (22 ± 1 ng Ru

$x10^6$ cells). It would indicate that, in this series of complexes, there is no direct correlation between potency and total cellular accumulation.

Table 4.5. Total accumulation of Ru in A2780 cells for complexes **24–33** after 24 h of drug exposure at 310 K with no recovery time, compared to their IC_{50} values in the same cell line..

	Compound	ng Ru $x10^6$ cells [a]	IC_{50} (μM)
24	[Ru(η^6-*p*-cym)(Phimqn)Cl]PF_6	6.19 ± 0.09	15 ± 1
25	[Ru(η^6-*p*-cym)(Anthimqn)Cl]PF_6	9.1 ± 0.4	28 ± 3
26	[Ru(η^6-*p*-cym)(Anthimqn)I]PF_6	11.7 ± 0.9	1.56 ± 0.08
27	[Ru(η^6-*p*-cym)(Anthimpy)Cl]PF_6	10.9 ± 0.8	4.4 ± 0.7
28	[Ru(η^6-*p*-cym)(Anthimpy)I]PF_6	17 ± 2	1.7 ± 0.3
29	[Ru(η^6-*p*-cym)(Qnimpy)Cl]PF_6	6.7 ± 0.4	>200
30	[Ru(η^6-*p*-cym)(Qnimpy)I]PF_6	4.2 ± 0.8	156 ± 4
31	[Ru(η^6-*p*-cym)(Indoimpy)Cl]PF_6	22 ± 1	>200
32	[Ru(η^6-bip)(Anthimpy)Cl]PF_6	10.9 ± 0.6	9.2 ± 0.4
33	[Ru(η^6-m-terp)(Anthimpy)Cl]PF_6	8.5 ± 0.6	1.7 ± 0.3

[a] Concentrations used were in all cases 1/3 x IC_{50}

4.3.3.4 Determination of partition coefficient (Log P)

Partition coefficients of chlorido complexes **27**, **32** and **33** were determined using the shaking flask method, as described in Chapter 2. These three complexes were selected with the aim of studying the effect of the changes of the arene group on the lipophilicity of the complexes. They all include the same *N,N*-chelating ligand (Anthimpy), and the same leaving group (Cl).To ensure that any of the complexes would not exist in the hydrolysed form during the experiments, 150 mM NaCl was added to the octanol-saturated water. Results are presented in Table 4.6. As expected, the Log P values of the complexes increase with increasing number of aromatic rings in the arene unit.

Table 4.6. Log P values for ruthenium complexes **27**, **32** and **33** determined using the shaking-flask method.

	Compound	Log P
27	[Ru(η^6-p-cym)(Anthimpy)Cl]PF$_6$	0.53 ± 0.04
32	[Ru(η^6-bip)(Anthimpy)Cl]PF$_6$	1.1 ± 0.4
33	[Ru(η^6-m-terp)(Anthimpy)Cl]PF$_6$	3.71 ± 0.09

4.3.3.5 DNA interactions

CT-DNA Melting. Thermal denaturation of CT-DNA was carried out using active complexes **7, 8, 24, 25, 27, 28, 32** and **33** (complexes **7** and **8** from Chapter 3 have been included for comparison purposes). Table 4.7 shows that the temperature in which 50% of the double stranded CT-DNA becomes single stranded is 335 K. There is a minor increase in melting temperature when co-incubating the CT-DNA with complexes **7, 8 24** and **25**. However there is no significant difference between each of the complexes. Highly active complexes **27**, **28**, **32** and **33** increase the melting temperature of CT-DNA in a range between 20 and 30 K.

CT-DNA Binding Kinetics. The kinetics of binding of complexes **7, 8, 24, 25, 27, 28, 32** and **33** to CT-DNA were determined in cell-free media. The results are expressed as the percentage of bound ruthenium against time. Figure 4.4 shows that the percentage of metal bound to CT-DNA after incubation at 310 K follows the order **25** < **24** < **27** < **28** < **32** < **33**. Highly active complexes **32** and **33** are the only ones that reach a percentage of bound ruthenium above 50%. Most of the

CT-DNA binding occurs within the first 10 h of reaction. Table 4.8 shows the values of the extent of CT-DNA binding after 48 h.

Table 4.7. T_m (K) values for complexes **7, 8, 24, 25, 27, 28, 32** and **33**. Melting curves of unruthenated and ruthenated CT-DNA were recorded using a fixed ratio of 1 : 5 Ru(II):CT-DNA (40 µM of the complex and 200 µM of CT-DNA).

	Compound	T_m (K)
7	$[Ru(\eta^6\text{-}p\text{-cym})(Impy)Cl]PF_6$	342 ± 1
8	$[Ru(\eta^6\text{-}p\text{-cym})(Impy)I]PF_6$	342 ± 2
24	$[Ru(\eta^6\text{-}p\text{-cym})(Phimqn)Cl]PF_6$	342 ± 1
25	$[Ru(\eta^6\text{-}p\text{-cym})(Anthimqn)Cl]PF_6$	342 ± 3
27	$[Ru(\eta^6\text{-}p\text{-cym})(Anthimpy)Cl]PF_6$	352 ± 1
28	$[Ru(\eta^6\text{-}p\text{-cym})(Anthimpy)I]PF_6$	358 ± 1
32	$[Ru(\eta^6\text{-bip})(Anthimpy)Cl]PF_6$	355 ± 2
33	$[Ru(\eta^6\text{-}m\text{-terp})(Anthimpy)Cl]PF_6$	362 ± 1
CT-DNA		**338 ± 1**
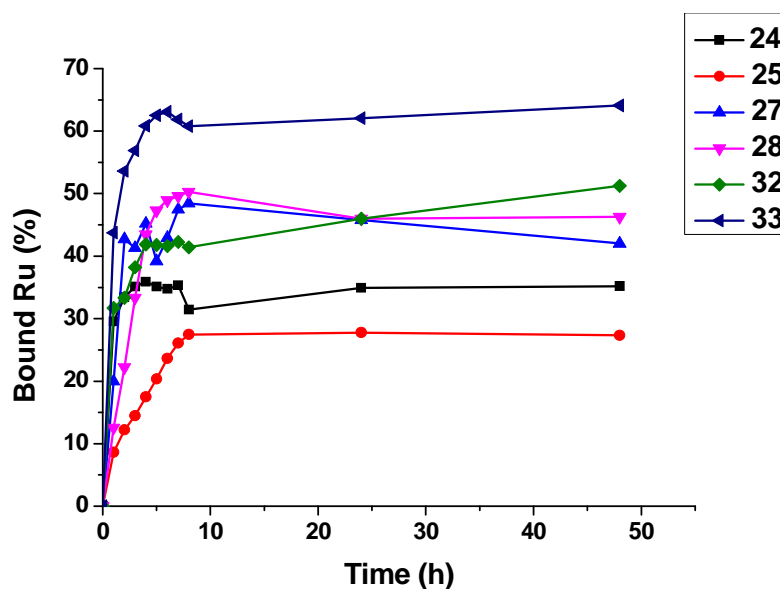
Figure 4.4. CT-DNA Binding kinetics for complexes **7, 8, 24, 25, 27, 28, 32** and **33** at 310K. Concentrations used were: CT-DNA 200 µM and Ru(II) complexes 40 µM. The solutions were stabilised for 5 min at RT before incubating them at 310 K.

Table 4.8. Extent of Ru bound to CT-DNA from complexes **7, 8, 24, 25, 27, 28, 32** and **33** after 48 h incubation at 310 K. Concentrations used were: CT-DNA 200 µM and Ru(II) arene complexes 40 µM.

	Compound	% bound Ru at 48 h
24	$[Ru(\eta^6\text{-}p\text{-cym})(Phimqn)Cl]PF_6$	35.1 ± 0.9
25	$[Ru(\eta^6\text{-}p\text{-cym})(Anthimqn)Cl]PF_6$	27.3 ± 0.8
27	$[Ru(\eta^6\text{-}p\text{-cym})(Anthimpy)Cl]PF_6$	42 ± 1
28	$[Ru(\eta^6\text{-}p\text{-cym})(Anthimpy)I]PF_6$	46.6 ± 0.7
32	$[Ru(\eta^6\text{-bip})(Anthimpy)Cl]PF_6$	51.2 ± 0.9
33	$[Ru(\eta^6\text{-}m\text{-terp})(Anthimpy)Cl]PF_6$	64.1 ± 0.9

CT-DNA UV-Vis Titrations. UV-Vis titrations were used to determine the binding affinity of complexes **7, 8, 24, 25, 27, 28, 32** and **33** to CT-DNA. Table 4.9 shows the binding constants determined. All binding constants are between 1.4 and 17 x 10^5 M^{-1} and follow the order: **27** < **7** < **8** < **32** < **28** < **25** < **24** < **33**. These values are within the reported range for complexes that intercalate into CT-DNA.[19,20]

Table 4.9. CT-DNA binding constants for ruthenium complexes **7, 8, 24, 25, 27, 28, 32** and **33** at 310 K. Concentrations used were: Ru(II) complexes 40 µM and CT-DNA 0, 20, 40, 60, 80, 100, 120, 160 and 200 µM.

	Compound	K_b x 10^5 (M^{-1})
7	[Ru(η^6-p-cym)(Impy)Cl]PF$_6$	1.6
8	[Ru(η^6-p-cym)(Impy)I]PF$_6$	2.5
24	[Ru(η^6-p-cym)(Phimqn)Cl]PF$_6$	8.0
25	[Ru(η^6-p-cym)(Anthimqn)Cl]PF$_6$	7.2
27	[Ru(η^6-p-cym)(Anthimpy)Cl]PF$_6$	1.4
28	[Ru(η^6-p-cym)(Anthimpy)I]PF$_6$	2.8
32	[Ru(η^6-bip)(Anthimpy)Cl]PF$_6$	2.7
33	[Ru(η^6-m-terp)(Anthimpy)Cl]PF$_6$	17

4.4 Discussion

Ru(II) complexes **24-31** were designed to include in their structures an increasing number of aromatic units, by modification of the *N,N*-chelating ligand, this in order to increase the likelihood of DNA-intercalation. This approach to fine-tuning the chemical and biological characteristics of metal complexes has been widely used previously with similar piano-stool structures.[21–23]

The start of the series is complex **7**, previously described in Chapter 3. From this starting point, an aromatic extension in the pyridine ring gives rise to complex **24**, while complex **25** includes extra aromatic units in both, the pyridine and the phenyl ring. The latter modification can also be seen in complexes **27**, **29** and **31**.

Data shown in Chapter 3 indicate that the cellular accumulation pathways used by chlorido complexes can be different from those involving iodido analogues. For this reason, this Chapter also included halogen exchange from Cl to I. This gives rise to complexes **8** (also reported in Chapter 3), **26**, **28** and **30**.

Finally, complexes **32** and **33** are a modification of chlorido complex **27**, in which the arene unit has been extended, this with the aim of correlating hydrophobicity and antiproliferative activity. A summary of the relation between the complexes investigated in this Chapter is shown in Figure 4.5.
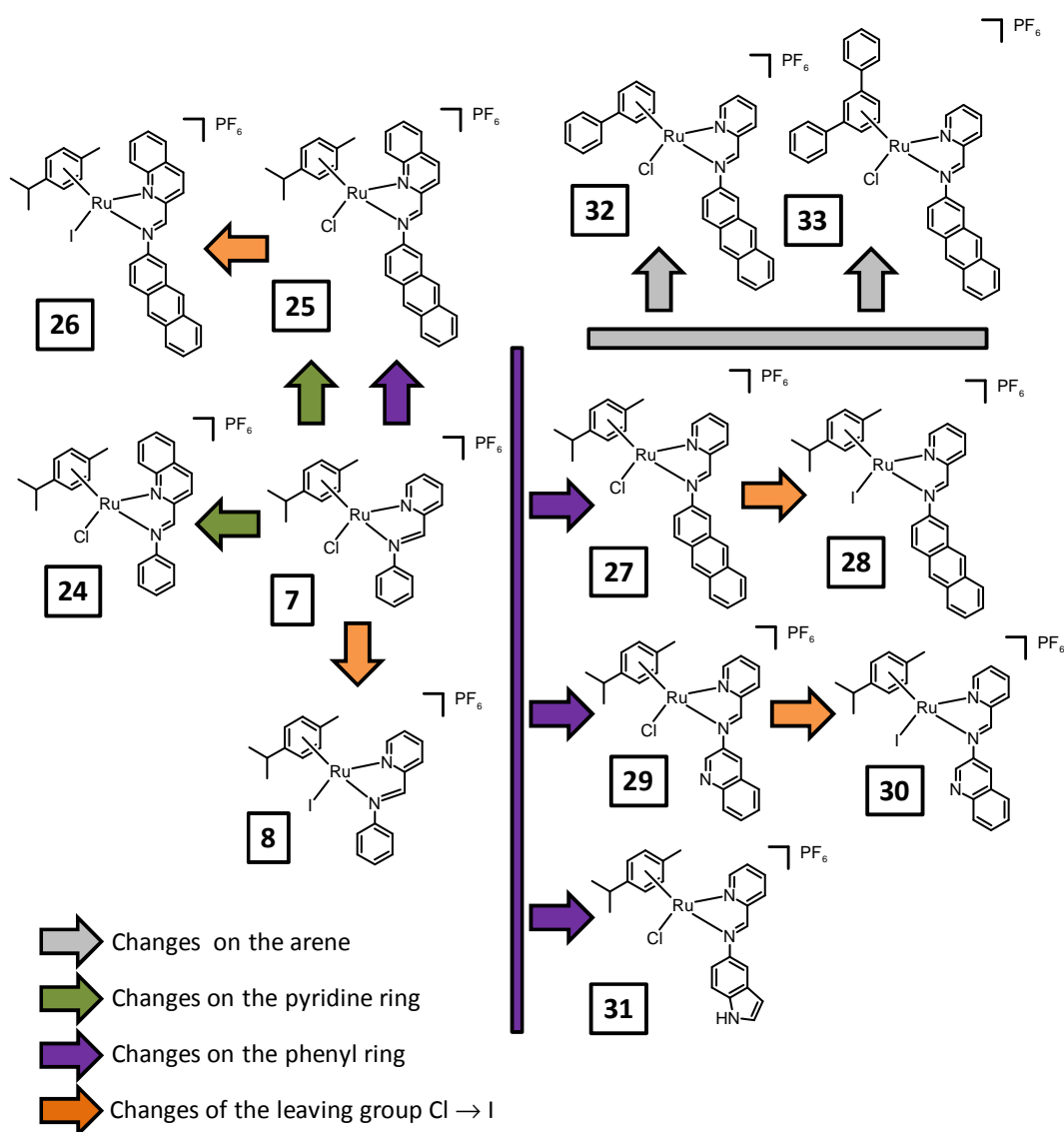
Figure 4.5 Relationship between the complexes investigated in this Chapter.

4.4.1 Aqueous chemistry

The aquation of complexes **24-31** was investigated, as it is thought that piano-stool complexes that bear halide ligands undergo aquation as an activation mechanism.[24] However, in the case of complexes **24-31** aquation could be

considered as an undesirable reaction, as the aim of these complexes is to interact with DNA by means of intercalation and not of covalent binding.

NMR was used to investigate the extent of aquation of complexes **24-31** after 24 h. Similarly to the data in Chapter 3, aquation was confirmed by means of its inhibition with NaCl/KI and by comparison to the aqua specie generated after AgNO$_3$ addition. The extent of 9-EtG binding was also investigated as a model for nucleobase interaction.

Figure 4.6 shows that the extent of aquation follows the order: **24** $=$ **26** $<$ **27** $<$ **28** $<$ **30** $<$ **31** $<$ **25** $<$ **29** and varies between 0 and 43%. This order cannot be related to the number of aromatic rings present in the structure, not even taken into account the differences in the monodentate ligands. For example, iodido complexes seem to follow a trend in which the modification on the pyridine ring caused less aquation than the modifications in the phenyl ring, such trend is not true for chlorido complexes, as complex **25** exhibits the second highest extent of aquation ($32 \pm 3\%$).

Also the same figure shows that there is no clear trend that correlates the observed extent of aquation to the extent of nucleobase binding. Interestingly, complex **24** [Ru(η^6-*p*-cym)(Phimqn)Cl]PF$_6$ does not undergo aquation nor does bind to 9-EtG; the same is true for complex **26** [Ru(η^6-*p*-cym)(Anthimqn)I]PF$_6$ for which the extent of nucleobase binding is negligible ($< 8\%$). These complexes, together with complex **25** [Ru(η^6-*p*-cym)(Anthimqn)Cl]PF$_6$ and **28** [Ru(η^6-*p*-cym)(Anthimpy)I]PF$_6$ have good potential as DNA intercalators as their binding to guanine is poor, regardless of their aquation.

Complexes **24-31** were further studied after 48 and 72 h to confirm that there was no decomposition in water or arene loss as it has been reported for similar complexes.[25,26] No variations were observed by NMR after this time.
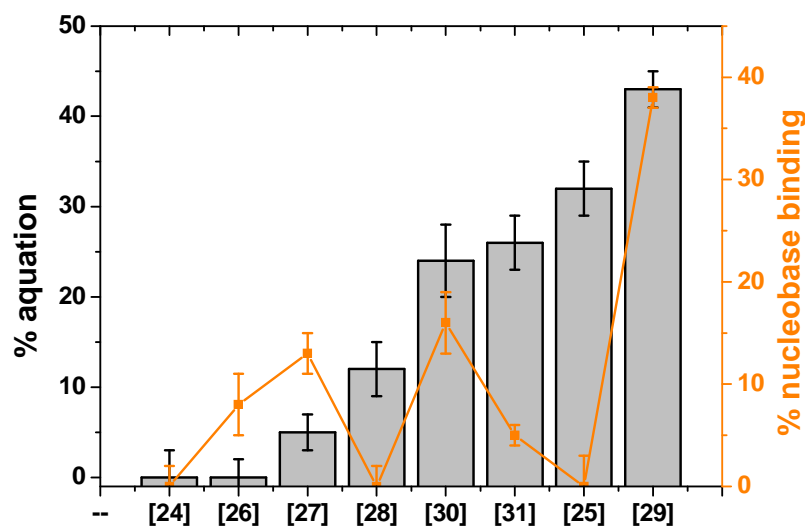
Figure 4.6. Comparison of the extent of aquation (left axis) and 9-EtG binding (right axis) of complexes **24-31** followed by ^{1}H-NMR at 310 K.

4.4.2 Antiproliferative activity

Antiproliferative activity of ligands **19**, **22** and **23** and complexes **24**-**33** was investigated in ovarian, lung, colon and breast cancer. It is noticeable that all the ligands tested were inactive in the chosen cell lines, under the conditions described. Ligands **20** Anthimqn, and **21** Anthimpy were not tested due to poor water solubility.

Complexes **29** - **31** are inactive in the four cell lines. Remarkably they all include in the structure an extra nitrogen atom in the *N,N*-chelating ligand. It is likely that

this heteroatom might be affecting the activity of these complexes. Comparing analogous complexes that vary only in their monodentate ligand (pairs **25** and **26**, **27** and **28**, **29** and **30**) it is observed that in all cases the iodido complexes are more active in all cell lines than the chlorido analogues. The highest improvement in potency is observed between complexes **25** and **26,** which share the ligand Anthimqn, in A2780 ovarian cells where the IC_{50} decreases by a factor of 18. This has been previously observed in Chapter 3 with similar Ru(II) complexes.

Results for time-dependence of IC_{50} values against time of exposure (Figure 4.3 on page 140) indicate that for complexes **25** and **26** the optimum period for drug-exposure is 24 h. However for complex **24** the highest potency is achieved after 48 h with a drop of IC_{50} from 15 to 9.1 μM between 24 and 48 h. The most interesting behaviour was that of complex **27**, which reaches its minimum IC_{50} at 24 h, but this value increases again between 48 and 72 h. This observation can be explained by the activation of detoxification mechanisms within the cell allowing for higher cell survival.

4.4.2.1 Metal accumulation in cancer cells

Metal accumulation in A2780 ovarian cells from complexes **24-33** was carried out in order to relate it to antiproliferative activity. Figure 4.7 and Figure 4.8 show that complexes with modifications on the *N,N*-chelating ligand do not accumulate in direct correlation to their potencies. Such observations have been previously reported for other related ruthenium arene complexes.[3] Complexes **24-26** have

been modified to include a quinoline as part of the *N,N*-chelating ligand. The difference between complexes **24** and **25** is two extra aromatic units in the imine moiety (ligand Phimqn vs Anthimqn). As expected this results in higher cellular accumulation. However, this improved accumulation does not achieve better potency.
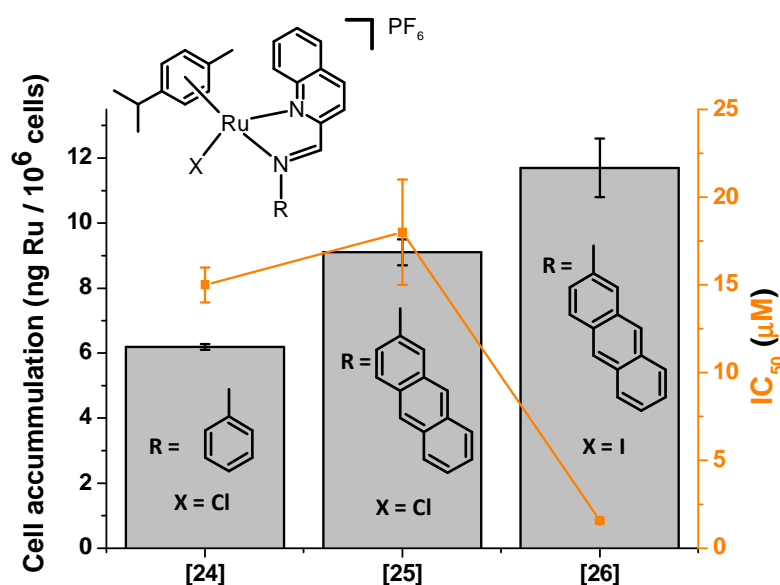
Figure 4.7. Comparison of the cellular accumulation of Ru from complexes **24-26** (left axis) and their antiproliferative activity (right axis). These complexes have in common the modification on the pyridine ring of the *N,N*-chelating ligand.

Complexes **27-31** have been modified on the phenyl ring of the *N,N*-chelating ligand. This series include complex **31** [Ru(η^6-*p*-cym)(Indoimpy)Cl]PF$_6$ which shows the highest cellular accumulation (22 ± 1 ng of Ru per 10^6 cells) however it is inactive with an IC$_{50}$ value > 200 μM. Another remarkable case is that of complexes **24** [Ru(η^6-*p*-cym)(Phimqn)Cl]PF$_6$ and **29** [Ru(η^6-*p*-cym)(Qnimpy)Cl]PF$_6$, both exhibit similar cellular accumulation (6.19 and 6.7 ng of Ru per 10^6 cells respectively) but the latter is inactive in A2780 cells while

complex **24** has an IC$_{50}$ of 15 ± 1 µM. This indicates that the cytotoxic effects caused by complex **24** inside A2780 cells are more efficient than those caused by complex **29**.

Active complexes that include different monodentate ligands (Cl vs I), pairs **25**, **26** with ligand Anthimqn and **27**, **28** with ligand Anthimpy have a common behaviour; in both cases the cellular accumulation of iodido analogue is higher than the chlorido analogues, with subsequent increased potency.
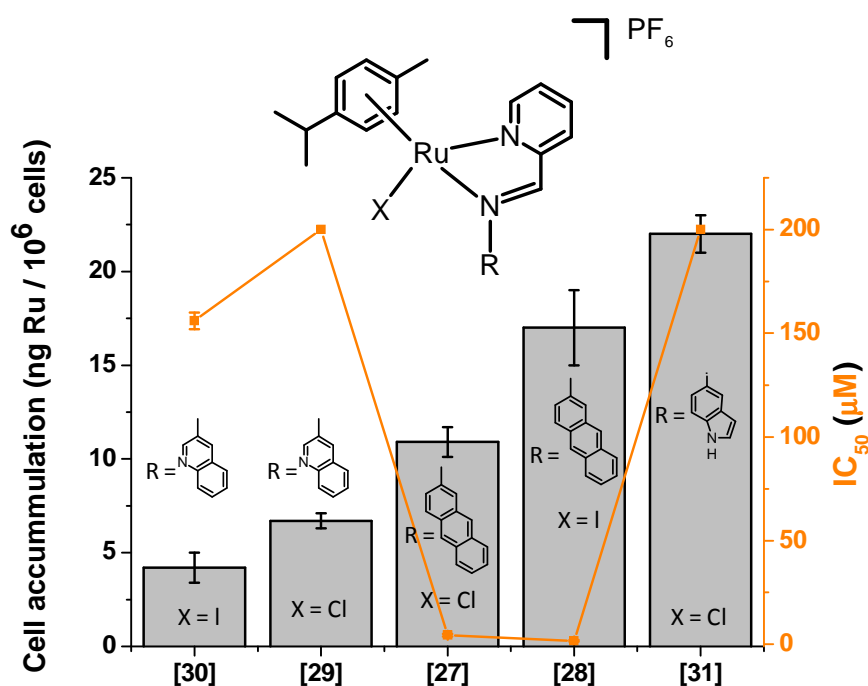
Figure 4.8. Comparison of the cellular accumulation of Ru from complexes **27-31** (left axis) and their antiproliferative activity (right axis). These complexes have all been modified on the phenyl ring of the *N,N*-chelating ligand.

Figure 4.9 shows the relation between cellular accumulation and potency when the arene unit of the complexes has been extended. Both complexes **27** and **32**

accumulate in the same extent inside A2780 ovarian cells, nonetheless, there is a two-fold difference in their cytotoxic activities, which reflects the variation in efficacy of the cytotoxic pathways activated. Complex **33** [Ru(η^6-*m*-terp)(Anthimpy)Cl]PF$_6$ which includes the most extended arene unit, terp, is the most active of this series, yet its cellular accumulation is only 8.5 ± 0.6 ng of Ru per 10^6 cells.
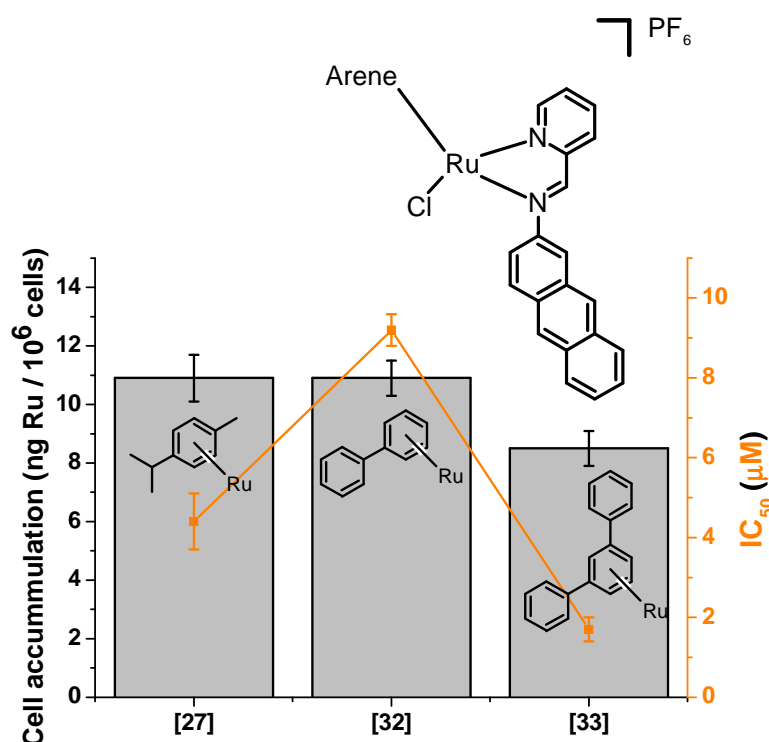
Figure 4.9. Comparison of the cellular accumulation of Ru from complexes **27**, **32, 33** (left axis) and their antiproliferative activity (right axis). These complexes have in common the *N,N*-chelating ligand, the monodentate ligand, Cl and include variations on the arene unit.

The cellular accumulation of complexes **27**, **32** and **33** can also be related to their log P values (Figure 4.10). Increasing hydrophobicity of the complexes follows

the expected trend **27** < **32** < **33** in which the arene unit increases in the number of aromatic rings, *p*-cym < bip < *m*-terp. Nonetheless, the increased lipophilicity of complex **33** does not result in higher cellular accumulation. This indicates that the transport of these complexes into A2780 cells do not rely solely on passive diffusion of the complexes, for which higher hydrophobicity should mean higher accumulation.
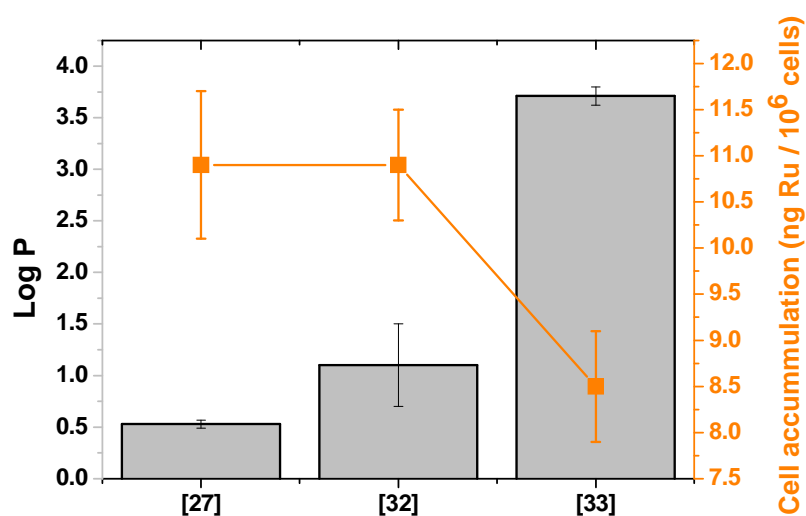
Figure 4.10. Comparison of the cellular accumulation of Ru from complexes **27**, **32, 33** (left axis) and their Log P values (right axis) determined using the shake flask method.

4.4.2.2 DNA interactions

CT-DNA Melting. Thermal denaturation is often used as a measurement of the interaction of metal complexes with DNA. Intercalating complexes tend to stabilise the double helix of DNA. This results in an increase of the melting temperature, as the point in which 50% of double-strand DNA becomes single-strand.[9,17] Such transformation is usually followed by UV-Vis spectroscopy,

measuring the hyperchromicity of the absorption band at 260 nm.[27] It can also be investigated by differential scanning calorimetry which measures the absorbance during denaturation.[28]

In the present Chapter thermal denaturation has been investigated by means of UV-Vis spectroscopy. Figure 4.11 shows the melting temperatures (T_m, K) determined and compares them to the corresponding value for free CT-DNA. Complexes **27** [Ru(η^6-*p*-cym)(Anthimpy)Cl]PF$_6$, **28** [Ru(η^6-*p*-cym) (Anthimpy)I]PF$_6$, **32** [Ru(η^6-bip)(Anthimpy)Cl]PF$_6$ and **33** [Ru(η^6-*m*-terp) (Anthimpy)Cl]PF$_6$ cause most stabilization of the double helix with ΔT_m values varying from 20 – 30 K. This result is consistent with previous reports that indicate that increasing the number of aromatic rings in the complex increases the T_m value for CT-DNA.[29] In particular Ru(II) complexes such as [(η^6-*m*-terp)Ru(en)Cl]PF$_6$ have been reported to stabilize DNA by effects of the positive charge on the metal centre, as well as the interactions between the arene unit and the base-pairs of DNA.[3]

In contrast complexes **7** [Ru(η^6-*p*-cym)(impy)Cl]PF$_6$, **8** [Ru(η^6-*p*-cym) (impy)I]PF$_6$ and **24** [Ru(η^6-*p*-cym)(Phimqn)Cl]PF$_6$ cause minimum variation to the T_m of CT-DNA (ΔT_m = 4 K). This is expected for complexes that do not intercalate. Given the structure of these complexes, it is a reasonable result. Ru(III) complex Na[trans-RuCl$_4$(DMSO)(Im)] is known to only cause slight stabilization of the double helix (ΔT_m = 2 K).[30]
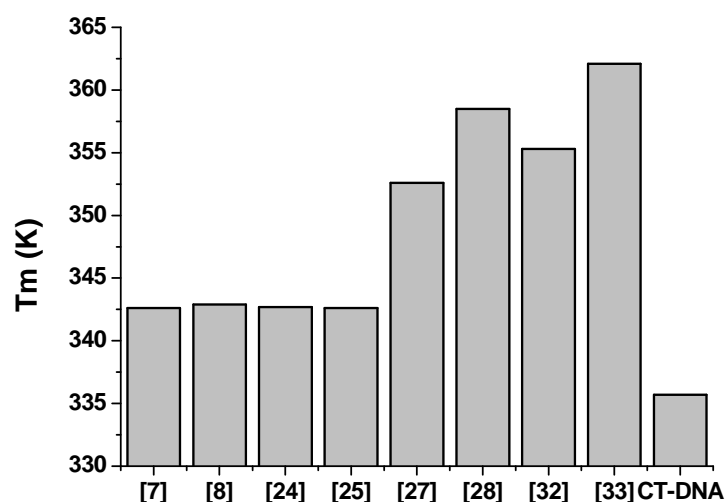
Figure 4.11. Comparison of the T_m (K) for CT-DNA when incubated with Ru complexes **7, 8, 24, 25, 27, 28, 32** and **33.**

Figure 4.12 compares the melting temperatures determined with the antiproliferative activity of the complexes in A2780 ovarian cancer cells. In this case there is a partial trend that correlates the extent of variation in T_m (K) to the cytotoxicity of the complexes in A2780 ovarian cells. Complexes **27, 28, 32** and **33** which caused the highest ΔT_m values are the most active in the series, with IC_{50} values varying from 9.2 to 1.7 µM. Remarkably, this trend is not always true for ruthenium complexes and depends greatly on the cell line.[16] Polypyridyl Ru(II) complexes with general formula $[(\eta^6\text{-}C_6Me_6)Ru(XY)]Cl$, where XY = dppz, dpq, dppn do not follow this trend. There is no correlation between their activity in MCF7 breast cancer cells or HT29 colon cancer cells and the ΔT_m values with CT-DNA.[29]
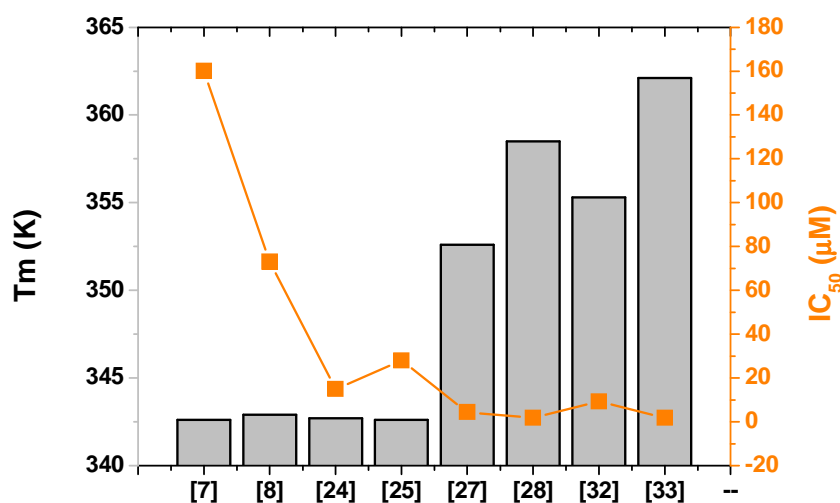
Figure 4.12. Comparison between the T_m (K) for CT-DNA when incubated with Ru complexes **7, 8, 24, 25, 27, 28, 32** and **33** (left axis) and the antiproliferative activity of the complexes in A2780 ovarian cells (right axis)**.**

Another possible correlation worth investigating is between melting temperatures and binding affinity of the complexes for CT-DNA. It has been reported that increasing ΔT_m values are related to increasing binding constants.[31,32] However this is not the case for complexes **7, 8, 24, 25, 27, 28, 32** and **33** as Figure 4.13 shows**.** One possible explanation relies on the different modes of intercalation.

Complete DNA intercalation is not the only non-covalent binding possible. There are two extra modes for DNA interaction: semi-intercalation and quasi-intercalation, both of which include partial intercalation of the aromatic unit between DNA base-pairs.[33] These interactions can cause enough stabilization of the double-helix to generate a difference in the melting temperature, without exhibiting high affinity between the metal complex and the CT-DNA.
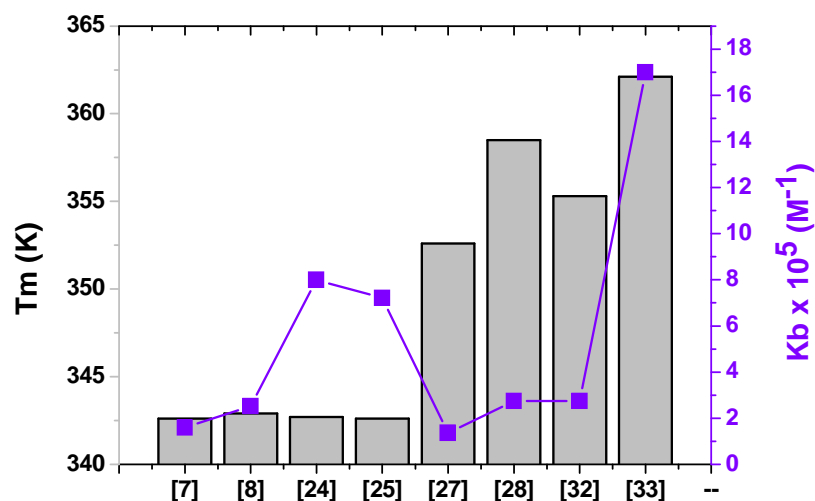
Figure 4.13. Comparison between the T_m (K) for CT-DNA when incubated with Ru complexes **7, 8, 24, 25, 27, 28, 32** and **33** (left axis) and their binding constants to CT-DNA (right axis)**.**

CT-DNA Binding Kinetics. The binding rate of complexes **7, 8, 24, 25, 27, 28, 32** and **33** to CT-DNA was determined using a constant ratio of CT-DNA to Ru(II). Figure 4.4 shows that all complexes bind rapidly to CT-DNA, reaching equilibrium after the first 10 h of incubation. The half-times of these reactions are lower that the equivalent process for **CDDP**.[3] It is interesting that only complexes **32** [Ru(η^6-bip)(Anthimpy)Cl]PF$_6$ and **33** [Ru(η^6-m-terp)(Anthimpy)Cl]PF$_6$ reach binding percentages above 50 after 48 h (Figure 4.14).

Complex **33** includes in its structure m-terp as the arene. This polyaromatic unit has been previously used with other Ru(II) complexes such as [(η^6-m-terp)Ru(en)Cl]$^+$.[3] Reports indicate that this complex binds to CT-DNA in cell-free media up to a 80% in 48 h. However it causes de-stabilisation of the double-helix and a subsequent decrease in the CT-DNA melting temperature ($\Delta T_m = -4$

K).[3] $[(\eta^6\text{-}m\text{-terp})\text{Ru(en)Cl}]^+$ is considerably less active than complex **33** in A2780 cells (42 ± 4 µM against 1.7 ± 0.3 µM) which indicates that the extent of metal binding to CT-DNA in cell-free media is not always directly proportional to the antiproliferative activity of the complexes, in contrast to the trend drawn by Figure 4.14. Interestingly, these results reflect only on the extent of intercalative binding between the Ru(II) complexes and CT-DNA, as the experiments are carried out in the presence of elevated NaCl concentrations which does not allow hydrolysis of the complexes and subsequent covalent binding to CT-DNA. Dinuclear Ru complexes that include in their structure the *p*-cymene unit such as $\{(\eta^6\text{-}p\text{-isopropyltoluene})\text{RuCl[3-(oxo-}\kappa\text{O)-2-methyl-4-pyridinonato-}\kappa\text{O}_4]\}$ have been reported to bind irreversibly to CT-DNA in cell-free media, reaching metal-bound percentages between 60 and 75%.[34]
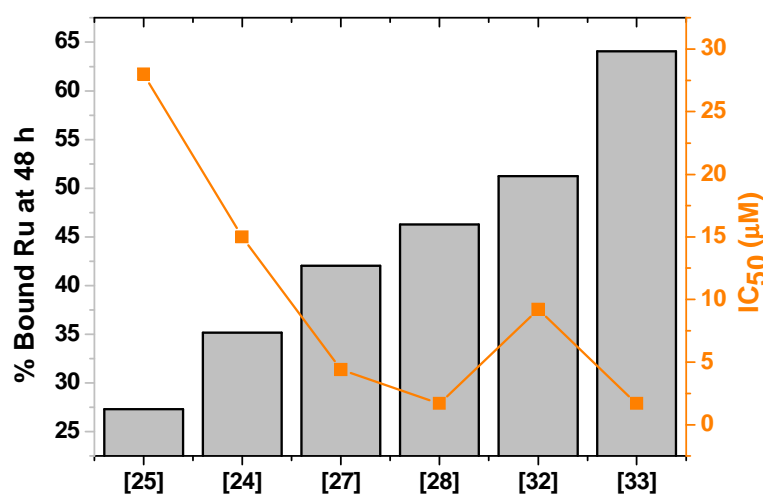
Figure 4.14. Comparison between the Ru bound to CT-DNA from complexes **7, 8, 24, 25, 27, 28, 32** and **33** (left axis) and their antiproliferative activities in A2780 ovarian cells (right axis).

CT-DNA Electronic Absorption Titrations. Binding interaction between complexes **7, 8, 24, 25, 27, 28, 32** and **33,** and CT-DNA were monitored by UV-Vis spectroscopy. In order to make sure that the interaction observed was indeed intercalation and not covalent binding, it was necessary to suppress the aquation of complexes **7**, **25**, **27**, **28**, **32** and **33**. Figure 4.15 (A) shows the aquation of complex **7** followed by UV-Vis in the course of 24 h at 310 K. Section (B) of the same figure shows how this reaction is suppressed by the use of 150 mM of NaCl, the spectrum obtained 5 min after mixing the sample overlaps completely with that obtained after 24 h. The suppression of the aquation by 150 mM of NaCl was also followed by ^{1}H-NMR. Finally section (C) in Figure 4.15 shows that there is no aquation of complex **24** over 24 h at 310 K.

Intercalation of metal complexes into CT-DNA usually results in batochromism of charge transfer bands.[17,18,35] This effect was observed in all the investigated Ru(II) arene complexes. Figure 4.16 shows the red-shift for complexes **7** (section A) and for complex **24** (section B) between 300 and 400 nm. At these wavelengths the π^* orbitals of the intercalated ligands could couple with the π orbital of the base pairs, thus decreasing the π-π^* transition energy. Bathochromism as a result of intercalation of a ligand into the base pairs of DNA has been widely studied.[9,20]
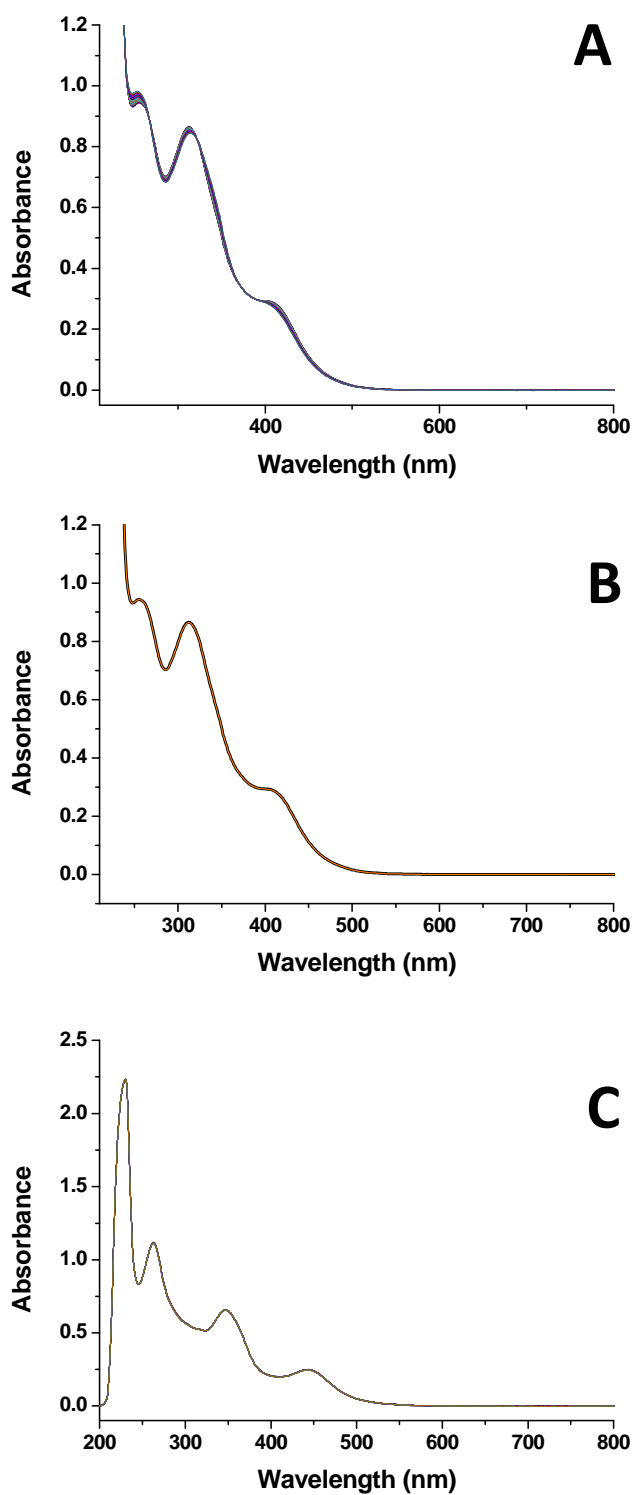
Figure 4.15. UV-Vis spectra of **(A)** aquation of complex **7**, **(B)** suppression of the aquation of complex **7** by addition of 150 mM of NaCl and **(C)** complex **24.** All experiments were carried out over 24 h at 310 K.
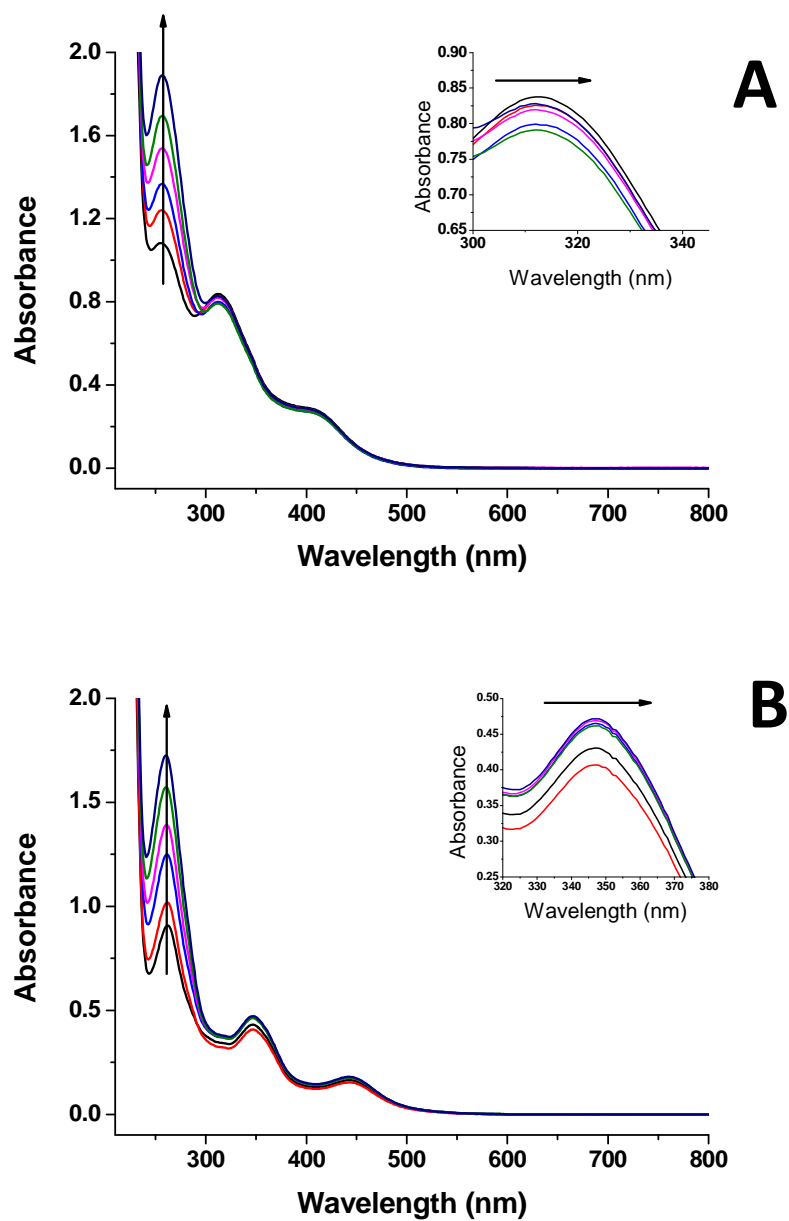
Figure 4.16. CT-DNA titrations with ruthenium complexes **7 (A),** and **24 (B).** Concentrations used were: Ru(II) complexes 40 µM and CT-DNA 0, 20, 40, 60, 80, 100, 120, 160 and 200 µM.

Titrations of complexes **7, 8, 24, 25, 27, 28, 32** and **33,** with CT-DNA were used to determine the binding constants of these compounds to the double helix. In

these experiments the NaCl concentration (150 mM) was fixed in order to suppress aquation and avoid covalent binding after activation of the arene complexes. Table 4.9 on page 165 lists the binding constants determined; all the values are in the order of 10^5 M^{-1} in comparison to other Ru(II) intercalators such as Ru(phen)$_2$(PHEHAT)$^{2+}$ which have K values in the order of 10^6.[19]

Figure 4.17 compares the binding constants for pairs of complexes. Complexes **7** and **8** are related by their *N,N*-chelating ligand, impy. These complexes differ in the monodentate ligand (Cl vs I). The same is true for complexes **27** and **28** which share the ligand Anthimpy. In both cases the binding constant Kb for the iodido analogues is higher than that for the chlorido complexes.
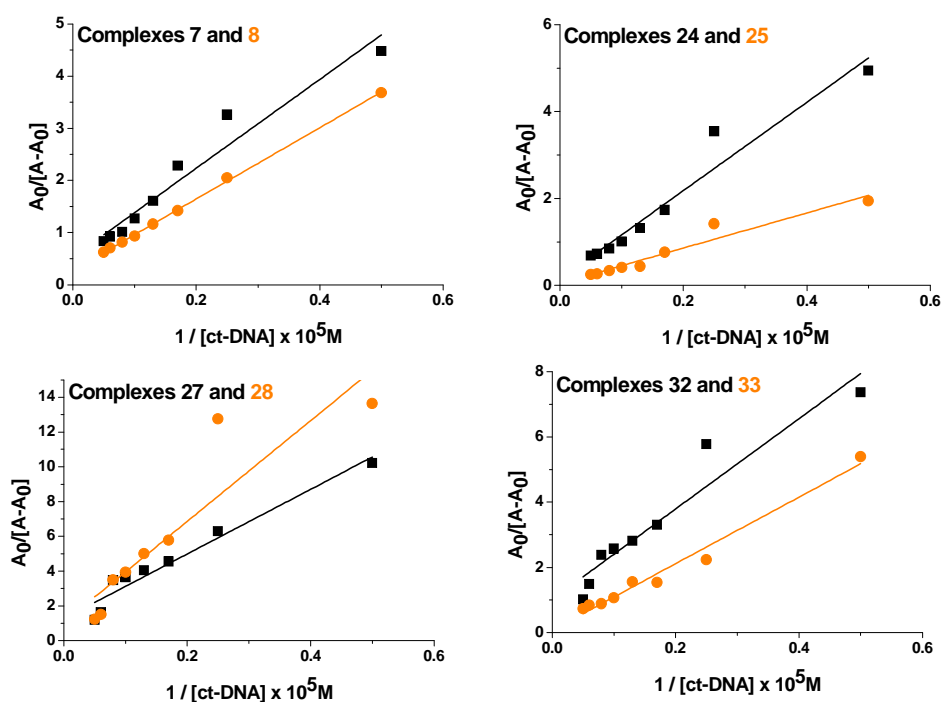
Figure 4.17. Comparison between the binding constants to CT-DNA of Ru complexes **7, 8, 24, 25, 27, 28, 32** and **33.**

In the case of the pair **24** and **25**, unexpectedly complex **25** exhibits a lower binding constant although it includes the Anthimqn ligand with a higher number of aromatic units. There is a marked difference between the binding constants of complexes the pair **24**, **25** and complex **33**. This could be attributed to the extended planarity of the arene unit. Such differences between the intercalative interaction of all-carbon aromatics and those containing nitrogen atoms has been previously reported[19,36] also the great importance of planarity in the intercalating ligand and its relation to the binding affinity has been investigated.[31,37]

Figure 4.18 relates the antiproliferative activity of the Ru(II) arene complexes and the observed K values for CT-DNA. For the extreme values of the IC_{50}, results seem to indicate that the potency of the complexes can be related to their ability to bind to CT-DNA. Inactive complex **7** has a low Kb value, while the contrary is true for complex **33,** which is highly active and exhibits the highest Kb. However, the relation between the middle values is not as clear. This inconsistency could indicate that these Ru(II) complexes are indeed multitargeted and that intercalation to DNA is not their main molecular mechanism. Ruthenium complexes, such as [Ru(terpy)(bpy)Cl]Cl, cis-[Ru(bpy)$_2$Cl$_2$], and mer-[Ru(terpy)Cl$_3$] do not show correlations between their reactivity towards CT-DNA and their antiproliferative activity.[38]

Complexes **7, 8, 24, 25, 27, 28, 32** and **33** all contain a chiral metal centre. Each separate isomer of a chiral complex can interact differently with DNA.[39–42] In the case of the present studies no attempt was made to separate the two isomers.
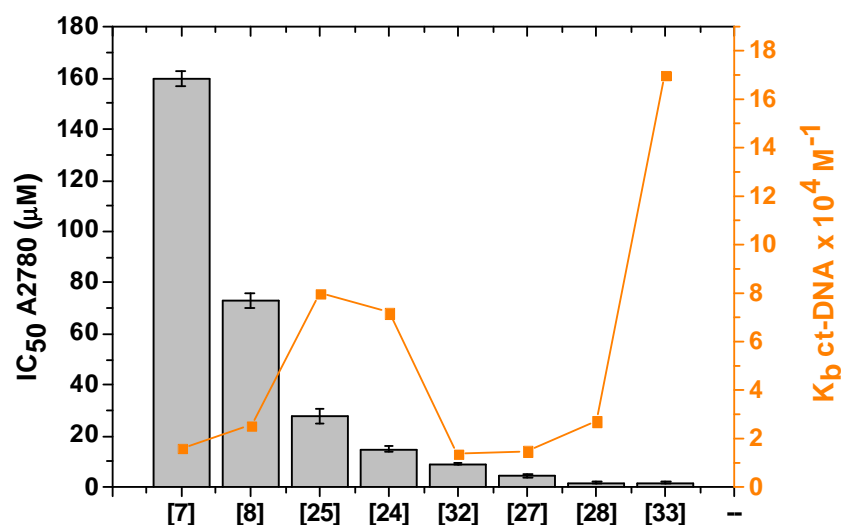
Figure 4.18. Comparison between the antiproliferative activity of Ru complexes **7, 8, 24, 25, 27, 28 ,32** and **33** in A2780 ovarian cells (left axis) and their binding constants to CT-DNA (right axis)**.**

4.5 Conclusions

The research presented in this Chapter aimed to investigate the potential of Ru(II) complexes for DNA intercalation, as a mechanism for antiproliferative activity. Iminopyridine ligands **19-23** were synthesised and characterised by conventional methods. This Chapter also describes the synthesis and characterization of complexes **24-33**. Aqueous chemistry of the Ru(II) complexes was investigated, with special attention to the relation between aquation and binding to 9-EtG as a model for nucleobase interactions. Results showed that there is no clear trend to correlate these parameters. The extent of aquation in complexes **24-33** vary from 0 to 43%. Antiproliferative activity of ligands and complexes was determined in A2780 ovarian, A549 lung, HCT116 colon and MCF7 breast cancer cells. All

ligands and complexes **29** [Ru(η^6-*p*-cym)(Qnimpy)Cl]PF$_6$, **31** [Ru(η^6-*p*-cym)(Indoimpy)Cl]PF$_6$ were inactive in the cell lines tested, while complexes **26** [Ru(η^6-*p*-cym)(Anthimqn)I]PF$_6$, **28** [Ru(η^6-*p*-cym)(Anthimpy)I]PF$_6$ and **33** [Ru(η^6-*p*-terp)(Anthimpy)Cl]PF$_6$ exhibited the most promising potency with IC$_{50}$ values comparable to those of **CDDP**. Time dependence of the antiproliferative activity on the length of the expose time was also determined for complexes **24-27**. Drug-exposure period of 24 h was optimum for complexes **25** [Ru(η^6-*p*-cym)(Anthimqn)Cl]PF$_6$ and **26** [Ru(η^6-*p*-cym)(Anthimqn)I]PF$_6$ as they reach their maximum potency at this time point. However, complex **24** [Ru(η^6-*p*-cym)(Phimqn)Cl]PF$_6$ is favoured by a longer exposure time, achieving best results after 48 h of incubation.

Cellular accumulation of complexes **24-33** was carried out in A2780 ovarian cells. The amount of Ru detected by ICP-MS ranges from 4.2 to 22 ng of the metal per 10^6 cells. This indicates that all the complexes, including inactives **29** and **31** are able to reach intracellular spaces. There was no direct relation between cellular accumulation and the antiproliferative activity exhibited by the complexes. Complexes **27, 32** and **33** share the *N,N*-chelating ligand, Anthimpy and the monodentate ligand, Cl. However they differ in the number of aromatic units in the arene (*p*-cym, bip and *m*-terp respectively). Determination of the Log P values confirms that increasing the number of aromatic rings increases the hydrophobicity of the complexes, although there is no direct correlation between these values and cellular accumulation or antiproliferative activity.

The most important results in this Chapter refer to the ability of the Ru(II) complexes to interact with CT-DNA. Thermal denaturation of CT-DNA was monitored by means of UV-Vis spectroscopy. Incubation with complexes **7, 8, 24** and **25** caused a minimum change of the melting temperature of the CT-DNA, indicating that intercalation is not likely to occur. In contrast, complexes **27, 28, 32** and **33** generated ΔT_m in the range of 20 – 30 K. The kinetics of CT-DNA binding in cell-free media was also investigated, in all cases the greatest extent of binding occurs during the first 10 h of incubation at 310 K. Only complexes **32** and **33** achieve binding above 50%. Finally DNA titrations were used to determine the affinity of the Ru(II) complexes to bind to CT-DNA. UV-Vis experiments showed bathochromic shifts for charge-transfer absorption bands which is indicative of DNA intercalation.

In general results indicate that although Ru(II) complexes synthesised in this Chapter interact with DNA mostly by means of intercalation, there is no direct correlation between these interactions and the antiproliferative activity exhibited by the complex. This supports the idea of piano-stool complexes being multitargeted, in this case DNA may well be one of the targets however it does not seem likely to be the principal target.

4.6 References

1.   E. Corral, A. C. G. Hotze, H. den Dulk, A. Leczkowska, A. Rodger, M. J. Hannon, and J. Reedijk, *J. Biol.Inorg. Chem.*, 2009, **14**, 439-448.

2.   O. Novakova, H. Chen, O. Vrana, A. Rodger, P. J. Sadler, and V. Brabec, *Biochemistry*, 2003, **42**, 11544-11554.

3.   T. Bugarcic, O. Nováková, A. Halámiková, L. Zerzánková, O. Vrána, J. Kaspárková, A. Habtemariam, S. Parsons, P. J. Sadler, and V. Brabec, *J. Med. Chem.*, 2008, **51**, 5310-5319.

4.   M. Melchart, A. Habtemariam, O. Novakova, S. Moggach, F. P. Fabbiani, S. Parsons, V. Brabec, and P. J. Sadler, *Inorg. Chem.*, 2007, **46**, 8950-8962.

5.   M. J. Clarke, *Coord. Chem. Rev.*, 2003, **236**, 209-233.

6.   B. M. Zeglis, V. C. Pierre, and J. K. Barton, *Chem. Commun.* , 2007, 4565-4679.

7.   H. Liu and P. J. Sadler, *Acc. Chem. Res.*, 2011, **44**, 349-359.

8.   L. Salassa, *Eur. J. Inorg. Chem.*, 2011, **2011**, 4931-4947.

9.   C. N. Sudhamani, H. S. Bhojya Naik, and D. Girija, *Synth. React. Inorg., Met.-Org., Nano-Met. Chem.*, 2012, **42**, 518-524.

10.   M. R. Gill and J. Thomas, *Chem. Soc. Rev.*, 2012, **41**, 3179-3192.

11.   L. N. Ji, X. H. Zou, and J. G. Liu, *Coord. Chem. Rev.*, 2001, **216-217**, 513-536.

12.   R. M. Hartshorn and J. K. Barton, *J. Am. Chem. Soc.*, 1992, 5919-5925.

13. K. J. Du, J. Q. Wang, J. F. Kou, G. Y. Li, L. L. Wang, H. Chao, and L. N. Ji, *Eur. J. Med. Chem.*, 2011, **46**, 1056-1065.

14. Y. J. Liu, H. Chao, L. F. Tan, Y. X. Yuan, W. Wei, and L. N. Ji, *J. Inorg. Biochem.*, 2005, **99**, 530-537.

15. M. S. Deshpande and A. S. Kumbhar, *J. Chem. Sci.*, 2005, **117**, 153-159.

16. H. Huang, Z. Li, Z. Liang, J. Yao, and Y. Liu, *Eur. J. Med. Chem.*, 2011, **46**, 3282-3290.

17. J. Lu, H. Guo, X. Zeng, Y. Zhang, P. Zhao, J. Jiang, and L. Zang, *J. Inorg. Biochem.*, 2012, **112**, 39-48.

18. C. Cai, X. Chen, and F. Ge, *Spectrochim. Acta, Part A*, 2010, **76**, 202-206.

19. C. Moucheron, A. Kirsh De Mesmaeker, and S. Choua, *Inorg. Chem.*, 1997, **2**, 584-592.

20. Q. Zhen, B. Ye, J. Liu, Q. Zhang, L. Ji, and L. Wang, *Inorg. Chim. Acta*, 2000, **303**, 141-147.

21. F. Wang, A. Habtemariam, E. van der Geer, R. Fernández, M. Melchart, R. J. Deeth, R. Aird, S. Guichard, F. P. Fabbiani, P. Lozano-Casal, I. D. H. Oswald, D. I. Jodrell, S. Parsons, and P. J. Sadler, *Proc. Natl. Acad. Sci. USA.*, 2005, **102**, 18269-18274.

22. A. Peacock, A. Habtemariam, R. Fernández, V. Walland, F. Fabbiani, S. Parsons, R. E. Aird, D. I. Jodrell, and P. J. Sadler, *J. Am. Chem. Soc.*, 2006, **128**, 1739-1748.

23. A. Peacock, S. Parsons, and P. J. Sadler, *J. Am. Chem. Soc.*, 2007, **129**, 3348-3357.

24. A. M. Pizarro, A. Habtemariam, and P. J. Sadler, *Top Organomet Chem*, 2010, **32**, 21-56.

25. T. Bugarcic, A. Habtemariam, R. J. Deeth, F. P. Fabbiani, S. Parsons, and P. J. Sadler, *Inorg. Chem.*, 2009, **48**, 9444-9453.

26. S. J. Dougan, M. Melchart, A. Habtemariam, S. Parsons, and P. J. Sadler, *Inorg. Chem.*, 2006, **45**, 10882-10894.

27. M. Ya, *Proc. Natl. Acad. Sci. USA.*, 1979, **76**, 101-105.

28. J. G. Duguid, V. Bloomfield, J. M. Benevides, and G. J. Thomas, *Biophys. J.*, 1996, **71**, 3350-3360.

29. S. Schäfer, I. Ott, R. Gust, and W. S. Sheldrick, *Eur. J. Inorg. Chem.*, 2007, 3034-3046.

30. C. Scolaro, A. Bergamo, L. Brescacin, R. Delfino, M. Cocchietto, G. Laurenczy, T. J. Geldbach, G. Sava, and P. J. Dyson, *J. Med. Chem.*, 2005, **48**, 4161-4171.

31. P. Zhao, L. C. Xu, J. W. Huang, K. C. Zheng, B. Fu, H. C. Yu, and L. N. Ji, *Biophys. Chem.*, 2008, **135**, 102-109.

32. C. C. Ju, A. G. Zhang, C. L. Yuan, X. L. Zhao, and K. Z. Wang, *J. Inorg. Biochem.*, 2011, **105**, 435-443.

33. P. Lincoln and B. Norde, *J. Phys. Chem. B*, 1998, **102**, 9583-9594.

34. O. Nováková, A. a Nazarov, C. G. Hartinger, B. K. Keppler, and V. Brabec, *Biochem. Pharmacol.*, 2009, **77**, 364-374.

35. H. Deng, J. Li, K. C. Zheng, Y. Yang, H. Chao, and L. N. Ji, *Inorg. Chim. Acta*, 2005, **358**, 3430-3440.

36. D. Lawrence Arockiasamy, S. Radhika, R. Parthasarathi, and B. U. Nair, *Eur. J. Med. Chem.*, 2009, **44**, 2044-2051.

37. P. Nagababu, J. N. L. Latha, and S. Satyanarayana, *Chem. Biodiversity*, 2006, **3**, 1219-1229.

38. O. Nováková, J. Kaspárková, O. Vrána, P. M. van Vliet, J. Reedijk, and V. Brabec, *Biochemistry*, 1995, **34**, 12369-12378.

39. J. K. Barton, A. T. Danishefsky, and J. M. Goldberg, *J. Am. Chem. Soc.*, 1984, **106**, 2172-2176.

40. N. Grover, N. Gupta, and H. H. Thorp, *J. Am. Chem. Soc.*, 1992, **114**, 3390-3393.

41. C. V. Kumar, J. K. Barton, and N. J. Turro, *J. Am. Chem. Soc.*, 1985, **107**, 5518-5523.

42. U. McDonnell, M. R. Hicks, M. J. Hannon, and A. Rodger, *J. Inorg. Biochem.*, 2008, **102**, 2052-2059.

Chapter 5

Antiproliferative pathways and mechanisms of action of half-sandwich Ru(II)/Os(II) arene complexes.

5.1 Introduction

There has been an important advance in the understanding of the mechanism of action of cisplatin and other platinum drugs.[1–7] However little is known on novel pathways followed by ruthenium or other transition metal complexes.[8] This impairs rational design and further improvement of drugs, especially of metal-based chemotherapeutics[9,10] Ruthenium/osmium based drugs are most likely multi-targeted,[11,12] which makes more difficult the study of the activation of cellular pathways that can lead to apoptosis.

In the present study, the activation of hallmark biochemical events in intrinsic and extrinsic apoptotic pathways has been investigated with the aim of gaining insight into the mechanism of action of half-sandwich arene complexes. For this, complexes **15** [Ru(η^6-p-cym)(p-Impy-NMe$_2$)Cl]PF$_6$, **16** [Ru(η^6-p-cym)(p-Impy-NMe$_2$)I]PF$_6$, **34** [Ru(η^6-p-cym)(p-Azpy-NMe$_2$)Cl]PF$_6$, **35** [Ru(η^6-p-cym)(p-Azpy-NMe$_2$)I]PF$_6$, **36** [Os(η^6-p-cym)(p-Impy-NMe$_2$)Cl]PF$_6$ and **37** [Os(η^6-p-cym)(p-Impy-NMe$_2$)I]PF$_6$ have been chosen. These compounds share important structural similarities and their differences will allow probing the impact of variation on activity and apoptosis mechanisms. The antiproliferative activity, metal accumulation and distribution of these complexes have been explored, as well as their effect on the cell cycle of A2780 ovarian cells.

Clinical drawbacks of platinum chemotherapeutics, such as acquired resistance give ruthenium /osmium complexes a potential clinical advantage.[7,13–15] Cisplatin cross-resistance in ovarian cancer cells has been evaluated in this Chapter as well

as oxaliplatin cross-resistance in colon carcinoma cells. Complexes **15, 16, 34–37** have been tested for induction of apoptosis and activation of caspase 3. Interestingly, the mechanism of action of chlorido complexes seems to be very different from that of the iodido analogues, as the latter are p53-independent. Finally, cellular detoxification mechanisms have been explored, especially those involving GSH, thus case co-incubation of complexes **15, 16, 34–37** with L-BSO achieves nanomolar antiproliferative activities. Figure 5.1 presents an overview of the apoptotic pathways investigated in this Chapter.

Figure 5.1. Overview of the apoptotic pathways investigated in Chapter 5.

5.2 Experimental section

5.2.1 Materials

Ruthenium(II) complexes **15** [Ru(η^6-*p*-cym)(*p*-Impy-NMe$_2$)Cl]PF$_6$ and **16** [Ru(η^6-*p*-cym)(*p*-Impy-NMe$_2$)I]PF$_6$ have been described in Chapter 3 and the arene dimer [(η^6-*p*-cym)RuCl$_2$]$_2$ in Chapter 2. Osmium(II) complexes **36** [Os(η^6-*p*-cym)(*p*-Impy-NMe$_2$)Cl]PF$_6$ and **37** [Os(η^6- *p*-cym)(*p*-Impy-NMe$_2$)I]PF$_6$ as well as the ligand *p*-Azpy-NMe$_2$ were kindly provided by Dr. Ying Fu.

L-Buthionine-sulfoximine L-BSO ($\geq$97%), auranofin ($\geq$98%), aphidicolin from *Nigrospora sphaerica* ($\geq$98%), etoposide ($\geq$98%), novobiocin sodium and staurosporine were purchased from Sigma Aldrich. Propidium iodide ($\geq$94%) and RNAse A for flow cytometry staining were also obtained from Sigma Aldrich together with the Annexin V-FITC Apoptosis Detection Kit for flow cytometry. Caspase activity was determined using the Caspase-3 Colorimetric Assay Kit from Cambridge Biosciences. Cell fractionation was carried out using FractionPREP kit from BioVision.

5.2.2 Preparation of complexes

[Ru(η^6-*p*-cym)(*p*-Impy-NMe$_2$)Cl]PF$_6$ [34][16]**.** Ruthenium *p*-cymene dimer [(η^6-*p*-cymene)RuCl$_2$]$_2$ (50 mg, 0.05 mmol) was dissolved in methanol (5 mL), placed in a round bottom flask, and two mol equiv of the ligand *p*-Azpy-NMe$_2$ were then added (23 mg, 0.10 mmol). The reaction mixture was left at ambient temperature

with constant stirring for 5 h. After this time 5 mol equiv of NH_4PF_6 were added to the mixture, which was left stirring for a further hour. The solid residue obtained was collected by filtration and recrystallised from ether (Yield 74%). Elemental analysis calc. for $C_{24}H_{28}N_4ClF_6PRu$, C: 45.05%, H: 2.21%, N: 8.76%. Found: C: 44.85%, H: 2.32%; N: 8.46%. NMR-δ_H (500 MHz; DMSO-d_6) 0.87 (6H, dd, J = 23.93, 11.51, 6.66 Hz) 2.26 (3H, s) 2.31 (1H, m) 2.52 (3H, s) 6.02 (1H, d, J = 5.75 Hz) 6.11 (2H, t, J = 11.51, 5.71 Hz) 6.32 (2H, d, J = 6.31 Hz) 6.99 (2H, d, J = 9.09 Hz), 7.69 (1H, t, J = 11.8, 6.66 Hz) 8.17 (2H, d, J = 8.18 Hz) 8.29 (1H, t, J = 14.24, 6.97 Hz) 8.39 (1H, d, J = 8.18 Hz) 9.41 (1H, d, J = 5.45 Hz). m/z (ESI) found 494.0 (calc. M^+ $C_{24}H_{28}N_4ClRu$ = 494.92).

[Ru(η^6-*p*-cym)(*p*-Impy-NMe$_2$)I]PF$_6$ [35][16]**.** Prepared as above, using 50 mg, (0.08 mmol) of [(η^6-*p*-cymene)RuI$_2$]$_2$ and 37 mg, (0.16 mmol) of *p*-Azpy-NMe$_2$ Yield 68%. Elemental analysis calc. for $C_{24}H_{28}N_4 F_6IPRu$ C: 39.42%, H: 1.93%, N: 7.66%. Found: C: 39.60%, H: 2.02%; N: 7.54%. NMR-δ_H (500 MHz; DMSO-d_6) 0.89 (6H, d, J = 6.70 Hz) 2.51 (6H, s) 2.58 (3H, s) 3.00 (1H, m) 5.95 (1H, d, J = 7.31 Hz) 6.11 (2H, t, J = 13.8, 6.01 Hz) 6.31 (1H, d, J = 6.70 Hz) 6.95 (2H, d, J = 9.75 Hz), 7.60 (1H, t, J = 14.10, 6.70 Hz) 8.16 (2H, d, J = 9.14 Hz) 8.23 (1H, t, J = 15.24, 8.53 Hz) 8.43 (1H, d, J = 7.75 Hz) 9.37 (1H, d, J = 5.44 Hz). m/z (ESI) found 586.4 (calc. M^+ $C_{24}H_{28}N_4IRu$ = 586.37).

5.2.3 Methods

5.2.3.1 Antiproliferative activity

The antiproliferative activity of complexes **15**, **16**, **34**–**37**, (Table 5.1, on page 197) were determined for A2780, A549, HCT116 and MCF7 carcinoma cell lines of ovarian, lung, colon and breast origin, respectively. They were also studied in A2780cis and HCT116Ox which are the corresponding **CDDP** and **OXA** resistant carcinoma cell lines, as well as HCT116p53-/- and MRC5, the former are modified HCT116 which have knocked out the p53 tumour suppressor and the latter are human foetal lung fibroblasts. The experiments to determine IC_{50} values were carried out as described in Chapter 2.

Briefly, 96-well plates were used to seed 5000 cells per well. The plates were left to pre-incubate in drug-free media at 310 K for 48 h before adding different concentrations of the compounds to be tested. In order to prepare the stock solution of the drug, the solid complex was dissolved first in DMSO to be then diluted in a 50:50 mixture of PBS : saline. A drug exposure period of 24 h was allowed. After this, supernatants were removed by suction and each well was washed with PBS (100 µL). A further 72 h was allowed for the cells to recover in drug-free medium (200 µL per well) at 310 K. The SRB assay was used to determine cell viability. IC_{50} values, as the concentration which caused 50% of cell death, were determined as duplicates of triplicates in two independent sets of experiments and their standard deviations were calculated.

5.2.3.2 Metal accumulation in cancer cells

Cell accumulation studies for complexes **15**, **16**, **34**–**37**, were conducted on A2780 ovarian cells. Briefly, 4 x 10^6 cells were seeded on a Petri dish, after 24 h of pre-incubation time, the complexes were added to give final concentrations equal to $IC_{50}/3$ and a further 24 h of drug exposure was allowed. After this time, cells were treated with trypsin, counted and cell pellets were collected. Each pellet was digested overnight in concentrated nitric acid (73%) at 353 K; the resulting solutions were diluted using double-distilled water to a final concentration of 5% HNO_3 and the amount of ruthenium/osmium taken up by the cells was determined by ICP-MS. These experiments did not include any cell recovery time in drug-free media, they were all carried out in triplicate and the standard deviations were calculated. The statistical significance of all cellular accumulation values was determined using a two-sided t-test with P<0.05. More experimental details can be found in Chapter 2.

5.2.3.3 Metal distribution in cancer cells

In order to study metal distribution in A2780 cells for complexes **15**, **16**, **34**–**37**, FractionPREP kit from BioVision was used according to the manufacturer's instructions. Briefly, 4 x 10^6 cells were seeded on a Petri dish. After 24 h of pre-incubation time in drug-free media at 310 K, the complexes were added to give final concentrations equal to $IC_{50}/3$ and further 24 h of drug exposure were allowed. Cells were treated with trypsin, counted and cell pellets were collected

after 5 min centrifugation at 2000 rpm, 277 K. Samples were re-suspended in the cytosol extraction buffer provided in the kit (CEB, 400 µL) and were kept on ice for 20 min to be centrifuged at 277 K for 10 min at 2000 rpm. Supernatants containing the cytosolic fractions were collected. Pellets were re-suspended in the membrane extraction buffers A (400 µL) and B (22 µL), also provided in the cell fractionation kit and vortexed for 1 min before being centrifuged at 277 K for 5 min at 3400 rpm. Supernatants containing the membrane fractions were collected. Samples were re-suspended in the nuclear extraction buffer provided (NEB, 200 µL) and kept on ice for 40 min. After this time, pellets were centrifuged at 12000 rpm for 10 min. Supernatants containing the nuclear fractions were collected and the remaining pellets were kept as the cytoskeletal fractions. Samples were stored at 253 K until further analysis.

Each sample was digested overnight in concentrated nitric acid (73%, 150 µL) at 353 K; the resulting solutions were diluted with double-distilled water (to HNO_3 5%) and the amount of ruthenium/osmium taken up by the cells was determined by ICP-MS, as decribed in Chapter 2. These experiments were all carried out in triplicate and the standard deviations were calculated.

5.2.3.4 Antiproliferative pathways and mechanism of action

- **Cell cycle analysis using flow cytometry**

Complexes **15**, **16**, **34**–**37**, and **CDDP** were used to study their effects on the cycle of A2780 ovarian cells. For this, A2780 cells were seeded in a 6-well plate

using 1.5×10^6 cells per well. Cells were pre-incubated in drug-free media at 310 K for 24 h, after which drugs were added using equipotent concentrations equal to $IC_{50}/3$. After 24 h of drug exposure, supernatants were removed by suction and cells were washed with PBS (2 mL/well). Finally, cells were harvested using trypsin (0.5 mL/well). Samples were centrifuged to pellets at 1000 rpm for 4 min at 277 K. Cell pellets were washed with PBS (5 mL), re-centrifuged and the supernatant was removed. Cells were fixed for 2 h at 253 K using ice-cold ethanol (70%, 5 mL). DNA staining was achieved by re-suspending the cell pellets in 300 μL of PBS containing 7.5 μM propidium iodide (PI) and 100 μg/mL of RNAse A. After staining cell pellets for 30 min at ambient temperature, they were centrifuged at 1000 rpm, 277 K for 5 min, the supernatants were removed by suction and discarded. Cell pellets were resuspended in PBS (5 mL) before being analysed by flow cytometry using the maximum excitation of PI-bound DNA at 536 nm, and its emission at 617 nm. Data were processed using Flowjo software. Further studies on cell cycle were carried out using complex **16** [Ru(η^6-p-cym)(p-Impy-NMe$_2$)I]PF$_6$ and **CDDP** in order to determine the concentration dependence of the changes in the cell cycle. In these studies, A2780 cells were exposed to different concentrations of the compounds, including values below and above their IC_{50}'s. Sample treatment was as described above.

- **p53-activated apoptotic pathway**

IC_{50} values for complexes **15**, **16**, **34–37** were determined in the HCT116p53-/- cell line which has the tumour suppressor p53 knocked-out. Briefly, a 96-well plate was seeded with 5000 A2780 cells per well. Cells were pre-incubated in

drug-free medium for 48 h at 310 K before adding the corresponding metal complex for a 24 h period of drug exposure. Afterwards, drugs were removed by suction, cells were washed with PBS (100 μL/well) and fresh medium was added to the plate (200 μL/well). Cells were allowed to recover in drug-free medium for 72 h at 310 K. After this period of time, the SRB assay was used to determine cell viability. IC_{50} values were determined as duplicate of triplicates in two independent set of experiments and their standard deviations were calculated.

- **Induction of Apoptosis**

Flow cytometry analysis of apoptotic populations of A2780 cells caused by exposure to complexes **15**, **16**, **34**–**37**, were carried out using the Annexin V-FITC Apoptosis Detection Kit. This kit, from Sigma Aldrich, was used according to the manufacturer's instructions. Briefly, A2780 cells were seeded in a 6-well plate using 1.5 x 10^6 cells per well. Cells were pre-incubated in drug-free medium at 310 K for 24 h, after which drugs were added using equipotent concentrations of $IC_{50}/3$. After 24 h of drug exposure, supernatants were removed by suction and cells were washed with PBS (2 mL/well). Finally cells were harvested using trypsin (0.5 mL/well). Samples were centrifuged to pellets at 1000 rpm for 4 min at 377 K. Cell pellets were washed with PBS (1 mL), re-centrifuged and the supernatant was removed by suction. In this case, cell pellets were re-suspended in 500 μL of binding buffer containing Annexin V FITC conjugate (50 mg/mL in 50 mM Tris-HCl, pH 7.5, containing 100 mM NaCl) and a PI solution (100 mg/mL in 10 mM potassium phosphate buffer, pH 7.4, containing 150 mM NaCl).

After staining cell pellets for 10 min at ambient temperature, they were washed in PBS (2 mL) before being analysed in a Becton Dickinson FACScan Flow Cytometer. For positive-apoptosis controls A2780 cells were exposed for 2 h to staurosporine (1 µg/mL). Cells for apoptosis studies were used with no previous fixing procedure as to avoid non-specific binding of the annexin V-FITC conjugate. Data were processed using Flowjo software.

Further studies on cell apoptosis were carried out using complex **16** [Ru(η^6-*p*-cym)(*p*-Impy-NMe$_2$)I]PF$_6$. In these studies, A2780 cells were exposed to different concentrations of the compound, including values below and above its IC$_{50}$ in order to investigate the effect of the concentration of the drug on the extent of apoptosis observed. Sample treatment was as described above.

- **Caspase 3 apoptotic pathway**

Colorimetric analysis of caspase 3 activation caused on A2780 ovarian cells by exposure to complexes **15**, **16**, **34–37** was carried out using the Caspase-3/CPP32 Colorimetric assay Kit and used according to the manufacturer's instructions. Briefly, A2780 cells were seeded in a 6-well plate using 1.5×10^6 cells per well. Cells were pre-incubated for 24 h in drug-free media at 310 K, after which drugs were added using equipotent concentrations of IC$_{50}$/3. After 24 h of drug exposure, supernatants were removed by suction and cells were washed PBS (2 mL/well), finally cells were harvested using trypsin (0.5 mL/well). Samples were centrifuged to pellets at 1000 rpm for 4 min, 277 K. Cell pellets were washed with PBS (1 mL), re-centrifuged and the supernatant was removed by suction. In this

case cell pellets were re-suspended in cold lysis buffer (50 µL) provided in the kit. Cells were kept on ice for 10 min and then centrifuged at 10.000 g for 1 min at 277 K. The supernatants were collected in clean tubes and put on ice. To each sample cell lysis buffer, 2X reaction buffer (50 µL of each) and 5 µL of DEV-pNA substrate were added before incubating them for 2 h at 310 K. The resulting solutions were read in an absorbance plate reader at 410 nm. Samples were analysed in triplicate, and the standard deviations were calculated. For positive activation of caspase 3 A2780 cells were exposed to staurosporine (1 µg/mL) for 2 h.

- ## DNA replication

IC_{50} modulation experiments for complexes **15**, **16**, **34–37** by the inhibition of DNA polymerase α and topoisomerase II were performed using the protocol previously described for IC_{50} determination with the following modifications. Briefly, a 96-well plate was seeded with 5000 A2780 ovarian cells per well. Cells were pre-incubated in drug-free medium for 48 h at 310 K, before adding the metal complexes together with the appropriate co-incubating agent (aphidicolin, novobiocin or etoposide). In order to prepare the stock solution of the drug, the solid complex was dissolved first in DMSO to be then diluted in a 50:50 mixture of PBS : saline. Separately, a stock solution of the co-incubation agent was prepared in saline. Both solutions were added to each well independently, but within 5 min of each other.

After 24 of exposure, drugs were removed by suction, cells were washed with PBS (100 μL per well) and fresh medium was added to the plate (200 μL per well). Cells were allowed to recover in drug-free medium for 72 h at 310 K. At the end of this period, the SRB assay was used to determine cell viability. IC_{50} values, as the concentration which caused 50% of cell death, were determined as duplicates of triplicates in two independent set of experiments and their standard deviations were calculated. In all the experiments that involved modulation of IC_{50} values, the set up included two different negative controls; number 1 is untreated, while number 2 is treated only with the co-incubating agent. These controls are in place to make sure that the dose of the co-incubating agent is non-toxic. Their value was always within 5% difference to the negative control 1. The statistical significance of all cellular accumulation values was determined using a two-sided t-test with P<0.05.

- **Inhibition of DNA polymerase α - co-incubation with aphidicolin:** 1 μM, 5 μM or 10 μM of aphidicolin was used for co-incubation with complexes **15**, **16**, **34–37** (see aphicolidin structure in Figure 5.28 on page 253).

- **Inhibition of topoisomerase II - co-incubation with Novobiocin and Etoposide:** Complexes **15**, **16**, **34–37** were also coincubated with 5 μM of novobiocin, and separatedly with 10 μM of etoposide (see novobiocin structure in Figure 5.30 on page 256 and etoposide structure in Figure 5.29 on page 255).

- **Cellular detoxification mechanisms**

The possible involvement of GSH and thioredoxin reductase in modulating IC$_{50}$ values was investigated by using the protocol described in the above section (see DNA replication) with the following modifications.

- **Interaction with GSH:** complexes **15**, **16**, **34–37** were co-incubated with L-BSO 1 μM, 5 μM or 50 μM. (see L-BSO structure in Figure 5.31 on page 258).

- **Interaction with thioredoxin reductase:** complexes **15**, **16**, **34–37** were coincubated with 0.1 μM auranofin.

5.3 Results

5.3.1 Synthesis and characterization

Ruthenium(II) complexes **15**, **16**, **34**, **35** and osmium(II) complexes **36** and **37** shown in Table 5.1, were synthesised and characterised using NMR, ESI-MS and elemental analysis as well as ICP-MS for metal quantification. The purity of the compounds by elemental analysis was in all cases ≥ 95%.

Table 5.1. Complexes investigated in Chapter 5.
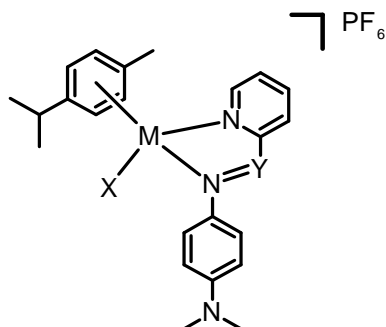
Compound		M	X	Y
15	[Ru(η^6-p-cym)(p-Impy-NMe$_2$)Cl]PF$_6$	Ru	Cl	C
16	[Ru(η^6-p-cym)(p-Impy-NMe$_2$)I]PF$_6$	Ru	I	C
34	[Ru(η^6-p-cym)(p-Azpy-NMe$_2$)Cl]PF$_6$	Ru	Cl	N
35	[Ru(η^6-p-cym)(p-Azpy-NMe$_2$)I]PF$_6$	Ru	I	N
36	[Os(η^6-p-cym)(p-Impy-NMe$_2$)Cl]PF$_6$	Os	Cl	C
37	[Os(η^6-p-cym)(p-Impy-NMe$_2$)I]PF$_6$	Os	I	C

5.3.2 Antiproliferative activity

Complexes **15**, **16**, **34**–**37** were tested in A2780, A549, HCT116 and MCF7 carcinoma cells, IC$_{50}$ values determined are shown in Table 5.2. All arene complexes investigated are highly active in all parental cell lines (IC$_{50}$ values < 17 µM), especially azopyridine iodido ruthenium complex **35** [Ru(η^6-p-cym)(p-Azpy-NMe$_2$)I]PF$_6$ which exhibits sub-micro molar activity in A2780 and MCF7 cell lines and is, in all cases, more potent than **CDDP**.

Table 5.2. Antiproliferative activity of complexes **15**, **16**, **34–37**, **CDDP** and **OXA** in A2780, A549, HCT116 and MCF7 cell lines. n/d = not determined.
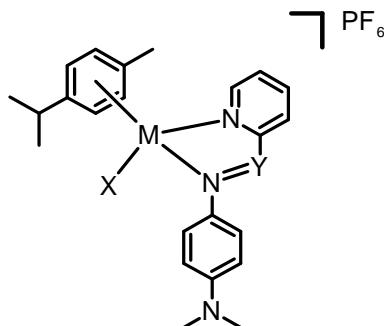
Compound			IC$_{50}$ (μM)			
	M	**X**	**Y**	**A2780**	**A549**	**HCT116**	**MCF7**
15	Ru	Cl	C	16.2 ± 0.9	10.5 ± 0.8	3.4 ± 0.4	12.1 ± 0.3
16	Ru	I	C	3.0 ± 0.2	15.3 ± 0.9	8.6 ± 0.8	4.4 ± 0.3
34	Ru	Cl	N	13.1 ± 0.5	15 ± 1	16.7 ± 0.8	11.9 ± 0.9
35	Ru	I	N	0.69 ± 0.04	1.27 ± 0.01	1.37 ± 0.04	0.8 ± 0.1
36	Os	Cl	C	3.0 ± 0.4	15.8 ± 0.2	3.26 ± 0.05	9.3 ± 0.6
37	Os	I	C	1.20 ± 0.02	3.31 ± 0.6	1.6 ± 0.1	1.2 ± 0.2
CDDP				1.2 ± 0.2	3.3 ± 0.1	5.1 ± 0.3	7.4 ± 0.2
OXA				n/d	n/d	3.99 ± 0.08	n/d

It is noticeable that in A2780 and MCF7 cells, both female cancers, all iodido complexes are more than 10X more active than their chlorido analogues. Osmium iodido complex **37** [Os(η^6-p-cym)(p-Impy-NMe$_2$)I]PF$_6$ is as active or better than **CDDP** in all cell lines tested.

Antiproliferative activity of complexes **15**, **16**, **34–37** was also investigated in resistant cell lines, A2780cis (**CDDP** resistant) and HCT116Ox (**OXA** resistant) and MRC5 human embryonal lung fibroblasts (non-cancerous cells). These results are shown in Table 5.3. In the case of resistant cell lines A2780cis and HCT16Ox, all iodido complexes **16**, **35** and **37** retain the activity previously observed in parental cell lines. In contrast, chlorido complexes **15**, **34** and **36** lose their

potency in A2780 cells resistant to cisplatin. All complexes exhibit higher $IC_{50,}$ values in MRC5 human fibroblasts than in any cancer cell line, between 8 and 30X improvement in comparison to A2780 cells.

Table 5.3. Antiproliferative activity of complexes **15, 16, 34–37**, **CDDP** and **OXA** in A2780cis, HCT116Ox and MRC5 cell lines. n/d = not determined.

	Compound	IC_{50} (µM)		
		A2780cis	HCT116Ox	MRC5
15	$[Ru(\eta^6\text{-}p\text{-cym})(p\text{-Impy-NMe}_2)Cl]PF_6$	52 ± 1	77.7 ± 0.9	190 ± 3
16	$[Ru(\eta^6\text{-}p\text{-cym})(p\text{-Impy-NMe}_2)I]PF_6$	3.3 ± 0.6	8.8 ± 0.7	89 ± 2
34	$[Ru(\eta^6\text{-}p\text{-cym})(p\text{-Azpy-NMe}_2)Cl]PF_6$	27.5 ± 0.9	1.18 ± 0.09	112 ± 8
35	$[Ru(\eta^6\text{-}p\text{-cym})(p\text{-Azpy-NMe}_2)I]PF_6$	0.60 ± 0.03	0.75 ± 0.01	18.2 ± 0.7
36	$[Os(\eta^6\text{-}p\text{-cym})(p\text{-Impy-NMe}_2)Cl]PF_6$	12.97 ± 0.07	3.6 ± 0.3	53.7 ± 0.8
37	$[Os(\eta^6\text{-}p\text{-cym})(p\text{-Impy-NMe}_2)I]PF_6$	1.27 ± 0.06	1.10 ± 0.08	31.9 ± 0.5
	CDDP	11.5 ± 0.3	n/d	16.2 ± 0.6
	OXA	n/d	32.2 ± 0.5	n/d

5.3.3 Metal accumulation in cancer cells

Total cellular accumulation of Ru/Os for complexes **15**, **16**, **34–37** was determined in A2780 cells in order to relate metal content to cytotoxicity. Values are expressed as ng of ruthenium/osmium per million cells and were determined as independent duplicates of triplicates.

Results are shown in Table 5.4. In the case of chlorido complexes **15**, **34** and **36**, their potency improves as their cellular accumulation increases. This trend is not observed for iodido complexes **16**, **35** and **37**. Cellular accumulation of Ru from

complex **35** is similar to Os accumulation from complex **37** (both approximately 15 ng of metal per 10^6 cells), however there is a significant difference in their IC_{50} values (13.1±0.5 for complex **35** and 3.0 ± 0.4 for complex **37**).

Table 5.4. Total accumulation of Ru/Os in A2780 cells for complexes **15**, **16**, **34–37** after 24 h of drug exposure at 310 K and no recovery time in drug-free media, together with their IC_{50} values. Concentrations used were equipotent, in all cases $IC_{50}/3$.

Compound			Cell accumulation (ng Ru/Os x 10^6 cells)	IC_{50} (µM)
	M	X	Y		
15	Ru	Cl	C	7.8 ± 0.5	16.2 ± 0.9
16	Ru	I	C	11.5 ± 0.8	3.0 ± 0.2
34	Ru	Cl	N	13.4 ± 0.9	13.1 ± 0.5
35	Ru	I	N	17.9 ± 0.8	0.69 ± 0.04
36	Os	Cl	C	15.2 ±0.9	3.0 ± 0.4
37	Os	I	C	18.1 ± 0.1	1.20 ± 0.02

5.3.4 Metal distribution in cancer cells

Metal distribution studies were carried out for complexes **15**, **16**, **34–37** in A2780 cells. The experiment allowed the separation of four cellular fractions: firstly, the cytosolic fraction which contains the total of soluble proteins from the cytoplasm,

secondly, the membrane fraction which included all membrane proteins plus all cellular organelles and its membranes. Thirdly, the nuclear fraction containing the total of nucleus soluble proteins and the nuclear membrane proteins and finally the cytoskeletal fraction that includes the total cellular insoluble proteins and genomic DNA. Figure 5.2 shows that all arene complexes **15**, **16**, **34–37** accumulate to a high extent in the membrane fraction. However the percentages for iodido complexes **16** [Ru(η^6-p-cym)(p-Impy-NMe$_2$)I]PF$_6$, **35** [Ru(η^6-p-cym)(p-Azpy-NMe$_2$)I]PF$_6$ and **37** [Os(η^6-p-cym)(p-Impy-NMe$_2$)I]PF$_6$ are higher than that for their chlorido analogues **15** [Ru(η^6-p-cym)(p-Impy-NMe$_2$)Cl]PF$_6$, **34** [Ru(η^6-p-cym)(p-Azpy-NMe$_2$)Cl]PF$_6$ and **36** [Os(η^6-p-cym)(p-Impy-NMe$_2$)Cl]PF$_6$.

It is also notable that although second highest concentration of ruthenium/osmium for chlorido complexes **15**, **34** and **36** is found in the cytosol, there is no significant amount of metal in this fraction for iodido complexes **16**, **35** and **37**. Concentrations of metal accumulated in the nuclear and cytoskeletal fraction are also higher for the chlorido complexes **15**, **34** and **36** than for the iodido analogues **16**, **35** and **37**.
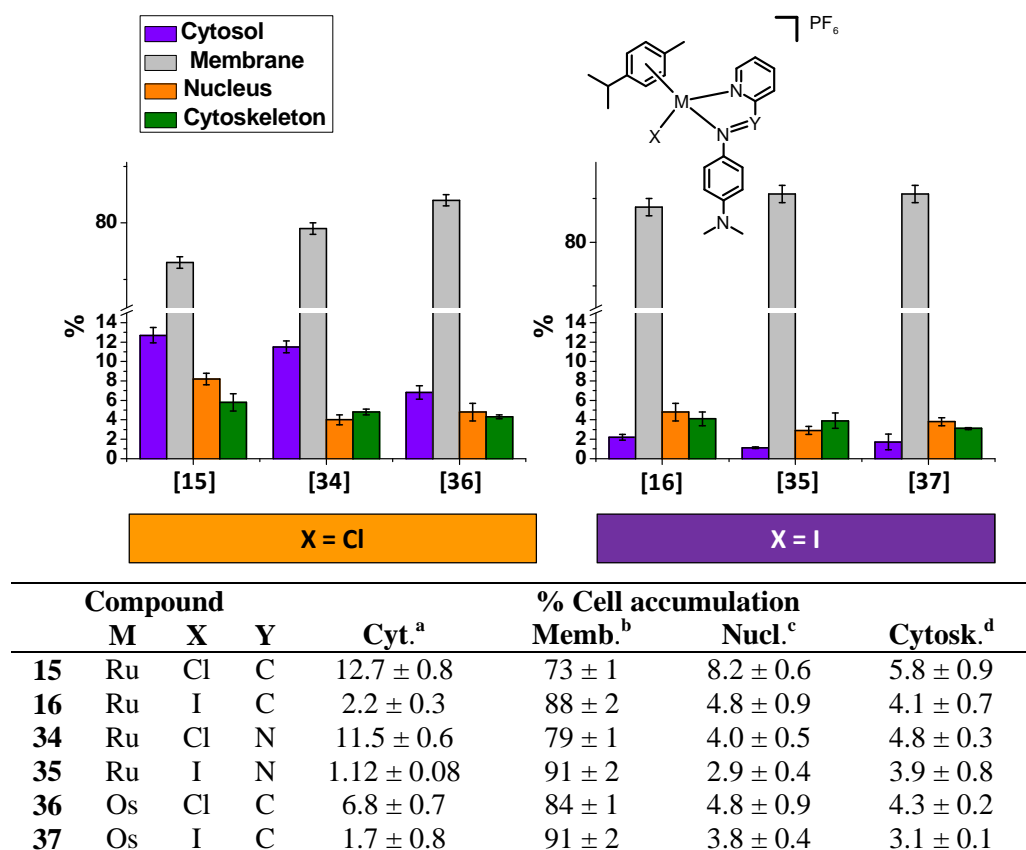
Figure 5.2. Distribution of metal for complexes **15**, **16**, **34–37** in A2780 ovarian cells. Concentrations used in all cases were $IC_{50}/3$, pre-incubation time in drug-free medium was 24 h and drug exposure time was 24 h. [a] **Cyt**. = cytosolic fraction (total soluble proteins from cytoplasm) [b] **Memb**. = Membrane fraction (membrane proteins, cellular organelles and organelles membranes) [c] **Nucl**. = Nuclear fraction (total nucleus soluble proteins and nuclear membrane proteins) [d] **Cytosk**. = cytoskeletal fraction (total cellular insoluble proteins and genomic DNA).

| | Compound | | | % Cell accumulation | | | |
	M	X	Y	Cyt.[a]	Memb.[b]	Nucl.[c]	Cytosk.[d]
15	Ru	Cl	C	12.7 ± 0.8	73 ± 1	8.2 ± 0.6	5.8 ± 0.9
16	Ru	I	C	2.2 ± 0.3	88 ± 2	4.8 ± 0.9	4.1 ± 0.7
34	Ru	Cl	N	11.5 ± 0.6	79 ± 1	4.0 ± 0.5	4.8 ± 0.3
35	Ru	I	N	1.12 ± 0.08	91 ± 2	2.9 ± 0.4	3.9 ± 0.8
36	Os	Cl	C	6.8 ± 0.7	84 ± 1	4.8 ± 0.9	4.3 ± 0.2
37	Os	I	C	1.7 ± 0.8	91 ± 2	3.8 ± 0.4	3.1 ± 0.1

5.2.3.4 Antiproliferative pathways and mechanism of action

- **Cell cycle analysis using flow cytometry**

Complexes **15**, **16**, **34–37** and **CDDP** were incubated in A2780 ovarian cells to study their effects on the cell cycle (See cell cycle scheme in Figure 5.22 on page 242). For this task, cells were stained using PI (Figure 5.3) as a fluorescent probe that interacts with DNA through intercalation.[17] The fluorescence emitted by PI is greatly enhanced (20–30 fold) when it is bound to nucleic acids allowing a sensitive method for DNA quantification. Since PI is membrane-impermeant, it is necessary to fix the cells with cold ethanol before the staining takes place, this treatment ensures that the dye enters intracellular compartments. Moreover, PI can also interact with RNA, which could cause false DNA readings. To avoid such interference, cells were also treated with RNAse.

Data obtained by flow cytometry were analysed using Flowjo software. For all experiments, data were gated using a forward scatter vs side scatter plot (FSC vs SSC plot) before obtaining histograms for the FL2-H channel (which is used to read PI fluorescence). Examples of these histograms are shown in Figure 5.4.
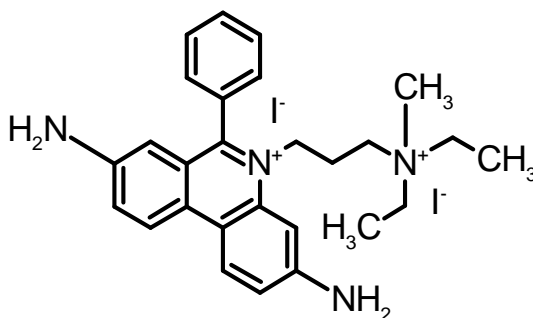
Figure 5.3. Structure of propidium iodide (PI)
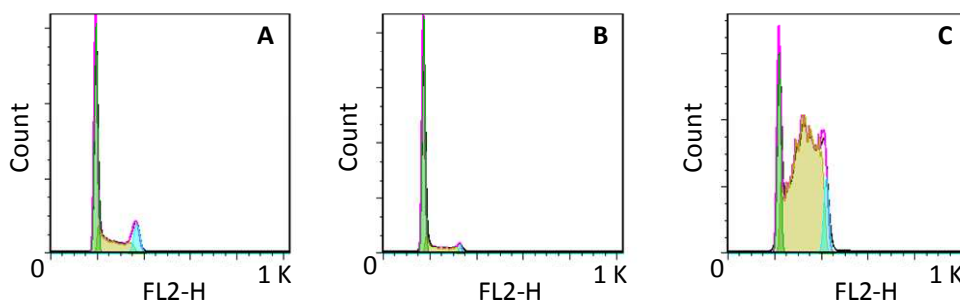
Figure 5.4. FL2-H histograms obtained by flow cytometry for cell cycle analysis (A) Control untreated cells; (B) Cells treated using 1 μM of complex **16**; (C) Cells treated using 0.4 μM of **CDDP**; For all experiments, drug exposure time was 24 h, cells were treated with RNAse and stained using PI.

By comparison to the control population, data in Figure 5.5 clearly show that **CDDP** causes cell cycle arrest in the S phase. The population in this phase increases after 24 h of exposure to the platinum drug (from $21.0 \pm 0.6\%$ for the control versus $25.2 \pm 0.6\%$), together with a significant reduction of the population in G1 phase (from $59.9 \pm 0.9\%$ to $47.2 \pm 0.2\%$). In contrast, the half-sandwich arene complexes cause arrest in the G1 phase regardless of the nature of their metal centre (Ru/Os) or the monodentate ligand (Cl/I). Ruthenium chlorido complexes **15** and **34** generate a slightly higher population in the G1 phase compared to their iodido analogues **16** and **35**. Interestingly, Impy-NMe$_2$ complexes **15** and **16** cause the S phase population to double the G2/M population ($12.7 \pm 0.9\%$ and $14 \pm 1\%$ in S phase for **15** and **16** respectively, versus $6.5 \pm 0.8\%$ and $6.3 \pm 0.7\%$). In contrast, Azpy-NMe$_2$ **34** and **35** complexes do not cause this effect and their G2/M and S phase populations are not significantly different.

	Compound			Cell cycle phase		
	M	**X**	**Y**	**G1**	**G2/M**	**S**
15	Ru	Cl	C	80.3 ± 0.7	6.5 ± 0.8	12.7 ± 0.9
16	Ru	I	C	78.6 ± 0.8	6.3 ± 0.7	14 ± 1
34	Ru	Cl	N	73 ± 1	11 ± 1	13.2 ± 0.5
35	Ru	I	N	69.7 ± 0.9	10.7 ± 0.9	10.3 ± 0.9
36	Os	Cl	C	77.8 ± 0.8	9 ± 1	11.9 ± 0.4
37	Os	I	C	78.4 ± 0.9	10.9 ± 0.8	9.7 ± 0.4
CDDP				47.2 ± 0.2	26.2 ± 0.4	25.2 ± 0.6
Control				59.9 ± 0.9	18.5 ± 0.9	21.0 ± 0.6
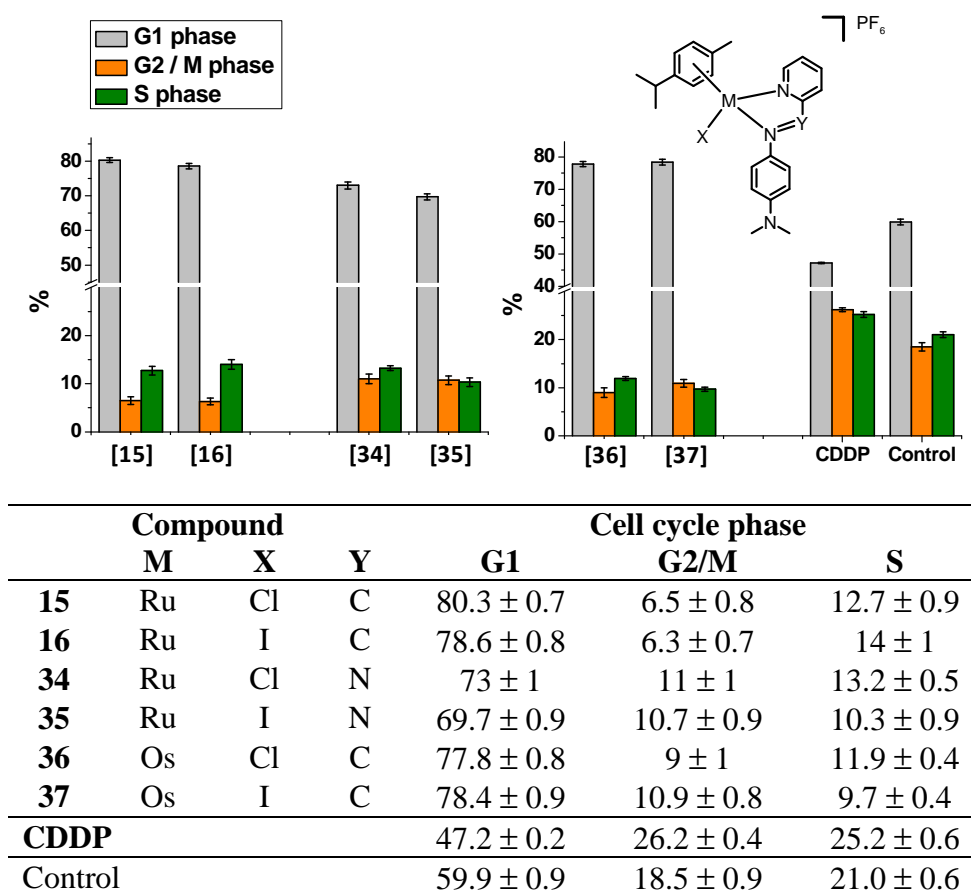
Figure 5.5. Cell cycle analysis carried out by flow cytometry using PI staining after exposing A2780 cells to complexes **15**, **16**, **34–37** and **CDDP**. Concentrations used in all cases were $IC_{50}/3$, pre-incubation time in drug-free medium was 24 h and drug exposure time was 24 h.

Further studies were carried out using ruthenium Impy complex **16** and **CDDP** to study the effect of drug concentrations on the cell cycle. Data obtained for these experiments are shown in Figure 5.6.

Compound	Concentration (μM)	G1	G2/M	S
			Cell cycle phase	
16	1	64.2 ± 0.6	21.9 ± 0.4	14.5 ± 0.8
	3	66.4 ± 0.1	19.5 ± 0.5	14.0 ± 0.6
	9	65.6 ± 0.8	21.4 ± 0.6	12.9 ± 0.5
CDDP	0.4	51.1 ± 0.3	32.6 ± 0.8	16.5 ± 0.6
	1.2	43 ± 1	33.2 ± 0.5	22 ± 1
	3.6	31.2 ± 0.4	23.9 ± 0.9	44 ± 2
Control	0	59.9 ± 0.9	18.5 ± 0.9	21.0 ± 0.6
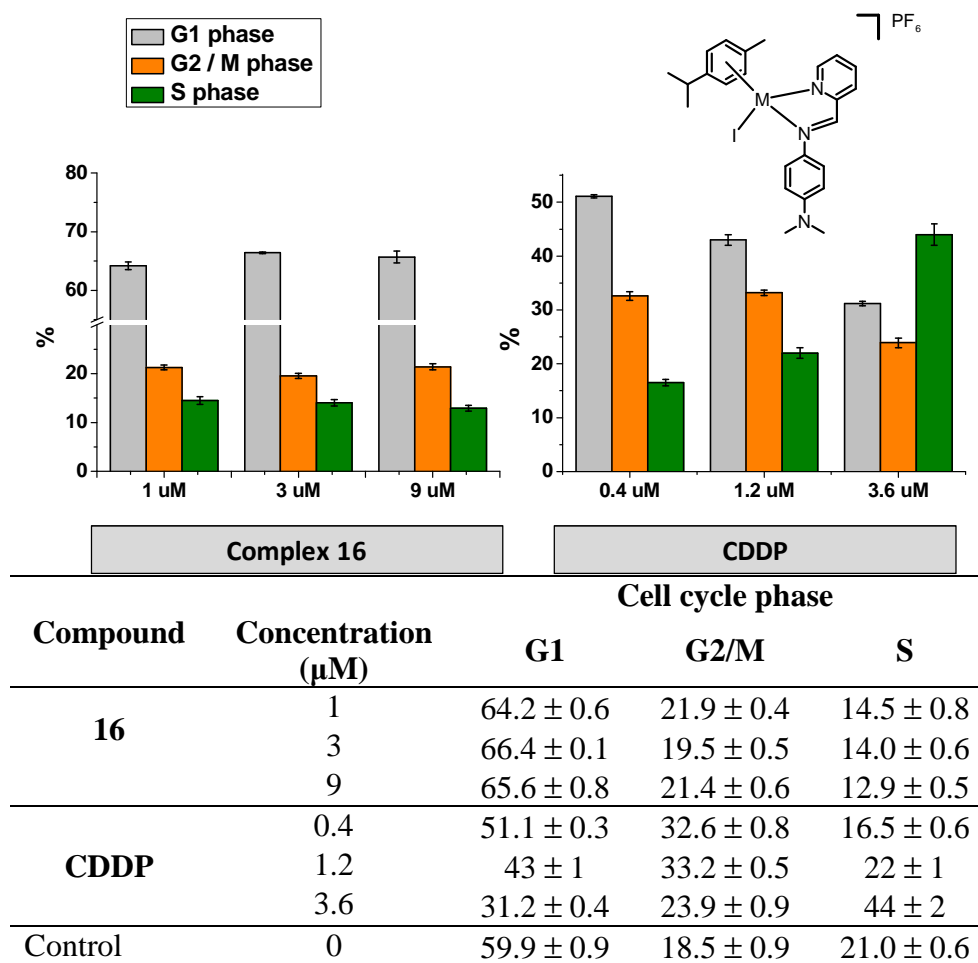
Figure 5.6. Cell cycle analysis carried out by flow cytometry using PI staining after exposing A2780 cells to complex **16** and **CDDP.** Concentrations used were 1, 3 and 9 μM for complex **16** and 0.4, 1.2 and 3.6 μM for **CDDP.** Pre-incubation time in drug-free medium was 24 h and drug exposure time was 24 h.

It is observed that the **CDDP** cell cycle arrest in S phase is concentration-dependent. The population in the G1 phase decreases with increasing drug concentration (from $51.1 \pm 0.3\%$ at 0.4 μM to $31.2 \pm 0.4\%$ at 3.6 μM **CDDP**). At the same time, the S phase population increases (from $16.5 \pm 0.6\%$ at 0.4 μM to $44 \pm 2\%$ at 3.6 μM **CDDP**). As shown above, iodido ruthenium complex **16**

arrests the cell cycle in the G1 phase. However this effect does not seem to depend on the concentration of the drug used. Samples exposed to concentrations above the IC_{50} (9 μM) exhibit approximately the same proportion of population in the cell cycle phases than those cells exposed to concentrations below the IC_{50} (1 μM). For example, the G1 phase population is 65.6 ± 0.8% at 9 μM, a concentration three times higher than the IC_{50}, and 64.2 ± 0.6% at 1 μM, which is three times lower than the IC_{50}. The same observation is true for the population in the G2/M phase (21.9 ± 0.4% at 9 μM and 21.4 ± 0.6% at at 1 μM).

- **p53-activated apoptotic pathway**

Antiproliferative activity for complexes **15**, **16**, **34–37** was determined using the SRB assay[18,19] on HCT116 cells as well as their derived cell line HCT116p53-/- which has knocked-out tumour suppressor p53 a regulator of the cell cycle. Table 5.5 shows that the antiproliferative activity of chlorido complexes **15**, **34** and **36** decreases significantly, especially ruthenium *p*-Impy-NMe$_2$ complex **15**, as its IC_{50} value increases a twenty-fold (from 3.4 ± 0.4 μM to 69.9 ± 0.9 μM) compared to the wild-type HCT116. On the contrary, ruthenium iodido complexes **16**, **35** and osmium iodido complex **37** retain their potency in the p53 mutant cell line at the same level as in the parental cell line HCT116.

It is remarkable that the differences in the IC_{50} values for complexes **15**, **16**, **34–37** seem to be associated with the halogen used as monodentate ligand and not to the nature of the metal centre nor the *N,N*-chelating ligand. It is also remarkable

that the IC_{50} value for **CDDP** in HCT166p53-/- is 36.7 ± 0.3 μM was five times

that for the parental cell line (5.1 ± 0.3 μM). Similar results are obtained for OXA,

for which the decrease in potency is higher than twenty-five fold as its IC_{50} in the

p53-knock out cell line is above 100 μM.

Table 5.5. Antiproliferative activity of complexes **15**, **16**, **34–37, CDDP** and OXA in HCT116 parental cell line and modified HCTp53-/-.

	Compound	IC_{50} (μM)	
		HCT116	**HCT116p53-/-**
15	$[Ru(\eta^6\text{-}p\text{-cym})(p\text{-Impy-NMe}_2)Cl]PF_6$	3.4 ± 0.4	69.9 ± 0.9
16	$[Ru(\eta^6\text{-}p\text{-cym})(p\text{-Impy-NMe}_2)I]PF_6$	8.6 ± 0.8	8.73 ± 0.05
34	$[Ru(\eta^6\text{-}p\text{-cym})(p\text{-Azpy-NMe}_2)Cl]PF_6$	16.7 ± 0.8	38 ± 1
35	$[Ru(\eta^6\text{-}p\text{-cym})(p\text{-Azpy-NMe}_2)I]PF_6$	1.37 ± 0.04	1.59 ± 0.04
36	$[Os(\eta^6\text{-}p\text{-cym})(p\text{-Impy-NMe}_2)Cl]PF_6$	3.26 ± 0.05	21.5 ± 0.8
37	$[Os(\eta^6\text{-}p\text{-cym})(p\text{-Impy-NMe}_2)I]PF_6$	1.6 ± 0.1	1.12 ± 0.07
	CDDP	5.1 ± 0.3	36.7 ± 0.3
	OXA	3.99 ± 0.08	> 100

- **Induction of Apoptosis**

Flow cytometry was also used to investigate the extent of apoptosis caused by

complexes **15**, **16**, **34–37**. Phosphatidylserine is a phospholipid component that is

found on the internal/cytosolic side of the membrane in healthy cells. However, in

early stages of apoptosis there is a loss of phospholipid asymmetry and

phosphatidylserine is translocated to the outer side of the membrane.[20] There it is

exposed to annexin V which in this case has been modified to include the FITC

fluorescent probe shown in Figure 5.7.
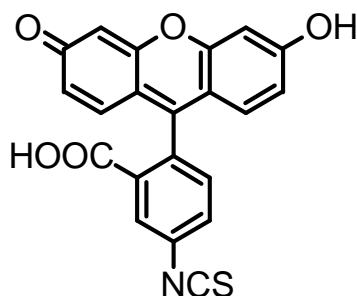
Figure 5.7. Structure of fluorescein isothiocyanate (FITC)

The binding of annexin V-FITC to phosphatidylserine is calcium-dependent. Hence the cells were not treated with trypsin-EDTA (only trypsin) when preparing the pellets. The binding buffer used in this experiment contains calcium and magnesium for the same reason. In the last stages of apoptosis, the integrity of the cellular membrane is compromised, allowing for PI (which is normally membrane impermeant) to enter the cell and bind to DNA.

Flow cytometry was used to monitor the fluorescence emitted by the FITC conjugate at the same time as the PI, making it possible to distinguish four sets of populations: viable cells, early and late apoptotic cells and non-viable cells. For all experiments, data were gated using a forward-scatter vs side-scatter plot (FSC vs SSC plot). The gated population was used to graph FL2-H vs FL1-H plots for each sample (FL1-H channel reading FITC fluorescence and FL2-H reading PI fluorescence). An example of this is shown in Figure 5.8.
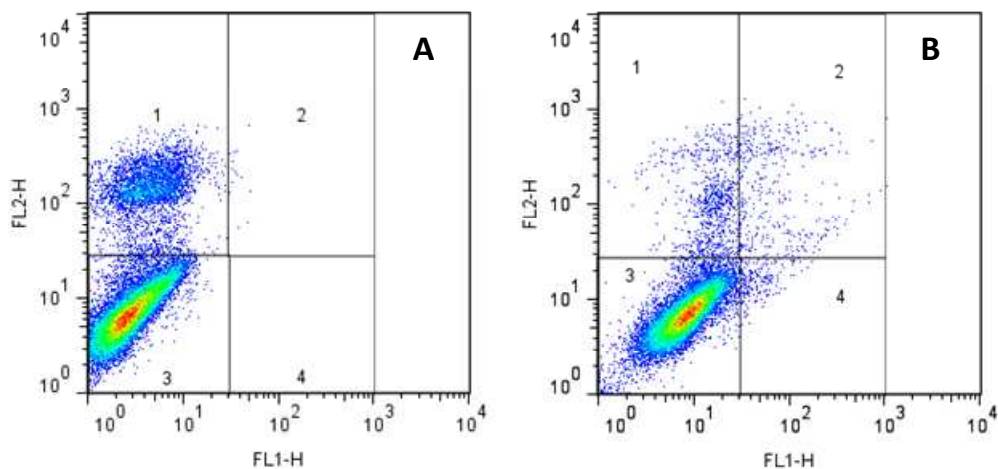
Figure 5.8. FL2-H vs FL1-H dot plots obtained by flow cytometry for apoptosis analysis using FITC (FL1-H channel) and PI (FL2-H channel) staining. (A) Cells treated with 1 μg/mL of staurosporine, (B) Cells treated with 1 μM of complex **16** for 24 h at 310 K.

Figure 5.9 shows that the ratio of apoptosis caused by exposure to the arene complexes can be divided into two groups, in which the patterns are similar. The first group includes the three chlorido complexes **15**, **34** and **36** that cause high late apoptotic populations. The second group, the iodido complexes **16**, **35** and **37** cause a large number of cells to be in the non-viable stage. Additionally, after 24 h of drug exposure, the extent of late apoptotic cells is close to zero.

Compound				Population (%)			
	M	**X**	**Y**	**Viable**	**Early Apoptotic**	**Non viable**	**Late Apoptotic**
15	Ru	Cl	C	91.2 ± 0.5	1.87 ± 0.03	4.3 ± 0.4	2.03 ± 0.09
16	Ru	I	C	88.5 ± 0.4	0.78 ± 0.02	10.7 ± 0.7	0.22 ± 0.08
34	Ru	Cl	N	92 ± 1	1.61 ± 0.06	3.94 ± 0.08	2.8 ± 0.3
35	Ru	I	N	92.3 ± 0.6	0.06 ± 0.02	7.4 ± 0.3	0.10 ± 0.02
36	Os	Cl	C	87.4 ± 0.9	1.29 ± 0.08	3.5 ± 0.6	7.8 ± 0.7
37	Os	I	C	87 ± 1	0.30 ± 0.04	11.9 ± 0.8	0.95 0.03
Staurosporine (Sta)				84.3 ± 0.5	0.41 ± 0.06	13.2 ± 0.4	5.66 ± 0.09
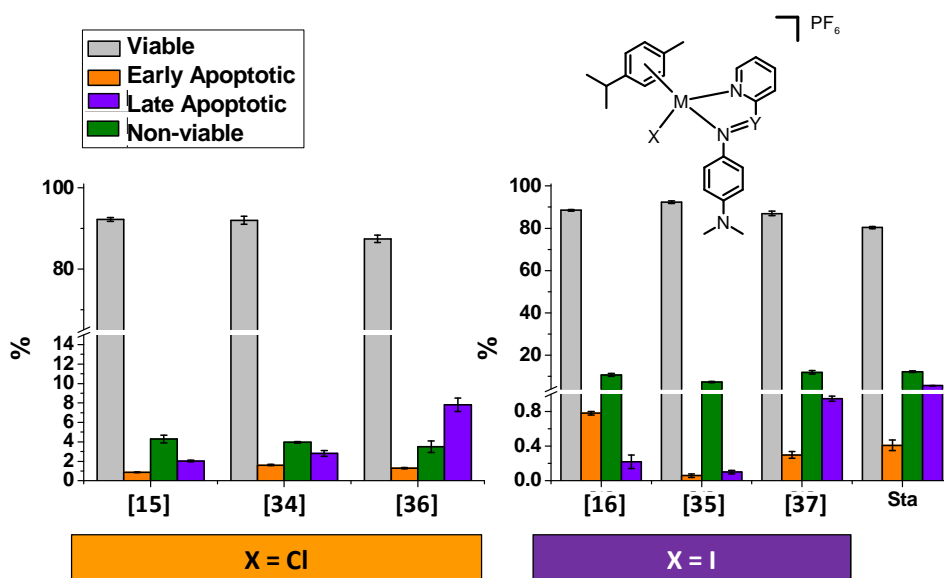
Figure 5.9. Flow cytometry analysis to determine the percentages of apoptotic cells, using Annexin V-FITC vs PI staining, after exposing A2780 cells to complexes **15**, **16**, **34–37** and staurosporine. Concentrations used were $IC_{50}/3$ for complexes and 1 μg/mL for staurosporine (Sta), pre-incubation time in drug-free medium was 24 h and drug exposure time was 24 h.
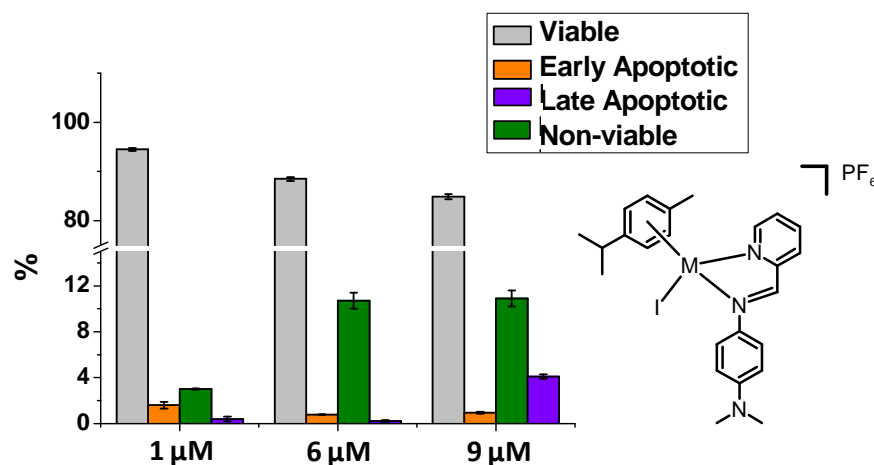
Compound	μM	Population (%)			
		Viable	Early Apoptotic	Non-viable	Late Apoptotic
16	1	94.5 ± 0.3	1.6 ± 0.3	3.02 ± 0.05	0.4 ± 0.2
	3	88.5 ± 0.4	0.78 ± 0.02	10.7 ± 0.7	0.22 ± 0.08
	9	84.9 ± 0.5	0.95 ± 0.08	10.9 ± 0.7	4.1 ± 0.2

Figure 5.10. Flow cytometry analysis to determine the percentages of apoptotic populations, using Annexin V-FITC vs PI staining, after exposing A2780 cells to various concentrations of complex **16**. Concentrations used were 1, 3 or 9 μM, pre-incubation time in drug-free medium was 24 h and drug exposure time was 24 h.

Further studies were carried out using complex **16** to study the effect of drug concentration on the extent of apoptosis, results are shown in Figure 5.10. As expected, complex **16** causes a decrease in viable cell population with increasing concentration changing from 94.5 ± 0.3% at 1 μM, which is a concentration equivalent to a third of the IC_{50} to 84.9 ± 0.5% at 9 μM, which is 3 x IC_{50} concentration. The percentage of late-apoptotic cells increased with concentration as expected.

- **Caspase 3 apoptotic pathway**

The caspase-3/CPP32 colorimetric assay kit from BioVision, was used to determine the level of activation of these proteins caused by 24 h of exposure of A2780 cells to complexes **15**, **16**, **34–37** in comparison to untreated cells. For positive activation of caspase 3, control A2780 cells were exposed for 2 h to staurosporine (1 µg/mL). It is known that the amino acid sequence Asp-Glu-Val-Asp (DEVD) is cleaved by caspase 3 during the activation of apoptosis in mammalian cells.[21] The cellular assay is based on the colorimetric detection and quantification of *p*-nitro aniline (*p*-NA) after it has been cleaved from the labelled substrate (DEVD-*p*-NA) which is incubated with treated cells. The absorbance of *p*-NA was determined for a triplicate of samples for each complex and the standard deviation of the experiment was calculated.

The data for the absorbance of free *p*-NA at 410 nm are shown in Figure **5.11**. Although all the complexes **15**, **16**, **34–37** activate caspase 3, it is worth highlighting that chlorido complexes **15**, **34** and **36** give rise to higher absorbance than their corresponding iodido analogues **16**, **35** and **37** regardless of the nature of their metal centre or their *N,N*-chelating ligand.
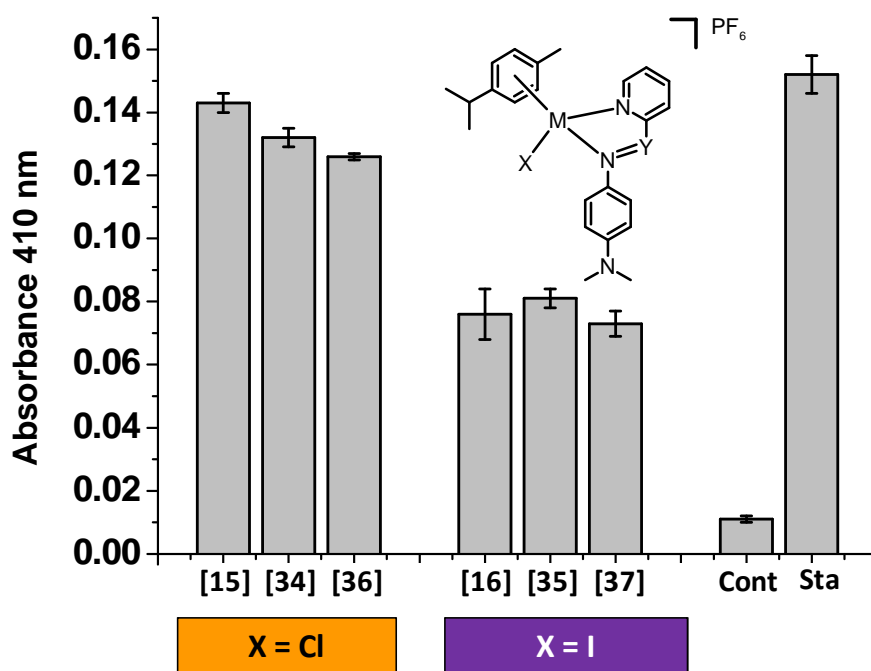
	Compound			Absorbance at 410 nm
	M	**X**	**Y**	
15	Ru	Cl	C	0.143 ± 0.003
16	Ru	I	C	0.076 ± 0.008
34	Ru	Cl	N	0.132 ± 0.003
35	Ru	I	N	0.081 ± 0.003
36	Os	Cl	C	0.126 ± 0.001
37	Os	I	C	0.073 ± 0.004
Control (Cont)				0.011 ± 0.001
Staurosporine (Sta)				0.152 ± 0.006

Figure 5.11. Caspase 3 activation in A2780 cells caused by 24 h exposure to complexes **15**, **16**, **34–37** at 310 K. Results are expressed as the samples' absorbance at 410 nm (maximum absorbance of free *p*-NA). Concentrations of the complexes used were equipotent at $IC_{50}/3$. Cont: control cells not treated, Sta: cells treated with staurosporine (1 µg/mL)

- **DNA replication**

IC_{50} modulation by inhibition of DNA polymerase α by aphidicolin and topoisomerase II by etoposide and novobiocin were investigated for complexes **15**, **16**, **34–37** in A2780 cells. Results for co-incubation with aphidicolin are shown in Figure 5.12. Complex **15** $[Ru(\eta^6\text{-}p\text{-cym})(p\text{-Impy-NMe}_2)Cl]PF_6$ loses potency at all concentrations of the co-incubating agent. Its IC_{50} values increases from 16.2 ± 0.9 μM to 71 ± 2 μM when co-incubated with 10 μM of aphidicolin. In contrast, its analogous iodido complex **16** $[Ru(\eta^6\text{-}p\text{-cym})(p\text{-Impy-NMe}_2)I]PF_6$ shows an increase in potency, as its IC_{50} value decreases from 3.0 ± 0.2 μM to 0.62 ± 0.08 μM when co-incubated with 10 μM of the polymerase α inhibitor. The antiproliferative activity of ruthenium p-Azpy-NMe$_2$ complexes **34** and **35** do not seem to be affected by the addition of aphidicolin, as their potency is the same in all experiments. Finally, the same is true for osmium p-Impy-NMe$_2$ complex **36** and its iodido analogue **37** which are only affected by the highest concentration of aphidicolin (10 μM).

Figure 5.13 shows the results obtained when complexes **15**, **16**, **34–37** were co-incubated with 5 μM of novobiocin, a topoisomerase II inhibitor. In this case, the only complex to show a decrease in potency is the chlorido complex **15** (IC_{50} value increases from 16.2 ± 0.9 μM to 28 ± 2 μM) while the changes in the antiproliferative activity of complexes **34**, **35** and **37** are not statistically significant. Interestingly, the potency of chlorido complex **36** $[Os(\eta^6\text{-}p\text{-cym})(p\text{-Impy-NMe}_2)Cl]PF_6$ is improved as its IC_{50} value decreases from 3.0 ± 0.4 μM to 0.77 ± 0.06 μM when incubated with 5 μM of novobiocin.

Compound			Aphidicolin (μM)			
	M	X	Y	0	1	5	10
15	Ru	Cl	C	16.2 ± 0.9	32.5 ± 0.8	67 ± 1	71 ± 2
16	Ru	I	C	3.0 ± 0.2	2.3 ± 0.2	0.75 ± 0.04	0.62 ± 0.08
34	Ru	Cl	N	13.1 ± 0.5	12.8 ± 0.5	12.73 ± 0.09	12.5 ± 0.5
35	Ru	I	N	0.69 ± 0.04	0.61 ± 0.08	0.60 ± 0.09	0.60 ± 0.03
36	Os	Cl	C	3.0 ± 0.4	2.8 ± 0.8	1.09 ± 0.06	1.02 ± 0.03
37	Os	I	C	1.20 ± 0.02	1.17 ± 0.06	0.80 ± 0.02	0.60 ± 0.04
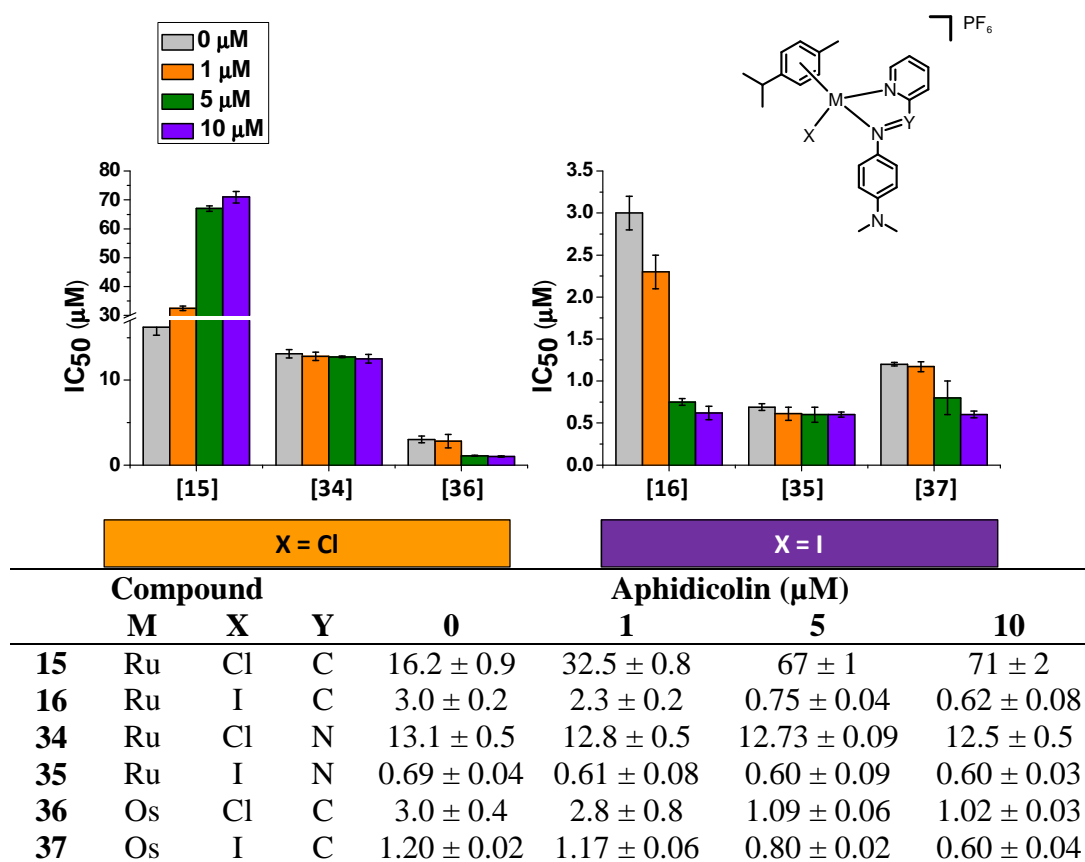
Figure 5.12. IC_{50} values for complexes **15**, **16**, **34–37** in A2780 cells after co-incubation with various concentrations of aphidicolin. Concentrations of the complexes used were equipotent, at $IC_{50}/3$. Aphidicolin concentrations used were: (■) 0 μM, (■) 1 μM (■) 5 μM and (■) 10 μM. All concentrations of aphidicolin used were non-toxic.

Results for co-incubation with etoposide are also shown in Figure 5.13. the potency of ruthenium complexes **15**, **16** and **35** decreases with increasing concentration of etoposide, especially for the iodido Impy complex **16**. Its IC_{50} increases from 3.0 ± 0.2 μM to 14.1 ± 0.8 μM when incubated with 10 μM of etoposide. In contrast, the potency of osmium complexes **36** improved. Notably,

the latter increases its activity ten-fold when co-incubated with 10 μM of etoposide. No significant changes in IC$_{50}$ were observed for complexes **34** and **37**.

| Compound | | | | IC$_{50}$ (μM) | |
	M	**X**	**Y**	**0**	**5 μM Novobiocin**	**10 μM Etoposide**
15	Ru	Cl	C	16.2 ± 0.9	28 ± 2	43 ± 1
16	Ru	I	C	3.0 ± 0.2	2.3 ± 0.3	14.1 ± 0.8
34	Ru	Cl	N	13.1 ± 0.5	12.8 ± 0.8	16.8 ± 0.9
35	Ru	I	N	0.69 ± 0.04	0.60 ± 0.09	2.0 ± 0.1
36	Os	Cl	C	3.0 ± 0.4	1.7 ± 0.2	0.33 ± 0.02
37	Os	I	C	1.20 ± 0.02	0.77 ± 0.06	0.89 ± 0.03
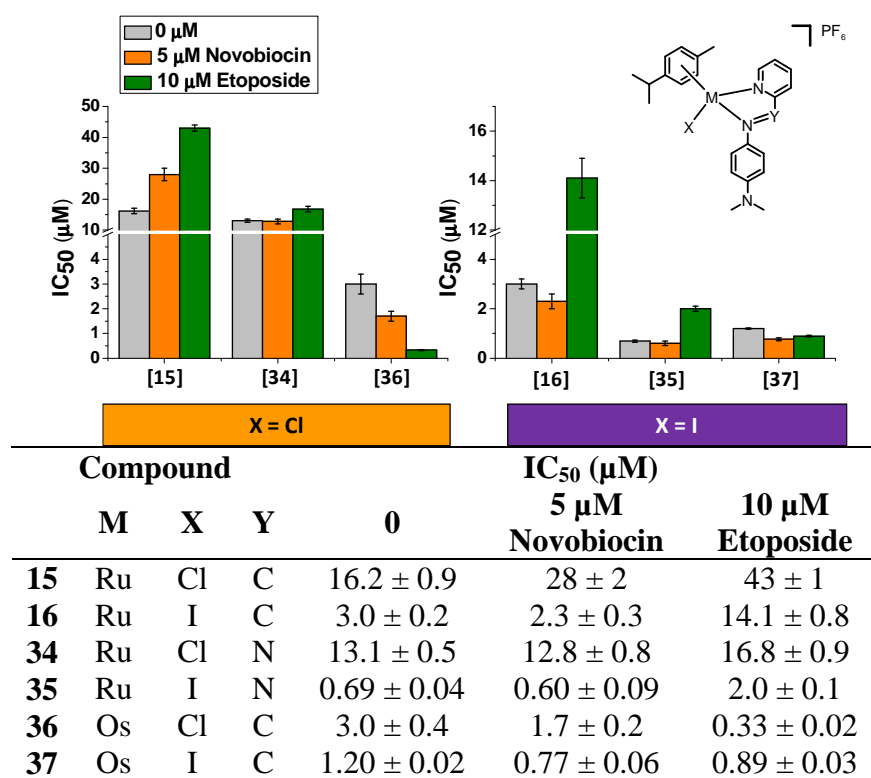
Figure 5.13. IC$_{50}$ in A2780 cells for complexes **15**, **16**, **34–37** after co-incubation with 5 μM novobiocin or 10 μM etoposide. Concentrations of the complexes used were equipotent at IC$_{50}$/3. For all complexes (■) no co-incubation agent, (■) co-incubation with 5 μM novobiocin and (■) co-incubation with 10 μM etoposide. Both concentrations of the co-incubating agents were non-toxic.

- **Cellular detoxification mechanisms**

The effect of modification of GSH levels and inhibition of thioredoxin reductase on IC_{50} values of complexes **15**, **16**, **34–37** was investigated. These complexes were co-incubated with various concentrations of L-BSO (1, 5 or 50 μM) as well as 0.1 μM of auranofin in independent experiments. Figure 5.14 shows the results when L-BSO was used to inhibit γ-glutamylcysteine synthetase and, consequently lower intracellular GSH concentrations.[22] Complexes **15**, **16**, **34–37** greatly improve their potency when co-incubated with L-BSO. The antiproliferative activity of ruthenium complex **15** [Ru(η^6-*p*-cym)(*p*-Impy-NMe$_2$)Cl]PF$_6$ improved more noticeably when co-incubated with 5 μM of L-BSO as its IC_{50} value decreased from 16.2 ± 0.9 μM to 1.0 ± 0.3 μM. The activity of the iodido analogue **16** is not affected by the presence of 1 μM L-BSO, but, its potency increases equally when using 5 μM or 50 μM of L-BSO. The activity of the ruthenium *p*-Azpy-NMe$_2$ complex **34** improved eight-fold (from 13.1 ± 0.5 to 1.63 ± 0.02 with using 5 50 μM of L-BSO present). Meanwhile the IC_{50} value of its iodido analogue **35** and both the osmium complexes **36** and **37** decreased to the sub-micro molar range, especially complex **37** [Os(η^6-*p*-cym)(*p*-Impy-NMe$_2$)I]PF$_6$ which improved its potency to nano molar values (80 ± 2 nM when co-incubated with 5 μM L-BSO). Interestingly, it is observed that the optimum concentration of L-BSO to achieve the maximum potency with all complexes is 5 μM.

| Compound | | | | L-BSO (µM) | | |
	M	X	Y	0	1	5	50
15	Ru	Cl	C	16.2 ± 0.9	3.8 ± 0.4	1.0 ± 0.3	2.93 ± 0.09
16	Ru	I	C	3.0 ± 0.2	2.9 ± 0.1	1.05 ± 0.07	1.05 ± 0.02
34	Ru	Cl	N	13.1 ± 0.5	1.71 ± 0.09	1.63 ± 0.02	6.6 ± 0.2
35	Ru	I	N	0.69 ± 0.04	0.22 ± 0.01	0.14 ± 0.01	0.15 ± 0.03
36	Os	Cl	C	3.0 ± 0.4	1.46 ± 0.02	0.42 ± 0.06	1.8 ± 0.1
37	Os	I	C	1.20 ± 0.02	0.48 ± 0.01	0.08 ± 0.02	0.60 ± 0.04
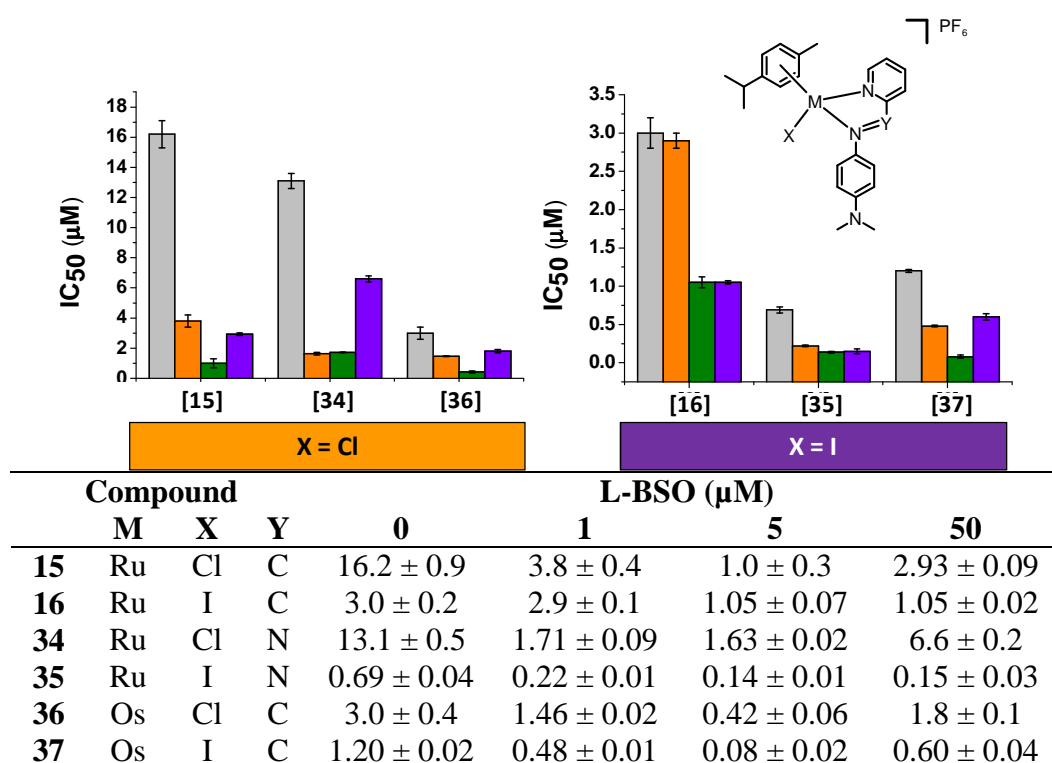
Figure 5.14. IC_{50} in A2780 cells for complexes **15**, **16**, **34–37** after co-incubation with various concentrations of L-BSO. Concentrations of the complexes used were equipotent at $IC_{50}/3$. L-BSO concentrations were (▦) 0 µM, (▦) 1 µM, (▦) 5 µM and (▦) 50 µM.

In a series of independent experiments, shown in Figure 5.15, auranofin, which is an effective inhibitor of thioredoxin reductase was co-incubated with arene complexes **15**, **16**, **34–37**. This gold complex can trigger mitochondrial-dependent apoptosis pathways and there are indications that mitochondrial oxidative stress is a central event in its mechanism of action. However, the concentration used in these experiments (0.1 µM) is non-toxic and too low to initiate the apoptotic cascade.

Compound			Auranofin (µM)	
	M	**X**	**Y**	**0**	**0.1**
15	Ru	Cl	C	16.2 ± 0.9	11.5 ± 0.5
16	Ru	I	C	3.0 ± 0.2	0.93 ± 0.05
34	Ru	Cl	N	13.1 ± 0.5	4.48 ± 0.09
35	Ru	I	N	0.69 ± 0.04	0.16 ± 0.01
36	Os	Cl	C	3.0 ± 0.4	0.30 ± 0.05
37	Os	I	C	1.20 ± 0.02	0.60 ± 0.09
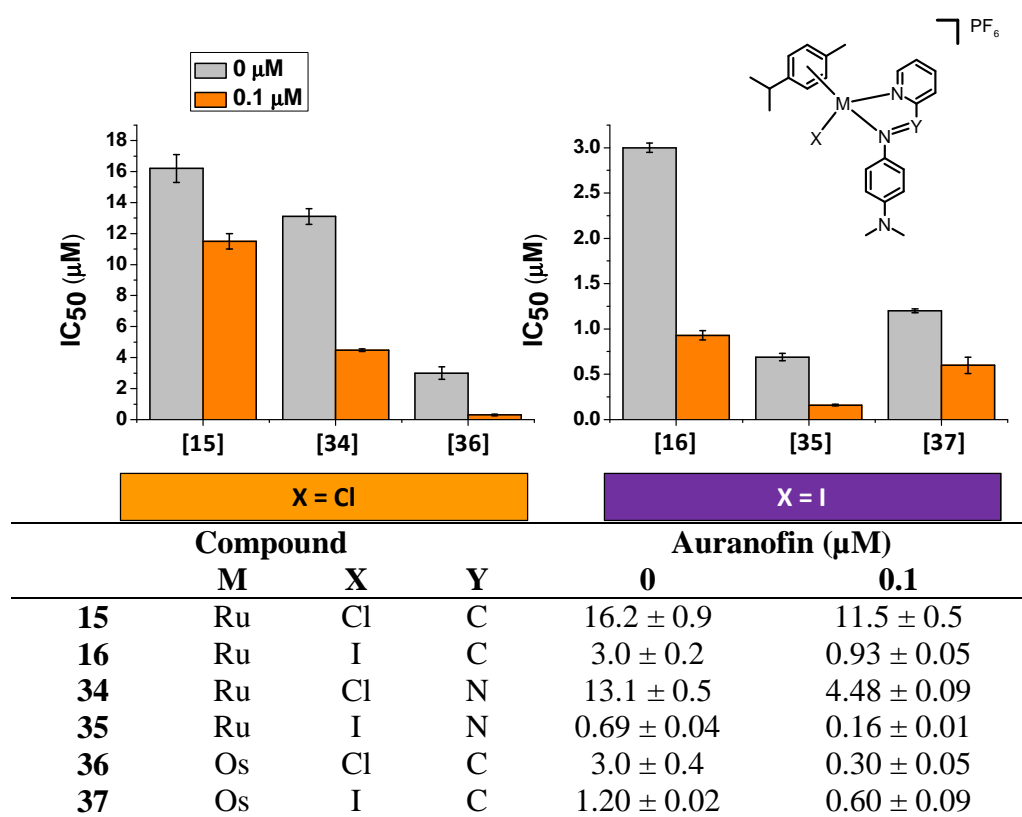
Figure 5.15. IC_{50} in A2780 cells for complexes **15**, **16**, **34–37** after co-incubation with 0.1 µM of auranofin. Concentrations of the complexes used were equipotent at $IC_{50}/3$. Auranofin concentrations were (■) 0µM and (■) 0.1 µM. The concentration of auranofin used were non-toxic.

It is observed that the potency of all complexes **15**, **16**, **34–37** improves when co-incubated with auranofin (Figure 5.15). In the case of ruthenium complexes, the antiproliferative activity of iodido compounds **16** and **35** is improved more significantly than their chlorido analogues **15** and **34**. The highest increase in potency is observed for osmium chlorido complex **36** [Os(η^6-*p*-cym)(*p*-Impy-NMe$_2$)Cl]PF$_6$; its IC_{50} value deceases 10X from 3.0 ± 0.4 µM to 0.30 ± 0.05 µM.

To confirm that the chosen concentration of auranofin was non-toxic, each 96-well plate had three independent series of control wells. The first one was negative control and was untreated at all times; the second control series was treated only with 0.1 μM of auranofin, and the last series was treated with different concentrations of **CDDP**. In all cases the difference in cell viability between series one (untreated) and two (plus auranofin) was never > 3%, and the IC_{50} value determined for CDDP was 1.2 ± 0.3 μM.

5.4 Discussion

5.4.1 Antiproliferative activity

Antiproliferative activity for complexes **15**, **16**, **34–37** was determined using the SRB assay for cell viability measurements. As shown in Table 5.2 on page 207, all complexes are highly active in the four cell lines used: A2780 ovarian, A549 lung, HCT116 colon and MCF7 breast lines with all IC_{50} values below 17 µM. Complexes **15**, **16**, **34–37** were chosen for the present study because of their structural similarities and with the aim of comparing the extent of variation in activity with changes in the structure.

As shown in Figure 5.16 all complexes have in common the arene, which is a *p*-cym unit. The starting point is chlorido complex **15** [Ru(η^6-*p*-cym)(*p*-Impy-NMe$_2$)Cl]PF$_6$ which includes the bidentate ligand *p*-Impy-NMe$_2$. A change in the chelating unit (a C atom replaced by N) generates azo complex **34** which has *p*-Azo-NMe$_2$ instead. In the opposite direction, Ru(II) complex **15** can be compared

to Os(II) complex **36**, they have in common the chelating ligand and the monodentate ligand. However the metal centre varying from ruthenium to osmium. According to the findings presented in Chapter 3, in which variations in the monodentate ligand modified substantially the cellular behaviour of ruthenium complexes, it was decided to include the comparison between complex **15** and **16**. Hence including as well iodido analogues **35** and **37**.
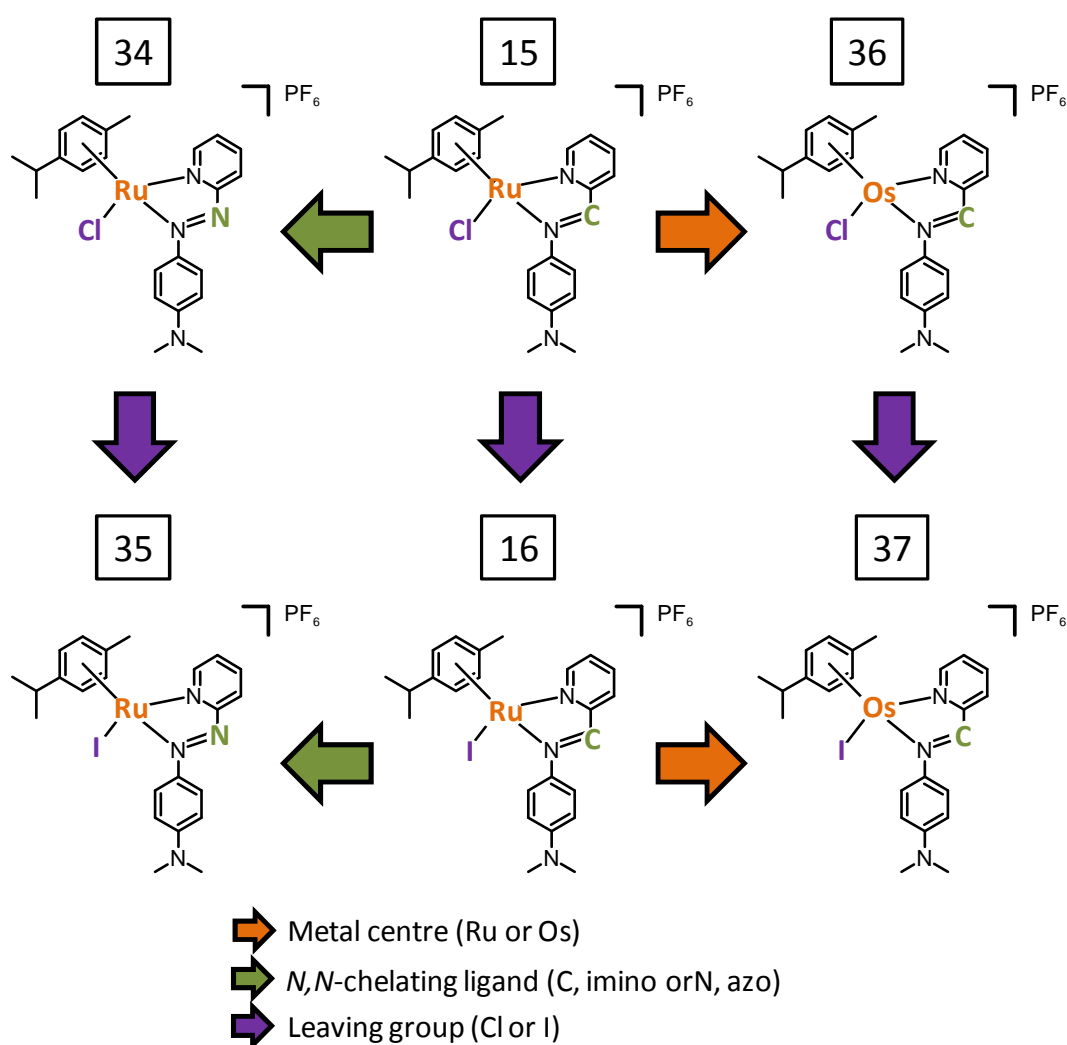
Figure 5.16. Relationship between the complexes **15**, **16**, **34–37** studied in Chapter 5.

It is remarkable that iodido complexes **16** and **35** are both highly active in all cell lines tested, although they exhibit different IC_{50} values caused by the variation of the C atom in the imine group. This structural modification causes ruthenium *p*-Azpy-NMe$_2$ complex **35** to be more active than the ruthenium *p*-Impy-NMe$_2$ complex **16** in all cell lines (eg. In A2780 cells IC_{50} changes from 3.0 ± 0.2 to 0.69 ± 0.04 µM). This observation could be explained by the electronic changes that the azo group generates in the structure. The electronic density of the ligand varies, affecting as well the electron-density of the metal centre and in consequence all reactions that involve it. The possibility of N=N bond reduction also adds to the electrochemical changes considered later when the metal centre varies between Ru/Os

It is observed that in A2780 ovarian and MCF7 breast cancer cells all iodido complexes **16**, **35** and **37** are more active than their chlorido analogues **15**, **34** and **36**. Antiproliferative activity variations after modifications on the monodentate ligand could be explained by the previous findings presented in Chapter 3. Changes in the halogen modify the cellular uptake and accumulation pathways involved in the first stages of drug action. This could lead to variations in cellular distribution of the drug, and in turn to different apoptotic pathways being triggered as a consequence of cellular compartamentalization,[23] hence resulting differences in IC_{50} values.

Finally, substitution of the metal centre is likely to explain why osmium *p*-Impy-NMe$_2$ complexes are more potent than their ruthenium analogues (with the exception of chlorido complex **36** compared to chlorido complex **15** exclusively in

A549 cells). This involves variation of the redox activity of the complex, a type of activity which has been related to the generation of ROS and modifications of mitochondrial activity.[24–27] Electron transfer agents such as metal complexes function catalytically in redox cycling with formation of ROS from oxygen. Electrochemical data add support to this mechanistic viewpoint. Generated secondary species generally exhibit reduction potentials amenable to electron transfer in vivo, thus giving rise to ROS.[24] Electrochemical reduction of ruthenium complex **35** has been previously investigated.[28,16] It was found that its first reduction potential is -0.40 V, which is considered to be within the biological relevant range of redox potential values (+ 0.40 V to – 0.50 V)[24] making possible its involvement in mitochondrial activity.

Experiments were also carried out with complexes **15**, **16**, **34–37** in order to investigate their antiproliferative activity in resistant cell lines. In the case of **CDDP** resistance, cisplatin-resistant A2780Cis cells were used. These results shown in Table 5.3 on page 208 also allow investigation of cross-resistance patterns with the platinum drug. **CDDP** is the metal-based anticancer drug most widely used. However, it shows major clinical drawbacks as very frequently patients treated with **CDDP** suffer from resistant cancer re-growth after remission. It is known that acquired **CDDP** resistance is mainly caused by changes in three cellular functions (A) reduced cellular accumulation which can be the result of impaired cell uptake or increased efflux, (B) increased cellular detoxification, especially mechanisms involving sulphur proteins, and (C) enhanced DNA repair.[29,30]

CDDP cross-resistance factors shown in Figure 5.17 are expressed as the ratio between the IC_{50} values in the resistant cell line divided by the IC_{50} values in the parental cell line. These results indicate that chlorido complexes **15**, **34** and **36** share, at least partially, some mechanisms of resistance to **CDDP**, as these complexes lose potency in the A2780Cis cells. Remarkably, the cross-resistance factors are always lower than the value for **CDDP**, which could mean a clinical advantage for the arene half-sadwich complexes.
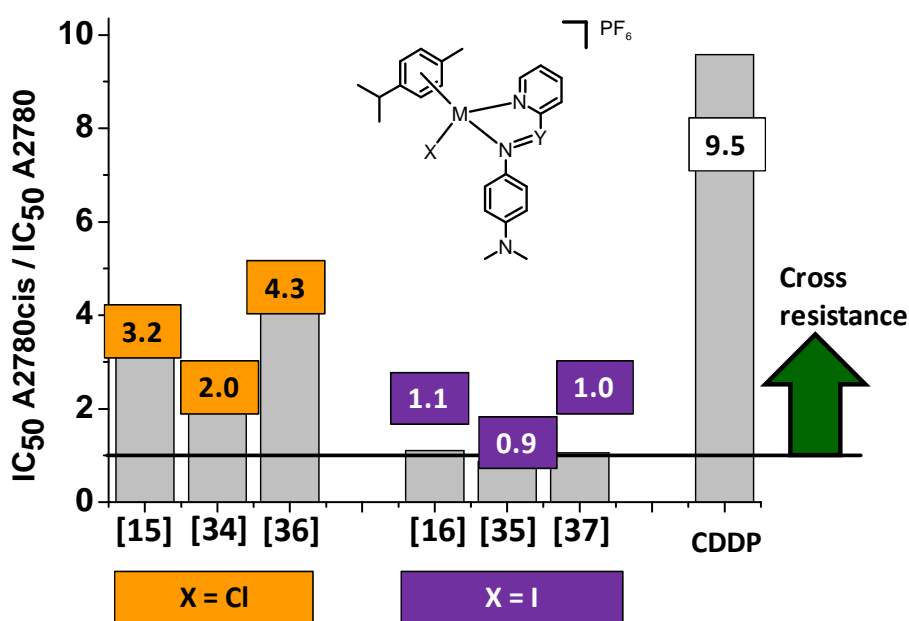
Figure 5.17. CDDP cross-resistance factors in A2780 cells when treated with complexes **15**, **16**, **34–37** for a 24 h period. Data are shown as the ratio of IC_{50} values in A2780cis divided by the IC_{50} value in the parental cell line. M = Ru/Os, Y = C/N

Iodido complexes **16**, **35** and **37** retain their potency in A2780Cis cells, as their cross-resistance factor is close to 1. This would suggest that there is at least one

major difference between these complexes and **CDDP**, with respect to the three main causes of resistance. Although cellular accumulation in A2780Cis has not been investigated, further results included in this Chapter that deal with the cell detoxification process involving sulphur proteins and DNA repair aim to establish the mechanism responsible for the lack of cross-resistance.

One common clinical strategy to treat cancers that have acquired resistance to **CDDP** is the use of OXA, even though this platinum based metallo-drug, shares some features of the mechanisms of action of **CDDP**. This clinical approach is especially important in the treatment of colorectal cancer with the common consequence of acquired resistance to both platinum drugs. To investigate whether ruthenium/osmium complexes can be an alternative for this particular case, the present research involved the analysis of cross-resistance with OXA using colon HCT116Ox cells. The results are shown in Table 5.3 on page 208, in this case, cross-resistance factors for complexes **15, 16, 34–37** were calculated using the corresponding data for IC_{50} values in HCT116 and in HCT116Ox, the latter being the OXA resistant cell line.

Figure 5.18 indicates that, similarly to **CDDP** resistance, iodido complexes **16** [Ru(η^6-*p*-cym)(*p*-Impy-NMe$_2$)I]PF$_6$, **35** [Ru(η^6-*p*-cym)(*p*-Azpy-NMe$_2$)I]PF$_6$ and **37** [Os(η^6-*p*-cym)(*p*-Impy-NMe$_2$)I]PF$_6$ retain their potency in the resistant cell line. Once again suggesting differences in the mechanism of resistance of these arene complexes compared to that of the OXA. In contrast, there is no uniform pattern for the chlorido complexes. Ruthenium *p*-Impy-NMe$_2$ complex **15** loses its potency greatly, with a cross-resistance factor of 22.5 while its equivalent osmium

complex **36** retains activity and its IC_{50} values does not change significantly. Remarkably, ruthenium complex **34** improves its activity in the resistant cell line compared to the parental cell line. Results also show that cells resistant to OXA HCT116Ox are also resistant to **CDDP**; this reflects the importance of the shared mechanism of action of these platinum drugs.
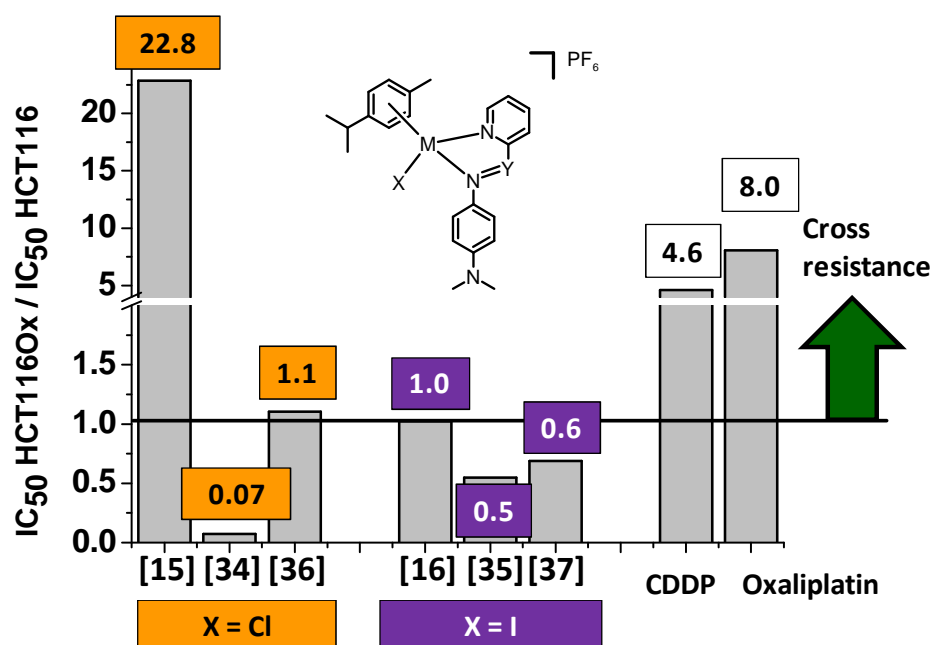
Figure 5.18. OXA cross-resistance factor in HCT116 cells when treated with complexes **15**, **16**, **34–37** for a 24 h period. Data are shown as the ratio of IC_{50} values in HCT116Ox divided by the IC_{50} value in the parental cell line. M = Ru/Os, Y = C/N

CDDP and OXA react with GC-rich sites in DNA and they are believed to form mainly intra-strand crosslinks.[31] However it has been reported that OXA requires lower intra-cellular concentrations and fewer DNA-Pt adducts to cause the same

extent of cell death to that of **CDDP**.[31] Both produce early SSB (single strand breaks) but it has been suggested that although there are more early lesions caused by **CDDP**, it is OXA which generates lesions that are more difficult to repair, as they are not recognised by MMR (mismatch repair) proteins.[31,32]

Another important point when investigating the antiproliferative activity of candidate drugs is their behaviour towards non-cancerous cells. For this, MRC5 human lung fibroblasts were used with complexes **15**, **16**, **34–37** (Table 5.3 on page 208). By comparing the IC_{50} value of a given drug in a cancer cell line against its activity in MRC5 is possible to determine the selectivity of the drug for a particular tumour tissue. As the difference between these two values increases the more likelihood of tumour specificity which may lead to reduce systemic effects for patients when in clinical use.

Figure 5.19 shows the ratios of IC_{50} values determined in MRC5 and the values obtained in A2780 cells. In this case the higher the value obtained, the more favourable is the selectivity of the studied drug for cancerous ovarian tissue. The best results are achieved by iodido complexes **16**, **35** and **37** suggesting that specific mechanisms of interfering with abnormal proliferation may be involved in the pathways activated by these complexes.

Tumour selectivity values determined for iodido complexes **16**, **35** and **37** are on average two-fold higher than those determined for chlorido complexes **15**, **34** and **36**, although the latter coincide with the value determined for **CDDP**. This indicates that in the case of ovarian carcinoma, these half-sandwich arene complexes are as selective as the platinum drug. MRC5 fibroblasts have been

used to evaluate this type of tissue selectivity for other chemotherapeutic drugs,[33] especially of natural origin[34,35] or even when using photodynamic therapy agents.[36]
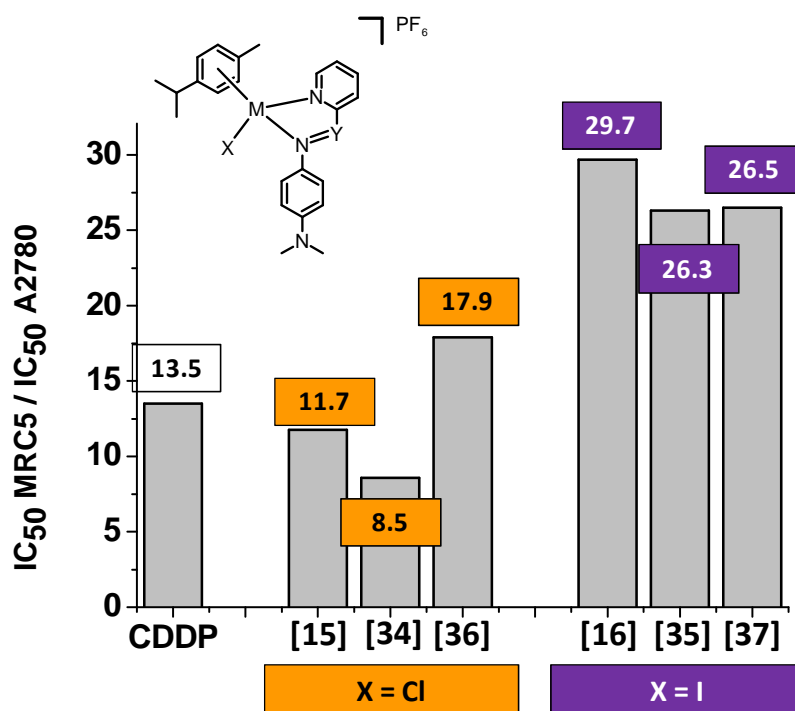
Figure 5.19. Ratio of IC_{50} values in MRC5 normal cells divided by the IC_{50} value in the A2780 cancer cells when treated with complexes **15**, **16**, **34–37** for a 24 h period. High values indicate good selectivity for tumour cells versus normal cells. M = Ru/Os, Y = C/N

5.4.2 Metal accumulation and distribution in cancer cells

The extent of metal accumulation (ruthenium /osmium) for complexes **15**, **16**, **34–37** was determined in A2780 cells in order to correlate it to the exhibited antiproliferative activity in this cell line. It was observed that in the case of chlorido complexes **15**, **34** and **36** there is a trend that correlates cellular

accumulation with potency as their IC_{50} values decrease when the cellular accumulation increases. However this trend was not observed for the iodido analogues **16**, **35** and **37** (Figure 5.20).
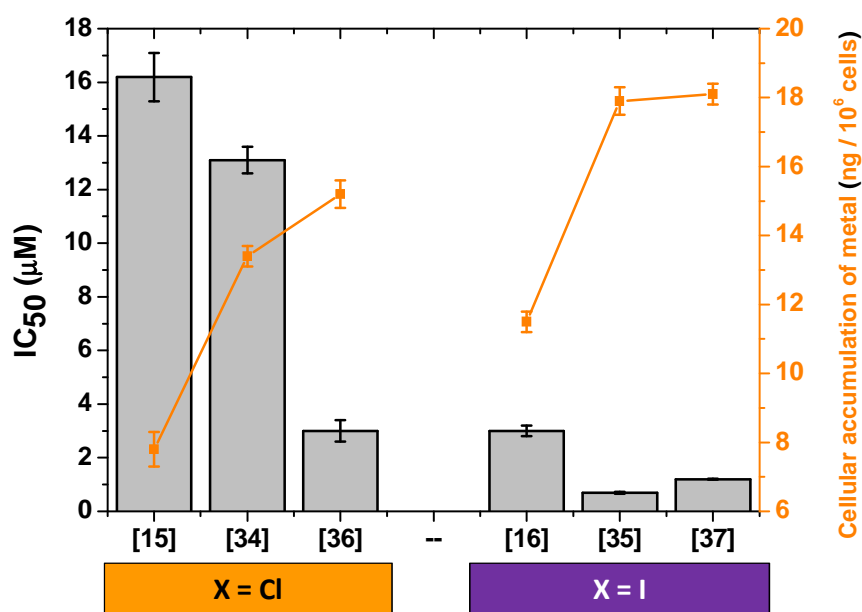
Figure 5.20. Comparison between cellular accumulation of Ru/Os (ng of metal per 10^6 cells)(left axis) and potency (IC_{50}, µM) of complexes **15, 16, 34–37** (right axis).

Differences in cellular accumulation cannot be explained by the extent of aquation exhibited by the complexes. As reported in Chapter 3, the *p*-Impy-NMe$_2$ complexes **15** and **16** aquate to a similar extent over 24 h (66% and 63% respectively). It has also been reported previously[16] that *p*-Azpy-NMe$_2$ complex **34** aquates up to 55% in the same period of time, while there is no aqua complex formation for the iodido complex **35**. Finally, the same process has been studied

for both osmium analogues;[37] chlorido complex **36** aquates 50% after 24 h and complex **37** is fully converted to the aqua species in the same time. Such marked differences do not allow for the establishment of any trend to account for the cellular accumulation. Besides, it is expected that plasma concentrations of chloride do not allow the complexes to hydrolyse before they enter the cells.[3,25] This is consistent with findings presented in Chapter 3 that indicate that there is no observable aquation of the complexes after 24 h in cell culture media and with previous reports that indicate that luminescent ruthenium complexes can reach the interior cell compartments with no structural changes.[38]

Interestingly, cellular compartmentalization studies on complexes **15**, **16**, **34–37** showed that the metal distribution in A2780 cells might not depend on the nature of the metal centre (Ru/Os) nor on the *N,N*-chelating ligand but on the monodentate ligand (Cl/I) instead. Results are shown in Figure 5.2 on page 211. The experiments carried out allowed the separation of four cellular fractions as shown in Figure 5.21.

Ru/Os from chlorido complexes **15**, **34** and **36** were retained highly in the membrane fraction. The extent of metal accumulation follows the order: membrane > cytosol > nuclear fraction > cytoskeleton. Ru/Os from the iodido complexes **16**, **35** and **37** is not retained in the cytosol ($< 2.2\%$ of the cellular Ru) and the percentages of metal in the nuclear and cytoskeletal fraction are lower than for chlorido analogues **15**, **34** and **36**.

Cytosolic Fraction	Membrane Fraction
total of soluble proteins from the cytoplasm	all membrane proteins plus all cellular organelles and its membranes
Nuclear Fraction	Cytoskeletal Fraction
total of nucleus soluble proteins and the nuclear membrane proteins	total cellular insoluble proteins and genomic DNA
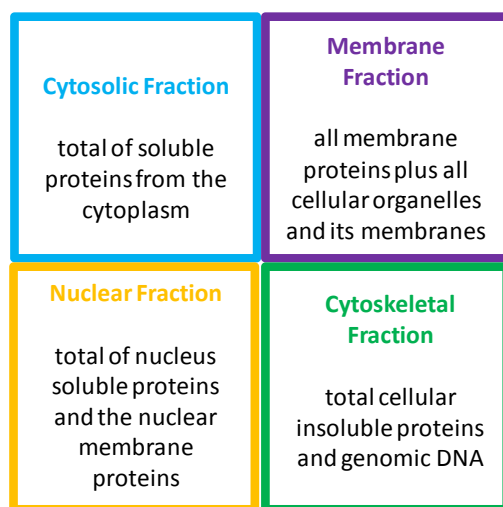
Figure 5.21. Cellular fractions for compartmentalization studies

Cellular accumulation pathways studied in Chapter 3, show that there are marked differences in the mechanism involved in cellular uptake and accumulation of chlorido complex **15** [Ru(η^6-p-cym)(p-Impy-NMe$_2$)Cl]PF$_6$ compared to iodido complex **16** [Ru(η^6-p-cym)(p-Impy-NMe$_2$)I]PF$_6$ in A2780 cells. It is possible that such differences can determine the distribution of ruthenium/osmium in cells and would explain why this process does not depend on the nature of the metal centre nor on the *N,N*-chelating ligand, but on the nature of the monodentate ligand. In consequence, it is also possible that the cellular metal distribution observed for complexes **34**-**37** is a consequence of the cellular uptake pathways involved in the metal accumulation of these complexes; moreover, this distribution can determine the different apoptotic pathways activated by chlorido / iodido complexes. This is consistent with recent studies that have linked endocytotic pathways to cellular signal transduction, suggesting bidirectional interplay between the two processes;[23] moreover, results suggest that cellular compartamentalization can

induce selective transmission of signals that can lead either to apoptosis or survival of the cell.[39,40]

5.4.3 Mechanism of action studies

- **Cell cycle analysis using flow cytometry**

The cell cycle in mammalian cells (Figure 5.22) consists of four distinct phases: an S phase during which the cell replicates its DNA and duplicates the chromosomes, an M phase in which the duplicated chromosomes are separated into two nuclei (mitosis) and consequently into two daughter cells (cytokinesis), and finally, two gap phases known as G1 (before S phase) and G2 (before M phase).[41,42]
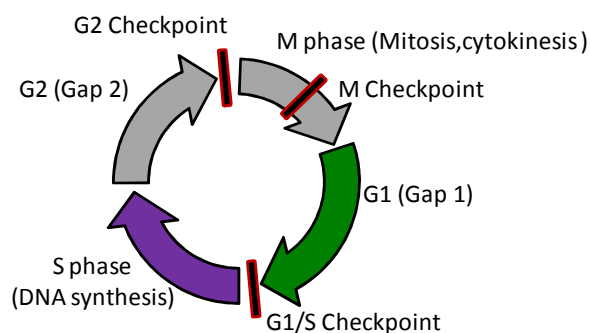
Figure 5.22. Cell cycle representation for mammalian cells.

Progression of the cells in this cycle is regulated by cyclin-dependent kinases (Cdks) and determined by three checkpoints.[43] The first of which occurs in late G1 phase, at this point G1/S and S phase cyclin-Cdk complexes are activated only

if the conditions for cell proliferation are ideal, then DNA replication starts. The second check point at the end of G2 phase controls DNA damage or completion of DNA replication, in this case the M-phase cyclin-Cdk complex is activated. The third checkpoint is responsible for deactivating all Cdks in the cell to allow spindle disassembly and later cytokinesis.

G1/S cyclins stimulate the cells to go into the cell cycle depending on external signalling that guarantee the rate of cell growth so it is possible to say that cell proliferation is controlled at the G1/S checkpoint.[44] Results shown in Figure 5.5 on page 214 indicate that complexes **15**, **16**, **34–37** do not allow A2780 cells to progress into the cell cycle hence they do not allow the cancer cells to multiply. Ruthenium and osmium complexes studied in this Chapter, have shown a significant arrest in G1 population compared to the untreated control. This has previously been reported for other ruthenium(II) complexes.[45] Interestingly, ruthenium Impy complexes **15** and **16** cause the S population to be twice as large as the G2/M phase population (12.7 ± 0.9% in S phase for **15,** compared to 6.5 ± 0.8 in G2/M phase and 14 ± 1% in S phase for **16,** compared to 6.3 ± 0.7 in G2/M phase). This possibly indicates that besides causing G1-arrest these ruthenium complexes interfere with DNA and/or chromosome replication as cells are partially retained in the second checkpoint which checks for DNA damage, which implies a secondary S arrest.

In contrast, results for **CDDP** (Figure 5.5 on page 214) show that the platinum drug causes arrest in the S phase, as expected.[46] It is known that the mechanism of action for **CDDP** involves covalent binding of the drug to DNA. This defective

DNA triggers cell cycle arrest and does not allow progression into cell division. Figure 5.6 on page 215 shows the results for the cell cycle analysis of A2780 cells when treated with different concentrations of **CDDP**. The arrest observed is concentration-dependent as the S phase population increases with concentration increase ($16.5 \pm 0.6\%$ when using 0.4 μM of **CDDP** to $44 \pm 2\%$ when using 3.6 μM). The explanation for this observation lies in that at higher concentrations of the platinum drug, the number of DNA-Pt lesions increases making the repair process slower and inefficient. This holds a greater population of cells in the S phase.

The same experiment was carried out using different concentrations of ruthenium complex **16** [Ru(η^6-p-cym)(p-Impy-NMe$_2$)I]PF$_6$. However in this case the population arrested in G1 phase does not increase significantly with the concentration of the complex ($64.2 \pm 0.6\%$ when using 1 μM of **16** to $65.6 \pm 0.8\%$ when using 9 μM), which indicates that the cell cycle arrest is concentration-independent. This could be an advantage for an anticancer drug, as its cytostatic activity would avoid cell proliferation at low concentrations.

- **p53-activated apoptotic pathway**

Protein 53 (p53) is a tumour-suppressor protein that interacts with the G1/S-Cdk complex involved in the first cell cycle checkpoint.[47] p53 is a zinc protein which contains 393 amino acid residues, divided into three domains[48] as shown in Figure 5.23.[49] It mediates cell cycle arrest, senescence or apoptosis after mutagenic

events. Disruption in the p53 pathway has been strongly correlated to tumorigenesis as it is considered to maintain genomic stability. Unfortunately, its inactivation is the most common event in human cancers, occurring in at least 50% of all cases.[50,51]

N-terminus		Central Core	C-terminus	
1-42	61-94	102-292	324-355	363-393
Transactivation domain	Proline-rich region	DNA-binding domain	Tetramerization domain	Regulatory domain
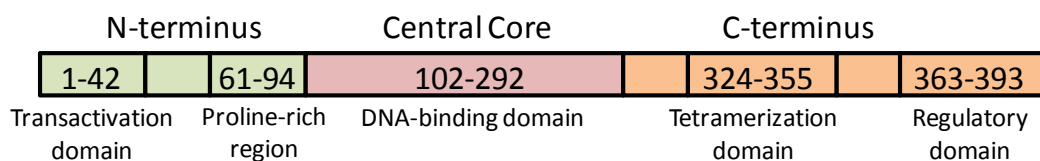
Figure 5.23. Schematic representation of the three protein domains in p53 according to Bai and Zhu.[49]

Figure 5.24 shows the ratios of IC_{50} values for HCT116p53-/- cells (p53 knocked out cells) over the parental line when treated with complexes **15**, **16**, **34–37** for a 24 h period (for IC_{50} values in each cell line see Table 5.5. on page 217). Figure 5.24 shows that there are different responses when the cells are exposed to the chlorido complexes **15**, **34** and **36**.

Although all chlorido arene complexes seem to lose potency, this effect is more pronounced for complex **15** [Ru(η^6-p-cym)(p-Impy-NMe$_2$)Cl]PF$_6$ which is 20X less active (IC_{50} increases from 3.4 ± 0.4 to 69.9 ± 0.9 μM). Activation of p53, by DNA damage, cytotoxic drugs, hypoxia or oncogenic signalling amongst others, is known to cause cell cycle arrest in G1 phase, as well as being involved in the intrinsic apoptotic pathway.[47]
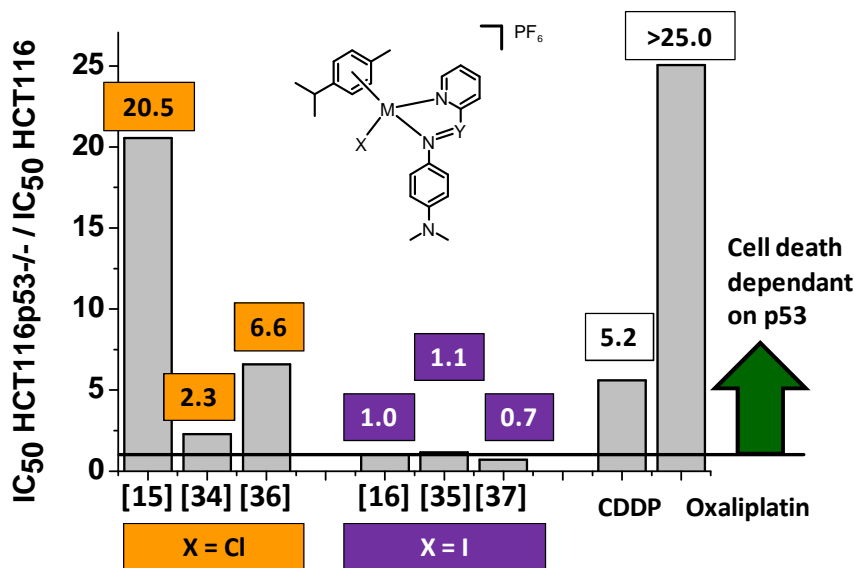
Figure 5.24. p53-dependent cell death of HCT116 cells when treated with complexes **15**, **16**, **34–37** for a 24 h period. Data are shown as the ratio of IC_{50} values in HCT116 p53 -/- divided by the IC_{50} value for the parental cell line. M = Ru/Os, Y = C/N

In previous sections, it was shown that these complexes cause the same effect on the cell cycle (G1 arrest). Both events may be related. It is possible that the chlorido complexes **15**, **34** and **36** activate p53 which in turns arrests the cell cycle, so when p53 is knocked out in HCT116 cells the arrest does not occur and cell proliferation increases, which is manifested as an increase in the IC_{50} value. Other ruthenium complexes have been previously studied in relation to their p53-dependence,[52,53] particularly, chlorido complex RM175 (Figure 5.25) which activates p53-dependent pathways.[54]
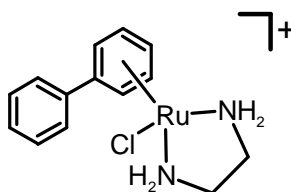
Figure 5.25. Structure of RM175

In contrast, Figure 5.24 also shows that iodido complexes **16**, **35** and **37** are as potent in the p53- null cell line as in the parental line. This is likely to indicate that their mechanism of action does not depend on the p53 apoptotic pathway, which might be advantageous for their clinical use, especially taking into account that the treatment of choice for colon cancer is OXA which shows a potency loss above 25-fold.
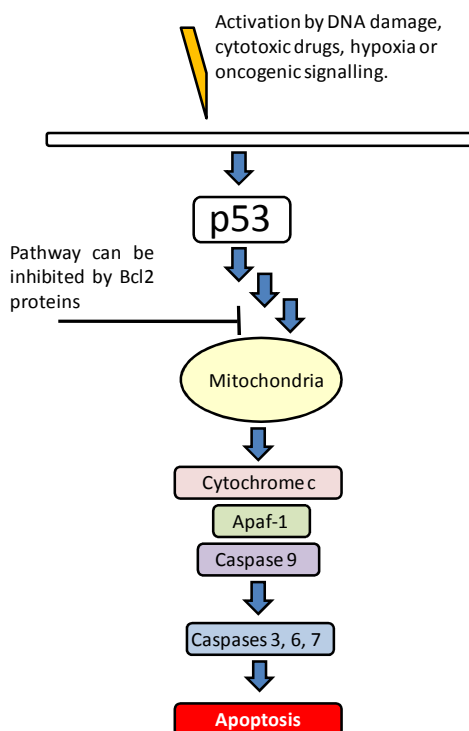
Figure 5.26. Schematic representation of the intrinsic apoptotic pathway.

The intrinsic apoptotic pathway, in which p53 is involved (Figure 5.26), is activated by cellular stress. Signalling in this pathway is amplified by mitochondria, which release cytochrome c and subsequently activate caspase 9, and downstream also activate caspase 3.[47]

- **Induction of apoptosis**

Apoptosis is the process of programmed cell death in which a cell goes through biochemical and morphological changes. Unlike necrosis, it produces fragments that other phagocytic cells are able to remove without causing damage to surrounding tissues.[55] There are basically two different pathways for cells to undergo apoptosis. The first one is the intrinsic pathway (initiated by internal stimuli) discussed in previous sections and the second is the extrinsic pathway initiated by external stimuli.[56] Nevertheless, there are several signalling mechanisms that can activate these pathways, for example external stimuli can be initiated by the TNF path (formerly known as tumour necrosis factor alpha-1) or the FAS path (apoptosis antigen 1) in which the death-inducing signalling complex DISC is formed and caspases 8 and 10 are activated.[56] Regardless of the mechanism that initiates the cascade of apoptotic stimuli, the process finishes with proteolytic caspases starting the organized degradation of cellular organelles.

In the present work, complexes **15**, **16**, **34–37** were used to investigate the extent of apoptosis in A2780 cells caused after a 24 h period of exposure. Results shown in Figure 5.9 on page 220 indicate that although all half-sandwich arene

complexes cause apoptosis there are differences in relation to early, late apoptotic and non-viable populations.

It was observed that early apoptotic populations of cells are practically non-existent after exposure to iodido complexes **16**, **35** and **37**, but they exhibit high incidence of non-viable cells. Also, the population for late-apoptotic cells in these iodido complexes **16**, **35** and **37** is very low. Morphological changes in early apoptotic cells include the loss of phospholipid asymmetry followed by the traslocation of phosphatidylserine to the outer membrane. The phospholipid component should be found in the internal/cytosolic side of the membrane in healthy cells. This protein translocation is key for the detection of apoptosis by annexin V.[20]

In late stages of apoptosis, the membrane is totally compromised as the cell breaks apart into several vesicles or apoptotic bodies. In the process, membrane blebbing allows formerly impermeant agents, like PI, to access inner cell compartments. In contrast to iodido complexes, the population of non-viable cells is lower for chlorido analogues **15**, **34** and **36**. These differences might indicate that although all complexes activate apoptotic cascasdes, the processes involving iodido complexes **16**, **35** and **37** are different from those involving chlorido analogues **15**, **34** and **36** generating variations in the time each pathway takes to cause cell death.

- **Caspase 3 apoptotic pathway**

Caspases, in general, are a family of cysteine proteases that play essential roles in apoptosis, necrosis, and inflammation.[57,58] Caspase 3, in particular, also known as CPP32, is encoded by the CASP3 gene in humans and recognises the peptide sequence DEVDG (Asp-Glu-Val-Asp-Gly), with cleavage occurring on the carboxyl side of the second aspartic acid residue[21,59] This peptide sequence preference allows the development of colorimetric methods to measure its activation, as used in this research, in which the DEVD sequence is labelled with p-NA.[21]
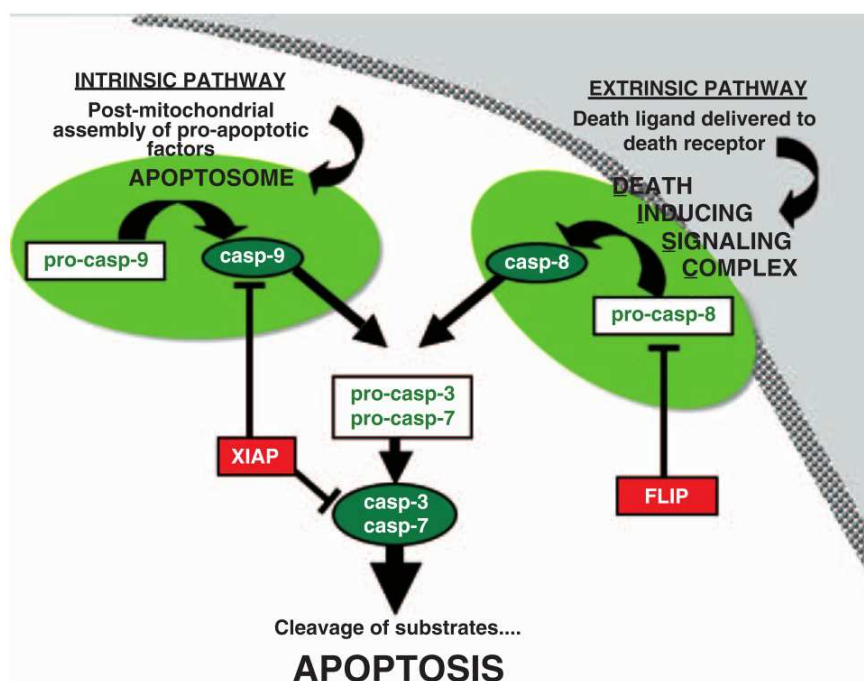
Figure 5.27. Involvement of caspase 3 in the intrinsic and extrinsic apoptotic pathways according to Salvesen and Riedl.[57]

The inactive form of caspase 3, known as the caspase 3 zymogen can be activated in both apoptotic pathways (Figure 5.27): (A) the intrinsic pathway, in which p53 activates the release of cytochrome c from mitochondria[56] and (B) the extrinsic pathway which is activated by DISC (death-inducing signalling complex) and is independent of Bcl2 activity. In the former, cytochrome c combines with caspase 9 and the apoptosis-activating-factor 1 (Apaf-1) to activate the zymogen. However, in the latter it is the sequential activation of caspases that plays a central role in the execution-phase of cell apoptosis.[57]

In the present research, complexes **15**, **16**, **34–37** were used to investigate the activation of caspase 3 in A2780 cells. For this, the absorbance of free p-NA was monitored, as caspase 3 specifically cleaves the adduct DEVD-pNA. Results shown in Figure 5.11 on page 223 indicate that all the studied arene complexes activate caspase 3. Remarkably, there is a difference (Ca. 1.5 X) between the levels of activation of the caspase 3 induced by the chlorido complexes **15**, **34** and **36** compared to that induced by the iodido complexes **16**, **35** and **37**. This difference again, indicates that the monodentate ligand plays a major role in determining the activity of these half-sandwich arene complexes. Staurosporine was used in this experiment as a positive control known to cause apoptosis.[60,61]

Polypyridyl ruthenium complexes have also been reported to induce apoptosis with activation of caspase 3 via the intrinsic pathway.[62] Interestingly, there are other reports[63] that indicate that anticancer agents that interact with DNA, specifically with mitochondrial DNA (mDNA), selectively enhance the generation of ROS in mitochondria and the release of cytochrome c, inducing apoptosis after

activating caspases 9 and 3. Cell compartmentalization studies showed that complexes **15**, **16**, **34–37** accumulate highly in the membrane fraction that includes the mitochondria, and they also activate caspase 3. However there are no data on their interaction with mDNA. Further studies will be needed to analyse ROS generation and the role of mitochondria in antiproliferative activity.

- ## **DNA replication**

DNA replication is a common target in the development of chemotherapeutic agents.[64] This process, used by the cell to copy its DNA, starts with the double helix being separated into two strands initiating the replication fork. For this a DNA helicase breaks the hydrogen bonds that keep the double strands together. In a following step, a DNA polymerase uses one of the newly-released single strands to match complementary nucleotides and synthesise a new strand. The formation of the replication fork causes rotation of the DNA and in consequence it builds up excess coiling that DNA gyrases relieve by unwinding the double helix. As a crucial step in cell multiplication, this process can be targeted to block abnormal cell proliferation.

In the present work, aphidicolin was used to inhibit DNA polymerase α in order to establish whether it has a role in the antiproliferative activity exhibited by arene complexes **15**, **16**, **34–37** in A2780 cells. It has been previously reported that aphidicolin is a reversible inhibitor of this polymerase[65,66] and shows a dose-dependent capacity to inhibit repair of **CDDP**-induced DNA damage.[65,67] Aphidicolin is a tetracyclic diterpene, (Figure 5.28) and has also been used as

synchronising agent in cell cycle studies.[65,68] It has been suggested that its mechanism of inhibition relies on conformational changes that inactivate the enzyme when aphidicolin binds to the dCTP binding site.[66]
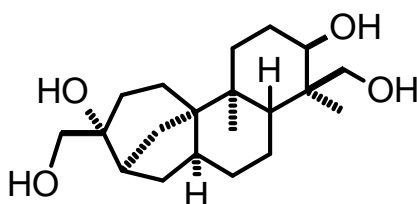
Figure 5.28. Structure of aphidicolin

Results (Figure 5.11 on page 225) suggest that the antiproliferative activity of ruthenium azpy complexes **34** [Ru(η^6-*p*-cym)(*p*-Azpy-NMe$_2$)Cl]PF$_6$ and **35** [Ru(η^6-*p*-cym)(*p*-Azpy-NMe$_2$)I]PF$_6$ may not involve mechanisms linked with DNA polymerase α inhibition, as their IC$_{50}$ values remain unchanged with the co-administration of different concentrations of aphidicolin. On the contrary, the activity of complexes **16**, **36** and **37** improves significantly. This may result from the lack of repair of DNA lesions caused by the half-sandwich arene complexes. Such results have been previously observed, the potency of **CDDP** improves when co-administered with aphidicolin, in this case, the diterpene partially prevents the repair of Pt-DNA by the polymerase α.[69,70]

Aphidicolin is widely used as a control for DNA polymerase inhibition studies as it exhibits a high affinity for the enzyme. [21,32,71,22] So it is possible that in a

competition reaction against a second inhibitor, the latter would be displaced. This explanation is consistent with the observations for the antiproliferative activity of complex **15** [Ru(η^6-p-cym)(p-Impy-NMe$_2$)Cl]PF$_6$ which decreases considerably when co-administered with aphidicolin. Inhibition of DNA polymerase might be one of the mechanisms of such a multitargeted drug.

Topoisomerases are a family of enzymes that cut DNA strands catalysing the hydrolysis of phosphodiesther bonds, whilst at the same time, are capable of rejoining the separated strands. In particular, topoisomerase II uses this mechanism to manage DNA tangles and supercoils that occur during DNA replication. Unlike topoisomerases type I, their processes are ATP-dependent. Etoposide, shown in Figure 5.29, is an inhibitor of topoisomerase II that binds to the enzyme and blocks the DNA re-ligation step.[72]

Figure 5.13 on page 226, shows the results of co-incubation of etoposide with complexes **15**, **16**, **34–37** in A2780 cells. The potency of complexes **34** and **37** towards these ovarian cells remains unchanged after the co-administration of etoposide. This might suggest that their mechanism of action does not involve disruption of DNA replication. In contrast, the chlorido complex **36** [Os(η^6-p-cym)(p-Impy-NMe$_2$)Cl]PF$_6$ exhibits a marked improvement of its activity (decrease in IC$_{50}$ value). It has been reported that this osmium complex undergoes full aquation after 24 h and is capable of binding to 9-EtG.[37] That together with the fact that in the cell compartmentalisation studies, Os from complex **36** is highly accumulated in the cytoskeletal fraction, (from which genomic DNA is isolated), suggesting that it is possible that the complex interacts directly with

DNA. Etoposide inhibition of topoisomerase II may allow complex **36** to promote double strand-DNA (DS-DNA) breaks. Such an observation has been previously reported for ruthenium complexes that bind directly to DNA inhibiting relaxation and repair by topoisomerase II.[64]
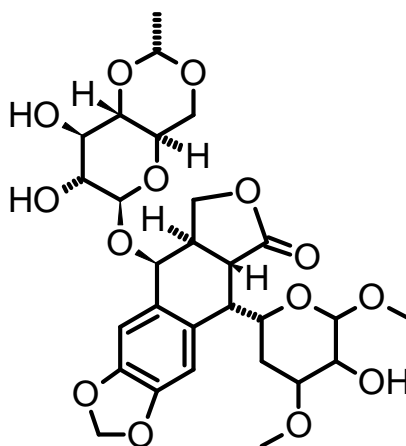
Figure 5.29. Structure of etoposide

Contrasting results were observed for complexes **15** [Ru(η^6-p-cym)(p-Impy-NMe$_2$)Cl]PF$_6$, **16** [Ru(η^6-p-cym)(p-Impy-NMe$_2$)I]PF$_6$ and **35** [Ru(η^6-p-cym)(p-Azpy-NMe$_2$)I]PF$_6$ which lose their antiproliferative activity towards A2780 cells when co-incubated with etoposide. This inhibitor is usually used as a positive control for topoisomerase II studies,[73,74] as it does not affect the activity of topoisomerase I enzymes[75] and exhibits a highly elevated affinity. The results are consistent with these complexes having a mechanism of action that inhibits topoisomerase II. However when co-incubated with etoposide the competition reaction favours the formation of the etoposide-enzyme complex which leads to a

decrease in the potency of the metal compounds. This result is consistent with the observations for DNA polymerase α inhibition shown earlier.

A particular type of topoisomerase II is DNA gyrase, which helps to minimize DNA unwinding problems by negatively supercoiling it. This enzyme can be inhibited by novobiocin (Figure 5.30) which is an aminocumarin that binds to the GyrB subunit.[76,77]
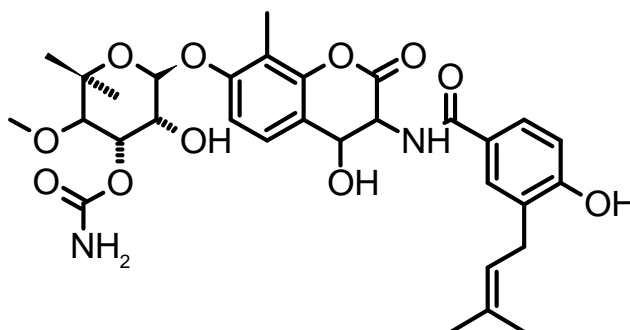
Figure 5.30. Structure of novobiocin, inhibitor of DNA gyrase.

In cell culture, co-administration of novobiocin with **CDDP** results in marked synergy as it allows a higher number of DNA interstrand cross-links to occur. [78] It has also been reported to improve the potency of several alkylating agents by increasing the formation of DNA-DNA cross-links.[78,79] In the results presented in Figure 5.13 on page 226, novobiocin was used as co-incubation agent for complexes **15**, **16**, **34–37** in A2780 cells. It was observed that the potency of ruthenium complexes **34** and **35** and iodido osmium complex **37** is not significantly modified by novobiocin, as their IC_{50} values remain unchanged. However, complexes **16** [Ru(η^6-p-cym)(p-Impy-NMe$_2$)I]PF$_6$ and **36** [Os(η^6-p-

cym)(p-Impy-NMe$_2$)Cl]PF$_6$ show an improvement in their activities. This result is consistent with some synergy between the arene complexes and the aminocumarin. It is possible that an increase in DNA-DNA cross-linking could be responsible for this improvement of the activity, particularly taking into consideration the observed secondary arrest in S phase caused by exposure of A2780 cells to complex **16**.

Interestingly, chlorido complex **15** [Ru(η^6-p-cym)(p-Impy-NMe$_2$)Cl]PF$_6$ loses potency towards A2780 cells in the presence of novobiocin. This observation can be explained if its mechanism of action includes targeting of topoisomerase II, with the possibility of deactivation in competition against novobiocin, as described earlier when analysing the results for co-administration of etoposide. Also, it has been reported that novobiocin induces mitochondrial damage that results in a moderate decrease of the ATP/ADP ratio and consequently a decrease in the ATP content of the cell.[80,81] Studies of cellular accumulation presented in Chapter 3 showed that the cellular uptake and accumulation in cells of complex **15** is highly dependent on ATP concentrations. Hence if the ATP concentration is lowered, it is possible that this affects the cell accumulation and in turn the antiproliferative activity of the arene complex.[80] It is notable that the results of the co-incubation of chlorido complexes with novobiocin are consistent with those observed on co-administration with etoposide.

- **Cellular detoxification mechanisms**

As previously noted, one mechanism for **CDDP** resistance involves an increase in intracellular GSH levels. Loss of antiproliferative activity of the platinum drug has been associated with covalent binding to the glutathione thiolate anion which reduces the possibility of DNA cross linking.[30] In the present study complexes **15**, **16**, **34–37** were co-administered with L-BSO to investigate the role of GSH in the cellular detoxification of half-sandwich arene complexes.

L-BSO, (Figure 5.31) is a specific inhibitor of γ-glutamylcysteine synthetase which is the enzyme involved in the rate-limiting step in GSH synthesis. The resulting action of the inhibitor is a significant decrease in GSH intracellular levels. When used as a single agent at high concentrations, L-BSO is capable of increasing ROS levels causing apoptosis.[82,83] However, it has been used at low doses to increase the sensitivity to certain anticancer drugs that depend on GSH-mediated detoxification.[3,70] L-BSO has also been entered phase I clinical trials, which indicate that its use is safe to the point of reducing GSH levels to 40%.[84]
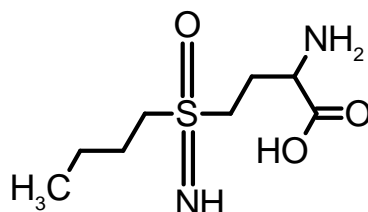
Figure 5.31. Structure of L-BSO

Results in Figure 5.14 on page 228 suggest that A2780 cells may use GSH as a detoxification mechanism for arene half-sandwich complexes. The potency of the complexes increases when co-administered to cells with L-BSO, especially iodido complex **37** [Os(η^6-p-cym)(p-Impy-NMe$_2$)I]PF$_6$ which exhibits a 15-fold reduction of its IC$_{50}$ value (from 1.2 ± 0.4 µM to 80 ± 2 nM). It is remarkable that the best improvements in activity are observed for chlorido complexes (16-fold improvement for complex **15** [Ru(η^6-p-cym)(p-Impy-NMe$_2$)Cl]PF$_6$ and 8-fold increase for complex **34** [Ru(η^6-p-cym)(p-Azpy-NMe$_2$)Cl]PF$_6$).

Inhibition of detoxification mechanisms by administration of L-BSO has been reported to improve the activity of a wide range of metal-based drugs.[70,82,85] For example L-BSO partially restores sensitivity to **CDDP** in several resistant cancer cell lines, and improves the activity of Pt-thiourea complexes,[86,87] It also lowers the IC$_{50}$ value of ruthenium(III) complexes such as KP1019[25] and osmium(II) azo complexes like FY26 (Figure 5.32).[85]
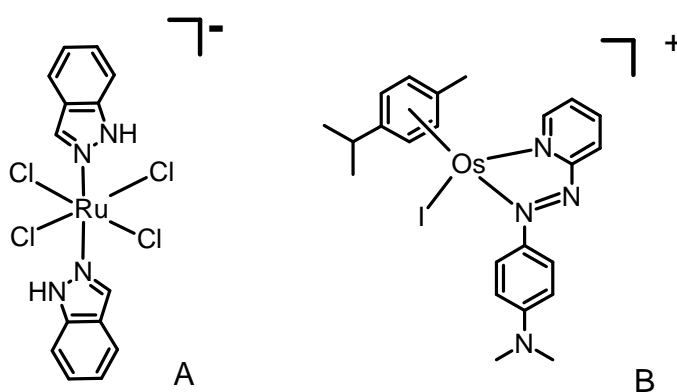
Figure 5.32. Structure of (A) KP1019 and (B) FY26.

The mechanism of action of L-BSO, involves the prevention of cellular detoxification by GSH through a decrease in GSH levels, as well as, an increase in redox activity. This imbalance in ROS levels in the cell, as the low levels of GSH affect the equilibria between GSH and its oxidised form GSSG.[83] (Figure 5.33)
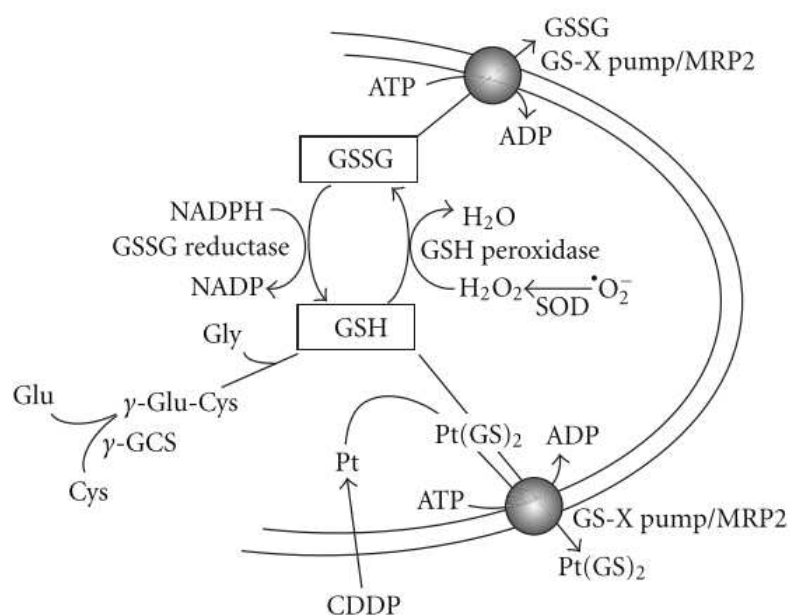
Figure 5.33. Generation of ROS caused by the imbalance in the equilibria GSH-GSSG, according to Chen and Kuo.[83]

Interestingly, in the case of complexes **15**, **16**, **34–37**, there is an optimum concentration of L-BSO (5 µM) which maximises the potency of the complexes tested. This dependence on the concentration of L-BSO is not linear, as the highest concentration (50 µM) does not achieve further improvement.

L-BSO causes deactivation of taxol, as it interferes with the cell cycle changes induced by paclitaxel.[88] It is possible that this interference, more obvious at

higher concentrations of L-BSO (50 µM) causes the decrease in activity of the complexes.

5.5 Conclusions

The aim of the research presented in this Chapter was to investigate the mechanisms involved in the antiproliferative activity of complexes **15**, **16** [Ru(η^6-p-cym)(p-Impy-NMe$_2$)X]PF$_6$, **34**, **35** [Ru(η^6-p-cym)(p-Azpy-NMe$_2$)X]PF$_6$, and **36**, **37** [Os(η^6-p-cym)(p-Impy-NMe$_2$)X]PF$_6$ where X = Cl or I. These complexes were chosen on the basis of their structural similarities, as they allow three types of structural modifications to be compared: (A) changes in the electronic structure of the *N,N*-chelating ligand (imine ligand vs isoelectronic azo ligand), (B) substitution of a chlorido monodentate ligand vs an iodido, and, finally (C) changes in the metal centre (ruthenium vs osmium).

Table 5.6 summarises the results obtained in this Chapter. They suggest that the apoptotic pathways involved depend to a great extent on the nature of the monodentate ligand. This is also reflected in variations of the cellular compartmentalization of the complexes due to different cellular accumulation mechanisms, as seen in Chapter 3. It is possible that iodido half-sandwich arene complexes could convert to their chlorido analogues. However there is evidence for the different behaviour of these two types of complexes, which is not consistent with such a conversion. If the iodido complex did convert to the chlorido complex, then more similarities in the activation of apoptotic pathways

would be observed, including similar antiproliferative activity and similar metal distribution, which is not the case. This and the stability of iodido complex **16** in cell culture media against conversion to its chlorido analogue was also demonstrated in Chapter 3.

Complexes **15**, **16**, **34–37** are highly active in all the cell lines tested (A2780, A549, HCT116, and MCF7). In terms of resistance and selectivity the iodido complexes **16**, **35** and **37** have an advantage over chlorido complexes **15**, **34** and **36** as they do not share mechanisms of resistance with **CDDP** nor with OXA, and they are more selective towards ovarian cancer than **CDDP**. Complexes **15**, **16**, and **34–37** cause a G1-arrest in the cell cycle of A2780 ovarian cells. This suggests that the complexes exhibit cytostatic activity as well as cytotoxicity, inhibiting cell proliferation. Iodido complexes **16**, **35** and **37** exhibited activity independent of p53 while the activity of chlorido complexes, **34** and **36** depends on this protein to cause cell death. Future work should include investigations of changes in mitochondrial function caused by chlorido complexes **15**, **34** and **36** to understand whether the intrinsic apoptotic pathway is involved in their mechanism of action. The production of ROS could play a significant role and trigger the release of cytochrome c into the cytosol.

Half-sandwich arene complexes initiated apoptosis in A28780 cells after 24 h of drug exposure. This was confirmed by the activation of caspase 3. It remains unknown if the activation of the caspase is the result of an intrinsic apoptotic pathway or a response to extrinsic stimuli. This should be further investigated.

Finally, co-treatment of complexes with L-BSO show that GSH levels are linked with the detoxification of arene complexes **15**, **16**, **34–37**, as their potency increases significantly with the co-administration. Complexes **35**, **36** and **37** in particular achieve nanomolar activities in the presence of a low L-BSO concentration (5 µM).

	Chlorido Complexes			Iodido Complexes		
	15	**34**	**36**	**16**	**35**	**37**
	Ru, *p*-Impy-NMe$_2$	Ru, *p*-Azpy-NMe$_2$	Os, *p*-Impy-NMe$_2$	Ru, *p*-Impy-NMe$_2$	Ru, *p*-Azpy-NMe$_2$	Os, *p*-Impy-NMe$_2$
IC$_{50}$(A2780, μM)	16.2 ± 0.9	13.1 ± 0.5	3.0 ± 0.4	3.0 ± 0.2	0.69 ± 0.04	1.20 ± 0.02
CDDP cross-resistance (A2780cis)	3.2	2.0	4.3	1.1	0.9	1.0
Oxaliplatin cross-resistance (HCT116Ox)	22.8	0.07	1.1	1.0	0.5	0.6
Selectivity MRC5 / A2780	11.7	8.5	17.9	29.7	26.3	26.5
Metal distribution (A2780)	Membrane Frac. > Cytosolic Frac. > Nuclear Frac. > Cytoskeletal Frac.			Membrane Frac. > Nuclear Frac. > Cytoskeletal Frac. Metal concentration in cytosolic fractions negligible		
Cell cycle arrest (A2780)	G1			G1		
P53 dependence (HCT116p53-/-)	20.5	2.3	6.6	1.0	1.1	0.7
Induction of apoptosis (A2780)	Population distribution: Viable > Late apoptotic > Non-viable > Early apoptotic			Population distribution: Viable > Late apoptotic. Non-viable and early apoptotic populations negligible		
Induction of caspase 3 (A2780)	Higher caspase 3 activation than iodido analogues			Caspase 3 activation		
Inhibition of DNA polymerase α Co-incubation with Aphidicolin	71 ± 2	12.5 ± 0.5	1.02 ± 0.03	0.62 ± 0.08	0.60 ± 0.03	0.60 ± 0.04
Inhibition of Topoisomerase II Co-incubation with Etoposide	43 ± 1	16.8 ± 0.9	0.33 ± 0.02	14.1 ± 0.8	2.0 ± 0.1	0.89 ± 0.03
Inhibition of DNA gyrase Co-incubation with Novobiocin	28 ± 2	12.8 ± 0.8	1.7 ± 0.2	2.3 ± 0.3	0.60 ± 0.09	0.77 ± 0.06
Depletion of GSH Co-incubation with L-BSO	1.0 ± 0.3	1.63 ± 0.02	0.42 ± 0.06	1.05 ± 0.07	0.14 ± 0.01	0.08 ± 0.02
	Complexes targeted by GSH cellular detoxification			Complexes targeted by GSH cellular detoxification		
Depletion of thioredoxin reductase Co-incubation with Auranofin	11.5 ± 0.5	4.48 ± 0.09	0.30 ± 0.05	11.5 ± 0.5	0.16 ± 0.01	0.60 ± 0.09
	Complexes targeted by thioredoxin detoxification			Complexes targeted by thioredoxin detoxification		

Additional annotations:
- CDDP cross-resistance: "Shares resistance patterns with CDDP" (chlorido); "No resistance pattern in common with CDDP" (iodido)
- Oxaliplatin cross-resistance: "No resistance pattern in common with Oxaliplatin" (iodido)
- Selectivity: ⭐ "Better selectivity than CDDP (13.5)"
- P53 dependence: "Activity depends on p53 activation" (chlorido); "Mechanism does not involve p53 activation" (iodido)

Table 5.6. Summary of Chapter 5. ⭐ Better than CDDP. Changes in potency: ⬆ improves, ⬇ decreases and ▬ unchanged. ⬤ Nanomolar activity.

5.6 References

1. A. M. Krause-Heuer, R. Grünert, S. Kühne, M. Buczkowska, N. J. Wheate, D. D. Le Pevelen, L. R. Boag, D. M. Fisher, J. Kasparkova, J. Malina, P. J. Bednarski, V. Brabec, and J. R. Aldrich-Wright, *J. Med. Chem.*, 2009, **52**, 5474-5784.

2. M. Jones, J. Siracky, L. R. Kelland, and K. R. Harrap, *Br. J. Cancer*, 1993, **67**, 24-29.

3. M. D. Hall, M. Okabe, D. W. Shen, X. Liang, and M. M. Gottesman, *Annu. Rev. Pharmacol. Toxicol.*, 2008, **48**, 495-535.

4. W. Qian, M. Nishikawa, A. M. Haque, M. Hirose, M. Mashimo, E. Sato, and M. Inoue, *Am. J. Physiol.Cell Ph.*, 2005, **289**, C1466-1475.

5. J. Reedijk, *Eur. J. Inorg. Chem.*, 2009, 1303-1312.

6. V. Cepeda, M. Fuertes, J. Castilla, C. Alonso, C. Quevedo, and J. M. Pérez, *Anti. Canc. Agents Med. Chem.*, 2007, **7**, 3-18.

7. C. Rabik and M. E. Dolan, *Cancer Treat. Rev.*, 2007, **33**, 9-23.

8. A. Bergamo and G. Sava, *Dalton Trans.*, 2007, 1267-1272.

9. L. Kelland, *Nat. Rev. Cancer*, 2007, **7**, 573-584.

10. A. Peacock and P. J. Sadler, *Chem-Asian J.*, 2008, **3**, 1890-1899.

11. M. Melchart and P. J. Sadler, in *Bioorganometallics: Biomolecules, Labeling, Medicine*, ed. G. Jaouen, Wiley, 2006, pp. 39-64.

12. M. G. Mendoza-Ferri, C. G. Hartinger, M. A. Mendoza, A. E. Egger, R. E. Eichinger, J. B. Mangrum, P. Nicholas, M. Maruszak, P. J. Bednarski, F.

Klein, M. A. Jakupec, A. A. Nazarov, K. Severin, and B. K. Keppler, *J. Med. Chem.*, 2010, **52**, 916-925.

13. M. J. Clarke, *Coord. Chem. Rev.*, 2002, **232**, 69-93.

14. I. Bratsos, S. Jedner, T. Gianferrara, and E. Alessio, *Chimia*, 2007, **61**, 692-697.

15. E. S. Antonarakis and A. Emadi, *Cancer Chemoth. Pharm.*, 2010, **66**, 1-9.

16. S. J. Dougan, University of Edinburgh, 2007.

17. I. Nicoletti, G. Migliorati, M. C. Pagliacci, F. Grignani, and C. Riccardi, *J. Immunol. Methods*, 1991, **139**, 271-279.

18. P. Skehan, R. Storeng, D. Scudiero, A. Monks, J. McMahon, D. Vistica, J. T. Warren, H. Bokesch, S. Kenney, and M. R. Boyd, *J. Natl. Cancer Inst.*, 1990, **82**, 1107-1112.

19. V. Vichai and K. Kirtikara, *Nat. Protoc.*, 2006, **1**, 1112-1116.

20. P. J. Quinn, *Plasma membrane phospholipid asymmetry*, Kluwer Academic, New York, 2002.

21. V. Gurtu, S. R. Kain, and G. Zhang, *Anal. Biochem.*, 1997, **102**, 98-102.

22. T. Tanaka, H. Kurokawa, K. Matsuno, S. Matsumoto, and Y. Hayashida, *Anti-Cancer Res.*, 2008, **28**, 2663-2668.

23. D. Teis and L. Huber, *Cell. Mol. Life Sci.*, 2003, **60**, 2020-2033.

24. P. Kovacic, *Medical Hypoth.*, 2007, **69**, 510-516.

25. U. Jungwirth, C. R. Kowol, B. K. Keppler, C. G. Hartinger, W. Berger, and P. Heffeter, *Antioxid. Redox Signaling*, 2011, **15**, 1085-1127.

26. G. T. Wondrak, *Antioxid. Redox Signaling*, 2009, **11**, 3013-3069.

27. G. Manda, M. T. Nechifor, and T. M. Neagu, *Curr. Chem. Bio.*, 2009, **3**, 342-366.

28. S. J. Dougan, A. Habtemariam, S. E. McHale, S. Parsons, and P. J. Sadler, *Proc. Natl. Acad. Sci. USA.*, 2008, **105**, 11628-11633.

29. G. Chu, *J. Biol. Chem.*, 1994, **269**, 787-790.

30. M. Kartalou and J. M. Essigmann, *Mutat. Res.*, 2001, **478**, 23-43.

31. S. Faivre, *Biochem. Pharmacol.*, 2003, **66**, 225-237.

32. T. Helleday, E. Petermann, C. Lundin, B. Hodgson, and R. Sharma, *Nat. Rev. Cancer*, 2008, **8**, 193-204.

33. E. van Niekerk, J. F. O'Sullivan, G. K. Jooné, and C. E. van Rensburg, *Invest. New Drugs*, 2001, **19**, 211-217.

34. C. Ngamkitidechakul, K. Jaijoy, P. Hansakul, N. Soonthornchareonnon, and S. Sireeratawong, *Phytother. Res.*, 2010, **24**, 1405-1413.

35. R. Tundis, B. Deguin, M. R. Loizzo, M. Bonesi, G. Statti, F. Tillequin, and F. Menichini, *Bioorg. Med. Chem. Lett.*, 2005, **15**, 4757-4760.

36. P. Sharma, T. Farrell, M. S. Patterson, G. Singh, J. R. Wright, R. Sur, and A. J. Rainbow, *Photochem. Photobiol.*, 2009, **85**, 99-106.

37. Y. Fu, University of Warwick, 2011.

38. C. Puckett, California Institute of Technology, 2007.

39. S. Schütze, V. Tchikov, and W. Schneider-Brachert, *Nat. Rev. Mol. Cell Biol.*, 2008, **9**, 655-662.

40.   K. H. Tan and W. Hunziker, *Exp. Cell Res.*, 2003, **284**, 281-288.

41.   D. Morgan, *The Cell Cycle: Principles of Control*, Oxford University Press, London, 2007.

42.   A. Murray and T. Hunt, *The Cell Cycle: An Indroduction*, Freeman, New York, NY, 1993.

43.   M. Malumbres and M. Barbacid, *Nat. Rev. Cancer*, 2009, **9**, 153-166.

44.   K. K. Dijkstra, C. Blanchetot, and J. Boonstra, *Evasion of G1 Checkpoints in Cancer*, 2010.

45.   C. Tan, S. Wu, S. Lai, M. Wang, Y. Chen, L. Zhou, Y. Zhu, W. Lian, W. Peng, L. Ji, and A. Xu, *Dalton Trans.*, 2011, **40**, 8611-8621.

46.   H. Zheng, W. Hu, D. Yu, D. Y. Shen, S. Fu, J. J. Kavanagh, C. Wei, and D. J. Yang, *Pharm. Res.*, 2008, **25**, 2272-2282.

47.   S. Wang and W. S. El Deiry, *P53, Cell cycle arrest and apoptosis*, Springer, Dordrecht, 2007.

48.   E. S. Stavridi, Y. Huyen, E. A. Sheston, and T. D. Halazonetis, in *The p53 tumor suppresor pathway and cancer*, ed. Zambeti, Springer, 2005, pp. 25-52.

49.   L. Bai and W. Zhu, *J.Cancer Mol.*, 2006, **2**, 141-153.

50.   U. M. Moll and N. Concin, *p53 in human cancer – Somatic and inherited mechanisms*, Springer Science, New York, 2005.

51.   S. M. Post, A. Quintás-Cardama, and G. Lozano, *Regulation of p53 activity and associated checkpoint controls*, Springer Science, New York, 2010.

52. C. Gaiddon, P. Jeannequin, P. Bischoff, M. Pfeffer, C. Sirlin, and J. P. Loeffler, *Pharmacology*, 2005, **315**, 1403-1411.

53. S. Chatterjee, S. Kundu, A. Bhattacharyya, C. G. Hartinger, and P. J. Dyson, *J. Biol. Inorg. Chem.*, 2008, **13**, 1149-1155.

54. R. L. Hayward, Q. C. Schornagel, R. Tente, J. S. Macpherson, R. E. Aird, S. Guichard, A. Habtemariam, P. J. Sadler, and D. I. Jodrell, *Cancer Chemoth. Pharm.*, 2005, **55**, 577-583.

55. V. Fadok, de Cathelineau Aimee, D. L. Daleke, P. M. Henson, and D. L. Bratton, *J. Biol. Chem.*, 2001, **276**, 1071-1077.

56. K. Kuribayashi and W. S. El Deiry, *Adv. Exp. Med. Biol.*, 2008, **615**, 201-221.

57. G. S. Salvesen and S. J. Riedl, *Adv. Exp. Med. Biol.*, 2008, **615**, 13-23.

58. T. J. Fan, L. H. Han, R. S. Cong, and J. Liang, *Acta Bioch. Bioph.*, 2005, **37**, 719-727.

59. P. Villa, S. H. Kaufmann, and W. C. Earnshaw, *Trends Biochem. Sci.*, 1997, 388-393.

60. A. Stepczynska, K. Lauber, I. H. Engels, O. Janssen, D. Kabelitz, S. Wesselborg, and K. Schulze-Osthoff, *Oncogene*, 2001, **20**, 1193-1202.

61. J. Manns, M. Daubrawa, S. Driessen, F. Paasch, N. Hoffmann, A. Löffler, K. Lauber, A. Dieterle, S. Alers, T. Iftner, K. Schulze-Osthoff, B. Stork, and S. Wesselborg, *FASEB J.*, 2011, **25**, 3250-3261.

62. T. Chen, Y. Liu, W. J. Zheng, J. Liu, and Y. S. Wong, *Inorg. Chem.*, 2010, **49**, 6366-6368.

63. K. Hara, E. Kasahara, N. Takahashi, M. Konishi, J. Inoue, M. Jikumaru, S. Kubo, H. Okamura, E. Sato, and M. Inoue, *J. Pharmacol. Exp. Ther.*, 2011, **337**, 838-845.

64. R. Gaur and L. Mishra, *Inorg. Chem.*, 2012, **51**, 3059-3070.

65. C. Sessa, M. Zucchetti, E. Davoli, R. Califano, F. Cavalli, S. Frustaci, L. Gumbrell, A. Sulkes, B. Winograd, and M. D'Incalci, *J. Natl. Cancer Inst.*, 1991, **83**, 1160-1164.

66. P. J. O'Dwyer, J. D. Moyer, M. Suffness, S. D. Harrison, R. Cysyk, T. C. Hamilton, and J. Plowman, *Cancer Res.*, 1994, 724-729.

67. H. Masuda, R. F. Ozols, G. Lai, A. Fojo, M. Rothenberg, and T. C. Hamilton, *Cancer Res.*, 1988, 5713-5716.

68. P. J. Smith, N. J. Blunt, R. Desnoyers, Y. Giles, and L. H. Patterson, *Cancer Chemoth. Pharm.*, 1997, **39**, 455-461.

69. H. Masuda, T. Tanaka, and H. Matsuda, *Cancer Res.*, 1990, **50**, 1863-1866.

70. H. Timmer-Bosscha, N. H. Mulder, and E. G. de Vries, *Br. J. Cancer*, 1992, **66**, 227-238.

71. C. Jaxel, G. Taudou, C. Portemer, G. Mirambeau, J. Panijel, and M. Duguet, *Biochemistry*, 1988, **27**, 95-99.

72. S. N. Powell and R. S. Bindra, *DNA Repair*, 2009, **8**, 1153-1165.

73. F. Beckford, J. Thessing, J. Woods, J. Didion, N. Gerasimchuk, A. Gonzalez-Sarrias, and N. P. Seeram, *Metallomics*, 2011, **3**, 491-502.

74. F. Beckford, D. Dourth, M. Shaloski, J. Didion, J. Thessing, J. Woods, V. Crowell, N. Gerasimchuk, A. Gonzalez-Sarrías, and N. P. Seeram, *J. Inorg. Biochem.*, 2011, **105**, 1019-1029.

75. H. Chao and L. Ji, *Helv. Chim. Acta*, 2008, **5**, 1962-1979.

76. A. O. Oliyide, X. Ji, P. Stapleton, A. Osbourn, Y. Pan, D. J. Bowles, B. G. Davis, and M. Yang, *Chem. Commun.* , 2011, **47**, 10569-10571.

77. M. Gellert, I. Tateo, M. O'Dea, and J. Tomizawa, *Proc. Natl. Acad. Sci. USA.*, 1976, **73**, 4474-4478.

78. J. P. Eder, C. A. Wheeler, B. A. Teicher, and L. E. Schnipper, *Cancer Res.*, 1991, **51**, 510-513.

79. J. P. Eder, B. A. Teicher, S. A. Holden, K. N. S. Cathcart, and L. E. Schnipper, *J. Clin. Invest.*, 1987, **79**, 1524-1528.

80. J. Nordenberg, D. Albukrek, T. Hadar, A. Fux, L. Wasserman, A. Novogrodsky, and Y. Sidi, *Br. J. Cancer*, 1992, **65**, 183-188.

81. M. L. Webb and S. T. Jacob, *J. Biol. Chem.*, 1988, **263**, 4745-4748.

82. C. P. Anderson and C. P. Reynolds, *Bone Marrow Transplant.*, 2002, **30**, 135-140.

83. H. H. W. Chen and M. T. Kuo, *Met Based Drugs*, 2010, **2010**, pii:430939.

84. D. Trachootham, W. Zhang, and P. Huang, *Oxidative stress and drug resistance in cancer*, Springer US, New York, NY, 2009.

85. S. D. Shnyder, Y. Fu, A. Habtemariam, S. H. V. Rijt, P. Cooper, P. M. Loadman, and P. J. Sadler, *MedChemComm*, 2011, **2**, 666-668.

86. G. Marverti, M. Cusumano, A. Ligabue, M. L. Di Pietro, P. A. Vainiglia, A. Ferrari, M. Bergomi, M. S. Moruzzi, and C. Frassineti, *J. Inorg. Biochem.*, 2008, **102**, 699-712.

87.   G. Marverti, A. Ligabue, M. Montanari, D. Guerrieri, M. Cusumano, M. L. Di Pietro, L. Troiano, E. Di Vono, S. Iotti, G. Farruggia, F. Wolf, M. G. Monti, and C. Frassineti, *Invest. New Drugs*, 2011, **29**, 73-86.

88.   J. E. Liebmann, S. M. Hahn, J. A. Cook, C. Lipschultz, J. B. Mitchell, and D. C. Kaufman, *Cancer Res.*, 1993, **53**, 2066-2070.

Chapter 6

Half-sandwich ruthenium tetrahydroquinoline complexes. Investigations into their use in combination therapy

6.1. Introduction

Multi-component therapy, also known as combination therapy, has emerged as an alternative in cancer chemotherapeutics as it allows dose-reduction and subsequent minimisation of adverse side-effects while avoiding the development of resistance.[1,2] Some examples of conventional combination therapy for cancer include the use of daunorubicin co-administered with ara-C for the treatment of acute nonlymphocytic leukaemia, aphidicolin glycinate and cisplatin in the treatment of melanomas[3] and paclitaxel combined with carboplatin[4] or gemcitabine with etoposide[5] for ovarian and NSCL cancer.

The start of combination therapy required intense empirical testing. However, several attempts have been made to understand the interaction of two or more drugs when they are co-administered.[6] The most-accepted theory is based on the additivity model designed by Loewe,[7] for which Chou and Talalay developed the median effect equations.[8–10] It indicates that two agents can interact in three different ways. 1) synergistically, 2) additively or 3) antagonistically. Synergistic interaction refers to the situation when the modulating effect of the combination of both drugs is greater than the addition of their single actions,[11] in comparison, in an antagonist interaction the modulating result is lower.[1,12] Carefully designed experiments allow the determination of the combination index, CI as an indication of synergy, it is also possible to determine the dose reduction index, DRI. Together the CI and DRI values are the two most important indicators of a successful combination of drugs.[8–10] Further mathematical analysis on the Chou and Talalay method can be used to determine the confidence intervals on the CI

value.[13] Important progress has been made in the development of methods to assess synergy, from experimental design to data manipulation.[6,7,14–16] However, the more widely used method is still the Chou and Talalay approach. In the present Chapter this method has been used to explore the potential of inactive Ru(II) piano-stool complexes to reduce the dose of clinically used Pt-based chemotherapeutics to stop cellular proliferation in ovarian cancer cells.

The inactive complexes used in this Chapter include in their structure tetrahydroquinolines as *N,N*-chelationg ligands. Quinolines and their hydrogenated derivatives are known for their wide pharmacological applications. They are active as antimalarials,[17] anticancer agents,[18–21] modulators of androgen receptors,[22,23] HIV-1 integrase inhibitors,[24] amongst others.[25,26] Therefore, it was expected that their use as *N,N*-chelating ligands for Ru(II) piano-stool complexes might render active compounds. However this was not the case for complexes **41-43**.

6.2 Experimental section

6.2.1 Materials

Ruthenium arene dimers used in this Chapter include [(η^6-*p*-cymene)RuCl$_2$]$_2$, reported in Chapter 2. 2-Pyridine carboxaldehyde (99%), 4-aminophenol (98%) and dicyclopentadiene were purchased from Sigma-Aldrich. 4-Aminobenzoic acid (≥99.0%) and ammonium hexafluorophosphate (≥98.0%) were obtained from Fluka. All deuterated solvents (D$_2$O, MeOD, DMSO-*d$_6$*, acetone-*d$_6$*, CDCl$_3$) were

obtained from Cambridge Isotope Laboratories. For the biological assays: cisplatin (**CDDP**), carboplatin and oxaliplatin (**OXA**) were obtained from Sigma Aldrich.

6.2.2 Preparation of ligands and complexes

The synthetic procedure 1, described below was used to generate all the tetrahydroquinolines used as ligands in this Chapter and listed in Table 6.1 on page 288.

Synthetic Procedure 1.
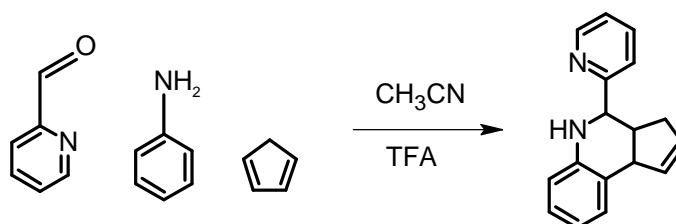
Scheme 4.1. Synthesis of 4-(pyridin-2-yl)-3a,4,5,9b-tetrahydro-3*H*-cyclopenta [*c*]quinoline **[Thq, 38].**

4-(pyridin-2-yl)-3a,4,5,9b- tetrahydro-3*H*- cyclopenta[*c*] quinoline [38]. Pyridine -2-carbaldehyde (100 mg, 102 µL, 0.93 mmol) was dissolved in acetonitrile (15 mL) at ambient temperature with stirring. Then 1 mol. equiv. of aniline was added (102 mg, 100 µL, 0.97 mmol). The reaction mixture was left to stand with stirring for 30 min. Then a few drops of TFA were added to the reaction, after 5 of stirring, freshly distilled cyclopentadiene (88 µL, 70.8 mg, 0.97

mmol) was added and the reaction mixture left under stirring for 10 h. The solvent was removed by rotary evaporation. A pale yellow solid was obtained, which was washed with ether (Yield 58%). Elemental analysis calc. for $C_{17}H_{16}N_2$, C: 88.22%; H: 6.49%; N: 11.28%. Found: C: 82.25%; H: 6.45%; N: 11.30%. NMR-δ_H (500 MHz; CDCl$_3$) 1.88 (1H, qt, J = 25.2, 16.4, 8.4, 4.3, 2.1 Hz) 2.45 (1H, qq, J = 25.2, 19.0, 7.3, 4.9, 2.4 Hz) 3.36 (1H, qd, J = 19.2, 9.0, 3.2 Hz) 4.18 (1H, d, J = 9.0 Hz) 4.74 (1H, d, J = 3.4 Hz) 5.62 (1H, m) 5.83 (1H, m) 6.71 (1H, dd, J = 7.8, 1.7 Hz) 6.75 (1H, td, J = 14.9, 7.4, 1.4 Hz) 7.00 (1H, td, J = 14.6, 7.1, 1.1 Hz) 7.07 (1H, d, J = 7.7 Hz) 7.21 (1H, q, J = 12.0, 4.6, 7.2 Hz) 7.46 (1H, dd, J = 7.7, 0.9 Hz) 7.72 (1H, td, J = 15.5, 7.6, 1.8 Hz) 8.61 (1H, d, J = 4.7 Hz). m/z (ESI) found 249.1 (calc. M + H$^+$. $C_{17}H_{17}N_2$ = 249.32), 271.1 (calc. M + Na$^+$, $C_{17}H_{16}N_2Na$ = 271.33).

4-(pyridin-2-yl)-3a,4,5,9b-tetrahydro-3*H*-cyclopenta[*c*]quinolin-8-ol [Thq-OH, 39] As synthetic procedure 1, using 2-pyridine carbaldehyde (100 mg, 102 μL, 0.93 mmol) 4-hydroxyaniline (106 mg, 0.93 mmol), cyclopentadiene (65 mg, 93 μL, 0.97 mmol). Yield 61%. Elemental analysis calc. for $C_{17}H_{16}N_2O$, C: 72.25%; H: 6.10%; N: 10.60%. Found: C: 77.30%; H: 6.12%; N: 10.63%. NMR-δ_H (500 MHz; CDCl$_3$) 1.75 (1H, m) 2.41 (1H, m) 3.24 (1H, qt, J = 27.5, 18.3, 9.3, 3.7 Hz) 4.11 (1H, d, J = 8.8 Hz) 4.83 (1H, d, J = 3.2 Hz) 5.63 (1H, m) 5.85 (1H, m) 6.66 (1H, d, J = 2.4 Hz) 6.92 (1H, d, J = 8.5 Hz) 7.49 (1H, t, J = 12.4, 6.2 Hz) 7.66 (1H, d, J = 7.9 Hz) 8.01 (1H, td, J = 15.3, 7.6, 1.7 Hz) 8.66 (1H, d, J = 4.8 Hz) 7. m/z (ESI) found 265.1 (calc. M + H$^+$. $C_{17}H_{17}N_2O$ = 265.32).

(4-(pyridin-2-yl)-3a,4,5,9b-tetrahydro-3*H*-cyclopenta[*c*]quinoline-8-

carboxylic acid [Thq-COOH, 40] As synthetic procedure 1, using pyridine-2-

carbaldehyde (100 mg, 102 μL, 0.93 mmol) 4-hydroxybenzoic acid (133 mg,

0.93 mmol), cyclopentadiene (65 mg, 93 μL, 0.97 mmol). Yield 54%. Elemental

analysis calc. for $C_{18}H_{16}N_2O_2$, C: 73.95%; H: 5.52%; N: 9.58%. Found: C:

73.90%; H: 5.59%; N: 9.51%. NMR-δ_H (500 MHz; CDCl$_3$) 1.66 (1H, m) 2.29

(1H, m) 3.19 (1H, qt, J = 27.0, 18.0, 9.1, 3.9 Hz) 4.12 (1H, d, J = 8.9 Hz) 4.80

(1H, d, J = 3.6 Hz) 5.58 (1H, d, J = 5.0 Hz) 5.93 (1H, m) 6.82 (1H, d, J = 8.4 Hz)

7.53 (2H, m) 7.62 (1H, m) 7.72 (1H, m) 8.06 (1H, m) 8.67 (1H, d, J = 5.2 Hz).

m/z (ESI) found 293.1 (calc. M + H$^+$. $C_{18}H_{17}N_2O_2$ = 293.31), 315.1 (calc. M +

Na$^+$, C $C_{18}H_{16}N_2O_2Na$ = 315.33).

Synthetic procedure 2 below was used to synthesise all the ruthenium complexes

described in this Chapter and listed in Table 6.2 on page 280.

Synthetic procedure 2.
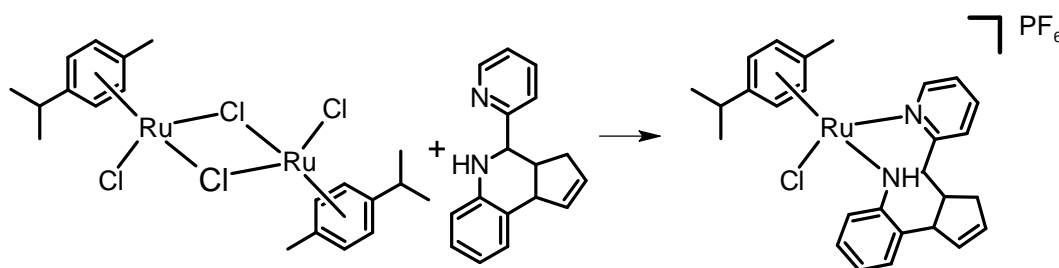
Scheme 4.2. Synthesis of the ruthenium complex [Ru(η^6-*p*-cym)(Thq)Cl]PF$_6$, **[41].**

[Ru(η^6-*p*-cym)(Thq)Cl]PF$_6$ [41]. Ruthenium dimer [Ru (η^6-*p*-cymene) Cl$_2$]$_2$ (100 mg, 0.16 mmol) was dissolved in methanol (5 mL) in a round bottom flask, then two mol. equiv. of the appropriate ligand was added, in this case, Thq (81 mg, 0.32 mmol). The reaction mixture was left at ambient temperature with constant stirring for 5 h. After this time 5 equivalents of NH$_4$PF$_6$ were added to the mixture, and left stirring for a further hour. A solid residue was collected by filtration and recrystallised. (Yield 76%). Elemental analysis calc. for C$_{27}$H$_{30}$N$_2$ClF$_6$PRu, C: 48.84%, H: 4.55%, N: 4.22%. Found: C: 48.80%, H: 4.50%; N: 4.26%. NMR -δ_H (500 MHz; DMSO-d$_6$) 0.95 (3H, d, J = 7.0 Hz) 1.20 (3H, d, J = 6.8 Hz) 2.27 (3H, s) 2.39 (1H, dd, J = 16.4, 6.2 Hz) 2.60 (1H, m) 2.76 (1H, q, J = 27.2, 20.4, 13.6, 6.6 Hz) 4.16 (1H, d, J = 5.1 Hz) 4.32 (1H, d, J = 9.2 Hz) 6.01 (1H, d, J = 4.1 Hz) 6.17 (3H, m) 6.20 (1H, d, J = 5.8 Hz) 6.22 (1H, d, 4.1 Hz) 6.75 (1H, d, J = 4.5 Hz) 7.50 (3H, m) 7.63 (1H, dd, J = 7.1, 1.71 Hz) 7.79 (2H, m) 8.25 (1H, td, J = 15.4, 7.8, 1.3 Hz) 9.40 (1H, dd, J = 6.4, 1.4 Hz). m/z (ESI) found 483.1 (calc. M$^+$ C$_{27}$H$_{30}$N$_2$Ru = 483.61).

[Ru(η^6-*p*-cym)(Thq-OH)Cl]PF$_6$ [42]. As synthetic procedure 2, using [Ru(η^6-*p*-cym)Cl$_2$]$_2$ (100 mg, 0.16 mmol) and Thq-OH (87 mg, 0.32 mmol). Yield 57%. Elemental analysis calc. for C$_{27}$H$_{29}$N$_2$ClF$_6$OPRu. C: 47.76%, H: 4.30%, N: 4.13%. Found: C: 47.69%, H: 4.24%; N: 4.08%. 0.92 (3H, d, J = 7.2 Hz) 1.10 (3H, d, J = 7.2 Hz) 2.24 (3H, s) 1.92 (1H, dd, J = 15.1, 5.8 Hz) 2.72 (1H, m) 2.66 (1H, q, J = 27.2, 20.4, 13.6, 5.8 Hz) 4.37 (1H, d, J = 4.9 Hz) 4.52 (1H, d, J = 8.1 Hz) 5.98 (1H, d, J = 5.8 Hz) 6.25 (3H, m) 6.27 (1H, d, J = 5.8 Hz) 6.32 (1H, d, 5.6 Hz) 6.70 (1H, d, J = 5.7 Hz) 7.50 (3H, m) 7.71 (1H, t, J = 12.3, 5.8 Hz) 7.84 (2H, m) 8.12

(1H, td, J = 15.1, 7.4, 1.5 Hz) 9.10 (1H, dd, J = 5.8, 1.2 Hz). m/z (ESI) found 498.5 (calc. M^+ $C_{27}H_{29}N_2ORu$ = 498.60).

[Ru(η^6-*p*-cym)(Thq-COOH)Cl]PF$_6$ [43]. As synthetic procedure 2, using [Ru(η^6-*p*-cym)I$_2$]$_2$ (100 mg, 0.16 mmol) and Thq-COOH   (96 mg, 0.32 mmol). Yield 51%. Elemental analysis calc. for $C_{28}H_{29}N_2ClF_6O_2PRu$ C: 46.71%, H: 4.06%, N: 3.89%. Found: C: 46.5%, H: 4.02%; N: 3.98%. NMR-δ_H (500 MHz; DMSO-d$_6$) 1.01 (6H, d, J = 2.8) 1.72 (1H, m) 2.22 (1H, m) 2.54 (3H, s) 2.62 (1H, m) 3.36 (1H, qt, J = 25.0, 19.1, 9.5, 4.2 Hz) 4.16 (1H, d, J = 9.2 Hz) 4.76 (1H, d, J = 4.2 Hz) 5.45 (1H, d, J = 4.8 Hz) 5.12 (2H, d, J = 6.2 Hz) 5.88 (1H, d, J = 6.1 Hz) 5.94 (1H, m) 6.54 (1H, d, J = 6.3 Hz) 6.95 (1H, d, J = 7.9 Hz) 7.48 (2H, m) 7.85 (1H, m) 7.92 (1H, m) 8.16 (1H, m) 9.05 (1H, d, J = 4.9 Hz). m/z (ESI) found 575.0 (calc. M^+ $C_{28}H_{29}N_2ClO_2Ru$ = 574.98).

6.2.3 Methods

6.2.3.1 Aquation studies

Aquation of complexes **41-43** was studied by proton NMR as described in Chapter 2, using 1 mM fresh solutions of each complex in D$_2$O at 310 K. To suppress the aquation observed in all complexes 150 mM NaCl was added to the deuterated solvent.

6.2.3.2 Nucleobase binding

Complexes **41-43** were reacted with to 9-ethylguanine, as a nucleobase model, the extent of binding after 24 h was followed by ^{1}H-NMR. The details of these experiments can be found in Chapter 2. Briefly, a fresh 1 mM solution of each complex was prepared in 50 mM sodium phosphate buffer (pH 7.5) with 5% DMSO. The solution also contained 9-ethylguanine for a final mol. ratio 1:1.25 where the nucleobase was in excess. As in the case of aquation studies, ^{1}H-NMR spectra were recorded at 298 K within the first 10 min after sample preparation and again after 24 h at 500 MHz. All experiments were carried out in triplicate and the standard deviations calculated. The formation of adducts was monitored by the formation of a second set of peaks that included bound-9-EtG.

6.2.3.3 Antiproliferative activity

The antiproliferative activity of ligands **38-40** and complexes **41-43** were determined in A2780 ovarian, A549 lung, HCT116 colon and MCF7 breast carcinoma cell lines. The experiments to determine IC_{50} values were carried out as described previously in Chapter 2. Briefly, 96 well plates were used to seed 5000 cells per well, they were left to pre-incubate in drug-free media at 310 K for 48 h before adding different concentration of the compounds to be tested. Stock solutions of ligands and complexes were prepared by dissolving the solids in DMSO to then be diluted with a mixture 50:50 PBS : saline. A drug exposure period of 24 h was allowed, after this, supernatants were removed by suction and

each well was washed with PBS (100 μL). Further 48 h were allowed for the cells to recover in drug-free media (200 μL per well) at 310 K. SRB assay was used to determine cell viability. IC_{50} values, as the concentration which caused 50% of inhibition of cell growth, were determined as duplicate of triplicates in two independent set of experiments, their standard deviations were calculated.

6.2.3.4 Metal accumulation in cancer cells

Metal accumulation studies for complexes **41-43** were conducted on A2780 ovarian carcinoma cell line. Briefly, 4 per 10^6 cells were seeded on a Petri dish, after 24 h of pre-incubation time in drug-free medium. The test complexes were added to give final concentrations equal to $IC_{50}/3$ and allowed further 24 h of drug exposure. After this time, cells were counted, treated with trypsin and cell pellets were collected. Each pellet was digested overnight in concentrated nitric acid (73%) at 353 K; the resulting solutions were diluted (HNO_3 5%) and the amount of ruthenium taken up by the cells was determined by ICP-MS. These experiments did not allow any cell recovery time in drug-free media. They were all carried out in triplicate and the standard deviations were calculated. Results are compared to the corresponding data for **CDDP**. More experimental details can be found in Chapter 2.

6.2.3.5 Combination therapy

- **Experiments with a fixed concentration of cisplatin.**

IC_{50} modulation experiments for complexes **41-43** by co-administration of Pt-chemotherapeutics were performed using the protocol previously described for IC_{50} determination (see 6.2.3.3 Antiproliferative Activity) with the following modifications. Briefly, a 96-well plate was seeded with 5000 cancer cells per well (A2780, A549, HCT116 or MCF7). Cells were pre-incubated in drug-free medium for 48 h at 310 K, before adding the metal complexes together with the **CDDP** (0.2 µM). In order to prepare the stock solution of the drug, the solid complex was dissolved first in DMSO to be then diluted in a 50:50 mixture of PBS : saline. Separately, a stock solution of **CDDP** was prepared in saline. Both solutions were added to each well independently, but within 5 min of each other. After 24 of exposure, drugs were removed by suction, cells were washed with PBS (100 µL per well) and fresh medium was added to the plate (200 µL per well). Cells were allowed to recover in drug-free medium for 72 h at 310 K. At the end of this period, the SRB assay was used to determine cell viability. IC_{50} values, as the concentration which caused 50% of cell death, were determined as duplicates of triplicates in two independent set of experiments and their standard deviations were calculated.

Figure 6.1 shows an example of the plate used for these experiments. The set up includes two different negative controls; number 1 is untreated, while number 2 is treated with 0.2 µM of **CDDP**. These controls are in place to make sure that the

platinum dose is non-toxic. Their value was always within 5% difference to the negative control 1.
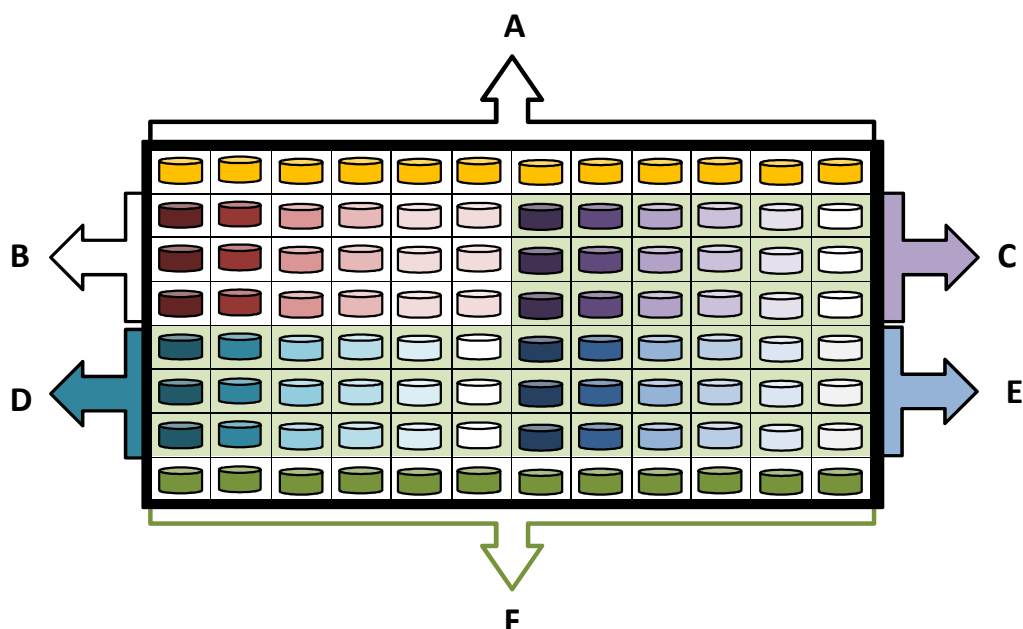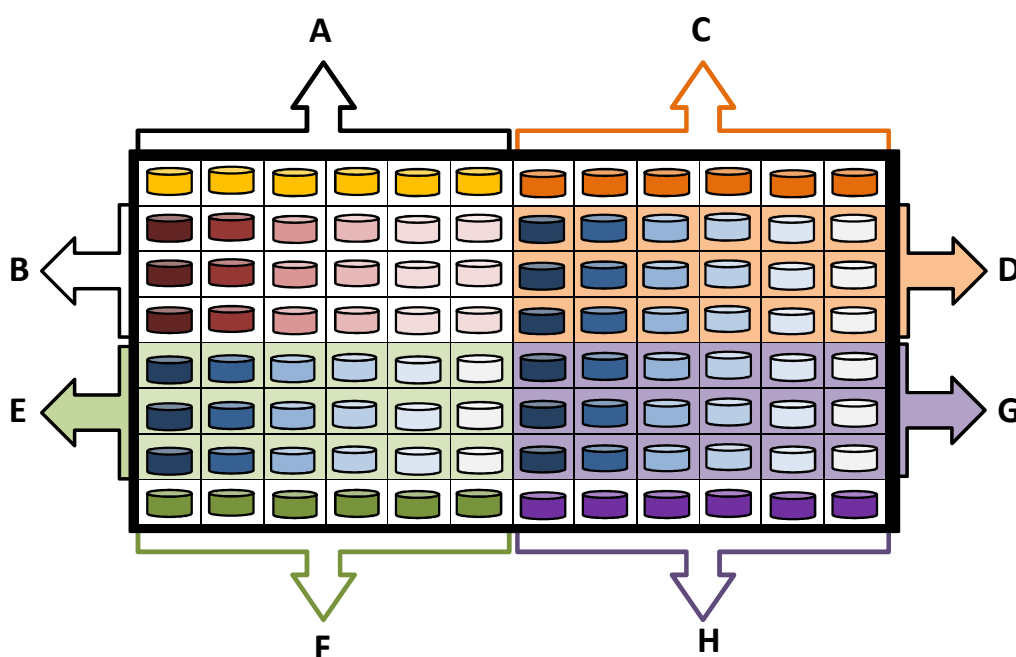

Figure 6.1. 96-well plate set up for experiments with fixed concentration of CDDP and Ru(II) complexes **41-43**. **(A)** Negative control 1: cells untreated, **(B)** Positive control, CDDP **(C)** Complex **41** with 0.2 µM of **CDDP**, **(D)** Complex **42** with 0.2 µM of **CDDP**, **(E)** Complex **43** with 0.2 µM of **CDDP** and **(F)** Negative control 2: cells treated with 0.2 µM of **CDDP**.

- **Experiments with complex 41 and a fixed concentration of cisplatin, oxaliplatin and carboplatin on A2780 cells.**

This experiment used the previously described protocol (see Experiments with fixed concentration of **CDDP**) modified as follows. A2780 cells were pre-incubated in drug-free medium for 48 h at 310 K, before adding complex **41** together with the appropriate co-incubating agent (**CDDP**, carboplatin or **OXA**,

all at 0.2 µM). The stock solution of the drug was prepared by dissolving the solid complex in DMSO to be then diluted in a 50:50 mixture of PBS : saline. Separately, a stock solution of the co-incubation agent was prepared in saline. Both solutions were added to each well independently, but within 5 min of each other.

Figure 6.2. 96-well plate set up for experiments with Ru(II) complex **41** and fixed concentration of the platinum chemotherapeutics. **(A)** Negative control 1: cells untreated, **(B)** Positive control, CDDP **(C)** Negative control 2: cells treated with 0.2 µM of carboplatin, **(D)** Various concentrations of complex 41 with 0.2 µM of carboplatin, **(E)** Negative control 3: cells treated with 0.2 µM of CDDP, **(F)** Various concentrations of complex 41 with 0.2 µM of CDDP, **(G)** Negative control 4: cells treated with 0.2 µM of OXA and **(H)** Various concentrations of complex 41 with 0.2 µM of OXA.

Figure 6.2 shows an example of the plate set up used for these experiments. The set up includes four different negative controls; number 1 is untreated, while numbers 2-4 are treated with 0.2 µM of **CDDP**, carboplatin and **OXA**, respectively. These controls are in place to make sure that the platinum dose is non-toxic. Their cell viability was always within 5% difference to the negative control 1. The figure shows how each ruthenium(II) complex was co-incubated separately with each of the platinum drugs. The plate was done in duplicate.

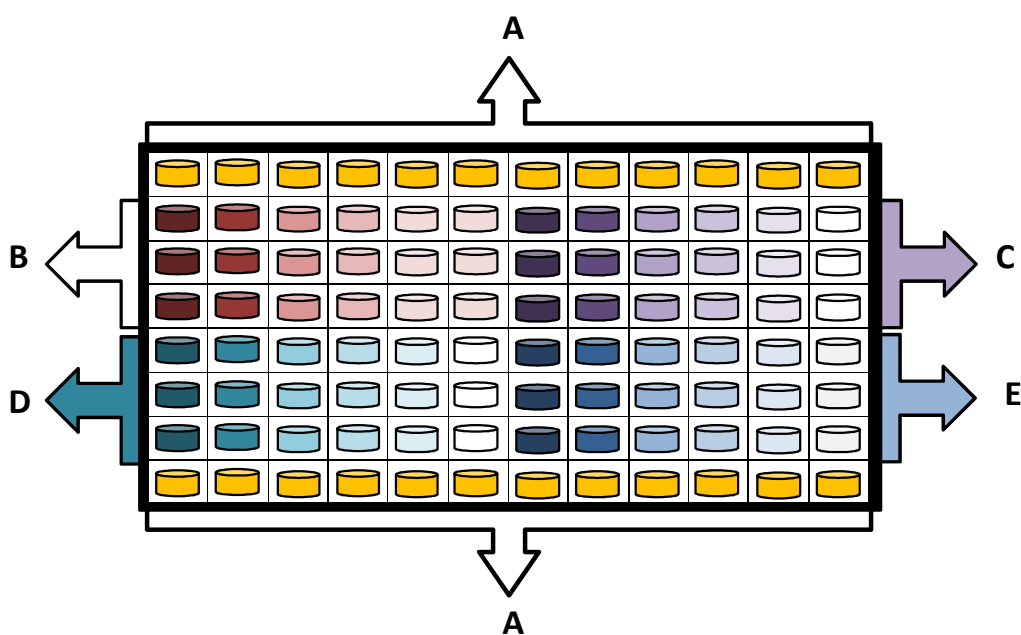- **Experiments according to the Chou and Talalay method.**

The Chou and Talalay approach to combination therapy requires the determination of the combination index, CI and the dose reduction index, DRI. This experimental design needs to include the co-administration of a fixed equipotent ratio of both drugs. The equipotent concentrations chosen for this set up were: 0, 0.25, 0.50, 0.75, 1, 2 and 4 x IC_{50} value as shown in Figure 6.3.

		Drug 1 (X IC_{50})						
		0	0.25	0.50	0.75	1.00	2.00	4.00
Drug 2 (X IC_{50})	0	■	■	■	■	■	■	■
	0.25	■	■					
	0.50	■		■				
	0.75	■			■			
	1.00	■				■		
	2.00	■					■	
	4.00	■						■

■ Equipotent combinations to be used

Figure 6.3. Fixed equipotent ratios of both drugs to be used, according to Chou and Talalay.

For this, the previous protocol (see experiments with fixed concentration of the platinum drug) was followed with a different plate setup. Figure 6.4 shows the plate setup used in the Chou and Talalay experiments.

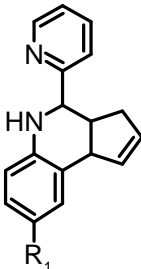**Figure 6.4.** 96-well plate set up for experiments using the Chou and Talalay method. **(A)** Negative control: cells untreated, **(B)** Positive control, CDDP **(C)** Various concentrations of complex **41** for median determination (0-4 x IC$_{50}$), **(D)** Various concentrations of **CDDP** for median determination (0-4 x IC$_{50}$) and **(E)** Complex **41** with **CDDP** at equipotent concentrations.

6.3 Results

6.3.1 Synthesis and characterization

Tetrahydroquinolines **38-40** shown in Table 6.1 below were synthesised and characterised using 1D and 2D, ^{1}H and ^{13}C-NMR 1D, 2D experiments, ESI-MS, and elemental analysis. Figure 6.5 shows the characteristic ^{1}H-NMR for the tetrahydroquinoline derivatives. Protons in the pyridine ring (a-d) are shown at higher chemical shifts (7.5-9 ppm), with the expected multiplicity pattern for a 1,2-disubstituted aromatic ring. Other aromatic protons from the quinolinyl system (k-m) are located between 6 and 7 ppm. Aliphatic protons e, f and j are shown at high field between 1-4 ppm. The structures described in Table 6.1 are consistent with the results from all the experimental techniques used to characterise the tetrahydroquinoline derivatives.

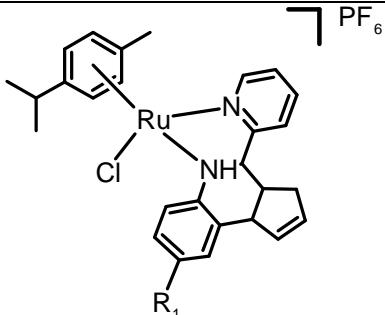**Table 6.1.** Tetrahydroquinoline derivarives studied in Chapter 6.

Basic Strucure	Ligands		R₁
	38	Thq	H
	39	Thq-OH	OH
	40	Thq-COOH	COOH
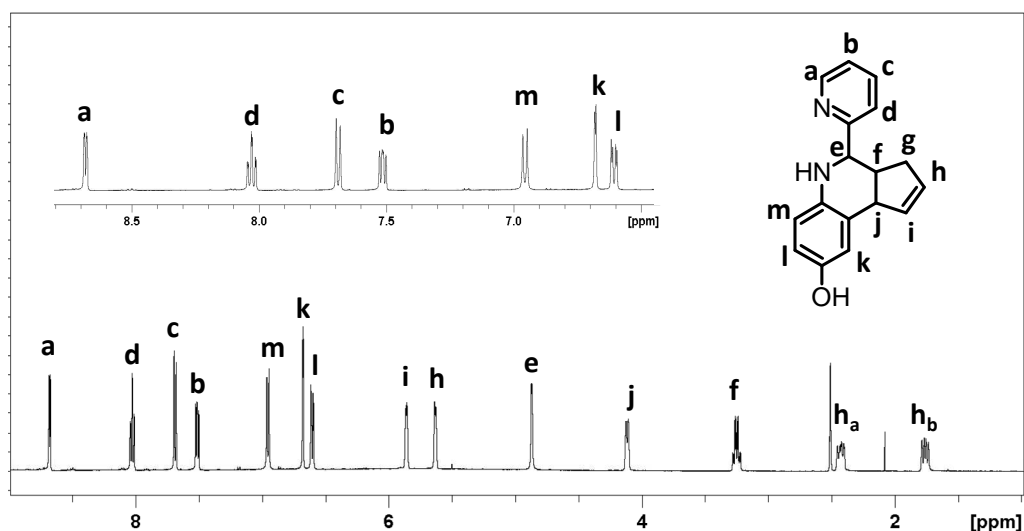
Figure 6.5. ^{1}H-NMR spectrum in dmso-d_6 of the tetrahydroquinoline derivative **39.**

Once the proposed ligands were fully characterised, complexes **41-43** in **Table 6.2** Table 6.2 below were synthesised. They were characterised using the same techniques as for the ligands, ^{1}H and ^{13}C-NMR (1D, 2D experiments), ESI-MS, and elemental analysis, as well as, ICP-MS for metal quantification. Although the structures proposed in Table 6.2 are consistent with all experimental data obtained, and the elemental analysis corresponds to cationic complexes with PF$_6$ as a counterion, further studies (eg. X-Rays) are needed to determine the structure of these complexes paying special attention to the presence of the hydrogen atom bound to the quinolinic nitrogen atom. The protonation/deprotonation of the carboxylic acid group in complex **43** would also give variations between a cationic and a neutral complex. The pK$_a$ of this acid group was not determined; however, it is expected that at biological relevant pH (7.2-7.4) the acid group would be deprotonated.

Table 6.2. Ruthenium (II) arene complexes studied in Chapter 6.

Basic Structure	Complex	Arene	Ligand	R_1	X
	41		Thq	H	Cl
	42	*p*-cym	Thq-OH	OH	Cl
	43		Thq-COOH	COOH	Cl

6.3.2 Aqueous solution chemistry

Aquation of complexes **41-43** was followed using ^{1}H -NMR using freshly prepared solutions of each complex in deuterated water. Each value represents the mean ± SD for three independent NMR experiments at 310 K. Results are shown in Table 6.3. Complex **41** does not undergo aquation while complexes **42** and **43** exhibit similar percentages of the aqua product formation (28 ± 3 and 23 ± 4 respectively).

Table 6.3. Extent of aquation and extent of 9-ethylguanine binding for complexes **41-43** after 24 h, using freshly prepared solutions of each complex in D_2O and a final ratio 1 : 1.25 for 9-EtG binding where the nucleobase was in excess.

	Compound	% aquation[a]	% 9-EtG binding[a]
41	[Ru(η^6-*p*-cym)(Thq)Cl]PF$_6$	0 ± 2	0 ± 4
42	[Ru(η^6-*p*-cym)(Thq-OH)Cl]PF$_6$	28 ± 3	12 ± 2
43	[Ru(η^6-*p*-cym)(Thq-COOH)Cl]PF$_6$	23 ± 4	25 ± 3

[a]Each value represents the mean ± SD for three independent NMR experiments at 310 K.

NMR was also used to follow the complexes binding to 9-ethylguanine (9-EtG) as a model for nucleobase interaction. Table 6.3 also includes the extent of nucleobase adduct formation after 24 h. The extent of guanine binding follows the order **41** < **42** < **43**. Complex **41** does not aquate nor binds to 9-EtG.

6.3.3 Antiproliferative activity

6.3.3.1 IC$_{50}$ determination in A2670, A549, HCT116

and MCF7 cells

Antiproliferative activity for ligands **38-40** and complexes **41-43** was determined using the SRB assay, this protocol is detailed in Chapter 2. For these experiments compounds with IC$_{50}$ values (concentration at which 50% of cell growth is inhibited) above 100 μM are inactive, while compounds with IC$_{50}$ values between 50 and 100 μM are moderately active. Values within the 15 - 50 μM range define a compound as active while below this range, compounds are considered highly active. All ligands and complexes tested were inactive against the chosen cell lines under the conditions described. Their IC$_{50}$ values are above 200 μM. All values reported in Table 6.4.

6.3.3.2 Metal accumulation in cancer cells

One time point, one concentration. Total cellular accumulation of ruthenium for complexes 41-43 was determined in A2780 ovarian cancer cell line in order to

relate amount of Ru accumulated to cytotoxicity. For these experiments drug exposure time was 24 h and cells were not allowed to recover. Values are expressed in ng of Ru per million cells and were determined as independent duplicates of triplicates. Results are shown in Table 6.5.

Table 6.4. Antiproliferative activity of ligands **38-40** and complexes **41-43** in A780, A549, HCT116 and MCF7 cell lines. IC_{50} is expressed as the concentration in which each ligand/complex causes 50% cancer cell growth inhibition.

		IC_{50} (μM)			
	Compound	**A2780**	**A549**	**HCT116**	**MCF7**
Ligands	**38**	>200	>200	>200	>200
	39	>200	>200	>200	>200
	40	>200	>200	>200	>200
Ru^{II} complexes	**41**	270 ± 3	>200	>200	>200
	42	>200	>200	>200	>200
	43	>200	>200	>200	>200

Table 6.5. Total accumulation of Ru in A2780 cells for complexes **41-43** after 24 h of drug exposure at 310 K with no recovery time, together with their IC_{50} values. Concentrations used were $IC_{50}/3$.

	Compound	**ng Ru x10^6 cells**	**IC_{50} (μM)**
41	[Ru(η^6-*p*-cym)(Thq)Cl]PF$_6$	2.3 ± 0.2	> 200
42	[Ru(η^6-*p*-cym)(Thq-OH)Cl]PF$_6$	2.5 ± 0.1	> 200
43	[Ru(η^6-*p*-cym)(Thq-COOH)Cl]PF$_6$	1.9 ± 0.4	> 200

6.3.4 Combination therapy studies.

Experiments with fixed concentration of cisplatin.

Complexes **41-43** were co-administered with **CDDP** to ovarian, lung, colon and breast cancer cell lines. All complexes were inactive when administered alone to

these cell lines. In contrast, their combination with a non-toxic concentration of the platinum chemotherapeutic caused drastic changes in cell viability.

Table **6.6** shows the IC_{50} values determined for the mixtures. The antiproliferative activity of complex **43** remains unchanged, while complexes **41** and **42** become active with potency increments in the range of 2 – 3 fold and IC_{50} values between 91 and 155 µM. The greatest improvement is achieved by complex **41** in ovarian cancer cells A2780, its IC_{50} value decreases from 270 ± 3 to 91 ± 2 µM.

Table 6.6. Antiproliferative activity of complexes **41-43** in A780, A549, HCT116 and MCF7 cell lines when co-administered with 0.2 µM of **CDDP**.

	IC_{50} (µM)			
	A2780	**A549**	**HCT116**	**MCF7**
41 + CDDP	91 ± 2	101 ± 3	142 ± 3	96 ± 2
42+ CDDP	109 ± 4	>200	119 ± 3	155 ± 1
43+ CDDP	>200	>200	>200	>200

- **Experiments with complex 41 and fixed concentration of cisplatin, oxaliplatin and carboplatin on A2780 cells.**

Complex **41** was co-administered to A2780 cells in combination with **CDDP**, carboplatin and **OXA** in order to determine whether the positive reduction on IC_{50} values observed in the section before was achieved with other platinum chemotherapeutics in clinical use. Table 6.7 shows that there are no significant differences between the platinum drugs used. The concentration of the platinum drugs was in all cases non-toxic.

Table 6.7. Antiproliferative activity of complex **41** in A2780 cells when co-administered with 0.2 µM of **CDDP,** carboplatin and **OXA**.

	Complex 41	**Complex 41 + CDDP**	**Complex 41 + carboplatin**	**Complex 41 + OXA**
IC$_{50}$ (µM) A2780	270 ± 3	91 ± 2	108 ± 3	96 ± 4

- **Experiments according to the Chou and Talalay method.** [8–10]

The median effects for the individual drugs, were determined using the equations in Eq. 6.1, 6.2 and 6.3. Where Fa = fraction of system affected, *Fu* = fraction of system unaffected, *D* = dose, *Dm* = dose for median effect, *m* = Hill-type coefficient: sigmoidicity of the curve. Figure 6.6 shows the median effect graphs used to calculate the individual values of *Dm*, dose for median effect, and *m*, the Hill-type coefficient described by Chou and Talalay for **CDDP** and complex **41**. Meanwhile, the determination of the median effect for the combination of the two drugs was carried out using the equation shown in Eq. 6.4, where Fa = fraction of system affected, Fu = fraction of system unaffected, D = dose, D$_m$ = dose for median effect, m = Hill-type coefficient: sigmoidicity of the curve.
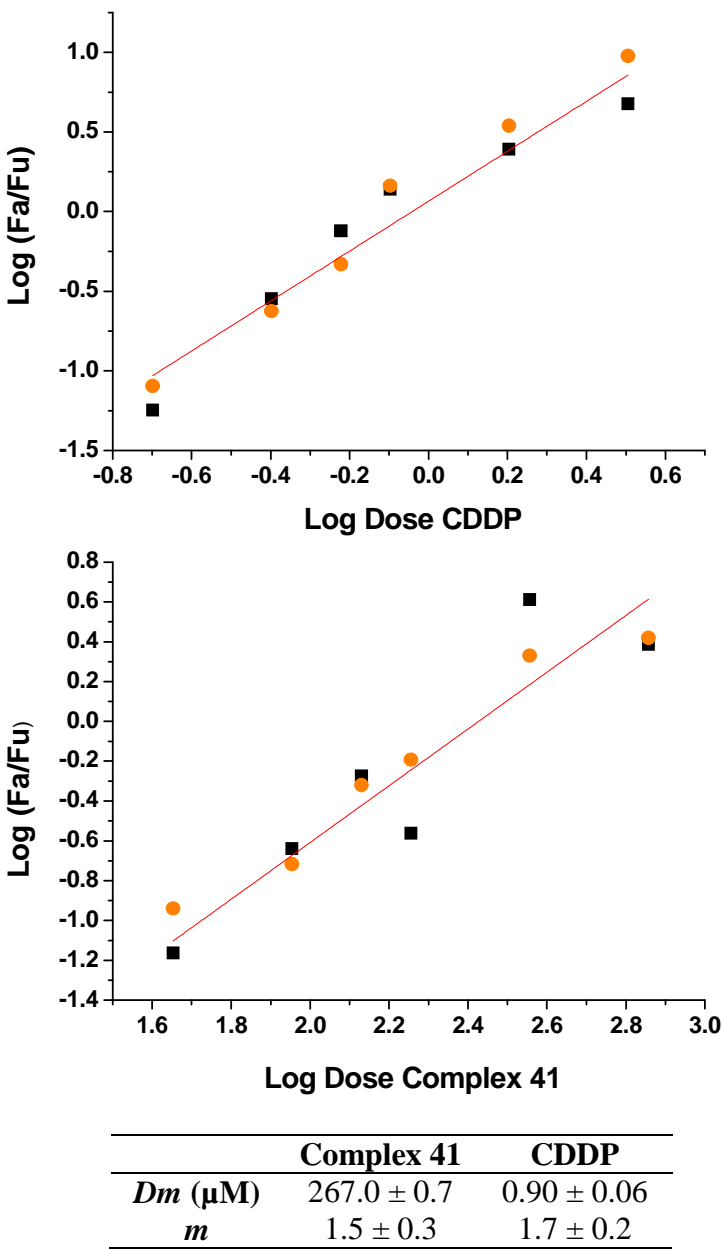
$$\frac{Fa}{Fu} = \left(\frac{D}{Dm}\right)^m \qquad\qquad \textbf{Eq.6.1}$$

$$Fa + Fu = 1 \qquad\qquad \textbf{Eq.6.2}$$

$$Log\left(\frac{Fa}{Fu}\right) = m\,Log\,D - m\,Log\,m \qquad\qquad \textbf{Eq.6.3}$$

$$\left(\frac{Fa_{1,2}}{Fu_{1,2}}\right)^{1/m_{1,2}} = \frac{D_1}{D_{m1}} + \frac{D_2}{D_{m2}} + \frac{D_1 D_2}{D_{m1} D_{m2}}$$

Eq.6. 4.

	Complex 41	**CDDP**
Dm (µM)	267.0 ± 0.7	0.90 ± 0.06
m	1.5 ± 0.3	1.7 ± 0.2

Figure 6.6. Median effect for complex **41** and **CDDP** according to Chou and Talalay.

Figure 6.7 shows the median effect graph obtained for the combination of **CDDP** and complex **41**. It also includes the *Dm* and *m* value determined for the combination of the two drugs. Using the median effects values for the individual drugs, it was posible to determine the combination index for the co-administration (Eq. 6.5). According to the method used, *CI* values above 1 denote an antagonist effect between the administered drugs, while *CI* = 1 shows an additive behaviour, and *CI* < 1 indicates positive synergy.
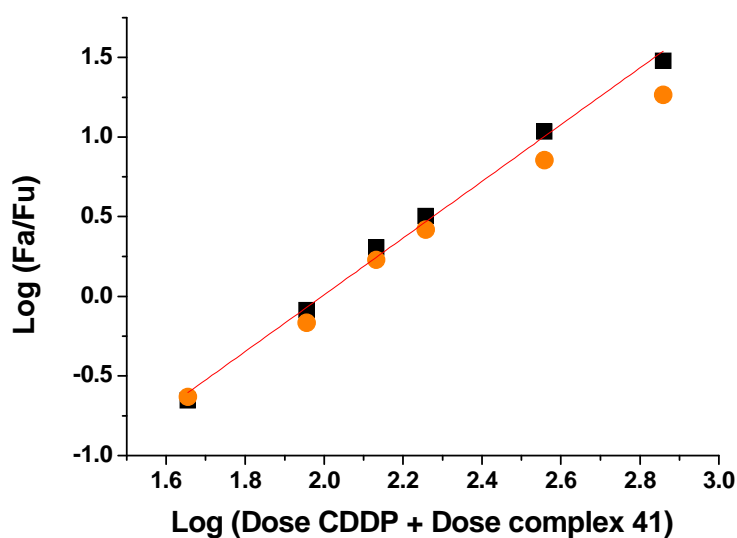
	CDDP + Complex 41
D_m (µM)	100 ± 3
m	1.7 ± 0.1

Figure 6.7. Median effect for the combination of complex **41** and **CDDP** according to Chou and Talalay.

$$CI = \frac{D_1}{Dx_1} + \frac{D_2}{Dx_2} = \frac{D_1}{D_{m1} \left(Fa/(1-Fa)\right)^{1/m_1}} + \frac{D_2}{D_{m2} \left(Fa/(1-Fa)\right)^{1/m_2}}$$ **Eq.6.5.**

Table 6.8 shows the *CI* values determined for the co-administration of **CDDP** and

complex **41** are < 1, which indicates a synergistic action that would allow a dose

reduction of **CDDP**. Table 6.8 also includes the dose reduction index values, *DRI*,

determined using the equation in Eq. 6.6. In this case, Chou and Talalay indicate

that *DRI* > 1 indicates a favorable dose reduction, while *DRI* < 1 is unfavorable.

The values determined for the dose reduction of **CDDP** by the use of complex **41**

range between 1.78 and 2.12.

$$DRI_1 = \frac{D_{m1} \left(Fa/(1-Fa)\right)^{1/m_1}}{D_1}$$ **Eq.6. 6.**

Table 6.8. Combination and dose reduction index determined for the co-administration of **CDDP** and complex **41**.

Dose (x IC$_{50,}$ µM)	Combination index, CI	Dose reduction index, DRI
4	0.96	1.82
2	0.88	1.99
1	0.83	2.10
0.75	0.83	2.12
0.50	0.99	1.78
0.25	0.98	1.79

6.4 Discussion

The mechanistic route for the ligand synthesis starts with the controlled distillation of the dicyclopentadiene. The five membered diene undergoes spontaneous Diels-Alder condensation. Therefore pre-reaction distillation is necessary as heat promotes the retro Diels-Alder reaction shown in Scheme 6.1Scheme 6. 1.


Scheme 6. 1. Retro Diels-Alder reaction to give cyclopentadiene from its dimer.

Tetrahydroquinolines used in this Chapter were obtained using the Grieco-Bahsas three component condensation,[27] in this reaction an imine intermediate is generated *in situ* by the condensation of the aniline and the aromatic aldehyde. The imine is used as a heterodiene in the subsequent hetero-Diels Alder reaction with inverse electron demand. The mechanism of this reaction is shown in Figure 6.16.

Complex **42** includes in its *N,N*-chelating ligand an electron donating group ($R_1 =$ OH) while complex **43** has an electron withdrawing group ($R_1 =$ COOH) in the same position, R_1. This electronic difference does not seem to influence their aqueous behaviour. Both complexes exhibit the same extent of aquation after 24 h period (23-28%). Complex **40**, which has no substituent ($R_1 =$ H), does not undergo aquation. Similar results were obtained for the extent of binding to 9-EtG. Complexes with substituted tetrahydroquinoline derivatives, **42** and **43**, bind

to the nucleobase, regardless of the nature of the R_1 substituent, while complex **41** remains unreacted. NMR studies show that the complexes are stable in aqueous solution for up to 96 h.
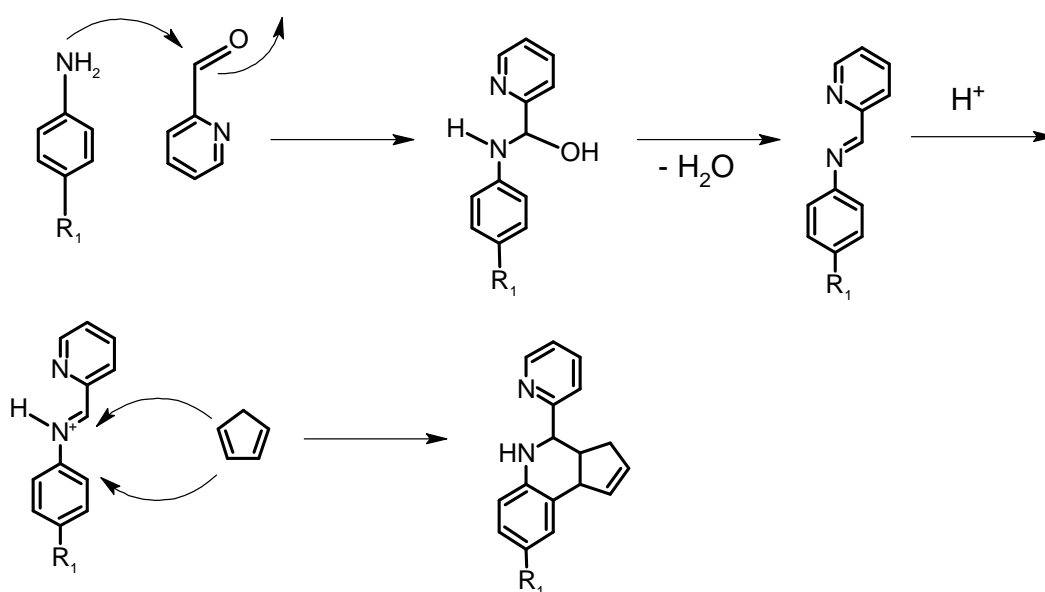
Figure 6.8. Reaction mechanism for the formation of the tetrahydroquinoline derivatives used in this Chapter as *N,N*-ligands.

Although the use of tetrahydroquinolines as *N,N*-chelating ligands in piano-stool Ru(II) complexes was expected to render active complexes, investigations on the antiproliferative activity of complexes **41-43** revealed that the complexes are inactive in all cell lines under the conditions described ($IC_{50} > 200$ µM). One possible explanation for the inactivity could be related to low cellular uptake. However metal accumulation studies in A2780 cells indicate that the complexes

do cross cellular membranes. Ruthenium accumulates in the order of 1.9 to 2.5 ng per million cells with no significant differences between the three complexes.

Investigations were carried out to explore the effect on the antiproliferative activity of complexes **41-43** of co-administration with a non-toxic dose of **CDDP** (0.2 µM). These experiments were carried out with the three complexes in four cell lines: ovarian, lung, colon and breast cancer.

Table 6.6 shows that in the case of complex **41**, the IC_{50} value in ovarian cells A2780 is reduced by a factor of 3, decreasing from 270 ± 3 µM to 91 ± 2 µM. Similar reductions were observed in the other cell lines, where the IC_{50} decreases between a 2-3 fold. The activity of complex **42** is also greatly improved in ovarian, colon and breast cancer, with IC_{50} values ranging between 109 to 155 µM. The activity of complex **43** remains unchanged in all cell lines. The most important result of this preliminary experiment is that the combination of a totally non-toxic dose of **CDDP** (0.2 µM) and inactive complexes **41** and **42** can dramatically alter cell viability. This is a major indication of a positive interaction between the platinum drug and these Ru(II) organometallic complexes.

The next question to be addressed was whether the observed potential for combination was limited to **CDDP** or if similar behavior was observed for other platinum chemotherapeutics in clinical use such as carboplatin and **OXA**. Complex **41** was chosen for this experiment as it showed the most promising results. The Ru(II) complex was co-administered with carboplatin or **OXA** in A2780 ovarian cancer cells. Table 6.7 shows that there are no significant differences between the increments in potency achieved by the three platinum

drugs (CDDP, OXA and carboplatin). This consistent behavior is another indication of the possible synergy existent between the two administered drugs. NMR studies carried out show that there is no chemical transformation after 24 h when complex **41** is co-incubated with **CDDP**.

In the light of the preliminary results, it was decided that the Chou and Talalay approach would be used to determine the type of interaction between complex **41** and **CDDP** in A2780 cells. According to this approach two drugs that cause a response in a biological system can be co-administered in a combination therapy setting. This co-administration can have three possible outcomes, as shown in Figure 6.9: 1) antagonism, 2) additivity or 3) synergy.
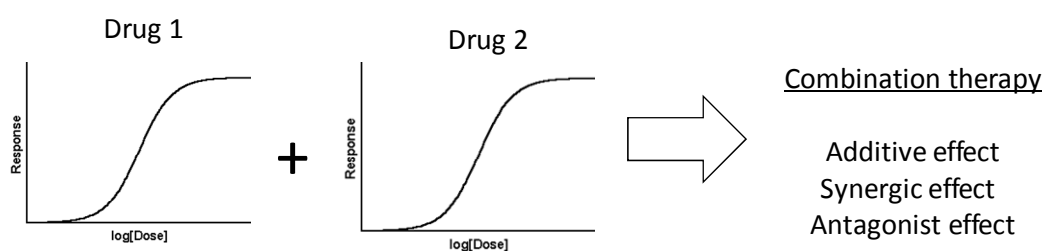

Figure 6.9 Possible outcomes of the combination of two drugs that cause a response in a biological system.

It is also possible to co-administer two drugs when one of them does not cause a response in the biological system, Figure 6.10 shows that the possible positive outcomes of the combination could be 1) potentiation or 2) enhancement.
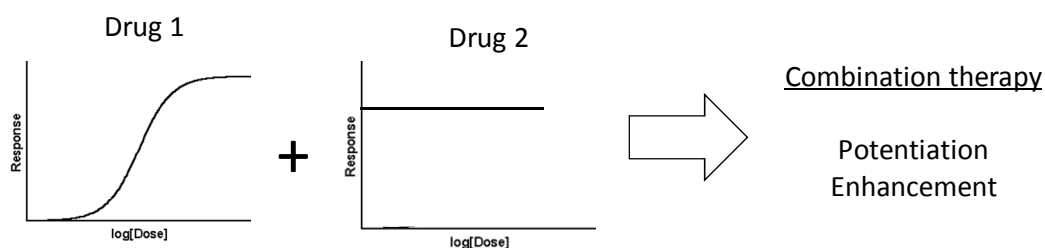
Figure 6.10 Possible outcomes of the combination of two drugs when one does not cause a response in a biological system

The Hill equation to describe nonlinear drug dose–response relationships is widely used in pharmacokinetic–pharmacodynamic models.[28] The Chou-Talalay approach includes the determination of a Hill-type coefficient, m. Sigmoidal dose-response curves, such as the ones observed for **CDDP** and complex **41**, should render m values higher than one. The Hill-type coefficient, m, for the individual drugs is defined by the slope of a median effect graph (Log (Fa/Fu) vs Log D) as shown in Figure 6.11. The value $m = 1$ denotes hyperbolic dose-response systems.[10] The Hill-type coefficients, m, for the individual drugs **CDDP** and complex **41**, were determined using the median effect equation in Eq. 6.2. Both values $m_{\textbf{CDDP}}$ and $m_{\textbf{Ru41}}$ are > 1 (1.5 ± 0.3 and 1.7 ± 0.2 respectively).
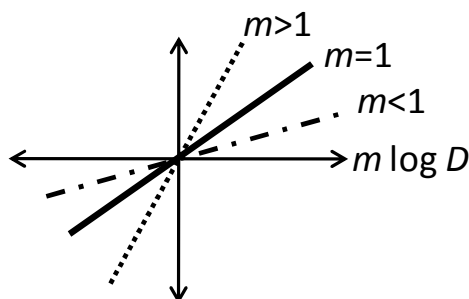
Figure 6.11. Median effect of one drug, as described by Chou and Talalay. m > 1 : sigmoidal dose-response systems, m = 1: hyperbolic dose-response systems.

The graph in Figure 6.11 also allowed the determination of the dose for median effect for CDDP and complex **41**. These values, 0.90 ± 0.06 and 267.0 ± 0.7 µM respectively, are in good agreement with the IC_{50} values for these two drugs determined by the SRB assay using a sigmoidal drug-response graph. Chou and Talalay establish two different approaches to determine the dose for median effect of the combination of two drugs. In the first case, the two drugs should have similar modes of action; in the second case the drugs involved can have a different or overlapping mode of action. At present, regarding the combination of **CDDP** and complex **41**, there is no information on the mechanism of action of the Ru(II) complex. It is expected that as for similar metal-based complexes, the mode of action of **41** is multitargeted. Therefore the determination of the dose for median effect of such combination used the equation in Eq.6. **4.**
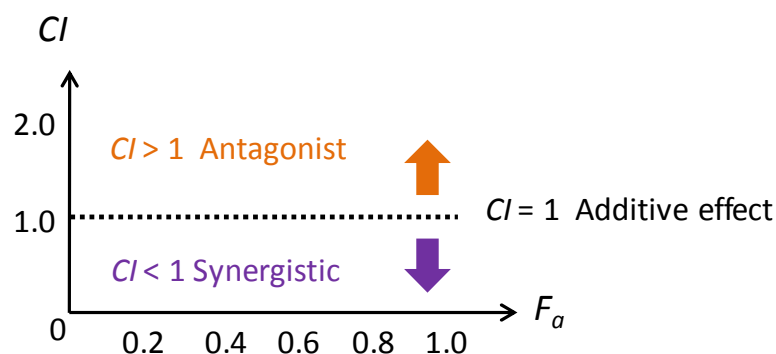
Figure 6.12. Predicted behaviour of two drugs according to their combination index, *CI*

A very important parameter to define the interaction between two co-administered drugs is the combination index, *CI*. As shown in Figure 6.12 the value of *CI* determines whether the drugs are antagonists or if their interaction is additive or

synergic.[8] In the case of **CDDP** and complex **41**, all equipotent combinations used gave *CI* values below 1, as shown in Figure 6.13. This confirms the synergistic interaction between the two drugs.
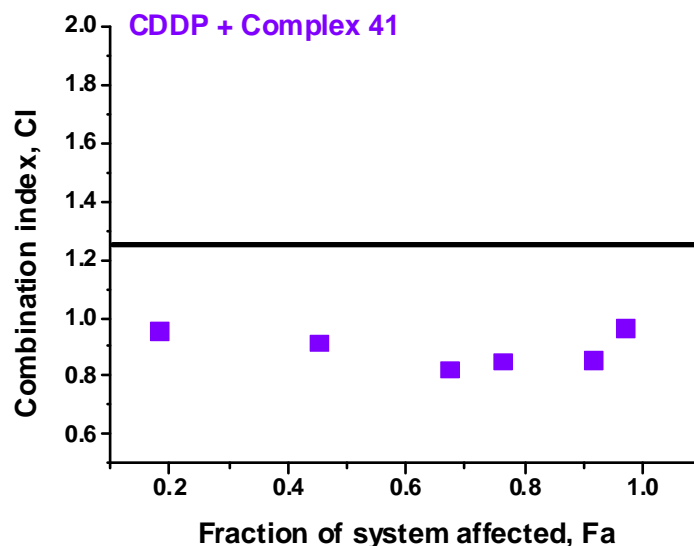
Figure 6.13. Combination index, *CI,* determined for the equipotent mixture of **CDDP** and complex **41**

Finally, it is possible to determine how favorable the dose reduction is when two drugs are administered in an equipotent setting. The dose reduction index, *DRI*, is established so that values above the unit are favorable while values lower than 1 represent an unfavorable combination (Figure 6.14).[8] As shown in Figure 6.15 all the values determined for the combination of **CDDP** and complex **41** are favorable.
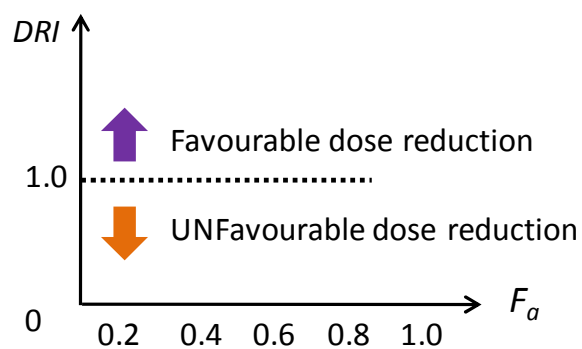
Figure 6.14. Predicted behaviour of two drugs according to their dose reduction index, *CI*
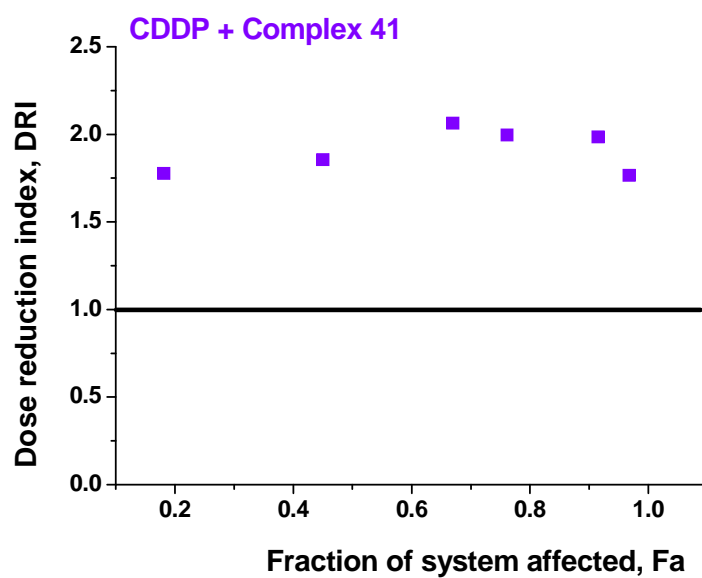
Figure 6.15. Dose reduction index, *DRI,* determined for the equipotent mixture of **CDDP** and complex **41**

6.5 Conclusions

This Chapter shows the successful use of Ru(II) half-sandwich complexes in combination therapy with platinum drugs in current clinical use. The results in this section indicate that it is possible to achieve considerable modulation of cell viability by co-administering an inactive Ru(II) complex and a non-toxic dose of **CDDP**. The enhancement of activity was independent of the platinum drug (**CDDP,** carboplatin or **OXA**). The Chou and Talalay approach has been used to establish the doses for median effect of an equipotent mixture of complex **41** and **CDDP**. The same approach allowed confirmation that the co-administration of these two chemotherapeutics results in a synergistic interaction with favorable dose reduction indices.

The results in this Chapter open up a new an interesting application for half-sandwich organometallic drugs that could lead to a significant dose reduction for Pt use and in consequence a reduction of undesirable side effects.

The Chou-Talalay method does not shed light on the mechanism of action of the drugs nor on the origin of the synergistic effect. These important questions need to be addressed in order to exploit the maximum potential of this new combination therapy approach.

6.6 References

1. W. R. Greco, G. Bravo, and J. Parsons, *Pharmacology*, 1995, 331-385.

2. W. R. Greco, H. Faessel, and L. Levasseur, *J. Natl. Cancer Inst.*, 1996, **88**, 699-700.

3. P. J. O'Dwyer, J. D. Moyer, M. Suffness, S. D. Harrison, R. Cysyk, T. C. Hamilton, and J. Plowman, *Cancer Res.*, 1994, 724-729.

4. F. Greco and M. J. Vicent, *Adv. Drug Delivery Rev.*, 2009, **61**, 1203-1213.

5. C. J. van Moorsel, H. M. Pinedo, G. Veerman, A. Guechev, K. Smid, W. J. Loves, J. B. Vermorken, P. E. Postmus, and G. J. Peters, *Biochem. Pharmacol.*, 1999, **57**, 407-415.

6. J. B. Fitzgerald, B. Schoeberl, U. B. Nielsen, and P. K. Sorger, *Nat. Chem. Biol.*, 2006, **2**, 458-466.

7. J. J. Lee, M. Kong, G. D. Ayers, and R. Lotan, *J. Biopharm. Stat.*, 2007, **17**, 461-80.

8. T. C. Chou, *Pharmacol. Rev.*, 2007, **58**, 621-681.

9. T. C. Chou, *Cancer Res.*, 2010, **70**, 440-446.

10. T. C. Chou and P. Talalay, *Adv. Enzyme Regul.*, 1984, **22**, 27-55.

11. M. C. Berenbaum, *Pharmacol. Rev.*, 1989, **1989**, 93-141.

12. W. Greco, H. Unkelbach, G. Poch, J. Suhnel, M. Kundi, and W. Bodeker, *ACES*, 1992, **4**, 65-69.

13. M. S. Belenkii and R. F. Schinazi, *Antiviral Res.*, 1994, **25**, 1-11.

14. D. M. Jonker, S. G. Visser, P. H. van der Graaf, R. Voskuyl, and M. Danhof, *Pharmacol. Ther.*, 2005, **106**, 1-18.

15. X. Li and H. Y. Zhang, *Trends Pharmacol. Sci.*, 2008, **29**, 331-2.

16. R. Straetemans, T. O'Brien, L. Wouters, J. Van Dun, M. Janicot, L. Bijnens, T. Burzykowski, and M. Aerts, *Biometrical J.*, 2005, **47**, 299-308.

17. C. Supan, G. Mombo-Ngoma, M. P. Dal-Bianco, C. L. Ospina Salazar, S. Issifou, F. Mazuir, A. Filali-Ansary, C. Biot, D. Ter-Minassian, M. Ramharter, P. G. Kremsner, and B. Lell, *Antimicrob. Agents Chemother.*, 2012, **56**, 3165-3173.

18. B. Heiniger, G. Gakhar, K. Prasain, D. H. Hua, and T. Nguyen, *Anti-Cancer Res.*, 2010, **30**, 3927-3932.

19. C. M. Bode, A. Boezio, B. K. Albrecht, S. F. Bellon, L. Berry, M. Broome, D. Choquette, I. Dussault, R. T. Lewis, M. H. J. Lin, K. Rex, D. Whittington, Y. Yang, and J. C. Harmange, *Bioorg. Med. Chem. Lett.*, 2012, **22**, 4089-4093.

20. A. Shi, T. Nguyen, S. K. Battina, S. Rana, D. J. Takemoto, P. K. Chiang, and D. H. Hua, *Bioorg. Med. Chem. Lett.*, 2008, **18**, 3364-3368.

21. A. R. Martirosyan, R. Rahim-Bata, A. B. Freeman, C. D. Clarke, R. L. Howard, and J. S. Strobl, *Biochem. Pharmacol.*, 2004, **68**, 1729-1738.

22. N. Nagata, M. Miyakawa, S. Amano, K. Furuya, N. Yamamoto, H. Nejishima, and K. Inoguchi, *Bioorg. Med. Chem. Lett.*, 2011, **21**, 6310-6313.

23. N. Nagata, K. Kawai, and I. Nakanishi, *J. Chem. Inf. Model.*, 2012, DOI: 10.1021/ci300219g.

24. L. Zai-gang, Z. Cheng-chu, W. Fang, H. Hong-qiu, and W. Cun-xin, *Chem. Res. Chinese Universities*, 2009, **25**, 841-845.

25. P. R. Graves, J. J. Kwiek, P. Fadden, R. Ray, K. Hardeman, A. M. Coley, M. Foley, and T. a J. Haystead, *Mol. Pharmacol.*, 2002, **62**, 1364-1372.

26. M. Rosini, F. Mancini, A. Tarozzi, F. Colizzi, V. Andrisano, M. L. Bolognesi, P. Hrelia, and C. Melchiorre, *Bioorg. Med. Chem.*, 2006, **14**, 7846-7853.

27. P. Grieco and A. Bahsas, *Tetrahedron Lett.*, 1988, **29**, 5855-5858.

28. S. Goutelle, M. Maurin, F. Rougier, X. Barbaut, L. Bourguignon, M. Ducher, and P. Maire, *Fundam. Clin. Pharmacol.*, 2008, **22**, 633-648.

Chapter 7

Conclusions & Future Work

7.1. Conclusions

Cancer has been defined by the WHO as the uncontrolled growth and spread of cells. During the first half of the 20th century surgery and radiotherapy were the preferred choice for cancer treatment. It was not until the 1940s when chemotherapy started to be considered as a viable alternative. Important research has been carried out in the last decades, rendering major achievements in the treatment and subsequent improvement of life expectancy in cancer patients.[1] The serendipitous discovery of cisplatin[2] started a new era in which transition metals have been used in the treatment of cancer. Coordination complexes are being developed in order to emulate and improve the activity of the platinum drug while reducing its unwanted side effects.[3–7] Ruthenium(II) complexes have been widely developed in this field as a viable alternative.[8–12]

This thesis deals with the design, synthesis and characterization of half-sandwich Ru(II) arene complexes as novel antineoplastic agents. This type of 'piano-stool' complexes allow fine tuning of the physical and chemical properties which should result in optimised biological activity.[13–16] They include three main building blocks:$[Ru(arene)(YZ)X]^{n+}$. An arene unit used to improve hydrophobicity and to stabilize the metal centre oxidation state, a monodentate ligand, X, initially included as an activation site, and a bidentate ligand, Y-Z.[5,17]

Chapter 3 is concerned with *N,N*-chelated ruthenium(II) iminopyridine complexes. In this case, electron-donating and electron withdrawing substituents were included in the Y-Z imino chelating ligand in order to investigate modifications on the antiproliferative activity. It was shown that complexes that

were substituted with electron donating groups such as NMe$_2$ were more active towards cancer cell lines (A2780, A549, HCT116 and MCF7) than those which included electron withdrawing groups (COOH, C$_3$H$_6$COOH).The investigation of the extent of aquation and 9-EtG binding of these complexes gave a correlation between the nature of the substituent group and their reactivity in aqueous media. A relevant finding was that the cellular accumulation of these Ru(II) impy complexes do not correlate with potency, showing that, the different ruthenium arene complexes may be involved in different antiproliferative mechanisms.

In the same Chapter, complexes **15** [Ru(η^6-p-cym)(p-Impy-NMe$_2$)Cl]PF$_6$ and **16** [Ru(η^6-p-cym)(p-Impy-NMe$_2$)I]PF$_6$ were used to investigate the possible pathways for cellular accumulation in comparison with cisplatin in A2780 ovarian cancer cells. The structural difference between these two complexes was the nature of the monodentate ligand (Cl vs I). Results indicate that the uptake pathways depend to a great extent on the halide present. Although maximum accumulation occurs at similar time period for both complexes (24 – 48 h) complex **16** showed partial energy-independent uptake which is enhanced by amphotericin B, a facilitative diffusion agent. The involvement of CTR1 copper transport protein was also investigated as well as the variations on the cellular accumulation caused by changes in the membrane potential. Results obtained indicate that P-gp could be involved in the efflux of Ru(II) complexes. Finally it was shown that the caveolae endocytotic pathway is not involved in the uptake of either of the ruthenium complexes **15** or **16**.

It is widely accepted that cisplatin targets DNA, and that this interaction is the main source of its antiproliferative activity.[18,19] However, the analogous mechanism of action of Ru(II) has not yet been fully established. Half-sandwich Ru(II) complexes can undergo aquation depending on the nature of their monodentate ligand. After this activation process, a vacant coordinative site is generated, allowing the interaction with different biomolecules.[20,21] Several Ru(II) complexes have shown to be able to interact with CT-DNA.[22] *In vitro* experiments have investigated the interaction between the Ru(II) complexes and cellular DNA[23,24] as well as the activation of nucleotide excision repair mechanisms after the formation of Ru-DNA adducts.[25] Based on this previous evidence, Chapter 4 was aimed at investigating whether DNA could be a molecular target for Ru(II) complexes **24**-**33**.

 Complexes **24-33** were designed to include extended planar aromatic units in the YZ chelating ligand as well as increased aromaticity in the arene building block, this in order to improve conditions for DNA intercalation. Investigations involved the synthesis of complexes and studies of their antiproliferative activity in ovarian, lung colon and breast cancer cells together with the extent of cellular accumulation. Determination of the Log P values confirmed that by increasing the number of aromatic rings in the arene unit it is possible to increase the hydrophobicity of the complexes. However, there was no direct correlation between these values and cellular accumulation or antiproliferative activity. Several experiments were carried out to investigate the interaction between active complexes and CT-DNA. Thermal denaturation of CT-DNA was monitored by

means of UV-Vis spectroscopy. Complexes **27, 28, 32** and **33** generated ΔTm in the range of 20 – 30 K which indicated that, as intercalators, they stabilised the double helix of DNA causing an increase in the energy required to separate the two strands. In all cases the greatest extent of binding occurs during the first 10 h of incubation at 310 K. UV-Vis titrations showed bathochromic shifts of DNA basis and for charge transfer absorption bands of the complexes which are again indicative of DNA intercalation. Ru(II) arene complexes are most likely to be multi-targeted. Research in Chapter 4 indicates that intercalative interactions do occur between CT-DNA and the synthesised complexes (**24-33**). Therefore DNA may well be one of the molecular targets.

In order to elucidate further the possible targets for Ru(II) complexes, possible molecular events activated during cell death were investigated using complexes **15, 16** [Ru(η^6-*p*-cym)(*p*-Impy-NMe$_2$)X]PF$_6$, **34, 35** [Ru(η^6-*p*-cym)(*p*-Azpy-NMe$_2$)X]PF$_6$, and **36, 37** [Os(η^6-*p*-cym)(*p*-Impy-NMe$_2$)X]PF$_6$ where X = Cl or I in Chapter 5. Results suggested that the apoptotic pathways depend to a great extent on the nature of the monodentate ligand. This is consistent with the findings of Chapter 3 regarding cellular accumulation pathways. Furthermore Cl vs I differences meant variations of cellular compartamentalization of the complexes, regardless of their metal centre (Ru vs Os). Complexes **15, 16, 34-37** are highly active in all the cell lines tested (A2780, A549, HCT116, and MCF7). Interestingly iodido complexes **16, 35** and **37** retain their potency in cisplatin and oxaliplatin resistant cell lines (A2780cis and HCT116Ox).

Resistance is one of the major challenges to overcome in the use of chemotherapy for cancer treatment.[26] Molecular mechanisms of acquired resistance include: increased drug efflux, mutations in drug targets, activation of downstream or parallel signalling pathways and altered drug metabolism.[27] Iodido complexes **16, 35** and **37** do not share mechanisms of resistance with cisplatin nor with oxaliplatin as they remain active in resistant cell lines. Other Ru(II) piano stool complexes have been reported to circumvent resistance to platinum chemotherapeutics. Such is the case for RM175, which is active in A2780cis.[28] Remarkably the iodido complexes studied in this Chapter are also more selective towards ovarian cancer than cisplatin. This was shown by measuring the activity of the complexes in MRC5 human fibroblasts.

Cell cycle studies in A2780 ovarian cells showed that complexes **15, 16, 34-37** exhibit cytostatic activity as well as cytotoxicity by causing G1-arrest that inhibits cell proliferation. Another important result concerns the involvement of tumour suppressor p53 in the apoptotic pathways activated by the Ru(II) complexes. Disruption of the activity of p53 has been strongly correlated to tumorigenesis as it is considered to maintain genomic stability.[29] Unfortunately, its inactivation is the most common event in human cancers, occurring in at least 50% of all cases.[30,31] Hence there is interest in novel chemotherapeutic agents that are active in the presence/absence of p53. Iodido complexes **16, 35** and **37** exhibited activity independent of p53, while the activity of chlorido complexes, **34** and **36** depends on this protein to cause cell death. Half-sandwich arene complexes **15, 16, 34-37** initiated apoptosis in A28780 cells after 24 h of drug exposure and moreover

activated caspase 3. It remains unclear if the activation of the caspase is the result of an intrinsic apoptotic pathway or a response to extrinsic stimuli. Finally, co-administration of complexes **15, 16, 34-37** together with L-BSO demonstrated that it is possible to achieve drug-dose reduction by depletion of GSH intracellular levels. In this case a non-toxic dose of L-BSO (5 µM) allowed nanomolar activities to be achieved in A2780 cells.

Combination of two or more drugs, such as the co-administration of L-BSO and ruthenium(II) complexes has been developed as an alternative in cancer chemotherapeutics. This approach, known as combination therapy, allows the reduction of un-wanted side effects by lowering drug doses. It can also help to minimise the development of resistance.[32,33] Using the Chou and Talalay[34–36] approach it is possible to determine whether the combination of two drugs results in a synergistic interaction and subsequent positive dose-reduction.

Chapter 6 showed the successful use of Ru(II) half-sandwich complexes in combination therapy with platinum drugs in current clinical use. Preliminary studies indicate that Ru(II) 'piano-stool' complexes that include in their structure tetrahydroquinoline derivatives as *N,N*-chelating ligands are capable of dramatically altering cell viability when in the presence of a non-toxic dose of cisplatin. The Chou and Talalay method was used to confirm the existing synergy and to calculate the favorable dose reduction indices. Results in this Chapter open a new and interesting application for half-sandwich complexes in the quest for novel chemotherapeutic treatments. Further studies need to be carried out in order to determine the molecular mechanism of action of the drug combination. Finding

out the molecular basis for the observed synergy will be key to exploit the maximum potential of this new combination therapy approach.

7.2. Future work

This section explores possible areas of future work based on the achievements of previous chapters.

### 7.2.1. Mechanism of action of half-sandwich organometallic complexes: in the search for multiple targets

Organometallic piano-stool complexes are most likely multitargeted. Chapter 5 explored the mechanism of action of ruthenium(II) and osmium(II) complexes. This Chapter showed the differences in the apoptotic pathways activated by chlorido complexes against those activated by iodido complexes. The latter are known to cause apoptosis via a p53-independent pathway. However little is known of the molecular targets within this important pathway. Future work should include investigation of the activation of signaling mechanisms in this pathway to narrow down their possible molecular targets.

Chapter 4 explored DNA as a target for ruthenium(II) complexes. Most of the studies in this Chapter were carried out using CT-DNA. Future work needs to confirm that the complexes are able to reach the cell nucleus; this can be achieved by studying cellular compartamentalization. Moreover it would be possible to

study Ru(II)-DNA binding in native DNA extracted from A2780 cells exposed to the ruthenium(II) complexes.

Further studies in cellular compartmentalization should include "fragment tracking". For this, a novel Ru(II) complex has already been synthesized (Figure 7.1) , it includes a bromide atom as a substituent in the *N,N*-chelating ligand as well as an iodide atom as the monodentate unit. The idea is to be able to follow the compartmentalization of three elements, Ru, Br and I which would give information on the distribution of the metal centre vs the monodentate unit vs the *N,N*-chelating ligand.
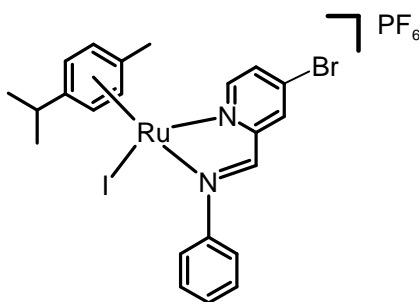
Figure 7.1. Ru(II) complex synthesised for cellular compartmentalisation studies

Activation of apoptotic pathways seem to rely heavily on cellular uptake pathways and subsequent compartamentalization - both of which depend on the nature of the monodentate ligand of the piano-stool complexes. In Chapter 5 only chlorido and iodido complexes were evaluated. It would be interesting to investigate also the analogous bromido complexes.

Chapter 5 also showed that the resistance to chemotherapeutics could be circumvented by using piano-stool complexes based on ruthenium and osmium. It is important that future work in this area include the analysis of the three major

causes of resistance. In the case of impaired cellular accumulation, future investigation needs to be based on the comparison of the metal content in resistant cells against their accumulation in parental lines and its subsequent compartamentalization.

7.2.2. Combination therapy, a viable alternative for dose reduction of platinum therapeutics

Chapter 6 showed the potential to use inactive Ru(II) complexes in combination with non-toxic doses of platinum chemotherapeutics to modulate cell viability. In this respect there are several unanswered questions: 1) is it possible to use this combination approach with other Ru(II) complexes?, 2) what is the origin of the synergistic effect?, 3) can *CI* and *DRI* be further improved?.

The used of the Chou and Talalay approach to combination therapy should be extended to other Ru(II) complexes, especially to those that do not include tetrahydroquinolines as *N,N*-chelating ligands, to investigate whether the antiproliferative activity is related to the presence of the quinoline derivative. It would also be pertinent to investigate the outcome of the co-administration of cisplatin with an active Ru(II) complex.

A comparative study of the mechanism of action of the drugs used in the combination therapy experiments is ultimately necessary to detect the origin of the synergistic effect observed. Starting with cellular uptake studies, it would be possible to compare the cellular accumulation of the individual drugs against their

accumulation after co-administration. In a similar fashion, the activation of landmark events in cellular apoptosis needs to be compared between the individual drugs and the co-administration. This would shed light to the understanding of the molecular basis of such interaction.

Finally, Chou and Talalay also explore the possibility of modulating cellular response using a variable ratio of both drugs, together with the analysis of the effect of co- and sequential administration (Figure 7.2). This has not yet been explored for the combination of cisplatin and Ru(II) complexes. Experimental settings as the ones shown in could be a way of improving *CI* and *DRI* values.
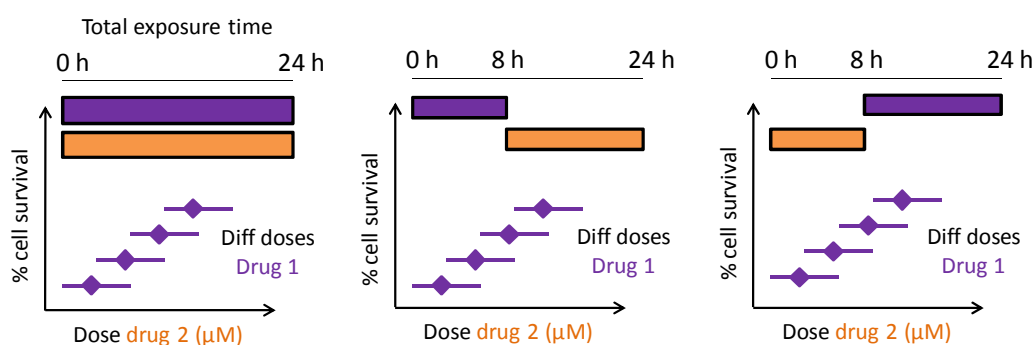
Figure 7.2. Suggested experimental settings to explore the effect of a variable ratio of both drugs, as well as the effect of co- and sequential administration

7.3   References

1.   V. T. DeVita and E. Chu, *Cancer Res.*, 2008, **68**, 8643-8653.

2.   B. Lippert, Ed., *Cisplatin*, Wiley, Zurich, 1999.

3.   S. P. Fricker, *Dalton Trans.*, 2007, 4903-4917.

4.   N. C. Institute, *August 2012*, www.cancer.gov.

5.   Y. K. Yan, M. Melchart, A. Habtemariam, and P. J. Sadler, *Chem. Commun.* , 2005, 4764-4776.

6.   B. Desoize, *Anti-Cancer Res.*, 2004, **24**, 1529-1544.

7.   I. Ott and R. Gust, *Archiv der Pharmazie*, 2007, **340**, 117-126.

8.   E. S. Antonarakis and A. Emadi, *Cancer Chemoth. Pharm.*, 2010, **66**, 1-9.

9.   I. Bratsos, S. Jedner, T. Gianferrara, and E. Alessio, *Chimia*, 2007, **61**, 692-697.

10.   R. E. Morris, R. E. Aird, P. D. S. Murdoch, H. Chen, J. Cummings, N. D. Hughes, S. Parsons, A. Parkin, G. Boyd, D. I. Jodrell, and P. J. Sadler, *J. Med. Chem.*, 2001, **44**, 3616-3621.

11.   C. Scolaro, A. Bergamo, L. Brescacin, R. Delfino, M. Cocchietto, G. Laurenczy, T. J. Geldbach, G. Sava, and P. J. Dyson, *J. Med. Chem.*, 2005, **48**, 4161-4171.

12.   S. Schäfer, I. Ott, R. Gust, and W. S. Sheldrick, *Eur. J. Inorg. Chem.*, 2007, 3034-3046.

13. F. Wang, A. Habtemariam, E. van der Geer, R. Fernández, M. Melchart, R. J. Deeth, R. Aird, S. Guichard, F. P. Fabbiani, P. Lozano-Casal, I. D. H. Oswald, D. I. Jodrell, S. Parsons, and P. J. Sadler, *Proc. Natl. Acad. Sci. USA.*, 2005, **102**, 18269-18274.

14. A. Habtemariam, M. Melchart, R. Fernandez, S. Parsons, I. D. H. Oswald, A. Parkin, F. P. Fabbiani, J. E. Davidson, A. Dawson, R. E. Aird, D. I. Jodrell, and P. J. Sadler, *J. Med. Chem.*, 2006, **49**, 6858-6868.

15. A. Peacock, A. Habtemariam, R. Fernández, V. Walland, F. Fabbiani, S. Parsons, R. E. Aird, D. I. Jodrell, and P. J. Sadler, *J. Am. Chem. Soc.*, 2006, **128**, 1739-1748.

16. P. C. Bruijnincx and P. J. Sadler, *Adv. Inorg. Chem.*, 2011, **8838**, 1-59.

17. G. Süss-Fink, *Dalton Trans.*, 2010, **39**, 1673-1688.

18. E. Corral, A. C. G. Hotze, H. den Dulk, A. Leczkowska, A. Rodger, M. J. Hannon, and J. Reedijk, *J. Biol.Inorg. Chem.*, 2009, **14**, 439-448.

19. O. Novakova, H. Chen, O. Vrana, A. Rodger, P. J. Sadler, and V. Brabec, *Biochemistry*, 2003, **42**, 11544-11554.

20. A. M. Pizarro, A. Habtemariam, and P. J. Sadler, *Top Organomet Chem*, 2010, **32**, 21-56.

21. A. M. Pizarro and P. J. Sadler, *Biochimie*, 2009, **91**, 1198-1211.

22. H. Kostrhunova, J. Florian, O. Novakova, A. Peacock, P. J. Sadler, and V. Brabec, *J. Med. Chem.*, 2008, **51**, 3635-3643.

23. A. Casini, C. G. Hartinger, A. A. Nazarov, and P. J. Dyson, *Top Organomet Chem*, 2010, **32**, 57-80.

24. T. Bugarcic, O. Nováková, A. Halámiková, L. Zerzánková, O. Vrána, J. Kaspárková, A. Habtemariam, S. Parsons, P. J. Sadler, and V. Brabec, *J. Med. Chem.*, 2008, **51**, 5310-5319.

25. O. Novakova, J. Kasparkova, V. Bursova, C. Hofr, M. Vojtiskova, H. Chen, P. J. Sadler, and V. Brabec, *Chem. Biol.* , 2005, **12**, 121-129.

26. J. M. Ford and W. N. Hait, *Cytotechnology*, 1993, **12**, 171-212.

27. R. H. Wilting and J.-H. Dannenberg, *Drug Resist. Update*, 2012, **15**, 21-38.

28. R. E. Aird, J. Cummings, A. A. Ritchie, M. Muir, R. E. Morris, H. Chen, P. J. Sadler, and D. I. Jodrell, *Br. J. Cancer*, 2002, **86**, 1652 - 1657.

29. S. Wang and W. S. El Deiry, *P53, Cell cycle arrest and apoptosis*, Springer, Dordrecht, 2007.

30. U. M. Moll and N. Concin, *p53 in human cancer – Somatic and inherited mechanisms*, Springer Science, New York, 2005.

31. S. M. Post, A. Quintás-Cardama, and G. Lozano, *Regulation of p53 activity and associated checkpoint controls*, Springer Science, New York, 2010.

32. W. R. Greco, G. Bravo, and J. Parsons, *Pharmacology*, 1995, 331-385.

33. W. R. Greco, H. Faessel, and L. Levasseur, *J. Natl. Cancer Inst.*, 1996, **88**, 699-700.

34. T. C. Chou, *Pharmacol. Rev.*, 2007, **58**, 621-681.

35. T. C. Chou, *Cancer Res.*, 2010, **70**, 440-446.

36. T. C. Chou and P. Talalay, *Adv. Enzyme Regul.*, 1984, **22**, 27-55.

Conferences and Meetings Attended

1. Biological and Medicinal Chemistry. BMCS 5th Postgraduate Symposium. Cambridge, UK. December 2011. Poster presentation.

2. 11th International Symposium on Applied Bioinorganic Chemistry. Barcelona, Spain. December 2011. Poster presentation.

3. Warwick University Postgraduate Symposium. Coventry, UK. June 2011. Poster presentation.

4. RSC Dalton Division Midlands Postgraduate Symposium. Coventry, UK. September 2011. Poster presentation.

5. RSC Dalton Division. Dalton Transactions Younger Researchers Symposium. Coventry, UK. April 2012. Poster presentation.

6. Warwick University Postgraduate Symposium. Coventry, UK. May 2012. Oral presentation.

7. 11th European Biological Inorganic Chemistry Conference. Granada, Spain. To be attended September 2012. Poster presentation.

8. Action Meeting COST CM1105. Functional Metal Complexes that Bind to Biomolecules. Granada, Spain. To be attended September 2012. Oral and poster presentation.

9. XI International Symposium on Platinum Coordination Compounds in Cancer Chemotherapy. Stem cells, DNA repair mechanisms, DNA-damaging agents. Verona, Italy. To be attended October 2012. Poster presentation.

10. 8th National Cancer Research Institute Conference. Liverpool, UK. To be attended November 2012. Poster presentation.

11. Development of Cancer Medicines: Preclinical in vivo models to interrogate cancer biology, biomarkers and therapeutic response - Joint BACR/Oncology Section, Royal Society of Medicine. London, UK. To be attended November 2012.